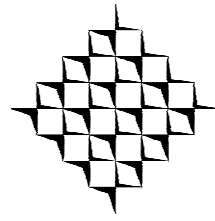




Universidade do Porto  
Faculdade de Engenharia  
**FEUP**  
Chemical Engineering  
Department



**Lepae**  
Laboratory for Process,  
Environmental  
and Energy Engineering

---

# On-line Monitoring of Deposits Formation and Removal on Solid Surfaces Using Vibration Techniques

---

**ANA ALEXANDRA DA SILVA PEREIRA**

Dissertation for Doctor Degree in Chemical and Biological Engineering  
Porto, 2008



The presented Thesis was supervised by:

**Supervisor:** Prof. Dr. Luís Manuel Ferreira de Melo

*LEPAE – Laboratory for Process, Environment and Energy Engineering  
Department of Chemical Engineering  
Faculty of Engineering, University of Porto*

**Co-Supervisor:** Prof. Dr. Joaquim Gabriel Magalhães Mendes

*IDMEC – Instituto de Engenharia Mecânica  
Department of Mechanical Engineering and Industrial Management  
Faculty of Engineering, University of Porto*



## ACKNOWLEDGEMENTS

I'm deeply grateful to Professor Luis Melo for all the patience, motivation and enthusiasm put within my work. His stimulating and enthusiastic conversations regarding our MSS always made me believe that it was possible. Furthermore, I can not forget when he told me 'Go home and think during the weekend! On Monday you will have grown'. Looking back I don't think I have grown (who knows if any day I will) but I know that I have made the right choice! I would also like to acknowledge Prof. Joaquim Mendes for teaching me that a Chemical Engineer is able to accomplish a mechatronic work without getting hurt and without damaging anything. His support and guidance have been of great value for the present Thesis.

During the past few years a lot of (philosophical) discussions about the vibrations on Lab 303 have been accomplished. I think I'm now able to conclude that the vibrations felt within a given work place are intrinsically related to the stimulus provided by the people that 'lives' there. I was quite lucky because when I started my work I met Roxane, who was/is always a supportive and full of joy friend. Thanks for all the things you taught me (you know you will always be my 'chefa') and mainly for showing me that a 'good person, with good vibrations' exist! I would also like to thank Jean (my godchild) for the translation of my abstract to French – Merci beaucoup! Most of these good/bad moments were also shared with my other friends: Bélinha our 'outsider' which always brought a fresh and kind air to my life; Carla, who is one of the nicest persons and efficient 'lab keeper' I ever met; and more recently Joana who was certainly a 'good acquisition' to the lab. A special recognition to Filipe who was always a good supportive friend.

The friends that I have made during the last years can not be forgotten. Thank you all for the good moments we spent together. A big kiss to: Adriano and Filipa (from older fights), Manela, Mónica, Olga, Ratola, and Susana.

A PhD is a many years journey, which is exciting and stimulating but also quite exhausting and difficult with many dark days. However during those dark and sparkling days I was accompanied by my Afonso, who walked with me side-by-side showing me what was the best way to follow (not only on a personal level but many times as my scientific adviser). Thanks for being there on the good and bad moments, full of friendship, love and a lot of patience. You were certainly a damper when my vibrating system was going uncontrolled and an additional source of energy when I needed.

My family was/is also one important and irreplaceable pillar of my life. Thanks to my mum, my dad and Bruno. I mostly acknowledge the education and the perseverance they taught me, but also the time they (specially my mum) spent hearing me (which is certainly not an easy task). Although I cannot

forget my grandma who was/is a second mother to me that was always present along this journey. I would also like to thank my new family (Teresa, Luis, Marta and Sofia) who ‘adopted’ me and make me feel that I also belong to them (and I do). I will never forget their friendship and care! Furthermore, I’m very touched with the efforts they made to help me concerning my work. A special kiss to my new-grandma D. Natália who blamed my PhD Thesis for the inexistence of great-grandsons.

During the last few months I also learned that there are persons with an incredible capacity to help the others... Dr. José Vieira Antunes (from ITN) is one of these persons who helped me a lot regarding the vibration characterization of my system as well as with the simulation/optimization software used in the last chapter. Thanks Zé for all the long talks, for answering all my ‘stupid’ questions but mainly for all the enthusiasm and kindness with which you helped me.

Another important contribution for the discussion of the vibration issues was provided by Dr. Pedro Ribeiro to whom I would like to express my gratitude. I would also like to thank Dr. Vincent Debut (from ITN) for his support and sympathy regarding the experiments that were performed in Lisbon.

I would also like to acknowledge the industrial inputs that my work gathered along the last years. I would like to thanks to Dr. Julian Clarke (from Unilever) for his important contribution regarding the shampoo trials. I would like sincerely to acknowledge Eng. Mário Freire and Eng. Jorge Martins (from Enkrott) for their enthusiasm and motivating contributions mainly concerning to what should be done to improve the MSS and regarding its (and mine) future. I would also like to thank Pedro, Telma and Catarina (from Enkrott) for their support regarding my ‘free’ MSS and mainly for showing me its fragilities.

I cannot forget the help of Mr. Santos on the assembling of my first setup, but also of Mr. Nelson for the patience and the good ideas that helped me to improve my last configurations. I would also like to thank Mrs. Fátima and Elisa for their patience and help regarding a lot bureaucratic issues.

I would also like to thank Fundação para a Ciência e a Tecnologia (FCT) for the financial support of the Surfcont project and of the graphical reproduction of the present Thesis.







## **ABSTRACT**

The adhesion of unwanted deposits to surfaces (fouling) is an economically and environmentally costly problem that gathers the attention of a vast scientific community. Several strategies have been studied and implemented in order to minimize fouling formation or to improve the cleaning procedures. One of these strategies is based on the implementation of on-line real-time monitoring techniques that provide information about the adhesion/removal of the fouling deposits. The information about the amount and nature of the deposits enables to take timely countermeasures in order to optimize the production and cleaning cycles as well as, in some cases, to prevent serious contaminations (e.g. food industry and drinking water distribution networks).

The present Thesis describes a new on-line monitoring device, the so called Mechatronic Surface Sensor (MSS). It uses an actuator that excites the monitored surface and a sensor that captures its vibration. The working principle of the MSS is based on the fact that the adhesion and the removal of deposits to/from the monitored surface affect the vibration properties of the surface-deposit system. The main features of the MSS concerning its practical implementation are mainly related with: i) its non-intrusive character; ii) the information gathered corresponds to an integrated measurement over a significant area (the area of the plate); iii) it can be applied to different types of surface materials.

Different MSS configurations have been experimentally tested along the work in parallel with two different methodologies (sinusoidal excitation *vs* experimental modal analysis). The results obtained when exciting the system with a sinusoidal signal indicate that the MSS is able to accurately monitor both the adhesion and removal of fouling layers to the monitored surface, through the evaluation of the highest amplitude (after applying FFT - Fast Fourier Transform) of the collected wave. This parameter was found to be inversely related with the amount of deposit attached to the monitored surface. Additionally, it was also possible to relate the damping factor with the type of deposit. Higher damping factor variations were observed for more viscoelastic deposits. For example, a biological deposit showed a higher damping factor variation than an inorganic one. Hair shampoos, due to their structural characteristics, affect differently the FFT amplitude, when compared to water. Being so, in a

cleaning procedure simulation it was possible to demonstrate that the MSS was able to accurately monitor different shampoo removal rates as well as to assess their cleaning endpoint.

The implementation of the experimental modal analysis methodology showed to be essential to assess the dynamic characteristics of the MSS: the system's modal frequencies and modal damping. The former characteristics were mathematically determined through the evaluation of the transfer function of the system. Furthermore, the information gathered from the transfer function enabled to conclude that the characteristic of the system affected by the deposit build-up is the damping ratio. The increase of the attached layer is an additional source of energy dissipation, which increases the damping ratio of the system. This former conclusion points out that the FFT amplitude is an indirect measurement of the effect that the deposit has on the modal damping of the system. It was also found out that the quantification of the RMS (root-mean square) of the transfer function is another indirect parameter able to accurately provide information about the build-up and the removal of calcium phosphate deposits. In fact the RMS and the FFT amplitude parameters showed similar behavior following the same fouling formation/removal process. However the use of the RMS showed to considerably improve the measurement resolution. Additionally, a preliminary study on the effect of temperature and flow velocity on the modal frequencies and on the damping ratios was also accomplished indicating that the effect of these variables should be regarded with some care when interpreting the overall results.

The use of a software to optimize the dimensions of the MSS plate (based on previously established criteria) was an important input not only to the improvement of the vibrating characteristics of the MSS but also to the theoretical discussion of some intrinsic aspects of the system. The effect of the plate dimensions and of the boundary conditions on the modal frequencies and on the vibrating shapes of the system are some of the studied aspects. Those results emphasized the importance that such simulation/optimization software assumes on the results interpretation and on the design of new MSS configurations.

The main conclusions that can be taken from the present Thesis is that the MSS showed to have a sound potential for laboratory and, most importantly, field applications regarding the monitoring of fouling and cleaning processes.

## SUMÁRIO

A adesão de depósitos indesejáveis a superfícies (sujamento ou 'Fouling') é um problema bastante grave do ponto de vista económico e ambiental que tem atraído a atenção de uma vasta comunidade científica. Têm-se estudado e implementado diversas estratégias para minimizar a formação de depósitos bem como para melhorar os procedimentos de limpeza. Entre essas estratégias encontram-se as técnicas de monitorização on-line e em tempo real da formação ou remoção de depósitos. A informação acerca da quantidade e tipo de depósitos permite uma intervenção atempada de forma a optimizar os ciclos de produção e de limpeza, bem como em alguns casos, prevenir sérias contaminações (e.g. indústria alimentar e redes de distribuição de água potável).

A presente Tese descreve um novo mecanismo de monitorização on-line, designado por Mechatronic Surface Sensor (MSS). Um actuador excita a superfície monitorizada e um sensor capta a vibração da mesma. A medida do MSS baseia-se no efeito que a adesão de depósitos à superfície monitorizada provoca nas propriedades vibratórias da mesma. As principais características do MSS são: i) carácter não intrusivo; ii) a informação fornecida corresponde a uma medida integrada do fenómeno numa área considerável (a área da placa); iii) pode ser aplicado a diferentes tipos de materiais.

Testaram-se diferentes configurações do MSS ao longo do presente trabalho em paralelo com duas metodologias diferentes (excitação sinusoidal vs análise modal). Os resultados alcançados quando o sistema é excitado com um sinal sinusoidal indicam que o MSS fornece informação precisa sobre a adesão e remoção de depósitos na superfície monitorizada, através da avaliação da maior amplitude (após aplicação de transformadas rápidas de Fourier – FFT) da onda da resposta vibratória. Observou-se uma relação inversa entre este parâmetro e a quantidade de depósito aderido à superfície monitorizada. Adicionalmente, foi possível relacionar o factor de amortecimento com o tipo de depósito, sendo que depósitos mais visco-elásticos provocam variações maiores do factor de amortecimento. Por exemplo, observou-se um factor de amortecimento mais elevado para um depósito biológico que para um depósito inorgânico. Os champôs devido às suas características estruturais afecta de forma diferente a amplitude FFT, comparativamente com a água. Assim sendo, durante um procedimento de

limpeza foi possível demonstrar que o MSS é capaz de monitorizar com elevada precisão diferentes taxas de remoção de champô bem como determinar o ponto final das mesmas.

A implementação da análise modal mostrou ser essencial na determinação das características dinâmicas do MSS: as frequências modais do sistema e o amortecimento modal. Estas características foram determinadas matematicamente através da avaliação da função de transferência do sistema. Adicionalmente, esta avaliação matemática, permitiu concluir que o parâmetro característico afectado pela adesão do depósito é o amortecimento. Verificou-se um aumento do amortecimento à medida que o depósito aderido aumenta uma vez que este funciona como uma fonte de dissipação de energia adicional. Esta conclusão clarifica que a amplitude (após FFT) é uma medida indirecta do efeito que o depósito exerce no amortecimento modal do sistema. Verificou-se, que a quantificação do RMS (root-mean square) da função de transferência é um outro parâmetro indirecto capaz de medir correctamente a adesão e remoção de depósitos de fosfato de cálcio. De facto, o RMS e a amplitude (após FFT) apresentaram comportamentos semelhantes na monitorização do mesmo processo de adesão/remoção, sendo que o uso do RMS permitiu melhorar consideravelmente a resolução da medida. Efectuou-se também um estudo preliminar sobre a influência da temperatura e da velocidade do escoamento nas frequências e amortecimentos modais indicando que o efeito destas variáveis deverá ser analisado com cuidado aquando da interpretação global dos resultados.

A utilização de um software para optimização das dimensões da placa (com base em critérios previamente estabelecidos) contribuiu não só para uma melhoria das características vibratórias do sistema mas também para a discussão de alguns aspectos intrínsecos ao sistema. O efeito das dimensões da placa e das condições fronteira nas frequências e nas deformadas modais foram alguns dos aspectos estudados. Os resultados obtidos enfatizaram a importância que tais simulações/optimizações assumem aquando da interpretação dos resultados e no design de novas configurações do MSS.

As principais conclusões que se podem tirar da presente Tese indicam que o MSS tem um elevado potencial para monitorizar a adesão e os processos de limpeza, quer a nível laboratorial que a nível industrial.

## RÉSUMÉ

La formation de dépôts indésirables sur les surfaces (encrassement) est un problème coûteux, aussi bien d'un point de vue économique qu'environnemental, qui retient l'attention d'une communauté scientifique étendue. Plusieurs stratégies ont été étudiées et mises en place pour minimiser l'encrassement et améliorer les procédures de nettoyage. Une de ces stratégies est basée sur l'implémentation de techniques de surveillance en temps réel qui fournissent des informations sur l'adhésion et l'enlèvement des dépôts formés lors de l'encrassement. Des informations sur la quantité et la nature des dépôts permettent la mise en œuvre rapide et opportune de contre-mesures en vue d'optimiser les cycles de production et de nettoyage ainsi que d'éviter l'apparition de sérieux problèmes de contaminations (comme dans l'industrie agro-alimentaire et les réseaux de distribution d'eau potable).

Cette thèse décrit un nouvel appareil de surveillance en ligne, le Mechatronic Surface Sensor (MSS). Cet appareil utilise un actuateur qui excite la surface surveillée et un capteur qui enregistre les vibrations de la surface. Le principe de fonctionnement du MSS est basé sur le fait que l'adhésion et l'enlèvement des dépôts à/de la surface surveillée vont affecter les propriétés vibratoires du système surface-dépôt. Les caractéristiques principales du MSS concernent sa mise en œuvre pratique et sont principalement liées à : i) son caractère non intrusif ; ii) les informations qu'il fournit correspondent à une mesure intégrée sur une aire significative (la superficie de la surface d'intérêt) ; iii) il peut être appliqué à des surfaces de différents matériaux.

Différentes configurations du MSS ont été étudiées expérimentalement au cours de ce travail au travers de deux méthodologies différentes menées en parallèle (excitation sinusoïdale vs analyse modale expérimentale). Les résultats obtenus en sollicitant le système avec un signal sinusoïdal indiquent que le MSS est capable de suivre avec précision l'adhésion et l'enlèvement des couches encrassant la surface d'intérêt par évaluation de l'amplitude la plus élevée de l'onde collectée (après application de la transformée de Fourier rapide – FFT). Ce paramètre s'est révélé être inversement corrélé à la quantité de dépôt fixée à la surface. De plus, le facteur d'atténuation a également pu être relié au type de dépôt. Des variations plus élevées du facteur d'atténuation correspondant à des dépôts plus viscoélastiques. Les dépôts biologiques par exemple donnaient une plus grande variation du facteur d'atténuation que les dépôts inorganiques. Les shampoings affectent différemment l'amplitude FFT que l'eau suite

à leurs caractéristiques structurelles différentes. Ainsi, il a été possible de montrer que le MSS permettait de suivre avec précision différentes vitesses d'enlèvement de shampoings durant une procédure de nettoyage ainsi que d'estimer le moment où le nettoyage pouvait être stoppé.

L'implémentation de la méthode d'analyse modale expérimentale s'est révélée essentielle pour évaluer les caractéristiques dynamiques du MSS, à savoir les fréquences modales du système et l'atténuation modale. Ces caractéristiques ont été déterminées mathématiquement par l'évaluation de la fonction de transfert du système. De plus, les informations collectées par la fonction de transfert ont permis de conclure que la caractéristique du système affectée par la formation du dépôt est le facteur d'atténuation. L'augmentation de la couche fixée est une source supplémentaire de dissipation d'énergie qui augmente le facteur d'atténuation du système. Cette conclusion montre que l'amplitude FFT est une mesure indirecte de l'effet que le dépôt a sur l'atténuation modale du système. La quantification de la racine carrée moyenne (RMS) de la fonction de transfert est un autre paramètre indirect permettant de rassembler des informations précises sur la formation et l'enlèvement des dépôts de phosphate de calcium. En fait, l'évolution de la RMS et de l'amplitude FFT était similaire pour les mêmes mécanismes de formation et d'enlèvement des dépôts. Cependant, l'utilisation de la RMS a permis d'améliorer considérablement la résolution des mesures. Une étude préliminaire réalisée sur les effets de la température et de la vitesse du fluide sur les fréquences modales et les rapports d'atténuation indique que ces variables devraient être considérées avec attention lors de l'interprétation des résultats globaux.

L'utilisation d'un logiciel pour optimiser les dimensions de la plaque MSS (basée sur des critères préétablis) a apporté une contribution importante à la discussion théorique de certains aspects intrinsèques du système. L'effet des dimensions de la plaque et des conditions limites sur les fréquences modales et les formes modales de vibration du système ont été étudiées. Les résultats ont souligné l'importance croissante de ces outils informatiques d'optimisation lors de la conception et l'interprétation des résultats de différentes nouvelles configurations de MSS.

Les conclusions principales émanant de cette thèse sont que le MSS a prouvé avoir un grand potentiel pour les études de laboratoire et, plus important encore, pour la surveillance des procédés d'encrassement et de nettoyage sur le terrain.







## **TABLE OF CONTENTS**

**Acknowledgements**

**Abstract**

**Sumário**

**Résumé**

|  |           |
|--|-----------|
| <b>1. State of the art .....</b>   | <b>1</b>  |
| 1.1. The problematic of fouling.....   | 1         |
| 1.1.1. Economic cost.....  | 2         |
| 1.1.2. Environmental impacts.....  | 3         |
| 1.1.3. Human-health problems .....   | 3         |
| 1.2. Anti-fouling strategies .....   | 4         |
| 1.3. Monitoring approach .....   | 7         |
| 1.3.1. Direct measurement of the deposit characteristics.....                          | 9         |
| 1.3.2. Heat transfer and/or pressure drop measurements .....                           | 10        |
| 1.3.3. Measurement of optical signals.....   | 11        |
| 1.3.4. Measurement of electric signals.....  | 12        |
| 1.3.5. Measurement of vibration signals .....  | 13        |
| 1.3.5.1. The deposit adheres directly to a crystal surface .....                       | 14        |
| 1.3.5.2. The transducers are not in contact with the deposit .....                     | 15        |
| 1.4. Requirements for a suitable monitoring device.....                                | 18        |
| 1.5. Estimation of the savings gathered with a monitoring systems implementation ..... | 19        |
| 1.6. Aims of the present Thesis .....  | 20        |
| References .....   | 22        |
| <b>2. Roadmap for the Thesis.....</b>  | <b>29</b> |
| 2.1. From the challenge to the idea .....  | 29        |
| 2.2. Monitoring device designation.....  | 30        |
| 2.3. Fundamentals of the Mechatronic Surface Sensor (MSS) .....                        | 30        |
| 2.4. First setup .....   | 32        |

|   |           |
|---|-----------|
| 2.5. Second setup.....  | 35        |
| 2.6. Third setup.....   | 38        |
| 2.7. Fourth setup.....  | 40        |
| References .....  | 41        |
| <b>3. Using nanovibrations to monitor biofouling.....</b>                                   | <b>43</b> |
| Abstract .....  | 43        |
| 3.1. Introduction .....   | 43        |
| 3.1.1. Description of the Mechatronic Surface Sensor (MSS).....                             | 46        |
| 3.1.2. Numerical computation study .....  | 48        |
| 3.2. Materials and methods .....  | 51        |
| 3.2.1. Adhesion studies .....   | 51        |
| 3.2.2. Sedimentation studies .....  | 53        |
| 3.3. Results and discussion.....  | 54        |
| 3.3.1. Biofilms: turbulent vs laminar flow .....  | 56        |
| 3.3.2. Biofilm vs silica deposit (turbulent flow).....                                      | 57        |
| 3.3.3. Sedimentation effect on the MSS signal .....   | 59        |
| 3.4. Conclusions .....  | 60        |
| References .....  | 60        |
| <b>4. Monitoring deposits build-up using a novel Mechatronic Surface Sensor (MSS) .....</b> | <b>63</b> |
| Abstract .....  | 63        |
| 4.1. Introduction .....   | 63        |
| 4.1.1. Description of the Mechatronic Surface Sensor (MSS).....                             | 65        |
| 4.2. Materials and experimental methods.....  | 67        |
| 4.3. Results and discussion.....  | 68        |
| 4.3.1. Calibration of the MSS normalized amplitude with the deposit dry mass.....           | 68        |
| 4.3.2. Monitoring deposition from SMUF solutions with the MSS and the heat flow cell.....   | 69        |
| 4.3.3. Damping factor for different deposits .....  | 70        |
| 4.3.4. Using the MSS to monitor cleaning .....  | 73        |
| 4.4. Conclusions .....  | 73        |
| References .....  | 74        |

|  |           |
|--|-----------|
| <b>5. Monitoring cleaning-in-place processes using nanovibration technology .....</b>                      | <b>77</b> |
| Abstract .....   | 77        |
| 5.1. Introduction .....  | 77        |
| 5.2. Materials and methods .....   | 79        |
| 5.2.1. Summary of the MSS working principle.....   | 79        |
| 5.2.2. Description of the MSS measuring system .....   | 80        |
| 5.2.3. Experimental cleaning conditions .....  | 81        |
| 5.2.3.1. Cleaning procedure .....  | 82        |
| 5.2.3.2. Cleanliness confirming methods.....   | 83        |
| 5.2.4. $A_{inv}$ normalization and determination of the error associated with it measurement.....          | 84        |
| 5.2.5. Repeatability experiments.....  | 85        |
| 5.2.6. Statistical analysis .....  | 85        |
| 5.3. Results and discussion.....   | 86        |
| 5.3.1. MSS repeatability.....  | 86        |
| 5.3.2. MSS reliability .....   | 87        |
| 5.3.3. Effect of different cleaning conditions (flow velocity and temperature) on the MSS<br>response..... | 89        |
| 5.4. Conclusions .....   | 93        |
| References .....   | 93        |
| <br>   |           |
| <b>6. Optimization of the MSS configuration .....</b>  | <b>97</b> |
| Overview of Chapter 6 .....  | 97        |
| 6.1. Introductory notes .....  | 97        |
| 6.2. Simulation study.....   | 98        |
| 6.2.1. Setup requirements.....   | 99        |
| 6.2.2. Optimization of the plate dimensions – governing equations .....                                    | 100       |
| 6.2.3. Software design.....  | 101       |
| 6.2.4. Dimensions optimization: clamped boundary condition.....  | 103       |
| 6.2.4.1. Criterion 1 – Maximization of the frequency separation between the n modes.....                   | 104       |
| 6.2.4.2. Criterion 2 – Minimization of the frequency of the first n modes .....                            | 105       |
| 6.2.5. Effect of the boundary conditions: free and simply-supported .....                                  | 107       |
| 6.2.6. Modal analysis of the new and of the old configurations .....                                       | 109       |
| 6.3. Methodologies for response analysis .....   | 110       |
| 6.3.1. Methodology 1 .....   | 111       |

|  |            |
|--|------------|
| 6.3.2. Methodology 2 .....   | 114        |
| 6.3.2.1. Transfer function determination.....                          | 116        |
| 6.3.2.2. Modal extraction .....  | 117        |
| 6.4. Preliminary tests of the new MSS setup.....                       | 119        |
| 6.4.1. Experimental modal analysis of the SS plate .....               | 119        |
| 6.4.2. Choice of system's best configuration .....                     | 121        |
| 6.4.2.1. Worst solution.....   | 122        |
| 6.4.2.2. Best solution.....  | 123        |
| 6.4.3. Linearity test .....  | 124        |
| 6.4.4. Effect of water on the transfer function of the system .....    | 126        |
| 6.4.5. Comparison of the 2 methodologies .....                         | 127        |
| 6.5. Experimental results .....  | 130        |
| 6.5.1. Error associated with each methodology .....                    | 130        |
| 6.5.2. Experimental results.....                                       | 131        |
| 6.5.3. Overall discussion of the results and methodologies .....       | 137        |
| 6.6. Other studies.....  | 141        |
| 6.6.1. Temperature .....   | 142        |
| 6.6.2. Flow velocities .....   | 144        |
| 6.6.3. Simultaneous effects of the temperature and flow velocity ..... | 146        |
| 6.7. Conclusions .....   | 149        |
| References .....   | 150        |
| <b>7. Main conclusions and forthcoming work.....</b>                   | <b>151</b> |
| 7.1. Conclusions .....   | 151        |
| 7.2. Future work .....   | 152        |
| 7.2.1. MSS configuration .....   | 152        |
| 7.2.2. Methodology .....   | 154        |
| 7.2.3. Reproducibility.....  | 155        |
| 7.2.4. Practical implementation.....                                   | 155        |
| <b>Appendix A - Theory of vibration .....</b>                          | <b>157</b> |
| A.1. Single-degree-of-freedom system .....                             | 157        |
| A.1.1. Measurement of damping .....                                    | 164        |
| A.1.2. Multi-degree-of-freedom systems .....                           | 166        |

|   |            |
|---|------------|
| A.2. Vibration signals.....   | 167        |
| A.2.1. Excitation methods.....  | 167        |
| A.2.2. Signal analysis.....   | 168        |
| A.3. Experimental modal analysis (EMA) of vibrating systems.....  | 170        |
| A.3.1. Vibration measuring system.....  | 173        |
| A.3.2. Digital signal processing.....   | 174        |
| A.3.3. Analysis of random signals.....  | 176        |
| A.4. Modal data extraction.....   | 179        |
| References.....   | 181        |
| <b>Appendix B - Actuator and sensor characteristics.....</b>  | <b>183</b> |
| B.1. Piezoelectricity.....  | 183        |
| B.2. Accelerometer.....   | 185        |
| References.....   | 186        |
| <b>Appendix C - Calibration of the <math>A_{FFT}</math> with the temperature and the flow rate.....</b> | <b>187</b> |
| <b>Appendix D - Transfer and coherence functions.....</b>   | <b>189</b> |

## NOMENCLATURE

### Abbreviations

|                  |  |
|------------------|--|
| $\beta$ -Lg      | $\beta$ -lactoglobulin   |
| A/D              | Analog to digital  |
| APM              | Acoustic plate mode  |
| ATP              | Adenosine tri-phosphate  |
| CFD              | Computer fluid dynamics  |
| CIP              | Cleaning-in-place  |
| DAQ              | Data acquisition   |
| DFT              | Digital Fourier transform  |
| DNS              | Dinitrosalicylic colorimetric method   |
| DSP              | Digital signal processing  |
| DTM              | Differential turbidity device  |
| EMA              | Experimental modal analysis  |
| FDG              | Fluid dynamic gauging  |
| FEUP             | Faculty of Engineering, University of Porto  |
| FFT              | Fast Fourier transform   |
| FLUS             | Fluorescence sensor  |
| FOS              | Fiber optical sensor   |
| FPW              | Flexural plate wave  |
| FTIR-ATR         | Fourier transfer infrared spectroscopy – attenuated total reflectometry                                    |
| GNP              | Gross national product   |
| HNO <sub>3</sub> | Nitric acid  |
| LEPAE            | Laboratory for Process, Environment and Energy Engineering   |
| MDOF             | Multiple degrees of freedom  |
| MIC              | Microbiologically influenced corrosion   |
| MSS              | Mechatronic Surface Sensor   |
| PAS              | Photoacoustic spectroscopy sensor  |
| PSD              | Power spectral density   |
| PVC              | Poly(vinyl chloride)   |
| PZT              | Piezoelectric material   |
| QCM              | Quartz crystal microbalance  |
| RF               | Fouling resistance   |
| RMS              | Root mean square   |
| SAFER            | Surveillance and control of microbiological stability in drinking water distribution networks (EU Project) |
| SAW              | Surface acoustic wave  |
| SDOF             | Single degree of freedom   |
| SEM              | Scanning electron microscope   |
| SMUF             | Simulated milk ultrafiltrate   |
| SS               | Stainless steel  |
| TF               | Transfer function  |
| TSM              | Thickness shear mode   |
| UTDR             | Ultrasonic time-domain reflectometry   |
| UV               | Ultraviolet  |
| VIS              | Visible  |
| WPI              | Whey protein isolate   |

| <b>Symbols</b> | <b>Meaning</b>  | <b>SI Units</b>   |
|----------------|---|-------------------|
| $A$            | Length  | m                 |
| $A$            | Amplitude   |                   |
| $A_{FFT}$      | Maximum amplitude after FFT                                 |                   |
| $A_{inv}$      | Normalized amplitude  |                   |
| $A_n^{er}$     | Modal amplitude coefficient                                 |                   |
| $Abs$          | Absorbance  |                   |
| $B$            | Width   | m                 |
| $c$            | Damping constant  | N s/m             |
| $C$            | Numerical constant  |                   |
| $c_L$          | Longitudinal wave velocity                                  | m/s               |
| $CA$           | Contact angle   | rad               |
| $D$            | Damping matrix  | N s/m             |
| $DF$           | Damping factor  |                   |
| $DR$           | Damping ratio   |                   |
| $E$            | Young's modulus   | N/m <sup>2</sup>  |
| $F$            | Forcing function or outside force                           | N                 |
| $F$            | Frequency   | Hz                |
| $F_{cutoff}$   | Cutoff frequency  | Hz                |
| $f_c$          | Viscous force   | N                 |
| $f_k$          | Spring force  | N                 |
| $f_{m,n}$      | Frequency of mode ( $m, n$ ) of a two dimensional structure | Hz                |
| $f_n$          | Frequency of mode $n$                                       | Hz                |
| $f_{sampling}$ | Sampling frequency  | Hz                |
| $Freq$         | Frequency   | Hz                |
| $h$            | Thickness   | m                 |
| $H$            | Magnitude of transfer function                              |                   |
| $H_{er}$       | Fitted modal model  |                   |
| $\hat{H}_{er}$ | Measured transfer function                                  |                   |
| $H0$           | Null hypothesis   |                   |
| $k$            | Spring stiffness  | N/m               |
| $K$            | Stiffness matrix  | N/m               |
| $L$            | Laminar flow  |                   |
| $m$            | Mass  | kg                |
| $M$            | Mass matrix   | kg                |
| $n$            | Number of modes   |                   |
| $N$            | Number of samples collected                                 |                   |
| $p$            | Statistical probability                                     |                   |
| $p$            | Position  | m                 |
| $Prot$         | Whey protein  |                   |
| $Q$            | Flow rate   | m <sup>3</sup> /s |
| $R^2$          | Correlation coefficient                                     |                   |
| $R_{xf}$       | Cross-correlation function                                  |                   |
| $R_{xx}$       | Autocorrelation function                                    |                   |
| $Re$           | Reynolds number   |                   |

|                                   |   |                   |
|-----------------------------------|---|-------------------|
| $S_{xf}$                          | Cross-power spectral density                                      |                   |
| $S_{xx}$                          | Auto-power spectral density                                       |                   |
| $Sig$                             | Statistical significance  |                   |
| $t$                               | Time  | s                 |
| $T$                               | Temperature   | K                 |
| $T$                               | Turbulent flow  |                   |
| $T$                               | Total record length   | s                 |
| $T$                               | Period  | s                 |
| $V$                               | Volume  | m <sup>3</sup>    |
| $W$                               | Weight  | kg                |
| $x$                               | Coordinate  | m                 |
| $x$                               | Displacement  | m                 |
| $x$                               | Response function   |                   |
| $x_i$                             | Amplitude of peak $i$   |                   |
| $\dot{x}$ or $\frac{dx}{dt}$      | First displacement derivative / velocity                          | m/s               |
| $\ddot{x}$ or $\frac{d^2x}{dt^2}$ | Second displacement derivative / acceleration                     | m/s <sup>2</sup>  |
| $Z$                               | Polar coordinate  | m                 |
| $\gamma^2$                        | Coherence function  |                   |
| $\Delta$                          | Variation   |                   |
| $\varepsilon$                     | Error function  |                   |
| $\zeta$                           | Damping factor  |                   |
| $\zeta$                           | Damping ratio   |                   |
| $\theta$                          | Polar coordinate  | rad               |
| $\lambda$                         | Wavelength  | m                 |
| $\lambda_1, \lambda_2$            | Roots of the characteristic equation                              |                   |
| $\mu$                             | Mean  |                   |
| $\nu$                             | Poisson coefficient   |                   |
| $\rho$                            | Density   | kg/m <sup>3</sup> |
| $\sigma$                          | Standard deviation  |                   |
| $\tau$                            | Time  | s                 |
| $\phi$                            | Phase of transfer function  | rad               |
| $\phi$                            | Modal shape   |                   |
| $\omega$                          | Angular frequency   | rad/s             |
| $\omega_d$                        | Damped angular frequency  | rad/s             |
| $\omega_n$                        | Angular frequency of mode $n$                                     | rad/s             |
| $\omega_{m,n}$                    | Angular frequency of mode $(m, n)$ of a two dimensional structure | rad/s             |



## Subscripts

|             |                      |
|-------------|----------------------|
| <i>0</i>    | Rest position        |
| <i>calc</i> | Calculated           |
| <i>e</i>    | Excitation           |
| <i>in</i>   | Input                |
| <i>m, n</i> | Two dimensional mode |
| <i>M1</i>   | Mode 1               |
| <i>M2</i>   | Mode 2               |
| <i>max</i>  | Maximum              |
| <i>min</i>  | Minimum              |
| <i>n</i>    | Natural              |
| <i>n</i>    | Number of modes      |
| <i>out</i>  | Output               |
| <i>Pk1</i>  | Peak 1               |
| <i>Pk2</i>  | Peak 2               |
| <i>r</i>    | Response             |
| <i>s</i>    | Stimulus             |
| <i>TF</i>   | Transfer function    |



# 1. STATE OF THE ART

## *1.1. THE PROBLEMATIC OF FOULING*

The adhesion of undesired material to the fluid/solid interface is known by fouling and is a complex problem that attracted the attention of a vast scientific and industrial community in the last four decades. Depending on the physico-chemical properties and on the experimental conditions (mainly temperature and flow velocity) of such fluids in contact with the material surface, different types of fouling formation may occur. Bott (1995) summarizes the common mechanisms of fouling formation: i) crystallization fouling occurs when the foulant deposit result from a crystallization phenomenon; ii) particulate fouling results from the deposition of particles existent on the processed fluid; iii) when the deposit is formed from the reaction of components in the fluid, the fouling is named chemical reaction fouling; iv) corrosion fouling is a particular type of the chemical reaction fouling and occurs when the chemical reaction takes place directly on the surface; v) biological fouling (or biofouling) results from the adhesion of biofilms to the surfaces.

Fouling occurs in a variety of fields such as: medical, industrial, domestic and natural processes. The contaminations of medical implants/instruments (Tunney et al. 2007) and the bacteria adhesion to contact lens (McLaughlin-Borlace et al. 1998) are examples of daily life biofouling that require special attention and concern. Particular emphasis is given to industrial fouling, since a large number of industrial operations potentiate the formation of such unwanted deposits. Many industries are subjected to extensive fouling resulting from the association of several fouling products (Kukulka 2005). The cleaning of fouling layers (i.e., the removal of such deposits from the equipment surfaces) is another point of interest, mainly for those industries that run their processes on a daily basis. The consequences of fouling and cleaning are mainly related to: i) economic costs; ii) environmental impacts; and iii) human-health problems. A brief discussion of each of these points will be presented, although it is important to recall that they are intrinsically connected and related.

### **1.1.1. Economic cost**

Heat exchangers, cooling water systems, and drinking water storage and network systems are some of the equipments typically affected by fouling formation. The effect that this phenomenon has on the overall process economy is highly dependent on the specific process, but is often related to a reduction of the thermal and hydrodynamic performance across a given operating line, respectively related to the increase of the heat transfer resistance and to the increase of the pressure drop. These constraints lead to higher costs associated with pumping, maintenance and energy.

The economic penalties associated with fouling in heat exchangers account for the costs related to: equipment over-sizing, additional fuel consumption, maintenance and loss of production. Those costs were estimated to be around 0.25% of the gross national product (GNP) in industrialized countries such as the USA (Müller-Steinhagen et al. 2005). Obviously, this number becomes smaller for less industrialized countries (such as New Zealand) but it is still very significant, around 0.15% of the GNP.

In addition to those concerns, it is important to highlight the importance that the removal of such deposits has on the overall operating efficiency of the process. In some industrial plants, those cleaning procedures are ‘manually’ performed and the equipment is opened, inspected and each zone is cleaned individually. This often includes the replacement of entire processing lines. In other processes, such as the dairy industry, due to the severity and high extent of fouling (Changani et al. 1997), cleaning is carried out on a daily basis and so more expedite and automated cleaning procedures were implemented, usually called cleaning-in-place, or CIP. In the CIP procedure chemical solutions are circulated through the processing plant in order to chemically remove the attached deposits. The consumption of large amounts of water and cleaning agents (e.g. biocides, acid and alkaline solutions, etc) and their subsequent wastewater treatment, the thermal and mechanical energy associated with its circulation and the fact that the production is stopped when a CIP is being performed, are examples of the economic impact that those cleaning procedure can have.

### **1.1.2. Environmental impacts**

Several factors associated with fouling and cleaning can contribute to the increase of the environmental risks: a) the formation of deposits on crucial pieces of equipment that can put in risk a given process, such as for example the formation of thick deposits in nuclear power plants, which diminishes the heat transfer between the nuclear reactors and the cooling water, can lead to fuel overheating and in last instances to a catastrophic environmental disaster; b) the use of chemical substances, during cleaning procedures or during treatment of water in cooling water systems, can be a hazard to the ecological system and can create microbiological resistance (Cloete 2003). For example, the most typically used biocide to control biofouling within water cooling systems is chlorine, which can lead to carcinogenic problems when it reacts with organic compounds (Zdaniuk et al. 2006); c) the demand for more energy. This last point is an important concern mainly related to the discussion of world environmental policies such as the reduction of the ‘greenhouse gas’ emissions and water sustainability. As already mentioned, fouling gives a high contribution to the increase in energy demands, due to the energetic inefficiency which (in the cases where energy is dependent on the combustion) also increases the emission of ‘greenhouse’ gas. It was demonstrated (Casanueva-Robles and Bott 2005) that the presence of fouling in power station steam condensers (on their heat transfer surfaces) can increase the emissions of ‘greenhouse’ gases and that its extent is related to the fouling layer thickness. Similar conclusions were taken on the effect of fouling in crude oil systems (Watkinson 2007) which has a significant weight on the fuel consumption of a refinery and on the greenhouse emissions. Regarding water sustainability, it becomes crucial to optimize the cleaning procedures in order to minimize water consumption, which will reduce the need for wastewater treatment.

### **1.1.3. Human-health problems**

Naturally, if fouling has a negative impact on the environment, human-health is also put in risk. Additionally, there are several industrial applications where the presence of microorganisms can lead to serious health problems. The food industry and drinking water distributions networks are some of the examples where biofouling may result in product or water contamination. In the food industry, if the cleaning and disinfection (disinfection is performed after cleaning and is related to the minimization of the number of microorganisms within the industrial plant) steps are not properly conducted, the safety and quality of the

product may be at risk (Hasting 2005). Concerning drinking water systems, the biofouling that exists along the several distribution networks are preferential shelters for growth of pathogenic microorganisms. The public health is at risk when a piece of those biofouling layers (often very thick) detaches and reaches the tap of the consumer.

## **1.2. ANTI-FOULING STRATEGIES**

It is consensual that fouling cannot be totally eliminated, although its mitigation has been object of many research efforts. The theoretical and experimental researches done by academia associated with the know-how gathered from industry allowed the devise of new solutions and strategies to alleviate the fouling problematic.

The study of the *mechanisms* behind the deposits formation (Bott 1995; Melo and Bott 1997) and their removal (Wilson 2005) has been the basis for most of the investigation around fouling and cleaning. Much work has been done regarding the determination of the effect of different experimental conditions such as temperature and flow velocity on fouling formation and removal in different equipments, particularly in heat transfer equipment in cooling water systems (Kukulka and Devgun 2007) and in dairy plant heat exchangers (Changani et al. 1997; Visser and Jeurnink 1997). A review on the main mechanisms and effects of some experimental parameters on fouling formation and removal within water side in cooling towers condenser has been provided recently by (Zdaniuk et al. 2006). Efforts have also been made in order to study the effect that the flow velocity, temperature and nutrients availability has on the formation and removal of biofilms, such as the ones formed by *Pseudomonas fluorescens* (Vieira and Melo 1999; Pereira et al. 2002; Chen et al. 2005).

Based on this type of studies several *predictive models* of fouling formation or cleaning have been designed and applied to real industrial processes. The conjugation of these models with the application of artificial neural networks for fouling prediction is being developed as a powerful tool for improving the operational equipment. These studies showed promising results concerning, for example, the prediction of the extent of fouling and the decrease of the heat transfer on a heat exchanger pre-heat train in an oil refinery (Radhakrishnan et al. 2007) and were able to determine the fouling expected in a nanofiltration plant (Shetty and Chellam

2003). Such approaches can be a powerful tool for the design and the optimization of the operation conditions that minimize fouling formation or that favor the deposits removal.

The study and optimization of the operational conditions at which a given processing plant should operate is another point of interest. The use of CFD analysis to simulate both the fouling formation and to optimize the equipment design in order to minimize its formation has become an interesting approach. Several works have been done in this area, applied to completely different situations such as for example: to the study fouling formation in an exhaust duct from a thermal treatment of pulp production sludge (Hajek et al. 2005); to understand the flow pattern within tubular heat-exchangers (Savtchenko et al. 2001); to predict cleaning in heat exchangers (Asteriadou et al. 2007); to simulate the gas flow within a spray dryer as a way to improve its design and to optimize it in terms of fouling minimization during its operation (Straatsma et al. 1999); the study of the ash formation in pipelines of pulverized coal/biomass burners to predict its effect on the equipment heat exchange loss (Losurdo et al. 2007). This wide range of application show how this simulation tool can be exploited and how it can contribute to fouling mitigation.

The use of chemical substances for cleaning purposes or for fouling minimization (e.g. biocides, corrosion inhibitors, dispersants, detergents, etc) is subjected to strict regulations since they can endanger the environment. In order to face this problem, 'environmental friendly' (Guamet and Gomez De Saravia 2005) chemical substances have being designed. An alternative approach was introduced by (Grant and Bott 2005) who proposed an efficient biocide dosage for biofilm control through the study of the best dosage concentration, frequency and duration of injection. The study of 'smart' materials capable of acting as biocides was suggested by (Cloete 2003), and this, when associated with drug delivery techniques for fouling mitigation, may become an interesting field of research (Ferreira et al. 2008).

The design of alternative approaches to chemical removal is also being studied. For example, the application of physical procedures, such as: the use of catalytic alloys to mitigate mineral fouling in heat exchangers (Tijing et al. 2007) or the implementation of crushed ice pigging systems to remove 'soft' fouling like toothpaste or jam (Quarini 2002) have been studied. The evaluation of ultrasound techniques to increase the removal forces (induced by microbubbles)

at the surface as a procedure to control biofouling formation was studied (Mott et al. 1998; Bott 2000) and its combination with a biocide showed to be much more efficient than their separate application (Bott and Tianqing 2004). The ultrasounds have also been applied to minimize milk fouling (Lin and Chen 2007), indicating that the fouling formation was delayed with the application of such technique. Some additional techniques applied to control biofilm formation within cooling water shell-an-tube exchangers are summarized by Bott (2000) and includes among other: i) the recirculation of sponge balls that wipe the dirty surfaces; ii) brush and cage, where a brush is placed inside each tube and the dirty is caught in a cage at the end of the tube; iii) ultraviolet light to kills bacteria, although this technique can not be directly applied to the equipment.

Another interesting area of research is related to the study of new surface materials that reduce the adhesion of unwanted materials or that favor its removal from such surfaces. Some work has been done regarding the modification of surfaces to reduce the formation of scales (Geddert et al. 2007), the attachment of bacteria (Zhao et al. 2005) or the adhesion of food deposits (Rosmaninho and Melo 2006; Saikhwan et al. 2006).

Monitoring adhesion and/or removal of deposits from surfaces is a complementary approach to minimize the effect of fouling and cleaning processes. The evaluation of the (non) existence of deposit on a given process through the use of conventional monitoring anti-fouling strategies relies often on indirect methods such as the process performance or product quality (Flemming 2003). This point becomes even more important since indirect measurements (of for example the bulk phase) do not provide any information about the location of the possible contamination. Conversely, the efficacy of a given countermeasure is also evaluated through the same indirect methods used to asses the presence of deposits. Those countermeasures become highly costly since in most cases they are quite inefficient once that biofouling effect is only detected at a very late phase. In fact, a similar idea is shared by Hastings (2002) and Wilson (2005) who state that the monitoring of current industrial processes is frequently very poor and the knowledge of the process is typically based on limited and retrospective data. This author reiterates the idea that a problem caused by an inefficient cleaning is typically not found at the start of the production cycle, when it would be easier to stop and re-clean the line.



The implementation of monitoring techniques in industrial processes subjected to fouling is one strategy that can be designed in order to increase the plant flexibility and to optimize both the production and cleaning cycles. This optimization is even more required when multi-processing plants are considered, which require a successful removal of deposits to avoid process contamination (Wilson 2005).

The previous examples of anti-fouling strategies, in spite of their different character are studied in order to minimize fouling. The interchange and integration of the information obtained with each of these techniques and methodologies is certainly the right way to accomplish fouling mitigation. The present Thesis discusses an on-line monitoring technique based on the propagation of acoustic waves to detect not only the adhesion/removal of fouling layers but also the type of deposit that is being formed. So, an overview of the monitoring importance and of the current methods used and reported in literature will be provided.

### **1.3. MONITORING APPROACH**

Milk processing is one of the industrial processes that better demonstrate the necessity to use and implement accurate monitoring techniques, due to the extensive fouling and to the regular cleaning procedures (often on a daily basis) that it demands. So, this particular case will be used to discuss in more detail the problems associated with the lack of timely information about the deposit, such as the amount and the type of deposit that forms on the equipment surface.

The importance of the CIP practices is totally recognized mainly in what concerns food industry. These automatic procedures involve typically (Fryer et al. 2006): i) *pre-rinse* step with circulation of water; ii) *detergent cycle* step with the circulation of chemical solutions (alkali and/or acid); iii) *post-rinse* step with circulation of water; iv) *sanitization* step with the use of disinfectants and surface conditioning; v) *final rinse* step with circulation of water (the step prior to the beginning of production). In fact, the main issue regarding CIP procedures is the inexistence of real time factual evidence about the type of deposit that is being formed on the surface and, additionally, the lack of information about the efficiency of the removal process (Wilson 2005). The procedure is established based on the assumption that the nature of fouling can be identified and is consistent during the process. However, most of the time

this is not true, since the nature of fouling depends on many factors, such as the seasonal variation of the raw material and the production of different products (in multi-product plants).

Taking into account that these cleaning cycles are currently employed semi-empirically, using a fixed time or a fixed cleaning solution concentration and/or volume, independently of the nature of the fouling that is formed on the surface in each particular case, it becomes clear that the costs associated with such removal can be higher than necessary (Fryer et al. 2006). The CIP procedures are designed in order to warrant that in a given plant the fouling layer is fully removed in spite of the actual nature and amount of deposit formed on the equipment walls. So, the cleaning commodities and cycles tend to be oversized – more chemicals and water are used, and the CIP operations are sometimes performed more often than needed. Regarding the first point, different chemical solutions are applied to remove different deposits (e.g. proteinoic layers are removed with alkaline solutions, while mineral deposits are removed with acid solutions). On the other hand, the CIP procedure is not fit to evaluate which chemical solution should be applied as a function of the deposit type.

The implementation of monitoring systems that provide on-line, in-real time, non-destructively and in-situ information has become one important strategy to minimize fouling (Hasting 2005). In fact, this approach can be used to simultaneously gather different types of information:

- to help in understanding the mechanisms behind fouling and cleaning - the study of the mechanisms behind the formation and the removal of such undesired processes would benefit from the implementation of appropriate on-line monitoring techniques. Furthermore, those studies can be done both in laboratorial and/or industrial environments and the information gathered in both cases can be compared in order to determine if the information coming from laboratorial prototypes and/or pilot-plants is close to what happens in real industrial operating conditions.

- to monitor the fouling extent – this approach is quite important since it enables the application of timely counter-measures when the problem starts to appear and it is possible to detect when the maximum amount of deposit (before) cleaning is achieved.

- to evaluate the efficacy of the applied counter-measures – several counter-measures are typically applied when fouling is detected. For example, the monitoring of the efficiency of a

given cleaning procedure or the evaluation of the effect that a given biocide has on the removal of the attached layer are some examples of the information that a monitoring system should be able to provide. During cleaning procedures it is of the utmost importance to detect the cleaning end-point.

The fouling monitoring systems can provide different levels of information (Flemming 2003) according to their specific design. For example, they are able to detect the fouling kinetics, attachment/detachment, but cannot differentiate between the constituents of such layers (e.g. biotic/abiotic). More specific monitoring devices are able to characterize the chemical/biological composition of a given fouling layer, although they are too sophisticated and costly to be operated in an industrial environment. There are several reviews (such as Nivens et al. 1995; Flemming 2003; Janknecht and Melo 2003) that describe the mostly studied monitoring techniques to detect biofouling formation. Such literature discusses in more or less detail both the traditional and the more recent techniques. In the following paragraphs, the physical principles behind the most well known/applied fouling monitoring techniques will be provided. Additional attention will be paid to the ‘measurement of vibration signals’, since the aim of the present Thesis is the study of a monitoring technique/device based on the surface acoustic propagation.

### **1.3.1. Direct measurement of the deposit characteristics**

Direct measurements of the deposit characteristics are still the most currently employed techniques (mainly when biological characterization is needed) and often require the sampling of a piece of deposit attached to the surface (off-line measurements). Those techniques are destructive and often time-consuming. Typically, mass determination, thickness measurements, microscopic analysis and quantification of the metabolic products (such as ATP) are evaluated.

Those samples can be directly collected from the equipment surfaces (when they are opened for maintenance or cleaning) or they can be sampled from a side-stream monitor containing coupons that can be periodically removed. Those monitors/reactors have been preferentially designed for laboratorial trials in order to evaluate, for example, the kinetics of formation of a given deposit or the effect of temperature and/or flow velocity on the deposit's formation. The most commonly known open continuous reactors can assume different configurations, like: i)

annular reactor; ii) Robbins device; or iii) flow cell reactor. The main differences between these devices can be read in Pereira et al. (2002), although they rely on the difficulty to sample the coupons as well as in their relative costs. The flow cell reactor (which was used in the present Thesis) is a vertical semi-cylindrical column made of PERSPEX<sup>®</sup> material with coupons placed in its flat surface. The main advantages over the other devices are: 1) the fact that it is possible to visually control what happens on the inner surface (the flow cell is transparent); 2) its simple design and low cost; 3) the fact that it is easy to sample the above mentioned coupons; 4) if flow recycling is introduced, it becomes possible to uncouple the effects of the flow velocity and of the residence time.

### **1.3.2. Heat transfer and/or pressure drop measurements**

The fouling adhesion and its subsequent removal affect the pressure and the temperature along the overall plant. In fact, the presence of fouling diminishes the internal diameter and increases friction in the pipes and so it increases the pressure drop. Additionally, the fouling acts as a resistance to the heat transfer and so it increases with the increase of the deposit. The measurement of the heat transfer and/or the pressure drop is a procedure not only applied industrially but also widely used for laboratorial research for fouling or cleaning quantification. The determination of the fouling extent through the evaluation of the plant performance (through pressure or temperature measurements) is one of the standard techniques industrially applied. In fact, these indicators are relatively insensitive during the formation of the initial layer of deposit and they act more as indicators of fouling/cleaning than as absolute measuring systems.

Another technique, the fluid dynamic gauging (FDG) based on pressure measurements has been used in laboratory research with good results to assess the thickness and strength of soft deposits (Chew et al. 2004) and to study (Chew et al. 2007) the deposition in porous membranes (like macro and micro-filtration processes). This technique is based on a nozzle that is inserted into the liquid and placed close and normally to the fouled surface. A suction pressure is applied and the flow passes into the nozzle which is quite a sensitive parameter to provide the distance between the tip of the nozzle and the top of the fouling layer (or in other words is a way to provide the thickness of the deposit).

### 1.3.3. Measurement of optical signals

There are some methodologies based on the detection of light signals (e.g. visible, infrared, ultraviolet) which rely on the fact that the light can be absorbed, emitted or scattered by matter. Some of the monitoring techniques that can be found within this group are the detection of the weak light signals that some organisms are capable to spontaneously emit and known as *bioluminescence*. This technique was successfully applied to measure the number of attached bacteria to different polymeric supports (Ludwicka et al. 1985). In other cases, if this bioluminescence can be genetically manipulated and ‘introduced into the biofilm’ the antibiotic and its effect on the biofilm removal can be successfully monitored (Kadurugamuwa et al. 2004). Associated with this, there is also the detection of *auto-fluorescence* of biomolecules such as amino acids.

Certain molecules have some characteristic wavelengths at which they absorb or emit radiation and this absorption or emission is related to the quantum energy levels associated with the vibration of the atoms. So, when a given sample is exposed to a continuum radiation it is possible to measure the absorbed radiation by *spectroscopy* methods and the emitted radiation by *fluorometry* methods (Janknecht and Melo 2003). One of the most well known (commercially available) systems is the FTIR spectrometer (Fourier transform infrared), which combines the measurement of the infrared spectroscopy and the use of Fourier transform techniques. The use of the Fourier techniques in comparison to the dispersive ones increases the sensitivity of the infrared analysis. This methodology was positively applied to detect antimicrobial agents within a biofilm structure in order to understand how the former act within the biofilm (Suci et al. 1998). These techniques are more suited to measure biomolecules signals and in many cases to distinguish between biotic and abiotic material, rather than to quantify the amount of deposit and they are typically not suited for industrial application. Furthermore, the measurements obtained with these techniques should be carefully analyzed since they can often suffer from interference of external factors (for example, temperature, pH, lack of discrimination between weak and scattering responses).

Regarding the measurement of the amount of deposited layer, other devices can be found, such as the *fiber optical sensor* (FOS) which assesses the thickness of the deposit or the number of microorganisms that adhere to the tip of an optical fiber that is inserted into the wall of the pipe through backscattered light (Tamachkiarow and Flemming 2003). The FOS

has been industrially implemented to detect the formation of biomass in brewery water pipelines.

Another example is the *photoacoustic spectroscopy sensor* (PAS) which is based on the fact that when a given sample absorbs energy it physically expands and creates an acoustic wave that propagates through the deposit and that can be measured by a vibration picking elements, such as piezoelectric films. The sample is excited with a short radiation impulse (electromagnetic radiation, such as laser light). The PAS has been applied to investigate the effect of soluble and colloidal substances on the structure and the stability of biofilms as well as to determine the efficacy of anti-fouling strategies (Schmid et al. 2003; Schmid et al. 2004).

When the measurement is based on the difference of two turbidity values, the device is named *differential turbidity device* (DTM). The DTM compares the turbidity of two systems, one that is measuring the adhesion process and the other is being continuously cleaned. The DTM device has been already industrially tested to detect the formation of biomass in water systems of a paper mill processing unit (Klahre and Flemming 2000). Regarding the industrial application, the main problems associated with these techniques is the fact that they are intrusive (a hole should be made in the tubing pipe) and they are not suited for thick deposits – above a given thickness threshold the optical signal gets saturated. The DTM requires that one of the turbidity devices is being constantly cleaned (e.g. by water jets or by using mechanical wipes) which is a constraint for practical implementation. Another limitation observed for these monitoring techniques is the fact that they do not integrate the measurement of the deposit over a suitable surface area, but rather perform a localized analysis.

#### **1.3.4. Measurement of electric signals**

The measurement of electric signals is quite popular among the reported monitoring techniques and it includes *electrochemical* measurements and *capacitance/impedance* determinations. The electrochemical measuring devices typically have two or more electrodes (in contact with the aqueous phase) to which a given voltage/current signal is applied. Those devices are based on the effect that the deposit build-up has on the electric conductivity of the surface/electrode and were applied to monitor for example the bio(fouling) formation in

nuclear power plants (Licina et al. 1993). Electrochemical measurements have also been applied to study the formation of scaling products on heat transfer surfaces (Tili et al. 2008). One of the most well known techniques within this group is the MIC (microbiologically influenced corrosion) monitor which detects the effect of the biocorrosion caused by microorganisms (due to their metabolic activity) on the electrodes. There are some commercially available MIC monitoring devices, such as the BIOX<sup>®</sup> (Mollica and Cristiani 2003). The BIOX<sup>®</sup> has also been used to optimize dosage of biocides in power station condensers (Cristiani 2005).

Concerning the capacitive/impedance devices, they are based on the fact that microorganisms (having liquid plasma with dielectric properties) can behave as electric capacitors. This means that microorganisms can store charges when exposed to electric fields and the movement of the electrical current between two electrodes can be used to measure the capacitance. A capacitive device typically includes two parallel plates (to which a voltage is applied to) separated by a non-conducting material. This methodology was applied to the detection of biofilm layers (Maurício et al. 2006) and the electric capacitance showed to be inversely related with the thickness of such deposit. It was also applied to follow both the formation and the degradation of biofilms in platinum and gold electrodes (Muñoz-Berbel et al. 2008).

### **1.3.5. Measurement of vibration signals**

The use of vibration measurements is widely reported and applied to different areas like civil and mechanical engineering and medicine. The ultrasound and acoustic techniques have been applied, as sensing/monitoring methodologies, to the inspection of material fractures/fatigue (e.g. in the aeronautical industry) and the examination of fetus during pregnancy. Most of the work in the gas and oil industries, regarding the application of ultrasound technique is focused on the detection of corrosion and fracture within pipelines (Lowe et al. 1998; Reber et al. 2002). Acoustic procedures have also been applied to monitor fouling layers. Two different approaches are typically found in the literature: i) the adhesion of the deposit occurs directly on the transducer (sensor) and then it is related with the sensor's vibration characteristics; ii) the transducer is placed on the outer part of the tubing and the amount of deposit is related to the acoustic properties of the wave that travels across the walls, the bulk and the deposit.

### ***1.3.5.1. The deposit adheres directly to a crystal surface***

One of the most reported devices is the *Quartz crystal microbalance* (QCM), which analyzes the effect that the adhesion of deposits directly to a quartz crystal causes to the vibration (frequency) of such a surface (Nivens et al. 1995). The QCM was firstly applied for vacuum and gas application, although the number of applications increased dramatically when it was setup to be used in the aqueous phase. It consists of thin quartz layers sandwiched between a pair of electrodes. When voltage is applied to the electrodes, thanks to the piezoelectric properties of the quartz crystal the structure can be excited to mechanically vibrate. Quartz is the preferred piezoelectric material when a precise vibration frequency (typical frequencies are between 5-10 MHz) is required, since its vibration is quite accurate and extremely repeatable. Because of these characteristics, it becomes quite reliable to relate the resonant frequency of the crystal to the deposit layer that attaches to its surface. As the deposit attaches to the crystal surface, its vibration frequency decreases. If the attached layer is thin and rigid, the frequency variation becomes proportional to the mass of such deposit. In those specific cases it is possible to determine the mass of deposit by applying the Sauerbrey relation - the mass is a function of some intrinsic properties of the crystal and of the frequency shift. However, in most of the situations the adhered layer is not rigid but rather viscoelastic and the former relation is not valid (Nivens et al. 1995). A viscoelastic deposit dampens the crystal oscillation, which with a correctly vibration analysis can give information about the viscoelasticity and the mass of the attached layer. Depending on the manufacturing characteristics (e.g. piezoelectric orientation and arrangement of the electrodes) different vibration modes can be obtained. Some examples are the thickness shear mode (TSM), surface acoustic wave (SAW), acoustic plate mode (APM) and flexural plate wave (FPW). In the literature, when no mention to the vibration mode is provided it means that the QCM is at the TSM configuration, indicating that the major surfaces of the crystal vibrate transversely in the thickness direction (bulk of the material). The TSM has been used to detect the bond of biological cells by antibody molecules that are immobilized on the resonator surface - (immunosensors configuration) and this was positively applied to detect microbiological infections in animals (Pohanka et al. 2007) like rabbits. The QCM has also been experimentally studied in order to determine the amount of attached bacteria (*P. Cepacia*) and its detection limit was found to be  $3 \times 10^{-5}$  cells/cm<sup>2</sup>, although a number of complications regarding temperature and flow velocity have been observed (Nivens et al. 1993). It was also applied to detect biofilm formation in quartz polished electrodes surfaces indicating that it



was able to monitor their adhesion (Helle et al. 2000), but the flow and the nutrients in the bulk seems to affect the measurement (frequency). Another commonly used configuration is the SAW, since it can be reproduced with precise characteristics using photolithography techniques directly on the piezoelectric substrate and it is widely used as immunosensors for chemical determinations (Hunt et al. 2003). As the name indicates, the propagation wave travels on the surface rather than on the bulk (as in the TSM).

There are many commercial versions of the QCM device (e.g. [www.Q-Sense.com](http://www.Q-Sense.com)) including some to detect the initial adhesion of bacteria to stainless steel surfaces. In fact, it showed to be quite efficient for identification of bacteria adhesion (in early initial periods) and on the identification of, for example, proteins. The above described QCM technique requires that the deposit is formed directly on the crystal surface and can only measure thin deposits. Because of these intrinsic characteristics, the QCM application to industrial processes is regarded with some concern mainly due to its intrusive character, to being appropriate for the detection of only small amounts of fouling, to the difficulty in using it with real industrial surfaces and to its high costs (that may reach more than 60 thousands Euros in the most sophisticated versions).

#### ***1.3.5.2. The transducers are not in contact with the deposit***

An alternative approach relies on the generation of an acoustic pulse that is transmitted through the bulk liquid and the deposit and measured on the wall of the tubing (under study). The measurement procedures implemented to detect/monitor fouling can assume different configurations, such as the *pulse-echo* and the *transmission* techniques (Withers 1996). The main differences between these two configurations rely on the use of one or more transducers and on the analysis of the output signal.

In the *pulse-echo technique* only one transducer (that acts as exciter and as sensor) is placed on the outer surface of the tubing and simultaneously transmits an ultrasound pulse to the piping and measures the echoed signals. For each boundary (wall/deposit, deposit/bulk) the wave gives rise to a reflection (echo) and so, the time that the reflection takes to return to the transducer can be related to the amount of fouling, the value being different according to the thickness of the deposit. In order to determine this thickness it is necessary to know the velocity of sound through the material, which is a difficult parameter to evaluate. The main

disadvantages associated with an efficient industrial implementation of this technique for fouling monitoring (Withers 1996) are: i) the echoed signal on the boundary deposit/bulk will be highly scattered since this boundary is not regular along the adhesion process. This signal will be very small compared to other reflections (e.g. from the wall/deposit); ii) the different acoustic properties of the deposit and the pipe will also contribute to decrease the already small deposit echoed signal; iii) it is different to distinguish the reflection introduced by the bulk and by the deposit, which will make it more difficult to quantify how much is the contribution of the deposit. So, this technique, in its fundamental application (normal beam), should be able to provide information about fouling severity rather than fouling amount. In order to overcome this problem some authors (Hay and Rose 2003; Lohr and Rose 2003) discussed the implementation of guided waves (which result from the interference of longitudinal and shear waves). The guided waves can be created by placing the transducer(s) within an oblique wedge. Figure 1.1, schematically compares the propagation of a normal beam and of the oblique incident waves. The use of the guided waves showed to be a good indicator of the medium viscosity, since an increase of this physical parameter corresponds to an increase in the energy loss. In spite of these still preliminary results (fouling was simulated by using only a viscous film on the pipe inner surface) this technique seems to have great potential on fouling detection and quantification.

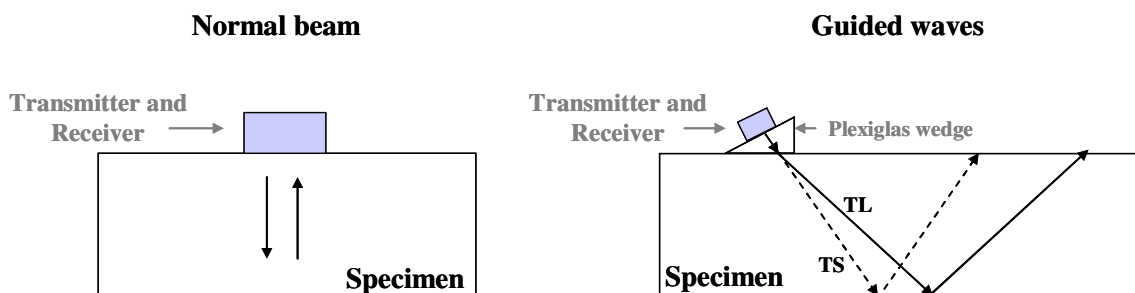


**Figure 1.1:** Schematic representation of the pulse-echo generation of normal beam and guided waves procedure (TL – transmission of longitudinal waves and TS – transmission of shear waves), for pulse-echo setups. The former schemes were based on (Lohr and Rose 2003)

Another example of the application of the pulse-echo technique is the ultrasonic time or frequency domain reflectometry. Several studies have been done with the ultrasonic time-domain reflectometry (UTDR) and they suggest that this methodology is able to detect the initial adhesion of different foulant layers such as: calcium sulphate on membranes of reverse osmosis systems (Mairal et al. 2000) or mixed deposits on ultrafiltration membranes (Li et al.

2003). The amplitude of the reflected wave showed to be the parameter that can be related to the amount of such deposits. The methodology for data analysis has been improved with the introduction of frequency domain (ultrasonic frequency-domain reflectometry) determinations since it allows measuring more mature biofilms and their detachment from the polymeric matrix (Fonseca et al. 2002; Kujundzic et al. 2007). These techniques can provide real-time information about the deposit, but they are intrusive methodologies. For example Kujundzic (2007) used an acoustic transducer (typically between 5-30 MHz) with a diameter of 0.6 cm placed on a polycarbonate coupon surface (contact area of the acoustic reflections:  $120 \times 10^3 \mu\text{m}^2$ ) to measure the biofilm formation.

The alternative approach, the *transmission technique* uses one transducer as an exciter and another one as receiver. When a pipe section is considered, the transducers are placed on opposite sides of the pipe walls so the traveling wave has to pass through the deposit and through the bulk liquid. In comparison to the pulse-echo approach, this technique introduces an advantage since the measured signal does not depend on the deposit characteristics for its reflection. The main drawback associated with this technique is that all existing boundaries will cause reflection, thereby reducing the signal that reaches the receiver. The guided waves approach has been also applied to the transmission setup leading to similar results to the ones already mentioned (Hay and Rose 2003; Lohr and Rose 2003) for the pulse-echo approach.

The equipment required for the actuation and signal analysis procedures in the ultrasound range (frequencies higher than 20 kHz) is quite complex and much more expensive than the one required for low-frequencies range. So, more recently acoustic techniques based on low-frequency (0-20 kHz) were designed to detect fouling and biofouling, the first one being the monitoring device discussed in the present Thesis (Pereira et al, 2006), followed by a similar technique applied to the detection of fouling in plate heat exchangers (Merheb et al. 2007). The latter uses an acoustic transducer that is placed on the upper section and excites the heat exchanger plate while 3 sensors are attached to the lower part of the equipment (at different zone of the heat exchanger). The signal responses are gathered by the 3 sensors and the acoustic power (integration of the output wave over time) and the delay of the acoustic signals are determined for each sensor. The results seem to indicate good sensitivity and it seems plausible that with further improvements this system can be industrially used to monitor

fouling. The comparison of the evolution of the acoustic parameters for the 3 sensors gives an idea of the amount of fouling on each zone of the heat exchanger.

#### **1.4. REQUIREMENTS FOR A SUITABLE MONITORING DEVICE**

It is clear from the above review that a good monitoring system should fulfill some basic requirements:

- It should be able to provide on-line, real-time, *in situ* information about the deposit adhesion and removal. The sampling rate at which the information is given should be several times higher than the adhesion/removal rates of the deposit. These features enable the operator to take timely counter-measures as well as being simple to use.

- It should not interfere with the process and so it should be non-intrusive. In fact, this is an important characteristic since intrusive sensors are sources of possible contamination (which is a huge concern for example for the food industry) and in some cases they can create fragilities in the piping (e.g. drinking water distribution network) structure.

- It should be robust and reliable. It should be able to operate and give accurate information under realistic industrial conditions, including high ranges of temperature, pressure and flow velocity. It is also consensual that in many cases the devices should be prepared to resist to severe chemical ‘attack’ (which might occur in some industrial facilities). Additionally, it should have a low cost due to the need to incorporate several of these monitors along each production line.

- The information provided by the device should be an integrated value of the deposit characteristics over a given area. The area of fouling considered for the measurement should be high enough to avoid biasing problems (the deposits are usually not uniformly distributed) but still keep the needed accuracy. For example, the pressure drop measurements detect fouling along a considerable area of pipe, although it does not have enough accuracy on this determination. Contrarily to this case, for example the FOS device measures the deposit that adheres to a fiber optical tip with diameter of 0.2 mm and, thus, in some cases it might give a non-representative result of what happens in a given equipment.

- It should be possible to apply it to different types of surface materials, since depending on the particular industrial case under study the equipment may be built with different materials.

One important concern regarding the implementation of monitoring devices is where to place the sensor. Assuming that the sensor is not portable (given the nature of the so far studied monitoring techniques) it is crucial to find out the location of the monitoring device taking into account (Withers 1996) that it should be placed where fouling is most likely to occur with an amount/way that is representative of what happens in the overall plant. The information gathered at this point should be used to infer about the fouling elsewhere in the plant. Additionally, more than one device can be implemented on critical points along the plant. A cost/benefit analysis of the implementation of more than one device should be done in order to evaluate the number of devices to be placed along a given processing line.

### **1.5. ESTIMATION OF THE SAVINGS GATHERED WITH A MONITORING SYSTEMS**

#### **IMPLEMENTATION**

It is accepted among the academic and industrial community that in spite of the great diversity of on-line monitoring technique described in literature, the majority of them have never crossed the frontier of the laboratory research to the industrial application. The main reason that is pointed out is the fact that most of them do not possess some of the key characteristics (previously mentioned) to allow their industrial application. Another disadvantage is related to how complex it is to evaluate the true costs associated with fouling within a given industrial plant. The lack of studies that can provide a figure about the savings that a given industrial facility is able to achieve with the implementation of accurate monitoring techniques is probably the major reason that separates scientific and industrial communities on this issue.

There are only a few reports that quantify the amount of savings that a given operation plant can achieve by implementing an efficient monitoring procedure. For example Tornqvist (2007) describes that the implementation of CIP procedures to other industrial applications than only to the food processing plants, together with the measurement of the equipment performance and estimation of cleaning cycles, can highly improve the production and cleaning cycles. The estimation of when the plant should be cleaned is based only upon the comparison between the heat exchangers performance under the actual operating conditions and the optimal performance expected. In fact, with this type of tool it was possible to

estimate that the losses associated with one heat exchangers (561 m<sup>2</sup>) working as a central cooler in a petrochemical plant was around 8 000 US\$/day (due only to the cost of energy) (Tornqvist 2007). If one accounts that the process has 4 heat exchangers the amount of money that is lost becomes very high.

Another study on the estimation of the savings in a dairy manufacturing plant (with 0.6 million liters of milk per day) is reported by an American company named 'Vigilistics' ([www.vigilistics.com](http://www.vigilistics.com)), which developed an optimization software based on the information gathered along several cycles of production/cleaning procedures. The information of each new operational cycle is then analyzed within the software and the optimization is always improved on each iteration. Based on the optimization procedure, they were able to actuate on the reduction of the cleaning cycles. The amount of water saved in this dairy plant by applying this methodology was around 110 000 l per day.

The previous studies give a figure of the savings that a given process can have when an efficient monitoring of the process is performed. Recall that the determinations were only based on the effect that the deposit has on the overall loss of efficiency of the heat exchangers, and that the savings would be even higher if a monitoring system able to provide information about the extent and type of fouling would be implemented, since it would give a more accurate idea of fouling severity and would help on devising a more appropriate CIP procedure. None of the previous monitoring procedures was based on the real evaluation of the deposit adhered to the surface, so those costs can decrease even more with the implementation of a monitoring technique that fulfils the requirements mentioned in Section 1.4.

## **1.6. AIMS OF THE PRESENT THESIS**

The work described and discussed in the present Thesis is focused on the development and application of an acoustic technique to measure the formation and the removal of fouling layers from a given monitored surface. From the text above, it seems quite obvious that there is a lack of monitoring devices that provide information about the attached or removed deposits and that can be industrially applied with suitably low costs. So, in order to fulfill these requirements as well as to provide information about the type of deposit that is being

formed on the surface a novel on-line monitoring device, the so called Mechatronic Surface Sensor (MSS) has been devised and assessed. In terms of its conceptualization, it is quite simple, similar to the one discussed for the vibration measurements through transmission technique, where two transducers are attached to the monitored surface: one acts as an exciter/actuator and the other as a sensor. Contrarily to what happened with the previous acoustic techniques described above, the MSS actuates the surface with a low-frequency excitation and measures the propagation of such vibration along the surface, rather than the reflection waves. The methodology used to process the output response and the fact that it uses low-frequency excitation brings some advantages to the MSS over the other vibrating monitoring devices previously described. Those advantages rely on its lower cost (typically the equipment required for ultrasound techniques are more expensive than for low-frequency excitations) and on the fact that it requires less complex equipment. According to Withers (1996), in the pulse-echo technique the 'signal processing and hardware were extremely complex particularly the need to generate a sufficient broad range of frequencies in the transducer to provide the necessary range of wavelengths required' (for example in the work described by Hay and Rose (2003) the system was actuated with a 50 kHz to 15 MHz frequency range at 300 V). For the transmission technique this equipment is simpler than the pulse-echo one but also more complex than the one used for the MSS (the MSS actuating characteristics - in its last and more accurate version - are within a frequency range between 0 and 20 kHz at 1.5 V). Another difference resides on the type of measurement made: localized *vs* integrated. Recall for example that the normal beam technique is a localized measurement in the both setup configurations (pulse-echo and transmission). The use of guided waves surpasses that limitation but is more complex from the analytical and assembling points of view since it requires the use of obliquous wedges. On the other hand the MSS integrates the measurement of the deposit information over the whole area of the monitored plate with the application of two small transducers. As regards the goals of assembling a monitoring device able to provide information about the fouling attachment or detachment, the main advantages of the MSS are the excitation techniques which enable to extract the parameters that can be related to the amount and the type of deposit that is being former on the monitored surface.

The methodology proposed by Merheb et al. (2007) which also uses low-frequency excitation was developed after the MSS one, described by Pereira et al. (2006) and their main

differences are on the treatment of the collected wave and on the number and type of sensors used.

The MSS was tested under three different situations giving quite accurate results and showing that it was able to: i) follow the build-up and detachment of biofilm deposits formed under different experimental conditions (different flow regimes) and distinguish between these biological layers and a silicate one (Chapter 3); ii) follow the formation of a calcium phosphate deposit and a protein one and to detect different formation and cleaning rates (Chapter 4); it was also able to distinguish their mineral/proteineous type; iii) to detect the cleaning end-point of shampoo removal under different cleaning conditions (Chapter 5). Furthermore, a more detailed analysis about the physical functioning and interpretation of the MSS output results will be provided in Chapter 6. That chapter also introduces an additional procedure to process the information gathered by the MSS giving some indications for the immediate future (Chapter 7) about what can be done to get this technology industrially applied.

## **REFERENCES**

- Asteriadou, K., T. Hasting, M. Bird and J. Melrose (2007). "Predicting cleaning of equipment using computational fluid dynamics." Journal of Food Process Engineering **30**(1): 88-105.
- Bott, T. R. (1995). Fouling of heat exchangers, Elsevier, Amsterdam.
- Bott, T. R. (2000). "Biofouling Control with Ultrasound." Heat Transfer Engineering **21**(3): 43-49.
- Bott, T. R. and L. Tianqing (2004). "Ultrasound enhancement of biocide efficiency." Ultrasonics Sonochemistry **11**(5): 323-326.
- Casanueva-Robles, T. and T. R. Bott (2005). The environmental effect of heat exchanger fouling: A case study. Heat exchanger fouling and cleaning - Challenges and opportunities. Irsee - Germany.
- Changani, S. D., M. T. Belmar-Beiny and P. J. Fryer (1997). "Engineering and chemical factors associated with fouling and cleaning in milk processing." Experimental Thermal and Fluid Science **14**(4): 392-406.
- Chen, M. J., Z. Zhang and T. R. Bott (2005). "Effects of operating conditions on the adhesive strength of *Pseudomonas fluorescens* biofilms in tubes." Colloids and Surfaces B: Biointerfaces **43**(2): 61-71.



- Chew, J. Y. M., W. R. Paterson and D. I. Wilson (2004). "Fluid dynamic gauging for measuring the strength of soft deposits." Journal of Food Engineering **65**(2): 175-187.
- Chew, Y. M. J., W. R. Paterson and D. I. Wilson (2007). "Fluid dynamic gauging: A new tool to study deposition on porous surfaces." Journal of Membrane Science **296**(1-2): 29-41.
- Cloete, T. E. L. (2003). "Biofouling control in industrial water systems: What we know and what we need to know." Materials and Corrosion-Werkstoffe Und Korrosion **54**(7): 520-526.
- Cristiani, P. (2005). "Solutions to fouling in power station condensers." Applied Thermal Engineering **25**(16): 2630-2640.
- Ferreira, C., M. C. Pereira, M. M. S. M. Bastos, O. C. Nunes, M. Coelho and L. F. Melo (2008). Functionalized nano-structures to combat biofilms. Chempor, Braga.
- Flemming, H.-C. L. (2003). "Role and levels of real-time monitoring for successful anti-fouling strategies - An overview." Water Science and Technology **47**(5 Number): 1-8.
- Fonseca, A. C., A. R. Greenberg and M. Hernandez (2002). Real time biofilm detection using ultrasonic frequency-domain reflectometry (UFDR). International Specialised Conference on BIOFILM MONITORING, Porto.
- Fryer, P. J., G. K. Christian and W. Liu (2006). "How hygiene happens: Physics and chemistry of cleaning." International Journal of Dairy Technology **59**(2): 76-84.
- Geddert, T., W. Bialuch, W. Augustin and S. Scholl (2007). Extending the induction period of crystallization fouling through surface coating. Heat Exchangers fouling and cleaning, VII. Tomar, Portugal.
- Grant, D. M. and T. R. Bott (2005). "Biocide dosing strategies for biofilm control." Heat Transfer Engineering **26**(1): 44-50.
- Guiamet, P. S. and S. G. Gomez De Saravia (2005). "Laboratory studies of biocorrosion control using traditional and environmentally friendly biocides: An overview." Latin American Applied Research **35**(4): 295-300.
- Hajek, J., V. Kermes, P. Stehlik and J. Sikula (2005). "Utilizing CFD as an efficient tool for improved equipment design." Heat Transfer Engineering **26**(5): 15-24.
- Hasting, A. P. M. (2002). Industrial experience of monitoring fouling and cleaning systems. Fouling, cleaning and disinfection in food processing. Cambridge, UK.
- Hasting, A. P. M. (2005). Improving the monitoring of fouling, cleaning and disinfection in closed process plant. Handbook of hygiene control in the food industry. H. L. M. Lelieveld, M. A. Mostert and J. Holah. Cambridge - UK, Woodhead Publishing limited.
- Hay, T. R. and J. L. Rose (2003). "Fouling detection in the food industry using ultrasonic guided waves." Food Control **14**(7): 481-488.

Helle, H., P. Vuoriranta, H. Valimaki, J. Lekkala and V. Aaltonen (2000). "Monitoring of biofilm growth with thickness-shear mode quartz resonators in different flow and nutrition conditions." Sensors and Actuators B-Chemical **71**(1-2): 47-54.

Hunt, W. D., D. D. Stubbs and S. H. Lee (2003). "Time-dependent signatures of acoustic wave biosensors." Proceedings of the IEEE **91**(6): 890-901.

Janknecht, P. and L. F. Melo (2003). "Online Biofilm Monitoring." Reviews in Environmental Science and Biotechnology **2**(2): 269.

Kadurugamuwa, J. L., L. V. Sin, J. Yu, K. P. Francis, T. F. Purchio and P. R. Contag (2004). "Noninvasive optical imaging method to evaluate postantibiotic effects on biofilm infection in vivo." Antimicrobial Agents and Chemotherapy **48**(6): 2283-2287.

Klahre, J. and H. C. L. Flemming (2000). "Monitoring of biofouling in papermill process waters." Water Research **34**(14): 3657-3665.

Kujundzic, E., A. Cristina Fonseca, E. A. Evans, M. Peterson, A. R. Greenberg and M. Hernandez (2007). "Ultrasonic monitoring of early-stage biofilm growth on polymeric surfaces." Journal of Microbiological Methods **68**(3): 458-467.

Kukulka, D. J. (2005). "An evaluation of heat transfer surface materials used in fouling applications." Heat Transfer Engineering **26**(5): 42-48.

Kukulka, D. J. and M. Devgun (2007). "Fluid temperature and velocity effect on fouling." Applied Thermal Engineering **27**(16 SPEC. ISS.): 2732-2744.

Li, J., D. K. Hallbauer and R. D. Sanderson (2003). "Direct monitoring of membrane fouling and cleaning during ultrafiltration using a non-invasive ultrasonic technique." Journal of Membrane Science **215**(1-2): 33-52.

Licina, G. J., G. Nekoksa, G. L. Ward, R. L. Howard and D. L. Cubicciotti (1993). Monitoring corrosion and biofilm formation in nuclear power plants using electrochemical methods. Proceedings of the 6th International Symposium on Environmental Degradation of Materials in Nuclear Power Systems-Water Reactors, Aug 1-5 1993, San Diego, CA, USA, Publ by Minerals, Metals & Materials Soc (TMS), Warrendale, PA, USA.

Lin, S. X. Q. and X. D. Chen (2007). "A laboratory investigation of milk fouling under the influence of ultrasound." Food and Bioproducts Processing **85**(1 C): 57-62.

Lohr, K. R. and J. L. Rose (2003). "Ultrasonic guided wave and acoustic impact methods for pipe fouling detection." Journal of Food Engineering **56**(4): 315-324.

Losurdo, M., C. Bertrand and H. Spliethoff (2007). Numerical studies on particle adhesion/deposition on pipelines. A novel lagrangian particle tracking code dedicated to CFD data post-processing. Heat exchanger fouling and cleaning - VII. Tomar, Portugal.

- Lowe, M. J. S., D. N. Alleyne and P. Cawley (1998). "Defect detection in pipes using guided waves." Ultrasonics **36**(1-5): 147-154.
- Ludwicka, A., L. M. Switalski and A. Lundin (1985). "Bioluminescent assay for measurement of bacterial attachment to polyethylene." Journal of Microbiological Methods **4**(3-4): 169-177.
- Mairal, A. P., A. R. Greenberg and W. B. Krantz (2000). "Investigation of membrane fouling and cleaning using ultrasonic time-domain reflectometry." Desalination **130**(1): 45-60.
- Maurício, R., C. J. Dias and F. Santana (2006). "Monitoring biofilm thickness using a non-destructive, on-line, electrical capacitance technique." Environmental Monitoring and Assessment **119**(1-3): 599-607.
- McLaughlin-Borlace, L., F. Stapleton, M. Matheson and J. K. G. Dart (1998). "Bacterial biofilm on contact lenses and lens storage cases in wearers with microbial keratitis." Journal of Applied Microbiology **84**(5): 827-838.
- Melo, L. F. and T. R. Bott (1997). "Biofouling in water systems." Experimental Thermal and Fluid Science **14**(4): 375-381.
- Merheb, B., G. Nassar, B. Nongaillard, G. Delaplace and J. C. Leuliet (2007). "Design and performance of a low-frequency non-intrusive acoustic technique for monitoring fouling in plate heat exchangers." Journal of Food Engineering **82**(4): 518-527.
- Mollica, A. and P. L. Cristiani (2003). "On-line biofilm monitoring by "BIOX" electrochemical probe." Water Science and Technology **47**(5 Number): 45-49.
- Mott, I. E. C., D. J. Stickler, W. T. Coakley and T. R. Bott (1998). "The removal of bacterial biofilm from water-filled tubes using axially propagated ultrasound." Journal of Applied Microbiology **84**(4): 509-514.
- Müller-Steinhagen, H., M. R. Malayeri and A. P. Watkinson (2005). "Fouling of heat exchangers-new approaches to solve an old problem." Heat Transfer Engineering **26**(1): 1-4.
- Muñoz-Berbel, X., C. Garcia-Aljaro and F. J. Muñoz (2008). "Impedimetric approach for monitoring the formation of biofilms on metallic surfaces and the subsequent application to the detection of bacteriophages." Electrochimica Acta **53**(19): 5739-5744.
- Nivens, D. E., J. Q. Chambers, T. R. Anderson and D. C. L. White (1993). "Long-Term, Online Monitoring of Microbial Biofilms Using a Quartz Crystal Microbalance." Analytical Chemistry **65**(1): 65-69.
- Nivens, D. E., R. J. Palmer and D. C. L. White (1995). "Continuous Nondestructive Monitoring of Microbial Biofilms - a Review of Analytical Techniques." Journal of Industrial Microbiology **15**(4): 263-276.

Pereira, A., R. Rosmaninho, J. Mendes and L. F. Melo (2006). "Monitoring deposit build-up using a novel mechatronic surface sensor (MSS)." Food and Bioproducts Processing **84**(4 C): 366.

Pereira, M. O., M. Kuehn, S. Wuertz, T. Neu and L. F. Melo (2002). "Effect of flow regime on the architecture of a *Pseudomonas fluorescens* biofilm." Biotechnology and Bioengineering **78**(2): 164-171.

Pereira, M. O., P. Morin, M. J. Vieira and L. F. L. Melo (2002). "A versatile reactor for continuous monitoring of biofilm properties in laboratory and industrial conditions." Letters in Applied Microbiology **34**(1): 22-26.

Pohanka, M., F. Tremel, M. Hubalek, H. Band'ouchova, M. Beklova and J. Pikula (2007). "Piezoelectric biosensor for a simple serological diagnosis of tularemia in infected European brown hares (*Lepus europaeus*)." Sensors **7**(11): 2825-2834.

Quarini, J. (2002). "Ice-pigging to reduce and remove fouling and to achieve clean-in-place." Applied Thermal Engineering **22**(7): 747-753.

Radhakrishnan, V. R., M. Ramasamy, H. Zabiri, V. Do Thanh, N. M. Tahir, H. Mukhtar, M. R. Hamdi and N. Ramli (2007). "Heat exchanger fouling model and preventive maintenance scheduling tool." Applied Thermal Engineering **27**(17-18): 2791-2802.

Reber, K., M. Beller, H. Willems and O. A. Barbian (2002). A new generation of ultrasonic in-line inspection tools for detecting, sizing and locating metal loss and cracks in transmission pipelines. Proceedings of the IEEE Ultrasonics Symposium.

Rosmaninho, R. and L. F. Melo (2006). "Calcium phosphate deposition from simulated milk ultrafiltrate on different stainless steel-based surfaces." International Dairy Journal **16**(1): 81-87.

Saikhwan, P., T. Geddert, W. Augustin, S. Scholl, W. R. Paterson and D. I. Wilson (2006). "Effect of surface treatment on cleaning of a model food soil." Surface and Coatings Technology **201**(3-4): 943-951.

Savtchenko, T., M. Fallen and F. Ebert (2001). "On flow fields in tubular heat exchangers - Numerical calculations and flow visualization." Chemical Engineering and Technology **24**(7): 706-711.

Schmid, T., C. Helmbrecht, U. Panne, C. Haisch and R. L. Niessner (2003). "Process analysis of biofilms by photoacoustic spectroscopy." Analytical and Bioanalytical Chemistry **375**(8): 1124-1129.

Schmid, T., U. Panne, J. Adams and R. L. Niessner (2004). "Investigation of biocide efficacy by photoacoustic biofilm monitoring." Water Research **38**(5 Number): 1189-1196.

Shetty, G. R. and S. Chellam (2003). "Predicting membrane fouling during municipal drinking water nanofiltration using artificial neural networks." Journal of Membrane Science **217**(1-2): 69-86.

- Straatsma, J., G. Van Houwelingen, A. E. Steenberg and P. De Jong (1999). "Spray drying of food products: 1. Simulation model." Journal of Food Engineering **42**(2): 67-72.
- Suci, P. A., J. D. Vraný and M. W. Mittelman (1998). "Investigation of interactions between antimicrobial agents and bacterial biofilms using attenuated total reflection Fourier transform infrared spectroscopy." Biomaterials **19**(4-5): 327-339.
- Tamachkiarow, A. and H. C. L. Flemming (2003). "On-line monitoring of biofilm formation in a brewery water pipeline system with a fibre optical device." Water Science and Technology **47**(5): 19-24.
- Tijing, L. D., B. C. Pak, B. J. Baek, D. H. Lee, C. S. Kim and Y. I. Cho (2007). Use of catalytic alloys for physical water treatment technology to mitigate mineral fouling in heat exchangers. Heat exchanger fouling and cleaning - VII. Tomar, Portugal.
- Tlili, M. M., P. Rousseau, M. Ben Amor and C. Gabrielli (2008). "An electrochemical method to study scaling by calcium sulphate of a heat transfer surface." Chemical Engineering Science **63**(3): 559-566.
- Tornqvist, A. (2007). A survey Alfa Laval's experience of fouling prevention in plate heat exchanger systems. Heat exchangers fouling and cleaning - VII. Tomar, Portugal.
- Tunney, M. M., N. Dunne, G. Einarsson, A. McDowell, A. Kerr and S. Patrick (2007). "Biofilm formation by bacteria isolated from retrieved failed prosthetic hip implants in an in vitro model of hip arthroplasty antibiotic prophylaxis." Journal of Orthopaedic Research **25**(1): 2-10.
- Vieira, M. J. and L. F. Melo (1999). "Intrinsic kinetics of biofilms formed under turbulent flow and low substrate concentrations." Bioprocess Engineering **20**(4): 369-375.
- Visser, J. and T. J. M. Jeurink (1997). "Fouling of heat exchangers in the dairy industry." Experimental Thermal and Fluid Science **14**(4): 407-424.
- Watkinson, A. P. (2007). "Deposition from crude oils in heat exchangers." Heat Transfer Engineering **28**(3): 177-184.
- Wilson, D. I. (2005). "Challenges in cleaning: Recent developments and future prospects." Heat Transfer Engineering **26**(1): 51-59.
- Withers, P. M. (1996). "Ultrasonic, acoustic and optical techniques for the non-invasive detection of fouling in food processing equipment." Trends in Food Science and Technology **7**(9): 293-298.
- Zdaniuk, G. J., L. M. Chamra and P. J. Mago (2006). "A literature survey of water-side fouling applicable to cooling tower condensers." Proceedings of the Institution of Mechanical Engineers, Part A: Journal of Power and Energy **220**(7): 815-827.

Zhao, Q., Y. Liu, C. Wang, S. Wang and H. Muller-Steinhagen (2005). "Effect of surface free energy on the adhesion of biofouling and crystalline fouling." Chemical Engineering Science **60**(17): 4858-4865.

## **2. ROADMAP FOR THE THESIS**

### ***2.1. FROM THE CHALLENGE TO THE IDEA***

The existence of monitoring techniques that provide information about fouling layers according to the requirements listed on Section 1.4 is still a necessity for industrial and academic communities. This same feeling was experienced a few years ago when the research work described in this Thesis started under the framework of the European project SAFER (Surveillance and control of microbiological stability in drinking water distribution networks). The main goal of the SAFER project was to control the microbiological stability and the quality changes of drinking water during its transport along the distribution systems. Drinking water networks are quite vulnerable systems, because they are not sterile and the biofilms that exists along them are the perfect shelter for pathogen microorganisms. The project was based on two main target areas: i) the development of new fast detection techniques that allow to implement early warning systems to control biofilms and pathogens (these techniques were based on microbiological or physical principles); ii) the optimization of disinfection of water systems in order to reduce the chemicals consumption based on the information gathered in point i). The present Thesis discusses one of the monitoring techniques (the MSS) proposed by the research group from LEPAE/FEUP with the aim of detecting biofouling adhesion/removal in drinking water systems. Besides the MSS, six more devices were worked out by other partners of the project. The 7 devices studied, relying on different physical principles, were the: i) fibre optical sensor (FOS); ii) differential turbidity measurement device (DTM); iii) FTIR-ATR spectroscopy; iv) Electrochemical sensor; v) capacitive sensor; vi) fluorescence sensor (FluS); and the vii) mechatronic surface sensor (MSS). The first three mentioned devices were developed for different applications (as can be read in the introduction section) and were experimentally tested in drinking water systems (to detect biofilm or other types of deposits). Four of these 7 devices have been abandoned along the project and only the FOS, the FTIR-ATR and the MSS were selected for further development and/or testing. So, the MSS was born within the SAFER project to detect biofilms adhesion/removal and since then it has been improved and applied to detect different types of fouling. The MSS is patented in Portugal (Mendes et al. 2005) and the respective European extension is pending (Mendes et al. 2006).

## **2.2. MONITORING DEVICE DESIGNATION**

The present Thesis discusses a *Mechatronic Surface Sensor* (MSS) which is an on-line monitoring device that measures changes in the vibration properties of the system introduced by the deposit. The first question that may arise is: what is mechatronic and why to use the mechatronic term to name this device?

In the recent decades, a more intrinsic relation has been established in different areas to integrate products/processes (mechanical systems) and electronics. The evolution of the last generation of automated mechanical systems is in fact quite new (since 1980) and the systems regarded so far as discrete mechanical and electrical parts became integrated electronic-mechanical systems with sensors, actuators and digital microelectronics components. And so, the designation for these integrated systems of *mechatronic systems* arises from the association of MECHANics and elecTRONICS. The 'Mechatronics is the synergetic integration of mechanical engineering with electronics and intelligent computer control in the design and manufacturing of industrial products and processes' (Bishop 2006).

The basis of the present Thesis relies on an interdisciplinary approach that conjugates several scientific-technological areas (mechanics, electronics, chemical and biological engineering) to create an efficient fouling monitoring device. The goal of the present work is not only to provide insights to and seek advances in scientific knowledge but also to discuss a solution that can contribute to increase the understanding and minimization of fouling/cleaning phenomenon in industrial facilities.

## **2.3. FUNDAMENTALS OF THE MECHATRONIC SURFACE SENSOR (MSS)**

The basic idea behind the MSS relies on the fact that the attachment, growth and detachment of deposits produce changes in the vibration properties of surface waves. This device has been designed based on the following requirements, which are essential for industrial applications:

- a) to be applied to different types of industrial surfaces (e.g. PVC, stainless steel - SS);
- b) to obtain an integrated measurement over a significant area, thereby minimizing biased conclusions taken from very small surface areas;



c) to be placed on the outer surface of the monitored surface, which is quite important to avoid being an additional source of contamination. Furthermore, the surface cleaning procedures (sometimes harsh) should not affect the integrity of the device;

d) it should be a robust device (or should have the possibility to be assembled in a robust configuration).

Four different configurations of the MSS device were experimentally built and tested and will be discussed along the present Thesis. In spite of the differences presented later on in this chapter, there is a general MSS configuration common to the four experimental setups. Their main differences come from: i) the sensing element (e.g. piezoelectric or accelerometer); ii) the material of the plate to be monitored (e.g. PVC or stainless steel); iii) the amplification and acquisition system; iv) the plate clamping type (e.g. glued or screwed); v) the use of a flow cell with or without coupons; vi) the excitation technique (sinusoidal *vs* random) as well as the mathematical processing of the collected data. These differences will be highlighted along the present chapter and the discussion about why they were made will also be provided.

The MSS monitor is composed of a PVC or SS plate that closes the open base of a semi-circular duct made of PERSPEX<sup>®</sup> (internal diameter = 30.0 mm, equivalent diameter = 18.3 mm). The flow cell where the MSS is inserted is similar to the one described by Pereira et al. (2002). An actuator and a sensor element are attached to the plate, on the face that is not in contact with the liquid flowing inside the duct, as schematically represented in Figure 2.1. The flow cell used in the first two and in the last configurations has 6 coupons that could be periodically removed in order to study the properties of the attached deposit (Figure 2.1). The response of the system captured by the sensor is mathematically processed on the computer.

**FIRST SETUP**

The work described in the present section can be read in further detail in **Chapter 3: ‘Using Nanovibrations to monitor biofouling’**, published as a paper in *Biotechnology and Bioengineering*, Vol. 99, No. 6, pp. 1407, 2008.

As previously mentioned the MSS was born within the SAFER project during which the first prototype has been assembled and its proof of concept was experimentally accomplished as described below.

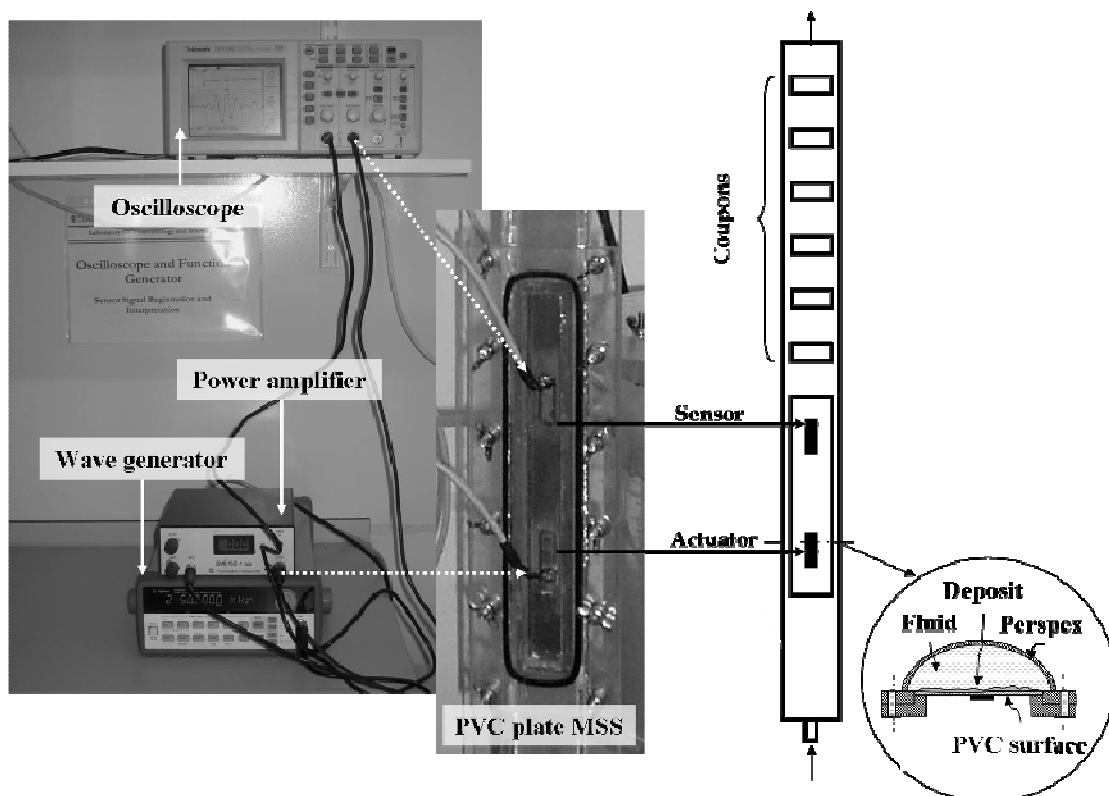


**Figure 2.1:** Picture of the generating/acquisition equipment and schematic representation of the experimental rig (detailed picture of the MSS plate). Note: the pointy arrows correspond to the connection between the generating/acquisition equipment and the sensor and actuator

**Summary of the setup characteristics**

- **Plate material:** PVC (length: 212 mm; width: 29 mm; thickness: 1.0 mm); the PVC is one of the materials that is typically used to build drinking water pipes. Besides that, the polymeric materials damp much more the vibrations than the metallic ones, so this PVC is one of the worse materials in terms of vibration propagation. Being so, the proof of concept of this technology to monitor the amount of attached deposit was done in one of the less favourable situations that may occur in terms of the material characteristics.

- Glue used: epoxy; the PVC plate was glued to a PERSPEX<sup>®</sup> support which was screwed to the flow cell. This way, the PERSPEX<sup>®</sup> support was designed in order to keep the PVC plate aligned by the inner flat surface of the flow cell.
- Actuation/Sensing elements type: piezoelectric material (BM 70/25/200 M). More information about these transducers can be read in Appendix B.
- Actuation characteristics: a sinusoidal wave with frequency of 3.2 kHz and 60 V is used to perform the actuation (the mentioned frequency matches one of the resonant frequency of the system). One of the key operating conditions of this configuration is the fact that it works at the system's *resonant frequency* that shows the maximum output amplitude guarantying that the maximum output signal is achieved.
- Generation/acquisition: are performed manually and require the following equipment (see Figure 2.1): waveform generator, power amplifier, digital oscilloscope and the computer where the information is saved and mathematically processed.
- Flow cell characteristics: the flow cell (internal diameter = 30 mm, length = 1200 mm) has 6 coupons;

The FFT amplitude (or  $A_{FFT}$ ) and the damping factor (or  $DF$ ), among other parameters determined, were found to be the parameters that respectively provide information about the amount and type/nature of the deposit. The  $A_{FFT}$  of the *output signal was found to be inversely proportional to the amount of deposit* attached to the surface. To obtain a curve similar to the ones usually reported in fouling studies (i.e., showing a direct relation between the measured variable and the amount of deposit), a normalization procedure was performed by subtracting all the values collected during the experiment from the initial value – this was called ‘normalized amplitude’. The damping factor was found to be another important parameter that can be determined from the MSS measurements and is related to the capacity that a mechanical system has to reduce the intensity of a vibration process. *Higher damping factors variations were observed for more viscoelastic deposits.*

## Conclusions

In order to study the MSS response to deposits with different physical and structural properties, three types of deposits that can be found in drinking water systems were monitored: i) *Pseudomonas fluorescens* biofilm under turbulent flow; ii) *Pseudomonas fluorescens* biofilm under laminar flow; and iii) Silicate under turbulent flow. A detailed

discussion about the obtained results can be read in *Chapter 3*. The main conclusions that can be taken from the present work are that:

- the MSS can give information not only about the amount of deposit formed on (or being removed from) the monitored surface, but also about the physical characteristics related to the viscoelasticity of the deposit, by determining the  $A_{FFT}$  and the damping factor of the output wave;
- when the analysis of each deposit is carried out separately, an increase of the mass causes an increase of the normalized amplitude – see Figure 2.2; a good correlation between these two parameters (normalized amplitude and wet mass) is observed.
- biological layers, which are usually more viscoelastic, can be distinguished from inorganic deposits by their damping factor, since more viscoelastic deposits showed higher damping factors.

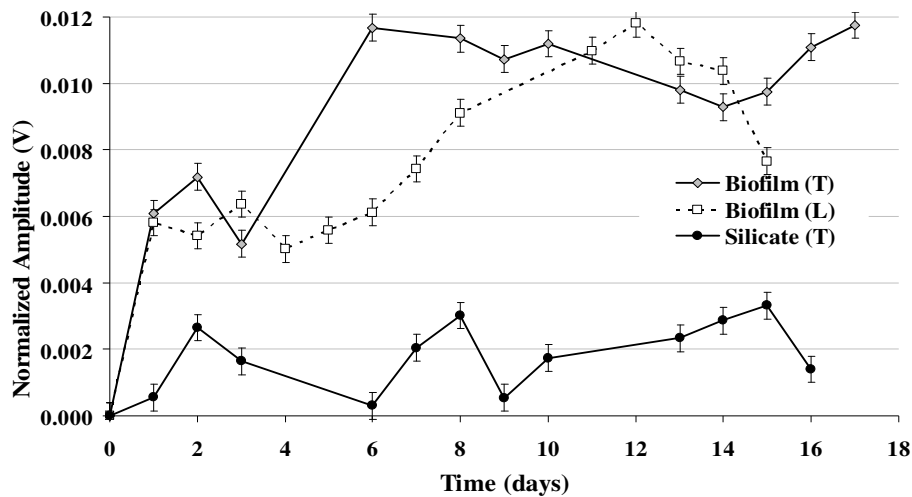


**Figure 2.2:** MSS normalized amplitude against time for the tested deposits: *Pseudomonas fluorescens* biofilm formed under turbulent (T) and laminar (L) flow, and silica deposit formed under turbulent flow (T)

Regarding the overall results of the SAFER project, the MSS showed to be one of the most promising sensors concerning the determination of the amount of biofilms in drinking water systems. Note that in spite of what is typically expected, the deposits observed in drinking water systems may be very thick, containing a mixture of biofilms and abiotic inorganic and organic solids.

## 2.4. SECOND SETUP

The work described in the present section can be read in further detail in **Chapter 4: ‘Monitoring deposits build-up using a novel Mechatronic Surface Sensor (MSS)’**, published as a paper in *Food and Bioproducts Processing*, Vol. 84 (4C), pp. 366, 2006.

As widely discussed in the state-of-the-art, the dairy industry is one of the most affected industries regarding fouling and cleaning severity. The implementation of a monitoring device that is able to provide on-line information not only about the amount but also about the type of deposit would be quite important to this industry. Thus, fouling caused by milk components was induced on the MSS in order to determine its ability to follow the adhesion and removal of those deposits. A second setup has been assembled overcoming some drawbacks observed in the first configuration (described in Section 0). The main problem associated with the latter was related to the fact that the generation/acquisition were performed manually. In order to face this problem, the equipment listed above (wave generator and oscilloscope) was replaced by a data acquisition board which is connected to the

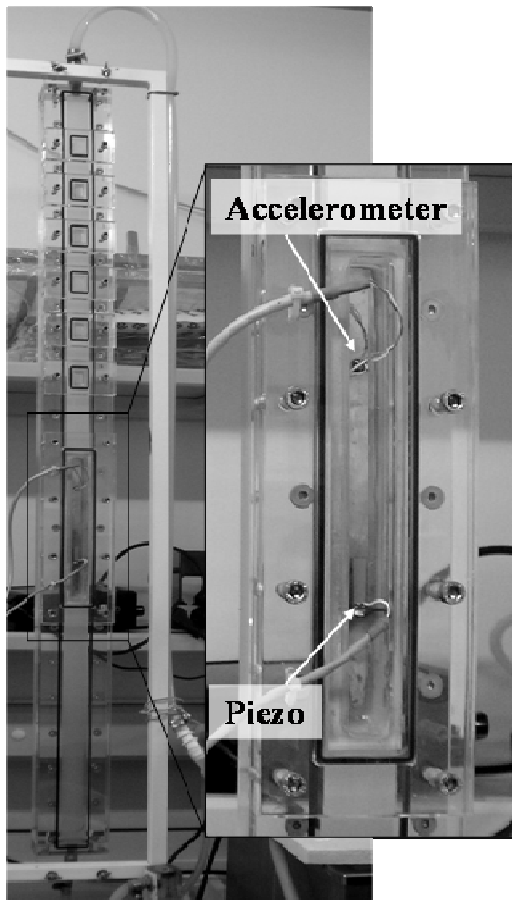


**Figure 2.3:** Picture of the experimental rig (with a detail of the MSS monitor)

computer. A full automatic measuring system was developed in LabVIEW<sup>®</sup> 7.1 in order to allow the generation, acquisition and mathematical procedure to be performed automatically after a given period of time. Besides the advantage inherent to this new procedure (automatic vs manual), the overall costs of the equipment decreased drastically. Furthermore, the piezoelectric sensor has been replaced by an accelerometer (More information about these accelerometers can be read in Appendix B) which is also a quite common type of sensor often

applied to the measurement of vibration. With the implementation of the accelerometer - see Figure 2.3 – with a smaller excitation voltage it was possible to read a higher output signal.

### Summary of the setup characteristics

Plate material: SS (length: 212 mm; width: 29 mm; thickness: 0.6 mm); the choice of the plate material is once again related to the application under study. The SS is one of most used materials for equipment used within the food industry.

Glue used: epoxy;

Actuation/Sensing elements type: a piezoelectric element as an actuator; an accelerometer element as a sensor;

Actuation characteristics: a sinusoidal wave with: 4.5 kHz and 9 V; recall that in the preceding configuration the actuation voltage was 60 V.

Generation/acquisition: are performed automatically;

Flow cell characteristics: similar to the one described and shown in Section 0.

### Conclusions

A more detailed discussion of the results can be read in *Chapter 4*, but the main conclusions were that:

- The  $A_{FFT}$  (or its normalized amplitude) and the damping factor of the vibration wave are the best parameters to characterize the deposition process. Variations of these parameters reflected not only changes in the mass of deposit attached to the surface, but also differences in the structural properties of the fouling layers (mineral *vs* protein deposit);
- The MSS is able to follow different cleaning rates: the cleaning rate of a mineral deposit and of a mixed deposit (mineral + whey protein) using an acid solution ( $\text{HNO}_3$ ) are quite different (see Figure 2.4);
- A relation between the MSS normalized amplitude and the thermal resistance (from a heat flow cell – traditional monitoring device) has been established.

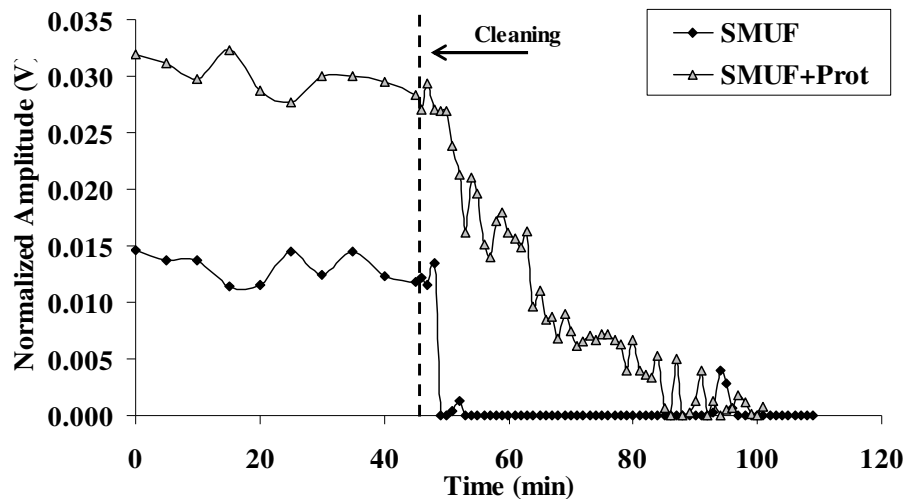


**Figure 2.4:** Cleaning of SMUF and SMUF with whey protein deposition curves assessed with the MSS

The adhesion of milk components to the MSS was performed at 50 °C (the biological ones were obtained at 27 °C) which brings some problems regarding the experimental design. It is widely known that the temperature has an effect on the material properties, such as the expansion and the rigidity of the system. And that an increase on the temperature decreases the rigidity of the glue. So, in order to guarantee that during the experiments the MSS was in fact measuring the parameters associated with the deposit effect rather than external effects associated for example with the rigidity of the glue (if the glue becomes less rigid it has an effect on the vibrating properties of the wave) an evaluation of the system properties was made. The fact that the SS plate is glued to the PERSPEX<sup>®</sup> structure showed to be a complicated procedure, since it required a proper and quite accurate gluing technique (improved after some frustrating attempts), which in some cases created leaking problems between the SS/PERSPEX<sup>®</sup> interface that might lead (among other problems) to an inaccurate measuring procedure. Before each trial, the system was set to run during 48 h at the experimental conditions under study (temperature and flow velocity) and the analysis of the output result showed that the  $A_{FFT}$  and the damping ratios were constant, which indicated that the system had not changed in terms of the system characteristics. Furthermore, after the cleaning procedures (when the  $A_{FFT}$  reached an  $A_{FFT}$  equal the initial one – clean state), the system was set to run (with water) over 24 h and the  $A_{FFT}$  and the  $DF$  were still constant, which confirms that the changes observed on these are associated only with the adhesion/removal of the deposit.

## **2.5. THIRD SETUP**

*The work described in the present section can be read in further detail on **Chapter 5: 'Monitoring cleaning-in-place processes using nanovibration technology'**, which was submitted as a paper to *Sensors and Actuators B: Chemical**

During the present Thesis a considerable collaboration between industry and the scientific community has been established, based on extensive discussions of the principles and practical applications of the monitor. From one of these discussions, the question of whether the MSS was able to monitor the removal and the cleaning end-point of the shampoo films removal arose. Note that this particular study does not deal with solid fouling deposits (as it happened until now) but with residual fluid films that stay attached to the monitored surface. Since the shampoo viscosity is quite different from water, the vibration that propagates along the tubing is affected by this property and so different  $A_{FFT}$  are observed for the water and for the shampoo. The effect of the temperature and of the flow velocity on such amplitude has been determined. Along the experimental trials the amplitude measurement was corrected as a function of these two parameters (temperature and flow velocity).

Contrarily to what happened in the previous sections, since the absolute  $A_{FFT}$  obtained with shampoo was smaller than the  $A_{FFT}$  obtained with water, the acquired signal was normalized in order to be similar to a typical cleaning curve (decrease with time). This signal varies between 0 and 1, these values corresponding, respectively, to the cleaned SS surface and to the MSS flow cell filled with shampoo (initial state). The  $A_{FFT}$  after introducing the correction (as a function of flow velocity and temperature) and after the normalization was named  $A_{inv}$ . The relation between the  $A_{FFT}$  and the external conditions (temperature and the flow rates) as well as the relation used to correct such parameter can be read in Appendix C.

In this configuration a SS plate replaces the flat base of a semi-circular smaller flow cell. The plate is screwed between the flow cell and another PERSPEX<sup>®</sup> structure (along its width) avoiding the use of glue, which as mentioned in Section 2.4 may, if not properly calibrated, affect the vibration signal.



### Summary of the setup characteristics

Plate material: SS (length: 350 mm; width: 88 mm; thickness: 0.6 mm);

Glue used: the plate is not glued, but screwed between the two structures of PERSPEX®;

Actuation/Sensing elements type: piezoelectric element as an actuator; an accelerometer element as a sensor;

Actuation characteristics: a sinusoidal wave with: 5.1 kHz and 0.4 V;

Generation/acquisition: are performed automatically;

Flow cell characteristics: smaller flow cell, with no coupons. A schematic representation of this flow cell configuration can be seen in Chapter 5, Figure 5.1.

### Conclusions

The results and respective discussion can be read in *Chapter 5*, and the main conclusions were:

- Different cleaning conditions lead to different curves, which were accurately monitored by the MSS. The  $A_{inv}$  was related to the amount of deposit that stays attached to the monitored surface – see Figure 2.5.
- The cleaning end-points have been positively confirmed by spectrophotometry and contact angle measurements.
- The MSS is a reliable device to monitor the cleaning of shampoo films;

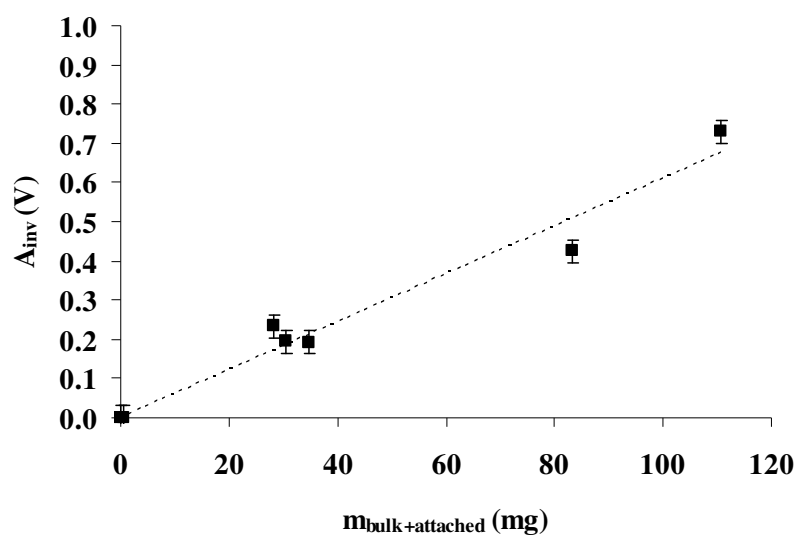


**Figure 2.5:** Relation between the  $A_{inv}$  and the mass of shampoo that remains in the flow cell after the cleaning procedure ( $R^2=0.9633$ )

## **2.6. FOURTH SETUP**

*The work described in the present section can be read in further detail on **Chapter 6: ‘Optimization of the MSS configuration’***

In parallel with the improvement of the different MSS configurations and with the experimental trials shown so far, a study of the fundamentals behind the MSS functioning principles was also carried out. *Chapter 6* provides a more detailed discussion about the basic idea behind the MSS and of how it operates. In order to reach a deeper understanding of the device functioning characteristics, a new configuration was designed which was used not only to describe in more detail the *modus operandi* of the procedure adopted in the previous chapters but also to introduce an alternative methodology to extract the information from the output signal.

Furthermore, along Chapter 6 some simulations were performed in order to determine the set of dimensions of the monitored plate that minimize of the frequencies of the first vibrating modes (this criteria allows a maximization of the output response). Additional simulations were carried out in order to evaluate the effect of the plate dimensions and of the boundary conditions on the modal shapes and frequencies of the system. In order to avoid the problems associated with the glue a new way to fix the monitored plate within the flow cell has been devised. In this alternative configuration, the SS plate is clamped between two PERSPEX<sup>®</sup> structures and sealed with O’rings.

The  $A_{FFT}$  and the damping factor used in the former chapters are able to provide informations about the amount and type of deposit but not about the vibrating characteristics of the system. In order to determine such vibrating characteristics (modal frequency and modal damping) an additional methodology was implemented: the experimental modal analysis (EMA). This technique showed to be a powerful tool to experimentally test the system in terms of its dynamic characteristics (i.e. it enable to decide between different configurations – e.g. different sealant materials - which were the best regarding the vibration properties of the system). The comparison between the EMA methodology (through the evaluation of the modal frequencies, the modal damping and of the root-mean-square of the transfer function -  $RMS_{TF}$ ) with the one used in the previous chapters has also been established, through the

monitorization of the attachment/detachment of a calcium phosphate (the procedure is similar to the one adopted in Chapter 4). The  $RMS_{FT}$  showed to be an interesting parameter to monitor the amount of deposit, which was able to increase the resolution of the system when comparing to the  $A_{FFT}$  parameter. With EMA it was also found that the amount of deposit affects the damping ratio and not the modal the frequencies of the system. Changes in the system's damping affects both  $A_{FFT}$  and  $RMS_{FT}$  parameters as proved with experimental trials.

A preliminary analysis of the effect of the temperature and flow velocity on the modal characteristics of the system is also provided. It was found that the modal frequency is highly affected by the temperature, while the effect on the damping ratio can be neglected for small temperature variation. Regarding the effect of the flow velocity and flow regime, they introduce a variation on the modal frequencies and damping although their effect seems to be neglected when the errors associated with their determinations are taken into account. It was also found that the effect of the temperature on the modal frequencies is higher for lower flow velocities. However, when simultaneous changes of temperature and of flow velocity occur, a rigorous analysis should be performed. When the effect of the external conditions on the modal parameters is high a calibration between the frequency or of the damping ratio with the temperature and with the flow velocity should be implemented.

## **REFERENCES**

Bishop, R. H. (2006). The Mechatronics Handbook, CRC Press.

Mendes, J., L. F. Melo, A. Mendes and A. Pereira (2005). Method and device for the measurement and identification of biofilms and other deposits using vibrations. FEUP. Portugal. N° 103 344.

Mendes, J., L. F. Melo, A. Mendes and A. Pereira (2006). Method and device for the measurement and identification of biofilms and other deposits using vibrations. FEUP. *Pending Patent* (PCT/IB2006/052992).

Pereira, M. O., P. Morin, M. J. Vieira and L. F. L. Melo (2002). "A versatile reactor for continuous monitoring of biofilm properties in laboratory and industrial conditions." Letters in Applied Microbiology **34**(1): 22-26.

### 3. USING NANOVIBRATIONS TO MONITOR BIOFOULING

#### ABSTRACT

The paper proposes the use of the Mechatronic Surface Sensor (MSS) to detect surface contamination. This methodology is based on the analysis of the vibration response of the monitored surface. In the present work a comparison between the responses of the MSS to different structural deposits build-up (*Pseudomonas fluorescens* biofilm – formed under turbulent and laminar flow and a silica deposit) were made. The results showed that the MSS response depends not only on the amount but also on the viscoelasticity of the attached deposit – different responses were obtained for the deposits according to their viscoelasticity. Another important conclusion is that the MSS response is not highly affected by solids that are not really attached to its surface.

#### 3.1. INTRODUCTION

The adhesion of unwanted deposits to industrial surfaces can be generically assessed in terms of its effects on the process (e.g. obstruction of pipes, decrease of the flow rates, increase of the thermal resistance and pressure drop) and on the product quality (e.g. microbial contamination of milk pasteurizing units). These problems lead, ultimately, to an increase in the costs of production and maintenance, as well as to public health problems (e.g. contamination in food industries and drinking water systems) and environmental impacts (discharge of cleaning agents and biocides and subsequent wastewater treatment costs). The build-up of biofilm layers is one of the most common forms of surface contamination (often called biofouling) in engineered water systems, particularly in cooling water units. In addition to the usual problems found in other fouling processes, microbial films favor pipe wall corrosion, create a suitable habitat for the incorporation of colloidal particles (iron oxides, clays, etc.) and can be a haven for the development of pathogens, particularly feared when potable water is required in hygienic procedures.

Although biofouling is practically impossible to eradicate, several actions can however be taken in order to mitigate its effects. Some of these strategies are related with the employment of treated/modified surfaces that delay the initial adhesion of such deposits (Rosmaninho et al. 2007) the optimization of both the design and operating conditions of the process plant, and the use of appropriate biocide and dispersant dosages (Flemming 2003). In parallel with such approaches, on-line monitoring of biofilm build-up and removal is a particularly effective way to minimize their formation and to optimize cleaning/disinfection cycles. With this tool it is also possible to understand the adhesion and removal dynamics, to apply timely counter-measures and to assess the efficacy of those actions on the biofilm removal process. The fact that microbial films often come together with other types of deposits (such as inorganic particles and precipitated salts) brings an additional complexity to the design of on-line monitors for field applications. In fact, the problem is not only to obtain a measure of the amount of surface contamination, but also to be able to identify the prevailing type of deposits in order to use the most appropriate antifouling programme (biocides, acid or alkali solutions, etc.)

There are numerous biofouling monitoring techniques and methods reported and reviewed in the literature (Nivens et al. 1995; Janknecht and Melo 2003), but only a few are applied in real industrial conditions. These techniques are based on different physical principles, e.g. measurement of pressure drop, electromagnetic radiation, thermal properties, vibration propagation, or simply direct weighing of removable coupons. On-line monitoring techniques, such as the one discussed in the present paper, rely upon sensors that receive a signal information and indirectly relate it to the phenomena happening on the surface. In practically all the reported cases, the signal acquired is not specific of a given deposit (Janknecht and Melo 2003), but requires proper calibration to produce a relation between the signal and at least one characteristic of the deposit (e.g. mass or thickness).

The aim of this work is to introduce and discuss a new on-line biofouling monitoring technology, the so called Mechatronic Surface Sensor (MSS). This sensor technology is based on the analysis of the change on the surface vibration properties caused by the adhesion, growth or detachment of deposits developing on the monitored surface. The vibration principles are also used in some other technologies, the most well-known being the QCM (Quartz Crystal Microbalance). The QCM is based on the vibration of a small quartz crystal

(an element with piezoelectric properties) and the adhesion of deposits to its surface causes a change on the natural vibration frequency of the crystal. The deposition must occur directly on the crystal surface that acts both as an excitation source and sensing element. For vacuum deposition studies of materials with similar rigidity as the quartz crystal, a direct proportionality between the frequency shift and the deposit mass was found, represented by the well known Sauerbrey equation (Nivens et al. 1995). This analysis becomes much more complex when there is a liquid phase and/or a non-rigid layer on the surface due to viscosity and viscoelastic effects. In biofilm studies, the relation between the frequency shift and the amount of adhered deposit is not linear, as observed by Nivens et al. (1993). Although it is a sophisticated and precise instrument, the QCM cannot be considered appropriate for field applications, because: i) the material is deposited directly on the crystal surface, implying a direct contact between the sensor and the liquid, that can be an additional contamination factor in food or pharmaceutical processes; ii) the measurement is made on a very small area, corresponding to the area of the crystal, with the risk of not being representative. The QCM is well fitted to monitor very small and thin films deposition and particularly designed for research laboratory applications.

The methodology presented in this paper is intended for field applications and is now patent pending (Mendes et al. 2005; Mendes et al. 2006). The goal is to be able to assess the amount and general physical properties of the contaminant layer by measuring different parameters (amplitude, time of flight, damping factor, etc) that mathematically define the acoustic waves moving along the surface. This propagation of nanovibrations is affected by the mass of the attached deposit and, at the same time, by the viscoelastic characteristics of the deposit/biofilm. It uses two independent piezoelectric elements to perform the actuation and sensing processes. Important features of the MSS are: a) it can be applied to any type of industrial surfaces (e.g. stainless steel, PVC, etc); b) the measurement is integrated over a significant area ( $\sim 12 \text{ cm}^2$ ), minimizing biased conclusions taken from very small surface areas; c) it is placed on the outer surface of the monitored pipe, thus there is no contact between the fluid and the device (this is very relevant, since the latter is not a source of contamination and the – sometimes harsh – surface cleaning procedures do not affect the integrity of the sensor). It is intended to be a robust instrument to be used in industrial environments, such as in pipes and it is able to monitor both the initial formation and the final amount of rather thick layers of biofilms or inorganic deposits.

### 3.1.1. Description of the Mechatronic Surface Sensor (MSS)

The MSS measures changes in the vibration properties of the surface due to the build-up/removal of deposits. In the present configuration, the MSS was composed of a PVC plate with two piezo elements (BM 70/25/200 M, Piezomechanik GmbH, Munich - Germany) 60 mm apart and glued on the outer surface of the material – Figure 3.1. The dimensions of the piezo elements are: 25 x 7.5 x 0.4 mm.

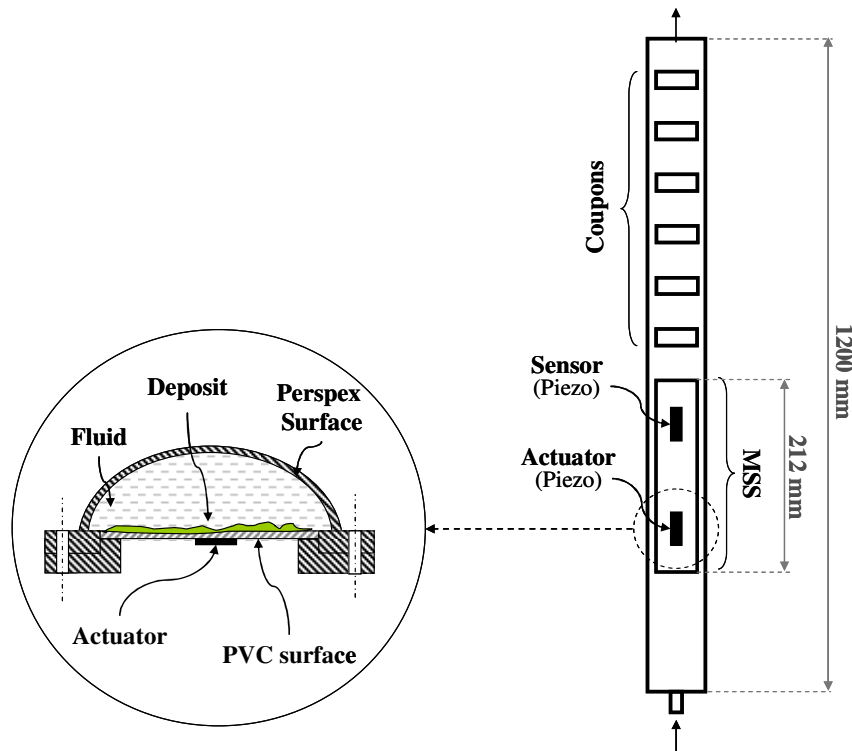


Figure 3.1: MSS schematic representation

The fluid flow and the biofilm formation occur in the inner surfaces of this flow cell, avoiding any contact with the piezo elements. One of the piezos acts as an actuator, stimulating the PVC plate to vibrate, while the other acts as a sensor capturing the vibration propagated along the surface. These two piezoelectric elements display a bending behavior when a voltage is applied to their terminals (see Appendix B).

The MSS measuring device used in the present work was inserted into a semi-cylindrical flow cell made of PERSPEX<sup>®</sup> (internal diameter = 30.0 mm, equivalent hydraulic diameter = 18.3 mm, length = 1200 mm) similar to the one described by Pereira et al. (2002). The flow cell contained several coupons (surface area per coupon = 2 cm<sup>2</sup>) that could be periodically removed in order to study the properties of the attached deposit.



The actuation element stimulates the PVC plate (length = 212 mm, width = 29 mm and thickness = 1 mm) with a 10 V and 3.2 kHz (which matches the resonant frequency of the system) sinusoidal signal generated via a wave or function generator (Agilent 33120A) and amplified 6 times on a power amplifier (Piezomechanik BM150). The vibration response to this actuation is then picked up by the other piezo element (the sensor) and collected via an oscilloscope (Tektronix, TDS 1002). This oscilloscope is connected to a computer via RS\_232 C (a standard interface for connecting serial devices) where the information is saved and mathematically processed. The synchronization between the signal generation and the signal acquisition is performed by an analogue trigger signal. Figure 3.2 shows a schematic representation of the generation and acquisition system of the MSS.

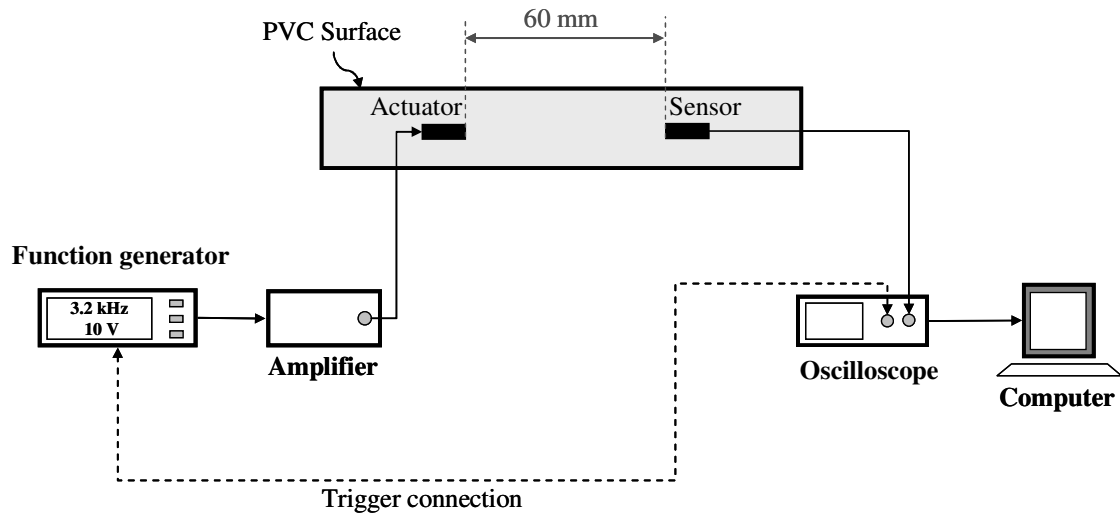


**Figure 3.2:** Schematic representation of the generation/acquisition system (the actuation is accomplished with a sinusoidal wave – 3.2 kHz and 60 V)

A different configuration of this system, without the need of the wave generator, the power amplifier and the oscilloscope, has been also developed with good results for calcium phosphate and protein deposits (Pereira et al. 2006). This alternative configuration uses a data acquisition board to generate and acquire the vibration signals, becoming a fully automatic measuring system. Also, a stainless steel plate was used instead of the PVC one, showing that the MSS can be applied to different surface materials.

The response of the system captured by the sensor is mathematically processed on the computer. Several wave characteristics are determined, such as: peak-to-peak amplitude, frequency and amplitude (after applying Fast Fourier Transforms – FFT), damping factor,

‘flight-time’, among many others. Among these wave parameters, the FFT amplitude showed to be the most representative of the amount of deposit on the surface (adhesion/removal of the deposits).

One of the key operating conditions of this device is the fact that it works at the system’s resonant frequency, guarantying that the maximum output signal is achieved. When the system is actuated by an external force (in the present case, the acoustic wave generated by the piezo actuator) and this force matches that of the natural frequency of the motion, the system will respond more energetically with an increase of the wave amplitude. If no energy dissipation (no damping) is observed, this amplitude will theoretically increase indefinitely. However, since damping exists, maximum amplitude is observed when the system is vibrating at resonance.

### 3.1.2. Numerical computation study

Since the wave picked up by the MSS sensor is the result of the vibration of a complex system, numerical computations were carried out in order to get theoretical information about the system. The complexity of this vibrating system comes from the interaction of different materials such as the acrylic duct, the PVC surface, the glue that fixes the two piezo elements to the outer surface of the PVC plate and the glue that fixes this plate to the PERSPEX<sup>®</sup> duct. Using a fundamental approach, the MSS can be assumed to be a damped system with one degree of freedom, subjected to a forcing function  $F(t)$ . In such a case, the response equation to an arbitrary forcing function, or Duhamel integral, can be applied (Shabana 1991). In order to simplify the simulations, some assumptions were made: the system is initially at a rest position ( $x_0 = 0$ , no displacement;  $\frac{dx_0}{dt} = 0$ , no velocity) and the damping factor is assumed to be constant along the simulations (no variation of the damping factor was introduced). With these conditions, the Duhamel integral becomes:

$$x(t) = \frac{1}{m\omega_d} \int_0^t F(\tau) e^{-\zeta\omega(t-\tau)} \sin \omega_d(t-\tau) d\tau \quad , \text{ for } t > \tau \quad (3.1)$$

where:  $m$  is the mass of the system;  $F(\tau)$  represents the forcing force acting during a short-lived interval  $d\tau$ ;  $\zeta$  is the damping factor;  $\omega_d$  is the damped resonant frequency of the system;  $\omega$  is the natural frequency of the system.

*Conditions of the simulation:* i)  $F(t)$  is the sinusoidal wave generated by the actuator with the generic form  $F(t) = A_0 \sin(\omega t)$ , where  $A_0$  and  $\omega$  were respectively 10 V and 20106 rad/s; ii)

$\omega = \frac{\omega_d}{\sqrt{1-\zeta^2}}$ ; iii)  $\zeta = 0.033$  and is constant; iv) the mass changes along the simulations.

The integral represented in Equation (3.1) has been numerically evaluated for different masses. For each of the masses considered, the following determinations were carried out: i) evaluation of the integral represented by Equation (3.1); ii) mathematical analysis of the  $x(t)$  response with calculation of the respective FFT (Fast Fourier Transforms) amplitude; iii) representation of the obtained “normalized” amplitude with the mass variation, as shown in Figure 3.3.

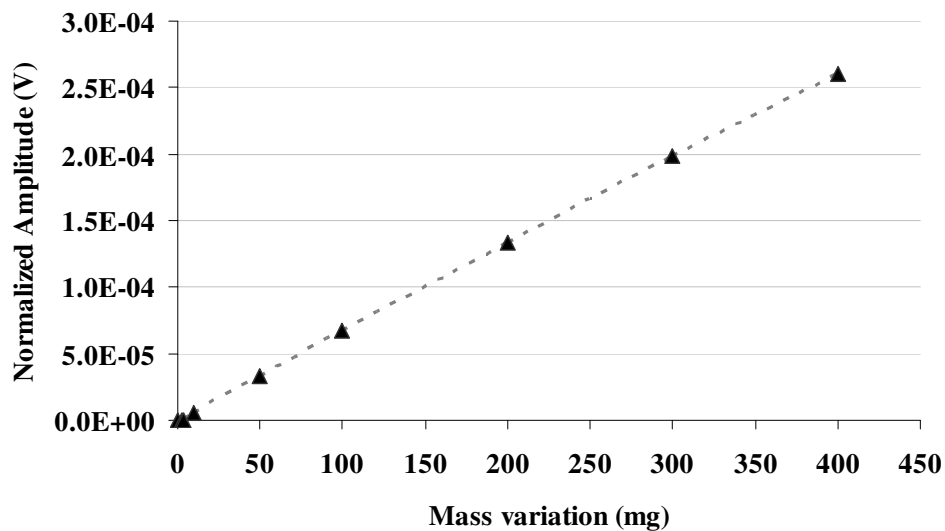


**Figure 3.3:** Variation of the normalized amplitude with the mass (simulation)

The  $A_{FFT}$  of the direct output signal is inversely related to the amount of mass of the system. To obtain a curve similar to the ones usually reported in biofilm growth studies (i.e., showing an increasing relation between the measured variable and the amount of deposit), a

normalization procedure was performed by subtracting all the values collected during the experiment from the initial value, resulting in the so called “Normalized Amplitude”.

Another important property of the wave that should be taken into account is the damping factor (it is an energy dissipation parameter). The damping factor is a structural property of vibrating materials which is widely used to characterize different structures. It represents the capacity that a mechanical system has to reduce the intensity of a vibration process along the time. The damping factor has been used, for example, to detect cracks in structures (Panteliou et al. 2001) or as vibration controller in machines and structures (Nakra 1998).

The initial vibrating system (MSS and water circulating in the duct) is characterized by a given damping factor. When a mass attaches to the sensor surface, the initial damping factor changes because the deposit acts as an additional ‘damper’ to the system. According to the structural nature of the deposit, different damping factors can be observed, since this parameter seems to depend on the viscoelastic characteristics of the adhered layer.

The damping factor was calculated from the output wave using the Logarithmic Decrement Method (Shabana 1991), which is based on the decrease of the maximum amplitude of the output (response) wave per unit time. The Logarithmic Decrement Method can be represented by the following equation:

$$\zeta = \frac{\frac{1}{n} \ln \left( \frac{x_i}{x_{i+1}} \right)}{\sqrt{(2\pi)^2 + \frac{1}{n^2} \ln^2 \left( \frac{x_i}{x_{i+1}} \right)}} \quad (3.2)$$

where  $\frac{x_i}{x_{i+n}}$  is the ratio of two (non) consecutive amplitudes;  $n$  is an integer value such as  $(n+1)$ =number of peaks, and  $\zeta$  is the damping factor (see Figure 3.4). The amplitude ratio is measured from the experimentally acquired wave signal  $x(t)$ .

Since the damping factor and the amplitude of the wave are independent parameters (two vibrations with equal amplitude can reach their rest positions more quickly or slowly depending on the structural properties of the material), the simulation previously presented, with a constant damping factor, is still valid. Figure 3.4 schematically represents this non-

dependence between the two parameters. It can be seen that, in spite of having the same initial amplitude, the wave A attenuates faster, that is, reaches its rest position more rapidly than the wave B.

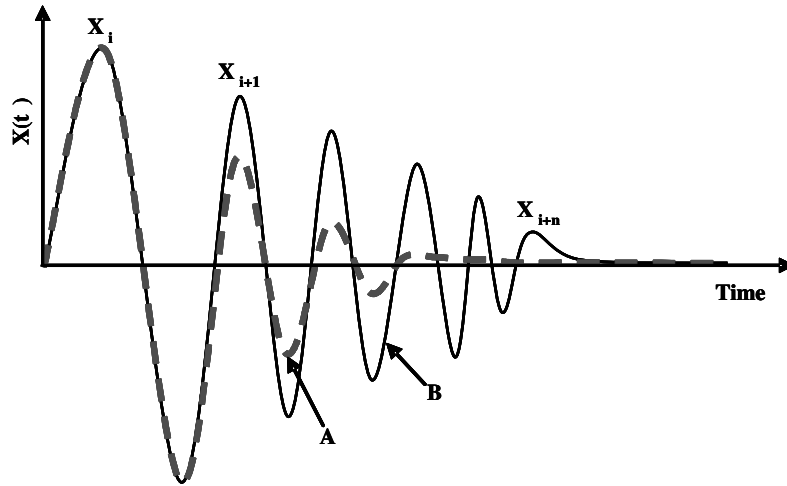


**Figure 3.4:** Schematic representation of two waves with the same peak-to-peak amplitude but with different damping factors (wave A has a higher damping factor than wave B)

### 3.2. MATERIALS AND METHODS

As mentioned in the ‘Description of the Mechatronic Surface Sensor’ section, the MSS monitor includes a flow cell (a PERSPEX<sup>®</sup> half-cylindrical duct with a flat PVC surface), on the outside of which the actuator and sensor elements are fixed. The water flows inside this duct and the biofilm is formed on its inner surface.

Two different mechanisms of deposit formation on surfaces were examined with the MSS: the adhesion and the sedimentation (without attachment).

#### 3.2.1. Adhesion studies

Deposits with different physical properties were formed and monitored in the flow cell in order to determine their influence on the MSS signal. The flow cell was placed in a vertical position to avoid deposition by sedimentation. The three tested layers were: i) *Pseudomonas fluorescens* biofilm formed under turbulent flow; ii) *Pseudomonas fluorescens* biofilm formed under laminar flow; and iii) Silica layer formed under turbulent flow.

Microorganism: a *Pseudomonas fluorescens* strain (ATCC 13515), known to be a good biofilm producer (Melo and Vieira 1999; Pereira et al. 2002), was used to develop biofilms subjected to laminar and turbulent flow regimes. It has the following optimal growth conditions:  $T = 27\text{ }^{\circ}\text{C}$ ,  $pH = 7$  and glucose as carbon source (Vieira and Melo 1995).

Growth medium: 50 mg/l glucose, 25 mg/l peptone, 12.5 mg/l yeast extract in phosphate buffer –  $pH = 7$ . The medium was sterilized.

Biofilm formation: A pure culture of *Pseudomonas fluorescens* was grown in a 4 l tank (Fermenter 1) for 24 h, using the optimum growth conditions reported above. After the incubation period, the suspension was diluted (1.6 l/h) in 5 l of sterilized and distilled water (Fermenter 2) that was put to recirculate between the fermenter and the flow cell. The bacterial concentration in the final suspension was  $6 \times 10^7$  cells/ml (measured by optical density, after calibration). The glucose concentration (determined by the Dinitrosalicylic Colorimetric Method – DNS) was maintained at 20 ppm by pumping sterile medium into the system.

Inorganic deposit: the inorganic deposit was obtained by recirculating a 400 ppm aqueous suspension of silica (micronized silica flour: Sikron SF600, Quartz-Werke Frechen, Germany) between the flow cell and the fermenter.

Flow regime: The biofilms were formed under two different flow regimes, by using different recirculation velocities between the fermenter and the flow cell: turbulent regime,  $Re = 5500$  (fluid velocity = 0.26 m/s) and laminar regime,  $Re = 1500$  (flow velocity = 0.07 m/s). The silica deposit was built up under turbulent flow,  $Re = 5500$  (fluid velocity = 0.26 m/s).

Experimental Procedures: In order to compare the MSS signal to the amount of deposit formed on the flat surface of the flow cell, coupons were periodically removed during the experiment at different stages of deposit formation. The following physical properties of the deposit were determined: wet mass, dry mass and thickness.

- The wet mass was determined by weighing (GR-200-EC  $\pm$  0.0001g) the coupons before and after deposit formation. Immediately after being collected, each coupon was weighed and the deposit thickness was measured. Then the coupon was dried until constant mass was reached. The difference between the latter value and the weight of the coupon without deposit gives the dry mass.

- The thickness of the wet deposit was also measured, with a digital micrometer device following the method described by Melo and Pinheiro (1984) and Brito and Melo (1999).
- The deposit density was assessed as the dry mass per unit of wet volume.

*Acquisition procedure:* During the experiments, the actuation/sensing process was activated at time intervals (approximately of 1 h) – for working days and during working periods. The normalized amplitude given by the MSS is measured at the beginning of the experiment (time = 0) and at each 1 h interval. The subtraction between the initial and final normalized amplitudes gives the MSS signal variation, which is related to the amount of deposit formed on the flat surface.

In order to determine the error associated with a given measurement, water was set to recirculate in the flow cell during one hour – it was assumed that no adhesion occurred because no bacteria or inorganic particles were introduced in the flow. The normalized amplitude was measured each 5 minutes and the standard deviation of these values is the error (electrical and mechanical) of the measuring system. Since the use of the device may increase the error of the measurement, this value was determined in the beginning of each experiment.

### 3.2.2. Sedimentation studies

In order to determine the contribution of the sedimentation of substances on the MSS signal, two different types of silica particles (SF 600 and SH 200, Quartz-Werke Frechen) were used. Their dimensions and the concentrations of the tested particle suspensions are indicated in Table 3.1.

**Table 3.1:** Silica particle suspensions used in the sedimentation tests

| Substance | Concentrations (% w/v) | Medium grain size ( $\mu\text{m}$ ) |
|-----------|------------------------|-------------------------------------|
| SH 200    | 0.1; 1; 10             | 24                                  |
| SF 600    | 10                     | 3                                   |

The sedimentation experiments were carried out in non-flow batch assays. After preparing the liquid suspension according to the desired concentration, the flow cell was filled with the suspension (~700 ml) and the MSS signal (normalized amplitude) was measured. Then the

system was left to rest during one hour, keeping the flow cell in a horizontal position with the MSS instrumented surface on the bottom part of the flow cell. After this period, the MSS signal was measured again. A control experiment has been performed with filtered and sterile water.

### 3.3. RESULTS AND DISCUSSION

The fouling curves of the three deposits, *Pseudomonas fluorescens* biofilm formed under turbulent flow, *Pseudomonas fluorescens* biofilm formed under laminar flow and silica deposit formed under turbulent flow, given by the MSS, are shown in Figure 3.5. Each of the points represented in this figure is the average of the ‘normalized amplitude’ values acquired each day. The deviation bars of the values are the error of the measuring system. It was found that this error is the same for the three experiments, being  $\pm 0.0004$  V. Figure 3.5 shows that the MSS normalized signal increases over time and reaches a higher value for the biofilms than for the silica deposit.

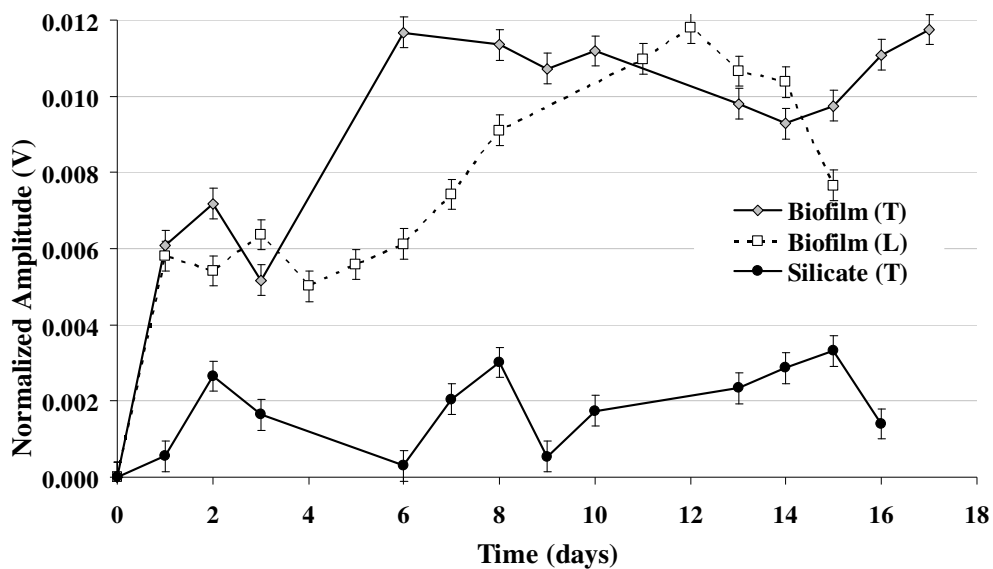


**Figure 3.5:** MSS normalized amplitude against time for the tested deposits: *Pseudomonas fluorescens* biofilm formed under turbulent (T) and laminar (L) flow, and silica deposit formed under turbulent flow (T)

To assess the physical meaning of the MSS normalized amplitude, calibration curves representing this parameter as a function of the wet mass (obtained by collecting coupons from the flow cell) were determined. The calibration results are plotted in Figure 3.6. The



error bars associated with the MSS response correspond to the average of three measurements carried out before and after collecting the sample (all the points have an error bar, but in some cases it is so small that it is not perceptible in the graph).

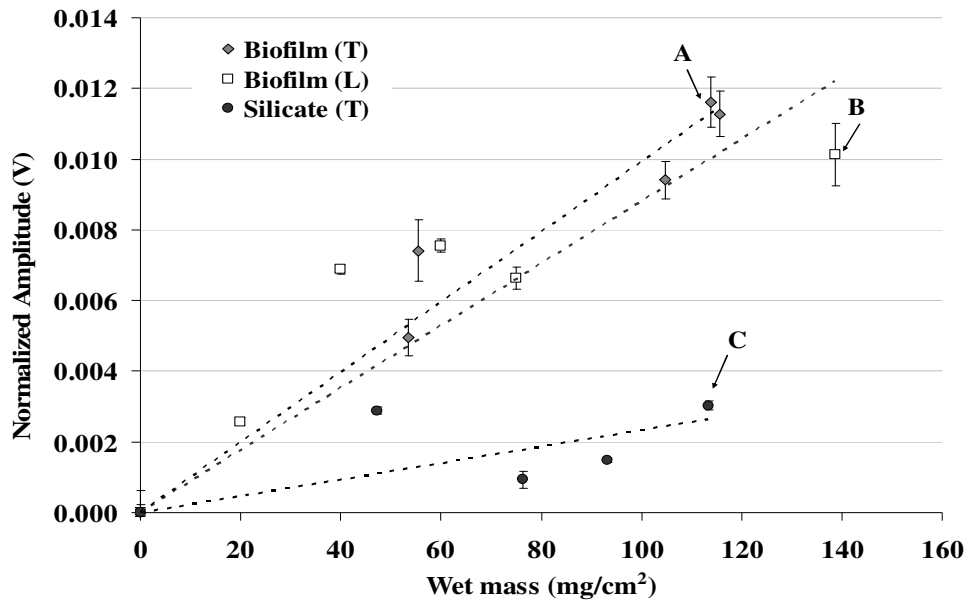


**Figure 3.6:** Variation of the MSS normalized amplitude with the wet mass per unit of area: *Pseudomonas fluorescens* biofilm under turbulent flow ( $\blacklozenge$ ), *Pseudomonas fluorescens* biofilm under laminar flow ( $\square$ ) and silica deposit under turbulent flow ( $\bullet$ )

Figure 3.6 shows that a satisfactory relation between the two measured parameters (normalized amplitude and wet mass) can be established for each of the deposits, according to the numerical computation presented in Figure 3.3. Table 3.2 indicates the mean relative error associated with the data in Figure 3.6.

**Table 3.2:** Mean relative error for the calibration curves for the three deposits

| Deposit  | Mean relative error (%) |
|--|-------------------------|
| <i>Pseudomonas fluorescens</i> biofilm (Turbulent) | 5.5                     |
| <i>Pseudomonas fluorescens</i> biofilm (Laminar)   | 11.6                    |
| Silica (Turbulent)                                 | 32.4                    |

These results indicate a better relation for the biofilm experiments (5.5% and 11.6% for the biofilm formed, respectively under turbulent and laminar regime) than for the silica one (32.4%). The silica deposits contain a much smaller water fraction (cf. wet masses and dry

densities in Table 3.3) than the biofilms, leading to larger experimental errors in measuring the wet masses due to unavoidable water evaporation.

**Table 3.3:** MSS signal characteristics and physical properties of the deposits studied

| <b>Deposit</b>     | <b>Regime</b> | <b>MSS normalized amplitude (V)</b> | <b>Damping factor variation</b> | <b>Wet mass (mg/cm<sup>2</sup>)</b> | <b>Dry Density (mg<sub>dry</sub>/cm<sup>3</sup><sub>wet</sub>)</b> |
|--------------------|---------------|-------------------------------------|---------------------------------|-------------------------------------|--|
| <b>Biofilm (A)</b> | Turbulent     | 0.0120 ± 0.0007                     | 0.033                           | 114.00                              | 121.31   |
| <b>Biofilm (B)</b> | Laminar       | 0.0100 ± 0.0009                     | 0.039                           | 138.60                              | 10.74  |
| <b>Silica (C)</b>  | Turbulent     | 0.0030 ± 0.0001                     | 0.023                           | 113.35                              | 1373.74  |

The results confirm that the MSS output signal can be used to monitor the build-up of deposits on surfaces, although the calibration curves are different from deposit to deposit. However, the data from the laminar flow experiments are much more scattered than the ones from turbulent flow runs, which seems to be due to the higher instability of the biofilm physical structure when formed under lower shear stresses.

### 3.3.1. Biofilms: turbulent vs laminar flow

In order to compare the two biological deposits, biofilm samples were collected from the laminar and turbulent flow experiments at approximately similar normalized amplitudes. These samples are represented in Figure 3.6 by points A and B that correspond to the biofilms formed respectively under turbulent and laminar flow and their characteristics are summarized in Table 3.3. The comparison shows that in spite of the similar slopes of the calibration curves in Figure 3.6, different dry densities are observed for the same normalized amplitude. For example, for approximately the same normalized amplitude of 0.011 V, the biofilm dry density is 121.3 mg<sub>dry</sub>/cm<sup>3</sup><sub>wet</sub> under turbulent flow and 10.7 mg<sub>dry</sub>/cm<sup>3</sup><sub>wet</sub> under laminar flow. These type of results confirm previous observations (e.g. Vieira et al. 1993) where higher densities were found in biofilms subjected to stronger shear stress conditions, suggesting that the compactness of the microbial layer is markedly affected by the hydrodynamic conditions of the fluid flowing over the biofilm surface. This effect is reflected on the damping factor variation which, as can be seen in Table 3.3, is lower for the more compact deposit (the one with higher density, i.e., the biofilm formed under turbulent flow, which absorbs less vibration energy).

### 3.3.2. Biofilm vs silica deposit (turbulent flow)

The biofilm formed under turbulent flow and the silica deposit (subjected also to turbulent regime) display different relations between the wet mass of deposit and the normalized amplitude (different slopes, see Figure 3.6). For example, if a wet mass of around  $114 \text{ mg/cm}^2$  is considered (sample represented by point A), the MSS normalized amplitude is 0.012 V for the biofilm (turbulent flow) and a much smaller value (0.003 V) is obtained for the silica deposit (represented by point C) – Table 3.3. This indicates that for the same mass of deposit, the normalized amplitude can assume different values according to the structural properties of the adhered deposit. In fact, Table 3.3 shows that for approximately the same wet mass ( $114.0 \text{ mg/cm}^2$ ), the dry density of the silica deposit is more than 10 times higher than the biofilm density.

The two comparisons previously presented (biofilms under turbulent vs. biofilm under laminar flow and biofilm vs. silica deposit, both under turbulent flow) seem to be in contradiction. On one hand, the two biofilms produced similar normalized amplitudes but have completely different dry densities; on the other hand, the silica deposit showed substantially lower normalized amplitude than the biofilm, in spite of its higher dry density. This apparent contradiction is due to the structural features of the deposits and is reflected on the damping factor variation. This parameter is related with the viscoelasticity of the body, the latter being a typical property of biofilms (Towler et al. 2003). Table 3.3 shows that the biofilm formed under laminar flow has the lowest density (lower compactness) and the highest damping factor (0.039), while the silica deposit has the highest density (more compact) and the lowest damping factor (0.023). The difference in damping factors observed for the three deposits is patent on the different wave intensity attenuations shown in Figure 3.7. This figure shows the real waves acquired, just before collecting the samples A, B and C (in Figure 3.6).

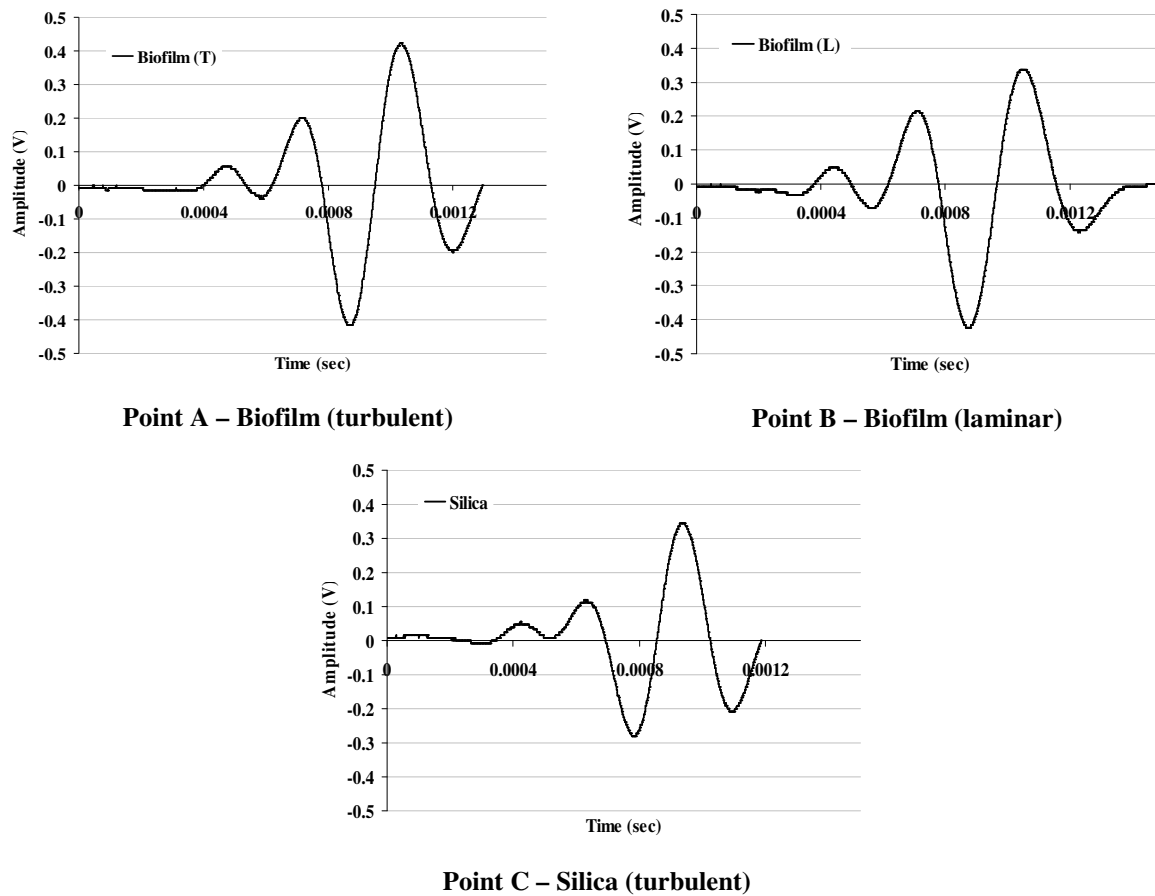


**Figure 3.7:** Real waves acquired with the MSS, immediately before collecting the samples A, B and C, represented in Figure 3.6

It is important to recall that the damping factor is determined using the Logarithm Decrement Method described in the ‘numerical computation’ section. Using two consecutive peaks (the valleys) and applying Equation (3.2), the silica deposit has a lower damping factor than the biofilm deposits, as indicated in Table 3.3.

The damping factor is specific of each type of deposit: a more viscoelastic layer will produce a higher damping factor variation than a more rigid deposit. When a deposit adheres to the surface it becomes part of the vibrating system and will have different effects on the attenuation of the vibrations according to its viscoelasticity (in the present case, the latter seems to be related to the dry density of the deposit).

These results emphasize the need to integrate the two wave parameters (normalized amplitude and damping factor) in order to obtain accurate information about the amount and the type of deposit (elasticity/compactness) attached to the surface.

### 3.3.3. Sedimentation effect on the MSS signal

Can the MSS signal variation be caused by any mass located on the surface, even if it is not actually attached to the surface? To answer this question, a few experiments were performed where simple sedimentation (deposition caused only by gravity effects) was induced. Aqueous suspensions with different silica particle concentrations and different particle dimensions were evaluated. These tests were carried out during only one hour, in the absence of flow, which favored the sedimentation process of the particles to the surface without firm attachment. The results are presented in Figure 3.8.

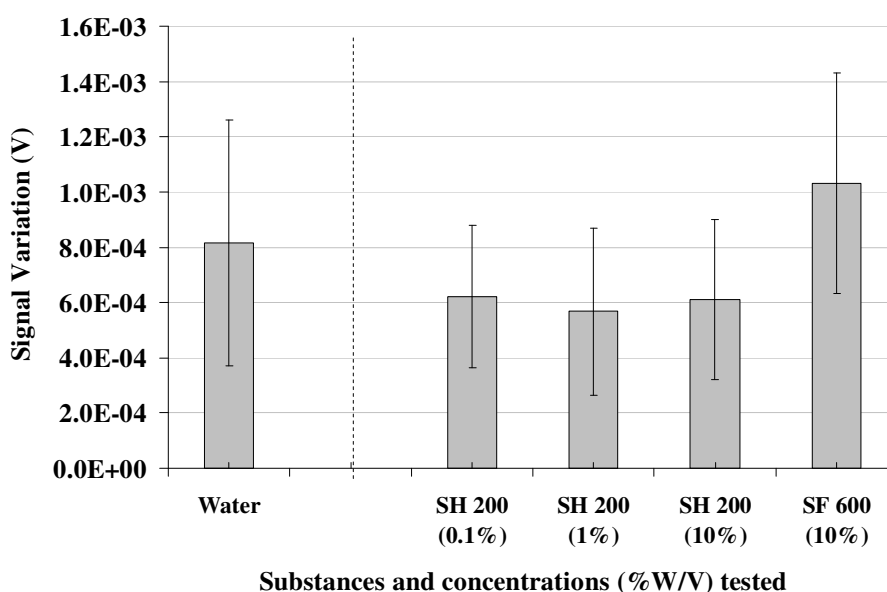


Figure 3.8: MSS signal variation due to the sedimentation of several silica deposits

Figure 3.8 show that the sedimentation of different types of silica deposits has no significant effect on the MSS output signal. It can be seen that the signal variation obtained with the particle suspensions is not different (attending to the standard errors associated with each determination) from the signal variation caused by the water with no particles. This means that without attachment the deposit is not properly integrated in the vibrating system and that the MSS is only fitted to monitor deposits which are actually adhered to the surfaces. Sedimentation effects can, therefore, be neglected when compared to the adhesion effects of the deposits.

### **3.4. CONCLUSIONS**

The MSS (Mechatronic Surface Sensor) is an on-line device that uses the propagation of nanovibrations along a surface to monitor the development of deposits attached to that surface. The results presented in this paper demonstrate that the MSS can give information not only about the amount of deposit forming on (or being removed from) the surface, but also about the physical properties related to the viscoelasticity of the deposit, by determining the FFT amplitude of the propagated wave and the damping factor (energy dissipation parameter). Therefore, biological layers, which are usually more viscoelastic, can be distinguished from inorganic deposits by their higher damping factor. Such information is of great importance in, for example, cooling water lines where the selection of adequate anti-fouling chemical treatments (biocides, acid cleaning solutions, etc.) depends on the type of deposit that is building up on the pipe walls. The on-line, real time information produced by the MSS will enable timely counter-measures to be taken.

An additional interesting feature of the MSS is the fact that it mainly detects deposits that are really attached to the surfaces and not simply located there by gravity effects without adhesion to the surface. The former are the ones that need special attention when choosing proper cleaning methods for their removal.

### **REFERENCES**

- Brito, A. G. and L. F. Melo (1999). "Mass transfer coefficients within anaerobic biofilms: Effects of external liquid velocity." Water Research **33**(17): 3673-3678.
- Flemming, H.-C. L. (2003). "Role and levels of real-time monitoring for successful anti-fouling strategies - An overview." Water Science and Technology **47**(5 Number): 1-8.
- Janknecht, P. and L. F. Melo (2003). "Online Biofilm Monitoring." Reviews in Environmental Science and Biotechnology **2**(2): 269.
- Melo, L. F. and J. D. Pinheiro (1984). Fouling tests: equipment and methods. In: Suitor JW, Pritchard AM, editors. Fouling in heat exchange equipment, New York: ASME-Heat transfer Division.
- Melo, L. F. and M. J. Vieira (1999). "Physical stability and biological activity of biofilms under turbulent flow and low substrate concentration." Bioprocess Engineering **20**(4): 363-368.

Mendes, J., L. F. Melo, A. Mendes and A. Pereira (2005). Method and device for the measurement and identification of biofilms and other deposits using vibrations. FEUP. Portugal. N° 103 344.

Mendes, J., L. F. Melo, A. Mendes and A. Pereira (2006). Method and device for the measurement and identification of biofilms and other deposits using vibrations. FEUP. *Pending Patent* (PCT/IB2006/052992).

Nakra, B. C. (1998). "Vibration control in machines and structures using viscoelastic damping." Journal of Sound and Vibration **211**(3): 449-465.

Nivens, D. E., J. Q. Chambers, T. R. Anderson and D. C. L. White (1993). "Long-Term, Online Monitoring of Microbial Biofilms Using a Quartz Crystal Microbalance." Analytical Chemistry **65**(1): 65-69.

Nivens, D. E., R. J. Palmer and D. C. L. White (1995). "Continuous Nondestructive Monitoring of Microbial Biofilms - a Review of Analytical Techniques." Journal of Industrial Microbiology **15**(4): 263-276.

Panteliou, S. D., T. G. Chondros, V. C. Argyrakis and A. D. Dimarogonas (2001). "Damping factor as an indicator of crack severity." Journal of Sound and Vibration **241**(2): 235-245.

Pereira, A., R. Rosmaninho, J. Mendes and L. F. Melo (2006). "Monitoring deposit build-up using a novel mechatronic surface sensor (MSS)." Food and Bioproducts Processing **84**(4 C): 366.

Pereira, M. O., P. Morin, M. J. Vieira and L. F. L. Melo (2002). "A versatile reactor for continuous monitoring of biofilm properties in laboratory and industrial conditions." Letters in Applied Microbiology **34**(1): 22-26.

Rosmaninho, R., O. Santos, T. Nylander, M. Paulsson, M. Beuf, T. Benezech, S. Yiantsios, N. Andritsos, A. Karabelas, G. Rizzo, H. Müller-Steinhagen and L. F. Melo (2007). "Modified stainless steel surfaces targeted to reduce fouling - Evaluation of fouling by milk components." Journal of Food Engineering **80**(4): 1176-1187.

Shabana, A. A. (1991). Theory of vibration - Volume I - An introduction. New York, Springer-Verlag.

Towler, B. W., C. J. Rupp, A. L. B. Cunningham and P. Stoodley (2003). "Viscoelastic Properties of a Mixed Culture Biofilm from Rheometer Creep Analysis." Biofouling **19**(5): 279-285.

Vieira, M. J. and L. F. Melo (1995). Effect of clay particles on the behaviour of biofilms formed by *Pseudomonas fluorescens*. Water Science and Technology. **32**: 45-52.

Vieira, M. J., L. F. Melo and M. M. Pinheiro (1993). "Biofilm formation - hydrodynamic effects on internal diffusion and structure." Biofouling **7**: 67-80.





## **4. MONITORING DEPOSITS BUILD-UP USING A NOVEL MECHATRONIC SURFACE SENSOR (MSS)**

### **ABSTRACT**

The formation and removal of deposits obtained from milk components (calcium phosphate and whey proteins) were monitored using a new device based on the effect of fouling on the vibration properties of the deposition surface. The MSS (Mechatronic Surface Sensor - pending Patent n° 103 344, Portugal) was able to detect the growth of the deposit mass (and its removal) and to distinguish between deposits with different structural properties (calcium phosphate *versus* protein deposits).

### **4.1. INTRODUCTION**

Fouling is a common, almost unavoidable hazard in food processing plants, since the material being processed often contains components such as proteins, microorganisms and inorganic salts that are natural precursors for the build-up of unwanted deposits on surfaces. Fouling occurs both on the process side and on the auxiliary heating/cooling fluid side of heat transfer equipment, as well as in isothermal units such as reverse osmosis membranes. In a milk pasteurizing unit, for example, fouling layers composed of proteins and mineral salts develop during the heating process, whereas microbial films appear predominantly on the cooling section of the pasteurizer.

The strategy to minimize the deleterious effects of fouling in food processing plants cannot be based on modification of the food fluids themselves. It has to consider a set of different approaches such as optimizing the design and operating parameters of the industrial equipment (heat exchangers, tanks, tubes, etc.), choosing surface materials that reduce initial adhesion or favour the cleaning procedures, and closely monitoring not only the formation of the fouling layer but also its removal (detachment) during the cleaning phase. Determining the right time to stop the heating/cooling process or to end the cleaning procedures are crucial

informations that improve the efficiency of the whole unit as regards energy saving, minimization of production losses, cleaning and wastewater treatment costs.

The present work addresses the question of on-line monitoring of fouling and cleaning, introducing a new device for use both in industry and in research labs. Although a number of fouling monitoring techniques have been reported (Flemming 2003; Janknecht and Melo 2003), not many can be said to be feasible for current industrial applications. Some do not display enough resolution to detect the initial deposit build-up (such as pressure drop measurements), others can be too expensive or technically difficult to be implemented in the field and operated by non-specialists (e.g., quartz crystal balance or photoacoustic spectroscopy).

The following requirements were taken into consideration when devising the new approach: (i) to have enough resolution and accuracy to detect the build-up of deposits virtually from the beginning of the fouling process; (ii) to be sufficiently robust for application in industrial plant conditions; (iii) to be applicable to practically all types of industrial surface materials (metals, plastics, glass); (iv) to be easily operated by non-specialists; (v) to be less expensive than most of the equivalent techniques; (vi) to be able to provide some information on the kind of material attached to the surface. After reviewing the existing methods (Janknecht and Melo 2003), a technique based on the propagation of nanovibrations along the deposition surface was developed and called Mechatronic Surface Sensor (MSS). This device is being patented (Mendes et al. 2005). The principles behind this technique had already been previously applied in totally different situations such as the detection of loose screws in mechanical equipment. The innovation here was to develop this technique for application in ducts where a fluid is flowing often in turbulent regime and to identify small amounts (masses) of deposits adhered to surfaces. Deposits with different composition were studied and in one case the fouling data obtained with the MSS were compared with the data obtained using heat transfer monitoring methods.

Contrarily to other devices that are based on similar principles (e.g., the quartz crystal microbalance), the MSS is not in direct contact with the fluid: this allows the use of different surface materials and avoids additional sources of contamination. Furthermore, the MSS is able to integrate the information obtained from deposits that occupy a sufficiently large area

to avoid possible misinterpretations when measuring very small localized deposits. In the present configuration, the MSS monitor is placed outside the industrial equipment, in a by-pass stream (i.e., with the real fluid flowing there), where the hydrodynamic conditions can be controlled in order to mimic the ones prevailing in the processing unit. One advantage of the by-pass option is that it allows to independently test various alternatives for cleaning (and various surfaces, if needed) before using them in the industrial process itself. However, if desired, it is possible to design these devices in order to be applied directly within the industrial equipment (in-line).

#### 4.1.1. Description of the Mechatronic Surface Sensor (MSS)

The basic idea behind the MSS relies on the fact that the attachment, growth and detachment of deposits produce changes on the vibration properties of surface waves. It also takes advantage of the resonant frequency of the system to work at the maximum output response.

The MSS monitor used in the present work is composed of a stainless steel (SS) plate (length = 212 mm, width = 29 mm and thickness = 0.6 mm) that occupies the flat base of a semi-circular duct made of PERSPEX<sup>®</sup> (internal diameter = 30.0 mm, equivalent diameter = 18.3 mm, length = 1200 mm) - Figure 4.1. This flow cell is similar to the one described in Chapter 3.

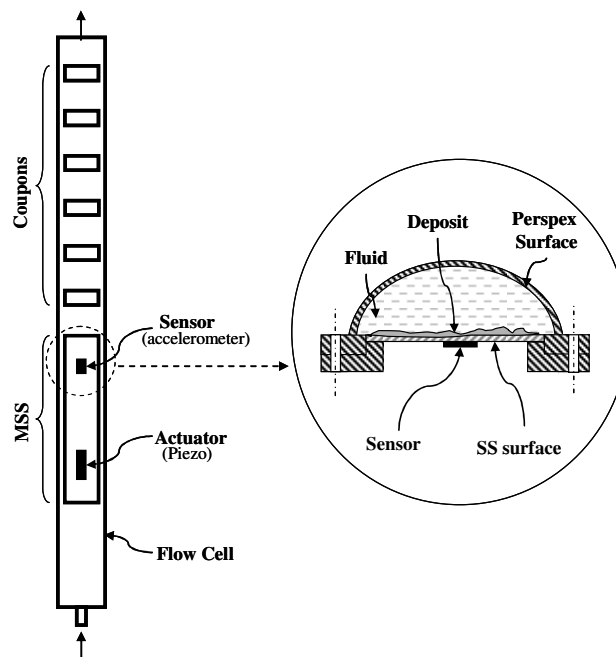


**Figure 4.1:** Schematic representation of the flow cell containing the MSS

An actuation and a sensor element are attached to the plate, on the face that is not in contact with the liquid flowing inside the duct. The actuation element makes the stainless steel vibrate. This vibration is then captured by the sensor. Both the actuation and sensing process are performed automatically at constant intervals. The actuator is a piezoelectric ceramic (BM 70/25/200 M, from Piezomechanick), so it produces mechanical stress (a bending deformation in the present case) when submitted to an electrical field. The accelerometer sensor is a small chip (ADXL-103, from Analog Devices) that measures acceleration and relates it to extremely small vibrations. Additional information about the used transducers can be read in Appendix B. Both the actuator and the sensor are glued on the outer surface of the plate at a distance of 9 cm, the monitored area being 18 cm<sup>2</sup>. The MSS semi-circular flow cell has 6 coupons. The coupons can be removed during the experiment, or at the end of it, to determine the physical characteristics of the deposit.

The excitation voltage is generated via a data acquisition board (National Instruments, NIDAQ-card PCI-6221) and directly applied to the piezo actuator. The measured vibration is also read by the same board. The synchronization between the signal generation and the signal acquisition is performed by a digital trigger signal. The vibration waves are collected periodically and automatically during the experiments (acquired each 5 minutes), and mathematically processed with proper digital signal processing (DSP) techniques. Some of the characteristics determined, are: frequency, amplitude, 'flight' time, peak-to-peak value, damping factor, and FFT amplitude ( $A_{FFT}$ ) among others. The amplitude nevertheless showed to be the best parameter to monitor the formation and removal (detachment) of the deposits. A full automatic measuring system was developed in LabVIEW<sup>®</sup> 7.1 and allows an easy operation and data interpretation.

The  $A_{FFT}$  of the output signal is inversely proportional to the amount of deposit attached to the surface. To obtain a curve similar to the ones usually reported in fouling studies (i.e., showing a direct relation between the measured variable and the amount of deposit), a normalization procedure was performed by subtracting all the values collected during the experiment from the initial value. The damping factor is another important parameter that can be determined from the MSS measurements and represents the capacity that a mechanical system has to reduce the intensity of a vibration process. Its calculation is based on the decrease of the maximum amplitude of the output (response) wave per unit time. The damping factor

variation is specific of each type of deposit a more viscoelastic deposit will have a higher damping factor variation than a more rigid deposit. This was shown in the present study, as described below.

#### **4.2. MATERIALS AND EXPERIMENTAL METHODS**

In this work, fouling caused by various fluids was induced on the MSS stainless steel surface in order to obtain deposits having different physical properties. Three types of deposits were monitored: (1) calcium phosphate deposit; (2) calcium phosphate and whey protein deposit; and (3) whey protein deposit alone.

Calcium phosphate deposits were obtained from SMUF (Simulated Milk Ultrafiltrate), which is an aqueous solution that simulates the mineral composition of milk. This solution was prepared according to Jenness and Koops (1962).

Calcium phosphate and whey protein deposits were obtained from SMUF with the addition of a commercial WPI (Whey Protein Isolate, Lacprodan DI-9224, provided by Arla Foods, Ingredients Amba, Denmark). The protein was dissolved in the SMUF solution in order to achieve a concentration 3 g/l of  $\beta$ -Lg. Whey protein deposits were obtained from a 3 g/l  $\beta$ -Lg solution prepared with the WPI.

The three experiments were performed at a constant temperature of 50 °C and the hydrodynamic conditions were also kept constant during the entire experiments at a Reynolds number of 8600 (turbulent regime). For comparison purposes, a calcium phosphate (SMUF) deposition test was carried out under the same conditions in another flow cell (a heat flow cell) where fouling monitoring is carried out by measuring the thermal resistance of the deposit over time. This flow cell has similar dimensions as the MSS flow cell and its main features are described elsewhere (Vieira et al. 1993). The *pH* of the three fluids in the MSS monitor, as well as for the SMUF deposition in the heat flow cell, was adjusted to 6.8 before the experiment started, but afterwards it was left free to vary throughout the experiment. Changes in *pH* (increasing from 6.8 to 7.6) were monitored and found to be similar in all the experiments. After a stable amount of deposit was reached (pseudo-steady state), the foulant

solution was replaced by a dilute solution of nitric acid (0.5%) at 50 °C in order to clean the surface and monitor the cleaning process.

In order to determine the error associated with the  $A_{FFT}$  measurement, 10 consecutive acquisitions at the same experimental conditions (temperature and flow velocity) before each experimental trial were accomplished. The standard deviation obtained for all the determinations were: 0.002 V, which correspond to the error bars in the following graphs.

### 4.3. RESULTS AND DISCUSSION

#### 4.3.1. Calibration of the MSS normalized amplitude with the deposit dry mass

A calibration procedure of the MSS normalized amplitude with the deposit dry mass was set, in order to evaluate the physical meaning of the sensor output response (Figure 4.2). The deposit was obtained from a SMUF solution composed mainly by calcium phosphate. The different dry masses were obtained by collecting coupons from the flow cell at different stages of deposit formation. The relation between these two measured parameters indicates that higher signal variations are observed for higher amounts of dry deposit.

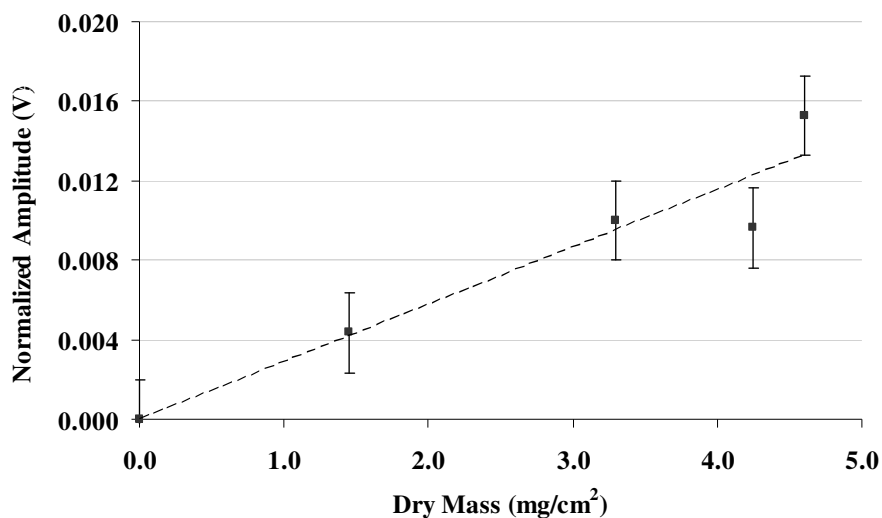


**Figure 4.2:** Variation of the MSS normalized amplitude with the deposit dry mass obtained from a SMUF solution

Every time a new device is set up, it is essential to perform a calibration similar to the one previously described since the specific numerical correlation between the MSS normalized amplitude and the deposit mass is dependent on the assembled system characteristics, although it always follows the same trend (the normalized amplitude increases with the increase of deposit).

**4.3.2. Monitoring deposition from SMUF solutions with the MSS and the heat flow cell**

With the purpose of comparing the information given by the MSS and the more traditional heat transfer technique, fouling caused by calcium phosphate from the SMUF solution was monitored by the MSS and by a heat flow cell in parallel identical experiments. The resulting deposition curves are similar, as shown in Figure 4.3.

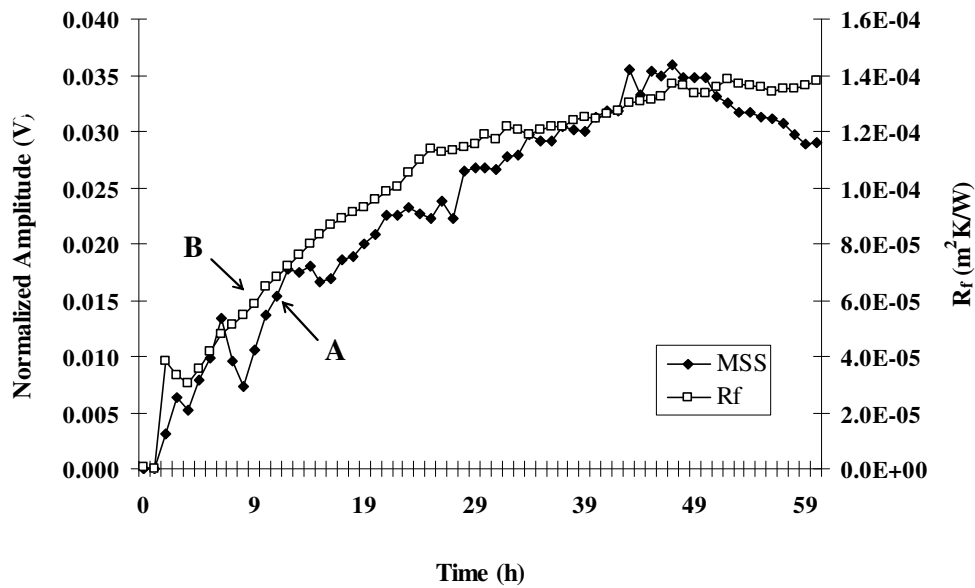


**Figure 4.3:** SMUF deposition curve assessed by MSS and heat flow cell ( $R_f$  – thermal resistance of the deposit,  $m^2/K W$ )

In order to verify the relative physical meaning of the curves, samples of the deposit were collected after similar deposition periods and the respective dry masses were determined (error associated with the mass determination  $\pm 0.0001$  g). Point A in Figure 4.3 indicates the sample collected from the MSS flow cell while point B represents the sample collected from the heat flow cell. The dry masses shown in Table 4.1 are comparable which allows to say that the two curves give similar information about the two identical fouling tests and that a

relation can be established between the normalized amplitude from the MSS and the thermal resistance from the heat flow cell.

**Table 4.1:** Correspondence between the mass of SMUF deposits and the measured parameters in two different sensors (MSS and heat flow cell)

| System   | Deposit dry mass (mg/cm <sup>2</sup> ) | MSS normalized amplitude (V) | Rf (m <sup>2</sup> K/W) |
|----------|--|------------------------------|-------------------------|
| SMUF (A) | 2.8                                    | 0.015                        | ----                    |
| SMUF (B) | 3.0                                    | ----                         | 6.0 x10 <sup>-5</sup>   |

### 4.3.3. Damping factor for different deposits

When we are dealing with similarly structured deposits, differences in the MSS response can be directly related to differences in the amount of deposit dry mass. However, how to interpret the MSS signal when comparing deposits with different physical properties? Previous studies carried out by the authors with SMUF alone and with SMUF plus whey protein (Rosmaninho and Melo 2005) under batch conditions showed that, for the temperature range used here, calcium phosphate is the component that determines the deposit structure in both cases. Images obtained with SEM (Scanning Electron Microscope) confirm that the structures of the two deposits are similar and dominated by calcium phosphate aggregates (Figure 4.4).

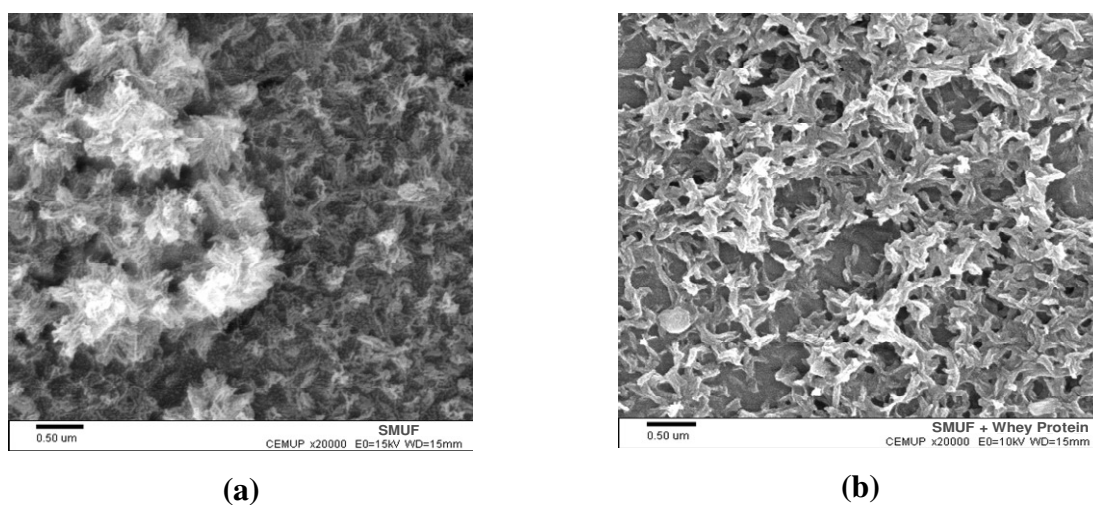


**Figure 4.4:** SEM images of: a) SMUF deposit and b) SMUF with whey protein deposit



A deposition experiment using a solution of SMUF with whey protein addition was performed and monitored with the MSS. The comparison of the latter with the original SMUF deposition curve is shown in Figure 4.5. Apart from a yet unexplainable “excursion” of the second experiment between hours 10 and 30, the two curves generally agree. The damping factor variation of these two deposits is the same (see Table 4.3), reinforcing the idea of their structural similarity as regards vibration properties.

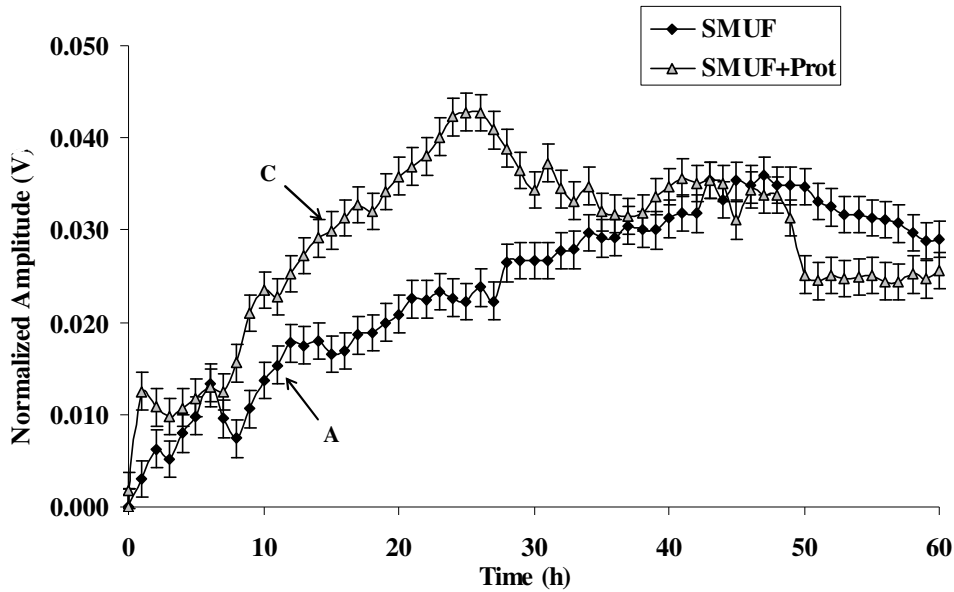


Figure 4.5: SMUF and SMUF plus whey protein deposition curves assessed by MSS

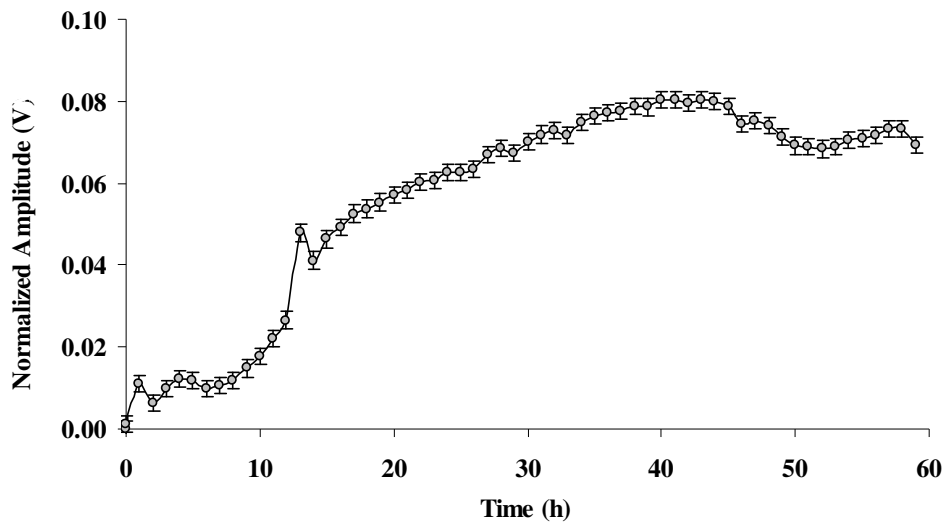
The correlation between the normalized amplitude in both systems and the dry mass of the correspondent deposits was once more obtained by collecting samples from the flow cell. Points A and C (Figure 4.5) represent, respectively, samples of SMUF and SMUF plus whey protein deposits taken at different time instants. Based on the relationship shown previously between the normalized amplitude and the dry mass of the deposit, it is clear that the higher MSS signal found for point C corresponded to a higher dry mass (Table 4.2).

Table 4.2: Relationship between the mass of SMUF, SMUF plus whey protein deposits and the output signal of MSS

| System                  | Dry mass (mg/cm <sup>2</sup> ) | MSS normalized amplitude* (V) |
|-------------------------|--------------------------------|-------------------------------|
| SMUF (A)                | 2.8                            | 0.015                         |
| SMUF + Whey protein (C) | 8.3                            | 0.030                         |

\* The relation between the normalized amplitudes and the dry masses provided in Table 4.2 (for the SMUF) is not comparable with the one shown in Figure 4.2 since they were obtained with two different MSS systems.

To evaluate the MSS response to the build-up of a deposit with a clearly different structure, the fouling curve of whey protein alone was monitored (Figure 4.6).



**Figure 4.6:** Whey protein deposition curves obtained by MSS

This type of deposit is much more gelatinous than the ones based on calcium phosphate controlled structures. This was reflected in a 50% increase of the damping factor variation when compared to the SMUF based deposits (Table 4.3). Thus, “different physical properties” mean different “rigidity” or different “elasticity”, corresponding to different vibration properties. This is a physical feature of the fouling layers that the MSS is able to distinguish among different deposits.

**Table 4.3:** Damping factor variation for different deposits

| System              | Damping factor variation |
|---------------------|--------------------------|
| SMUF                | 0.014                    |
| SMUF + Whey protein | 0.014                    |
| Whey Protein        | 0.021                    |

The mass of protein deposit determined at the end of the experiment was around  $1.0 \text{ mg/cm}^2$ , corresponding to a MSS signal of  $0.070 \text{ V}$  (see Figure 4.6). It is interesting to note that in the case of the calcium phosphate deposit, a larger mass, of around  $3.0 \text{ mg/cm}^2$ , resulted in a much smaller output signal ( $0.015 \text{ V}$ ), as indicated in Table 4.2. This confirms the effect of the viscoelasticity on the MSS signal and the relevance of determining the damping factor.

However, there are mutual interacting effects of the two parameters ( $A_{FFT}$  and damping factor) that need to be separately analysed and fully quantified in further experiments.

#### 4.3.4. Using the MSS to monitor cleaning

The MSS can also be used to follow the removal of deposits during cleaning. Two illustrative examples are presented in Figure 4.7.

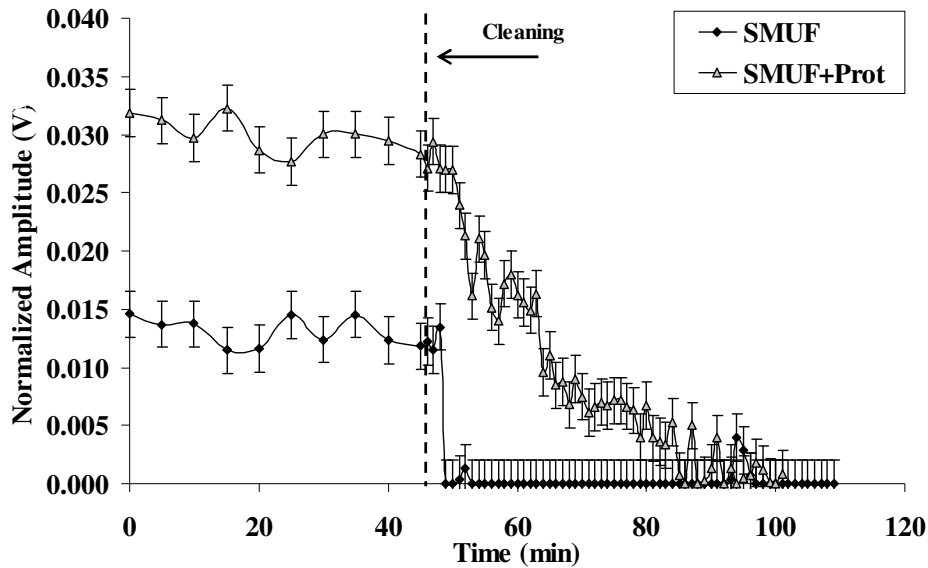


**Figure 4.7:** Cleaning of SMUF and SMUF with whey protein (SMUF+Prot) deposition curves assessed by MSS

The cleaning agent used in both cases was a dilute nitric acid solution which is widely used to clean mineral deposits. It was expected that under those cleaning conditions, the presence of whey protein in one of the deposits would be responsible for a longer cleaning period since it helps in keeping together the calcium phosphate aggregates (Visser and Jeurnink 1997) and, also, because protein layers are usually better cleaned with alkali solutions (Gillham et al. 1999). This was supported by the MSS data which showed a smoother (less steep) cleaning curve for the mineral-protein layer when compared to a pure mineral deposit.

#### 4.4. CONCLUSIONS

The MSS device measures changes in the vibration properties of the surfaces due to the build-up or removal of fouling layers. It gives quantitative information about two parameters of the

vibration wave that are used to characterize the fouling process: the normalized amplitude and the damping factor variations. For a given deposit, the normalized amplitude reflects changes on its amount: higher normalized amplitudes are observed for higher amounts of attached deposit. The damping factor variation contributes for the characterization of the deposit structure: higher damping factors variations are observed for more elastic deposits.

The main distinguishing features of MSS as compared to other known sensors like the QCM (Quartz Crystal Microbalance) or SAW (Surface Acoustic Wave) are: (1) this sensor can be applied to real industrial surfaces (stainless steel, PVC, etc) with any type of flow regime (laminar or fully turbulent); (2) the measurements are made without any contact with the fluid under study; (3) the sensor integrates measurements over a significantly larger area.

Another relevant feature of the MSS device is that the sensor is also capable of monitor with great accuracy the cleaning processes allowing the distinction between different cleaning rates.

Future work will be aimed at clarifying quantitative aspects of these issues and obtaining correlations for the identification of the main characteristics of the fouling material.

### **REFERENCES**

Flemming, H.-C. L. (2003). "Role and levels of real-time monitoring for successful anti-fouling strategies - An overview." Water Science and Technology **47**(5 Number): 1-8.

Gillham, C. R., P. J. Fryer, A. P. M. Hasting and D. I. Wilson (1999). "Cleaning-in-place of whey protein fouling deposits: Mechanisms Controlling Cleaning." Food and Bioproducts Processing: Transactions of the Institution of of Chemical Engineers, Part C **77**(2): 127-136.

Janknecht, P. and L. F. Melo (2003). "Online Biofilm Monitoring." Reviews in Environmental Science and Biotechnology **2**(2): 269.

Jeness, R. and J. Koops (1962). "Preparation and properties of a salt solution which simulates milk ultrafiltrate." The Netherlands Milk and Dairy Journal **16**(3): 153-164.

Mendes, J., L. F. Melo, A. Mendes and A. Pereira (2005). Method and device for the measurement and identification of biofilms and other deposits using vibrations. FEUP. Portugal. N° 103 344.

Rosmaninho, R. and L. F. Melo (2005). Assessment of the influence of the surface energy properties of stainless steel on fouling caused by calcium phosphate and by whey proteins. Proceedings of the 9th International Chemical Engineering Conference (Chempor'05). Coimbra, Portugal.

Vieira, M. J., L. F. Melo and M. M. Pinheiro (1993). "Biofilm formation - hydrodynamic effects on internal diffusion and structure." Biofouling 7: 67-80.

Visser, J. and T. J. M. Jeurink (1997). "Fouling of heat exchangers in the dairy industry." Experimental Thermal and Fluid Science 14(4): 407-424.



## **5. MONITORING CLEANING-IN-PLACE PROCESSES USING NANOVIBRATION TECHNOLOGY**

### **ABSTRACT**

Monitoring fouling and cleaning processes has become an important issue to optimize production cycles, increase the quality of the final product and reduce environmental impacts. The aim of the present study is to use nanovibrations to detect the cleaning end-point of hair shampoo removal under different cleaning conditions. A new monitoring tool (MSS – Mechatronic Surface Sensor) was found to be able to clearly identify when the equipment was cleaned and measure the rate of cleaning by showing the real-time cleaning curves, which depend on the operating conditions.

### **5.1. INTRODUCTION**

The problems associated with fouling are well known and well documented, and are usually associated with a decrease of the heat transfer rate, an increase of the pressure drop and, in food and biotechnological production plants, can endanger the process sterility. In order to keep the operational efficiency of the processing plant, removal of these deposits is required. Both the deposit formation and its removal/cleaning introduce huge costs (due mainly to maintenance, production breaks, consumption of water/chemicals and wastewater treatment) into the production processes.

During the last decade, different approaches have been assessed in order to reduce fouling or to easily remove these unwanted deposits. Such approaches go from the use of ‘Computer Fluid Dynamics’ (CFD) to optimize the design of the processing equipment and the production/cleaning cycles (e.g. Friis and Jensen 2002; Asteriadou et al. 2007), to the development of new surface materials that show promising results concerning the reduction of the initial adhesion and the improvement of the cleaning efficiency (Rosmaninho and Melo 2006; Rosmaninho et al. 2007).

Additionally, scientists and engineers have been looking for faster, more precise and less expensive ways to monitor the build-up and removal of fouling layers in order to optimize both the production and the cleaning cycles. Some authors reviewed the most well known fouling monitoring techniques (e.g. Janknecht and Melo 2003; Hasting 2005). Hastings (2002) lists temperature and pressure measurements among the most commonly applied industrial monitoring techniques. These techniques can provide valuable indications about the conditions of the deposits on the surfaces of the processing plant but they have their drawbacks: pressure drop is usually not sensitive enough to detect the first attached layers or accurately assess the cleaning status of the surfaces after CIP (Cleaning-in-place), while heat transfer techniques are either non-specific (if only the inlet and outlet fluid temperatures are measured) or rather expensive and subject to almost unavoidable errors in wall temperature measurements.

The authors of the present paper developed a new monitoring method based on the effect that the attachment and detachment of deposits have on the vibrations properties of the monitored surface. An on-line fully integrated device called MSS (Mechatronic Surface Sensor) was set-up using a piezoelectric element to produce surface vibration. This vibration propagates along the surface, is picked up by the sensor element (accelerometer) and is mathematically processed through: i) time-domain measurements (such as peak-to-peak amplitude, flight time among others); and ii) frequency domain measurements, namely FFT (Fast Fourier Transforms) determinations (the highest amplitude and frequency were analyzed). Other methods based on the propagation of acoustic waves have been reported. Hay and Rose (2003) and Lohr and Rose (2003) proposed the use of ultrasounds (such as guided waves, normal beam and pulse-echo) which require highly sophisticated and more expensive equipment than the MSS (which works with a much lower frequency – around 5 kHz). The work of Merheb et al. (2007) follows the principle previously applied to the MSS by the authors of the present paper Pereira et al. (2006) although with a different configuration since it uses one transducer in the upper part of the heat-exchanger to produce an acoustic impact which is then received by three sensors placed on the bottom part of the monitored structure. Furthermore, Merheb et al. (2007) also use different variables of the response curves to follow the fouling deposition: the acoustic power and delay of the acoustic signal. The former papers reported the application of ultrasounds for fouling detection mainly in the food industry.



The problem addressed in the present paper is the on-line measurement of the removal of the residual shampoo film that is found on the equipment walls during cleaning procedures. The work will then be focused on demonstrating that the structural properties of fluids/films (which are distinct from the usually more consistent fouling layers) will differently affect the vibration of the monitored surface and, therefore, can be measured by the nanovibration device. This will ultimately allow the optimization of the cleaning procedures which are so frequent in plants that produce a great diversity of personal care products such as shampoos and cosmetic creams.

## **5.2. MATERIALS AND METHODS**

### **5.2.1. Summary of the MSS working principle**

The MSS working principle is based on vibration analysis to detect and evaluate the amount and nature of a deposit that is attached to the surface. The adhesion or removal of the deposits affect the  $A_{FFT}$  of the output signal, which was found to be inversely proportional to the amount of deposit attached to the monitored surface. The damping factor (energy dissipation) is also another wave parameter that, complementarily to the amplitude, reflects the structural nature of the deposit. This previous work (Pereira et al. 2006) also reported that the MSS was found to accurately follow the build-up of a milk deposits obtained from mineral (Simulated Milk UltraFiltrate- SMUF) and whey protein solutions on a stainless steel surface, through the analysis of the properties of the surface wave. As regards the structural characteristics of the deposits, higher damping factors were observed for more elastic deposits: since the whey protein has a more elastic structure than the calcium phosphate layer, it presented a higher damping factor. That work (Pereira et al. 2006) also reported the capacity of the MSS to measure different cleaning rates, depending on the type of deposit and cleaning agents.

The cleaning end-point is one important issue concerning the optimization and flexibility of manufacturing plants (Wilson 2005). The question addressed in the present paper was to find out if the MSS could detect the cleaning end-point of the shampoo films removal on shampoo processing equipment. Shampoos and other personal care products are expected to have certain characteristics that make them unique to costumers. These characteristics rely basically on rheology (Balzer et al. 1995) which mainly affects the slow flow rate of the

shampoo from its bottle and the easy way it is distributed on the hair and on the scalp. Since shampoo has quite distinct physical properties from those of water (the cleaning medium), the vibration that propagates along the production plant tubing is affected by this difference and, therefore, different  $A_{FFT}$  values should be observed for the water and for the shampoo. It seems that the shampoo characteristic that mostly affects the MSS signal is its viscoelasticity. The absolute amplitude obtained with shampoo will be smaller than the amplitude obtained with water. Because of this, the acquired signal was normalized in order to be similar to a typical cleaning curve (amount of shampoo decreasing with time). This signal (represented by the variable  $A_{inv}$ ) varies between 0 and 1, these values corresponding, respectively, to the cleaned stainless steel (SS) surface and to the SS tube filled with shampoo (initial state).

### 5.2.2. Description of the MSS measuring system

In the present configuration, the actuating and sensing elements are attached to the outer surface of a stainless steel (SS) plate that replaces the flat base of a semi-circular flow cell made of PERSPEX<sup>®</sup> (internal diameter = 30.0 mm, equivalent diameter = 18.3 mm; length = 350 mm) – Figure 5.1. Two advantages of this system are: (i) the actuating and sensing elements are not in contact with the fluid, avoiding possible contamination; (ii) almost any type of industrial surface can be tested with this device.

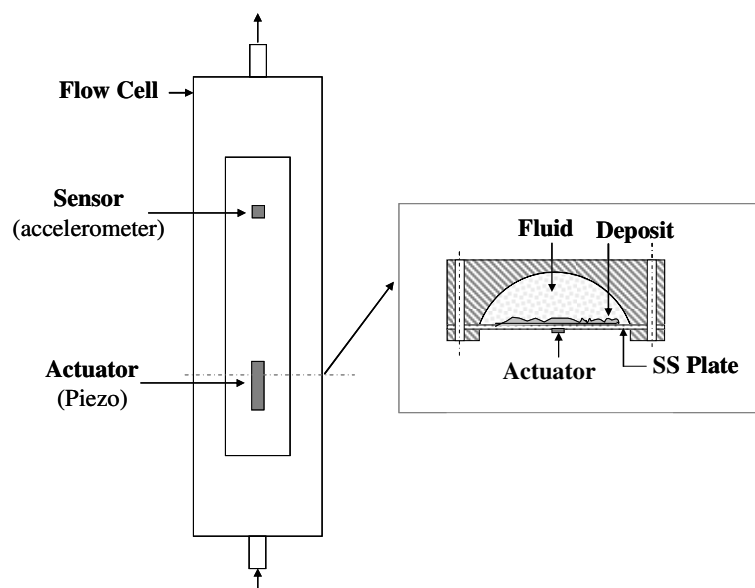


**Figure 5.1:** Schematic representation of the MSS inserted into the flow cell

The actuator (piezo) and the sensor (accelerometer) – see Appendix B - elements are glued to the outer surface of the SS plate at a distance of 9 cm, corresponding to a monitoring area of 18 cm<sup>2</sup>, giving therefore an average information about the contamination of this area which overcomes possible interpretation errors due to very localized measurements

One of the important characteristics of the MSS is the fact that it takes advantage of the resonance frequency of the system, guarantying that the maximum output signal is obtained. The MSS measures changes in the vibration characteristics of the surface due to fouling formation/removal (or in the present case due to the shampoo cleaning). Both the actuating and the sensing processes are automatically carried out via a data acquisition board (National Instruments, NIDAQ-Card PCI-6221) inserted into the computer. The SS plate is actuated by a piezo element (BM 70/25/200 M, Piezomechanik) with a sinusoidal wave with 5.1 kHz (which matches the resonant frequency of the system) and the vibration response is then captured by an accelerometer (ADXL-103, Analog Devices) and mathematically processed to determine the  $A_{FFT}$ .

### 5.2.3. Experimental cleaning conditions

The specific goals of the present experiments were to evaluate the MSS performance – repeatability and reliability - on following the removal of shampoo from the monitored surface. Furthermore, different cleaning conditions (temperature and flow velocity) were used to determine the influence of such parameters on the cleaning of shampoo layers (cleaning time and mass detached) – see Table 5.1.

**Table 5.1:** Experimental conditions used to remove the shampoo from the MSS duct

| Temperature (°C) | Velocity (m/s) | Reynolds number |
|------------------|----------------|-----------------|
| 31               | 0.14           | 3300            |
| 31               | 0.21           | 5000            |
| 51               | 0.14           | 4800            |
| 51               | 0.41           | 13800           |
| 51               | 0.47           | 16000           |

In order to fulfill these goals, a commercial hair shampoo with trade name SUNSILK<sup>®</sup> (color radiant) was used. The physical characteristics of this shampoo are: density - 1.03 g/l and viscosity 7000 cp (at 24 °C). The density was determined by weighing a given volume of shampoo. A viscometer ViscoStar Plus (from Fungilab) with spindle PB was used to assess the viscosity of the shampoo.

### **5.2.3.1. Cleaning procedure**

The same cleaning procedure was sequentially applied in each experiment:

1) The “water baseline” was determined by measuring the signal amplitude obtained with water recirculating at the defined temperature and velocity (see Table 5.1):  $A_{inv} = 0$  ( $A_{FFT}$  correspondent to the initially clean flow cell -  $A_{FFT\_water}$ );

2) The flow cell was filled with shampoo – Figure 5.2 (A). The  $A_{FFT}$  was determined for the shampoo at room temperature ( $A_{FFT\_shampoo}$ ) and with no recirculation:  $A_{inv} = 1$ .

3) The shampoo film was removed (with water under the conditions stated in point 1) and the  $A_{FFT}$  of the stabilization zone was determined – Figure 5.2 (B). When the MSS signal reaches the zero value ( $A_{inv} \approx 0$ ), it means that the flow cell is cleaned. On the other hand, if an output signal between  $0 < A_{inv} < 1$  is obtained it means that there is still a shampoo film attached to the sensor surface. It is important to notice that the cleaning experiments were carried out without recirculating the water.

It was found out that the experimental conditions affect differently the  $A_{FFT}$  parameter. Being so, a previous calibration between the  $A_{FFT}$  and the temperature and flow velocity has been performed – according to the results shown in Appendix C. Note that the  $A_{inv}$  was determined after a normalization procedure (based on the  $A_{FFT}$  measurements) which is described in Section 5.2.4.

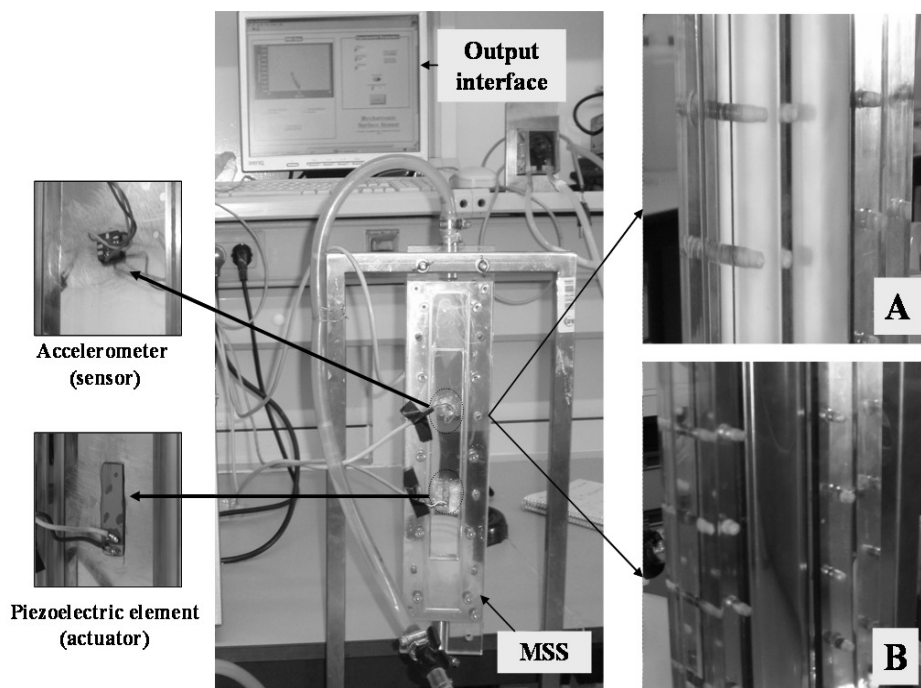


**Figure 5.2:** Picture of the experimental setup with a detailed view of the accelerometer and the piezoelectric element. Additionally the back view of the MSS flow cell is provided: A) flow cell filled with shampoo; B) flow cell after being cleaned

### 5.2.3.2. Cleanliness confirming methods

In several experiments the cleanliness of the flow cell was confirmed by visual inspection, absorbance and contact angle measurements.

- Visual inspection: photos and movies were taken during the cleaning process. The movies allow a qualitative checking of what happened in terms of the shampoo removal at a given cleaning time, for different removal conditions (for example as shown in Figure 5.2 B))
- Spectrophotometry: at the end of the experiment, the flow was stopped and the flow cell inner walls were brushed (keeping the water in the flow cell). Then the water was drained out of the flow cell and the absorbance of this bulk water was determined using a spectrophotometer (T80 UV/VIS Spectrometer, PG instruments Ltd) at  $\lambda = 225$  nm. The blank (control) sample was tap water (identical to the tap water used to remove the shampoo).

In order to perform the calibration of the MSS signal with the amount of shampoo film attached to the flow cell walls, a relationship of the shampoo absorbance vs shampoo mass was previously determined. Solutions with different concentration of shampoo were prepared and their absorbance measured with the spectrophotometer. This relation is indicated in the discussion section.

- Contact angle (CA) measurements: the basic procedure used to determine this parameter was similar to the one used to evaluate the absorbance of the bulk fluid. After draining the water out of the flow cell, the SS plate was unscrewed and the CA was determined on the MSS surface (fluid side). The CA values were determined by the sessile drop method in a contact angle equipment (DataPhysics OCA15 Plus) using water as reference liquid. The quantification of the contact angles was carried out using an image analyzing system. The comparison between the CA values for the initially clean stainless steel plate (before contacting the shampoo) and for the same plate after the removal experiments is a measure of the cleanliness of the surface.

#### 5.2.4. $A_{inv}$ normalization and determination of the error associated with it measurement

Appendix C shows the relation between the  $A_{FFT}$  and the temperature and flow velocity. During a given experimental trial, each  $A_{FFT}$  value acquired is corrected according to that relation previously obtained (for a standard temperature of 35 °C and flow velocity of 0.35 m/s). Then the respective  $A_{inv}$  calculation is performed according to the following relation:

$$A_{inv\_i} = \frac{A_{FFT\_water} - A_{FFT\_i}}{A_{FFT\_water} - A_{FFT\_Shampoo}} \quad (5.1)$$

The determination of the  $A_{FFT\_water}$  and of the  $A_{FFT\_shampoo}$  was based on 10 consecutive measurements obtained before each experimental trial. They correspond respectively to the  $A_{FFT}$  signal obtained for water (recirculating at the cleaning experimental conditions) and to the shampoo  $A_{FFT}$  signal (flow cell filled with shampoo). It was found that the standard deviation associated with the  $A_{FFT\_water}$  was independent of the experimental condition under study and equal to 0.003 V. The same standard deviation was observed for the  $A_{FFT\_shampoo}$ . The error associated with each  $A_{inv\_i}$  normalized value was determined (based on the error propagation theory), according to the following equation (Taylor 1997):

$$\sigma_{A_{inv\_i}} = \sqrt{\left( \frac{\partial A_{inv}}{\partial A_{FFT\_water}} \sigma_{A_{FFT\_water}} \right)^2 + \left( \frac{\partial A_{inv}}{\partial A_{FFT\_Shampoo}} \sigma_{A_{FFT\_Shampoo}} \right)^2 + \left( \frac{\partial A_{inv}}{\partial A_{FFT\_i}} \sigma_{A_{FFT\_i}} \right)^2}$$

Where,  $\sigma$  is the standard deviation associated with the subscripted quantity. This  $\sigma_{A_{inv_i}}$  value is the error determined for each specific case and shown in the graphs.

With the calibration and normalization implemented the  $A_{inv}$  value only reflects the effect of the shampoo removal, rather than the effects of temperature or flow velocity.

### 5.2.5. Repeatability experiments

In order to determine the repeatability of the MSS signal, 3 removal trials were made. The removal procedure and the experimental conditions were the same in the 3 assays:  $T = 51\text{ }^{\circ}\text{C}$  and flow velocity = 0.41 m/s.

### 5.2.6. Statistical analysis

To determine if it is possible to assume that the means of the 3 tests are equal, an independent  $t$ -test has been made (using a commercial statistical software SPSS<sup>®</sup>). This test is used to compare the statistical significance of a difference between the means of two groups when they are independent of each other. The test assumes that all sources of uncontrollable random variation will equally affect each treatment. The variable will be the  $A_{inv}$  value obtained with the MSS (for each of the 3 trials) which was independently obtained.

In order to correctly apply this statistical test, the data should meet some requirements: i) the samples should be randomly and independently taken from the population; ii) the population variances should be equal – homogeneity of variances; iii) the population should be normally distributed. All of the mentioned assumptions were truly confirmed for the tested data. The 3 trials have been compared in groups of two: repetition 1 with repetition 2; and repetition 1 with repetition 3. For each of the two groups the null hypothesis ( $H_0$ ) assumes equal means between the tested repetitions:

$$H_{0a}: \mu_{repetition1} = \mu_{repetition2}$$

$$H_{0b}: \mu_{repetition1} = \mu_{repetition3}$$

In order to test the null hypothesis, the significance level (set to 0.05 in the present case) is compared with the probability obtained from the significance test. The significance level is a probability (previously specified) that when compared with the test probability allows to

reject or accept the null hypothesis. If the test of significance gives a probability smaller than the one of the significance level then the null hypothesis should be rejected. The significance test shows stronger evidence when the significance level is smaller.

### 5.3. RESULTS AND DISCUSSION

#### 5.3.1. MSS repeatability

The first part of the present work was focused on the study of the repeatability of the MSS signal. The shampoo removal experiments were repeated three times at constant cleaning conditions. Water was flushed through the flow cell at 0.41 m/s and 51 °C. Figure 5.3 shows the shampoo removal curves obtained with the MSS for the 3 repetitions.

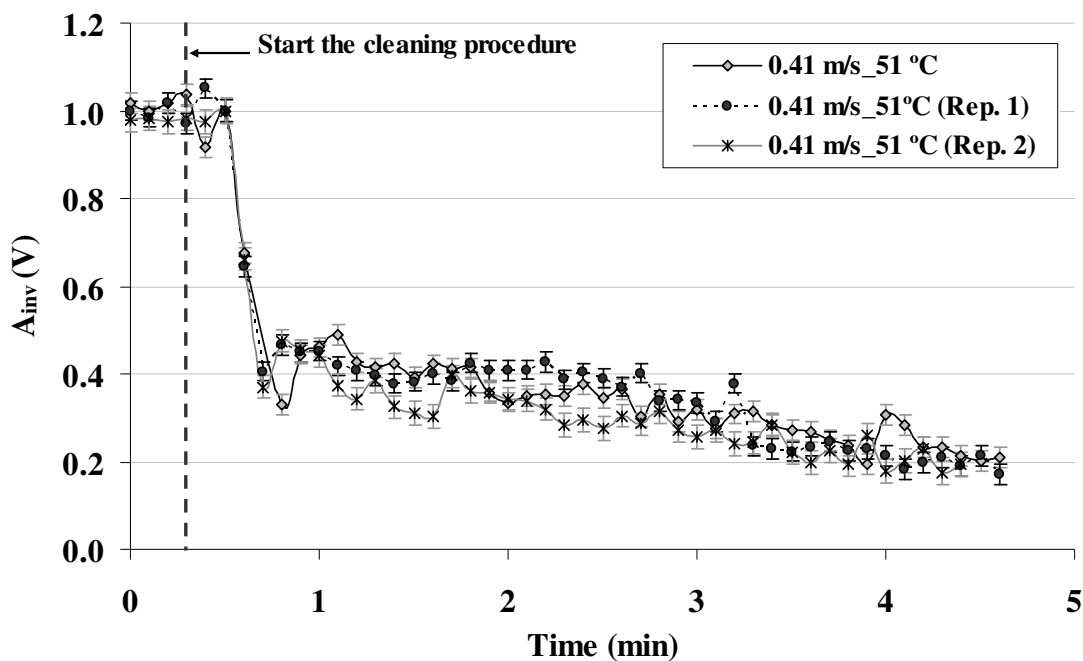


**Figure 5.3:** MSS output response when the shampoo is removed with water at 0.41 m/s and 51 °C (3 repetitions of similar conditions)

When the water enters the flow cell, the MSS output signal starts to decrease. This is in accordance to what is expected since (taking into account the normalization described in the ‘Material and Methods’ section), as far as the shampoo is removed, the  $A_{inv}$  signal starts to decrease, reaching 0 V when there is no film attached to the SS surface. On the other hand,  $A_{inv}$  does not start to decrease immediately when the water flushes the flow cell (first points



after starting the cleaning procedure), since the initial flush includes the removal of the bulk shampoo and of the loosely attached film. That is also why the rate of decrease is much higher ( $A_{inv}$  decreases abruptly) in the beginning of the cleaning procedure – during the first minute - than from this point until the end.

Figure 5.3 also shows that the 3 cleaning curves obtained for analogous cleaning conditions (0.41 m/s and 51 °C) are very similar. The results of the statistical analysis obtained for case A (repetition 1 is compared with repetition 2) and for case B (repetition 1 is compared with repetition 3) are shown in Table 5.2. It can be seen that in both cases the equality of variances is obtained, since the Levene’s Test has a  $p > 0.05$  (Sig. is 0.598 and 0.656 respectively for case A and for case B). Also, the  $t$ -test significance is higher (Sig. is 0.972 and 0.345 respectively for case A and for case B) than 0.05 indicating that in both cases the equality of means can be assumed for a confidence level of 95%.

**Table 5.2:** Significance results of the Levene’s and t-tests (confidence of 95%)

|   | <b>Sig. of Levene’s Test</b><br>(Equality of variances) | <b>Sig. (2-tailed) of <math>t</math>-test</b><br>(Equality of means) |
|---|---|--|
| Case A<br>(Rep.1 is compared with rep. 2) | 0.598   | 0.972  |
| Case B<br>(Rep.1 is compared with rep. 3) | 0.656   | 0.345  |

Therefore, the results in Table 5.2 demonstrates that there is statistical evidence to assume the equality of the data collected in the 3 repetitions and to conclude that the MSS produces repeatable data.

### 5.3.2. MSS reliability

Although the repeatability of the MSS has been demonstrated, it is still important to find out if the  $A_{inv}$  parameter does actually represent what is happening in the monitored surface. In order to study the reliability of the MSS output data, an independent method - spectrophotometric – was used. Figure 5.3 shows that after 4.5 min the shampoo was not fully removed from the SS surface ( $A_{inv} \approx 0.19$  V). So, at the end of each cleaning trial the procedure described in the ‘Cleanliness confirming methods – Spectrophotometry’ section

was performed. Figure 5.4 represents the end-point absorbance obtained for different  $A_{inv}$  values.

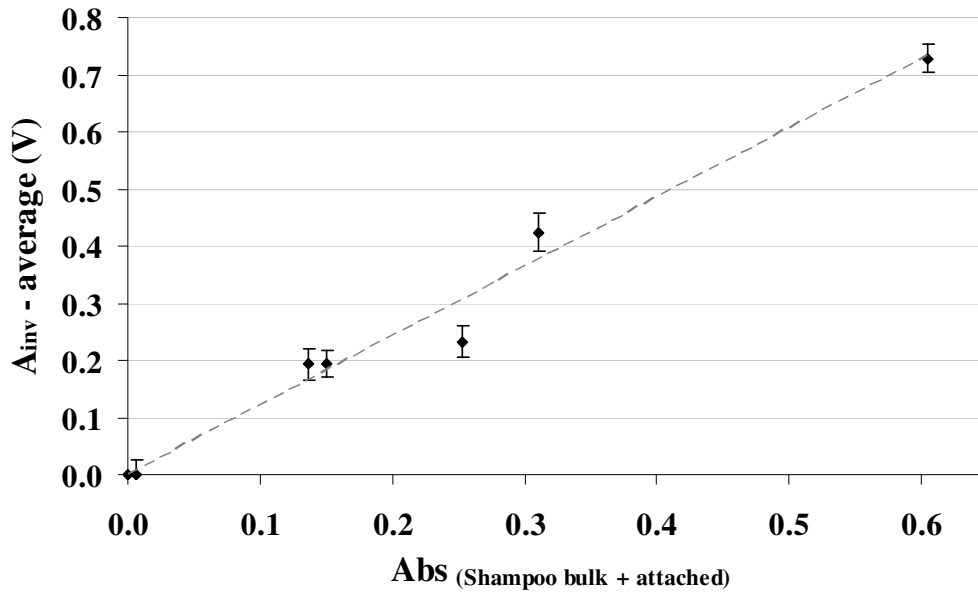


**Figure 5.4:** Relation between the  $A_{inv}$  (determined at the end of each trial) and the absorbance of the collected water – after brushing and draining the flow cell ( $R^2 = 0.9782$ )

Figure 5.4 shows a good fitting between the MSS output signal ( $A_{inv}$ ) and the absorbance of the water collected from the flow cell. This result suggests that the MSS can be used to reliably monitor the removal of shampoo layers from SS surfaces. Complementary experiments were made in order to relate the MSS output signal with the amount of shampoo that stays inside the flow cell. For such purpose, a previous calibration between the mass of shampoo and the absorbance was performed. This calibration is represented by Equation (5.2) ( $R^2 = 0.9984$ ).

$$\text{Absorbance} = 2.2507 \times \text{Mass of shampoo (mg)} \quad (5.2)$$

It is then possible to relate  $A_{inv}$  with the amount (mass) of shampoo that remains in the flow cell, by determining the absorbance after each trial and applying Equation (5.2). As shown in Figure 5.5, this relation ( $A_{inv}$  vs mass of shampoo) follows an approximately linear pattern.

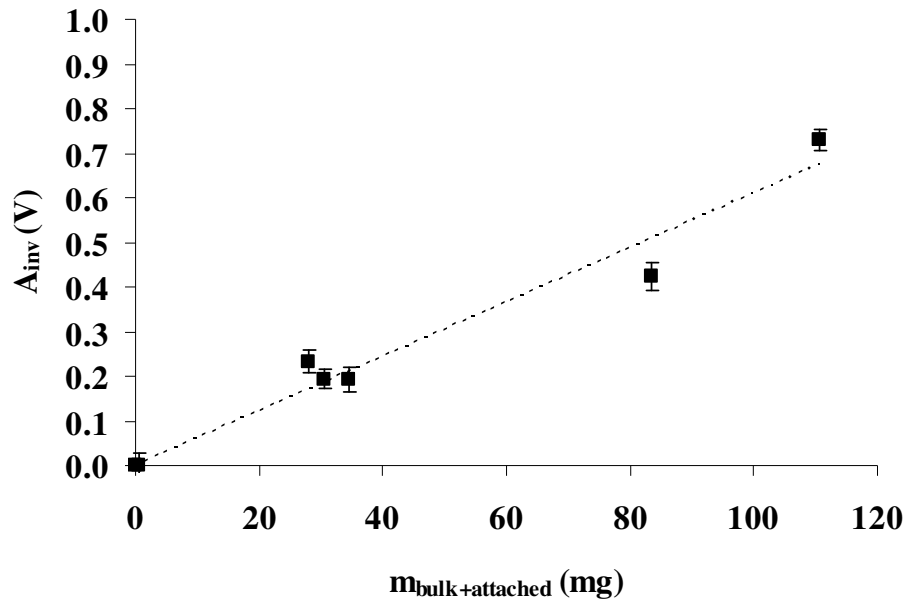


**Figure 5.5:** Relation between the  $A_{\text{inv}}$  and the mass of shampoo that remains in the flow cell after the cleaning procedure ( $R^2 = 0.9633$ )

Figure 5.5 re-emphasizes that when  $A_{\text{inv}}$  decreases there is also a decrease of the amount of shampoo in the flow cell. For example, looking at the removal of shampoo at 0.41 m/s and 51 °C, in Figure 5.3, it can be concluded that the amount of film that remains in the flow cell after 4.5 min is  $32.6 \pm 2.9$  mg (which corresponds to 12.7% of the total mass that filled the tube).

### 5.3.3. Effect of different cleaning conditions (flow velocity and temperature) on the MSS response

The former conclusions demonstrated the repeatability and reliability of the MSS, but they also suggested that an efficient shampoo removal process may be dependent on the cleaning conditions. In order to study the influence of the cleaning conditions on the shampoo removal, several trials at different conditions were performed. The experimental plan included the comparison of different flow velocities (0.14 m/s and 0.47 m/s) and different temperatures (31 °C and 51 °C). These results can be seen in Figure 5.6.

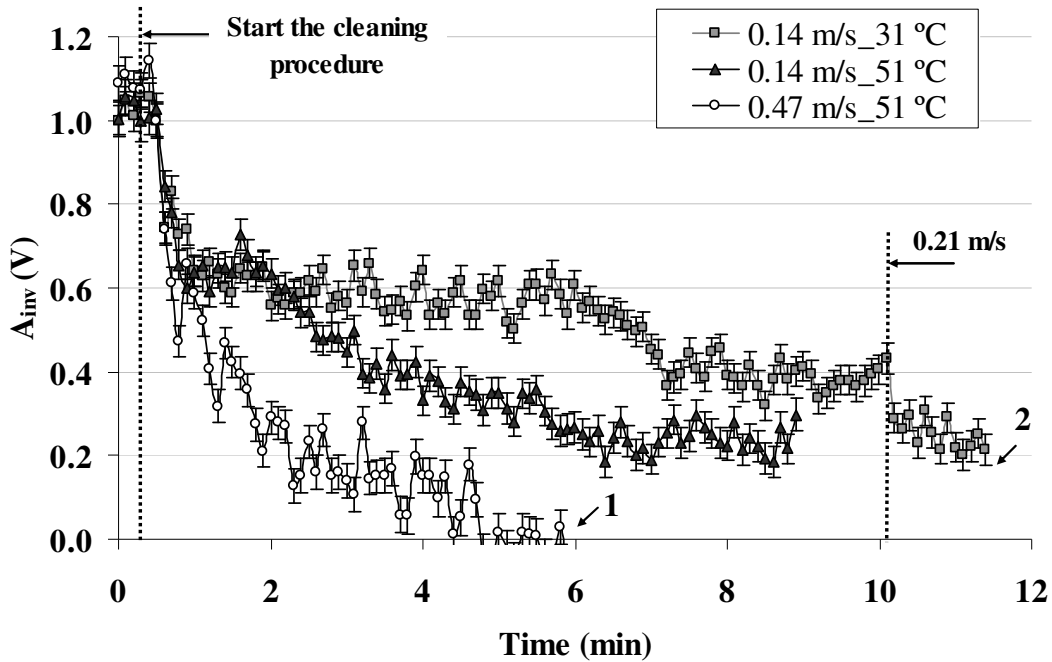


**Figure 5.6:** Cleaning of attached shampoo film with water at 0.47 m/s and 51 °C, 0.14 m/s and 31 °C and 0.14 m/s and 51 °C

The comparison of the shampoo removal curves in Figure 5.6 indicates that the removal process is highly dependent on the water flow velocity and temperature. The cleaning curves obtained with water flowing at 0.14 m/s present a final steady-state period after the bulk removal. It can also be seen that the steady-state period has a higher  $A_{inv}$  value for the removal at 31 °C (from 0.8 min to 6.0 min) than for 51 °C (from 0.8 min to 2.0 min). This observation confirms that the removal of shampoo layers is slower at lower temperatures, which can be explained by the well known fact that higher temperatures are more efficient in dissolving shampoo components.

On the other hand, when considering the curves obtained at the same temperature (51 °C), it can be seen that the higher flow velocity (0.47 m/s) is more efficient for the removal of the attached shampoo films. For example, an amount of shampoo equivalent to  $A_{inv} = 0.20$  V is removed in only 2 min at 0.47 m/s, while it takes almost 6 min to remove it at 0.14 m/s.

In the case of the removal experiment at 0.14 m/s and 31 °C, the flow velocity was increased, after about 10 min to 0.21 m/s (as indicated in Figure 5.6). After this procedure the  $A_{inv}$  decreased, corresponding to the removal of an additional amount of shampoo (as visually confirmed). At point 1 and 2 in Figure 5.6, corresponding to the time where the two

experiments were stopped, the water was drained, the monitored plate was removed from the flow cell and was set to dry. In both cases, the contact angle of the plate (i.e., of the face in contact with the fluid) was measured. These results were then compared with the contact angle of the clean SS plate (previously determined) and the results are shown in Table 5.3.

**Table 5.3:** MSS  $A_{inv}$  signal and contact angle measurement at points 1 and 2 (Figure 5.6) and of the initially clean stainless steel surface

|                     | Point 1        | Point 2        | Clean SS       |
|---------------------|----------------|----------------|----------------|
| MSS – $A_{inv}$ (V) | 0.00           | 0.22           | 0.00           |
| Contact angle (°)   | $41.6 \pm 3.8$ | $33.3 \pm 4.6$ | $46.6 \pm 2.0$ |

The data obtained with this independent method (the contact angle measurement) confirms that the MSS stainless steel plate is cleaned at point 1 (contact angle close to the one corresponding to the clean surface). On the other hand, at point 2, the contact angle is lower ( $33.3^\circ$ ) than the one obtained for the clean SS ( $46.6^\circ$ ) indicating the existence of a remaining film on the MSS surface. These results are in accordance with the conclusions taken from the absorbance method.

The importance of the temperature and of the flow velocity in the removal process has been already remarked. The next results will be focused on determining the influence of each of these parameters on the rate of the removal process. In order to do that, several removal curves (some of which using data already presented) corresponding to different removal conditions – different flow velocities and/or temperatures - were studied. For each pair of conditions (flow velocity and temperature), the  $A_{inv}$  value was determined after 2, 4 and 6 minutes. The results obtained are shown in Figure 5.7, where a), b) and c) correspond respectively to  $t = 2$  min,  $t = 4$  min and  $t = 6$  min.

It is perceptible from Figure 5.7 that the flow velocity and the water temperature have different contributions to the shampoo removal process. At the beginning of the cleaning procedure (graph 5.7a)), the effect of the flow velocity is much more noticeable than the effect of temperature, since for the two temperatures the lines of  $A_{inv}$  vs flow velocity are practically superimposed. On the other hand, as the removal process proceeds, the effect of the temperature becomes increasingly more important. For example, after 6 min (graph 5.7c)),

the amount of attached shampoo film is considerably different for  $T = 31\text{ }^{\circ}\text{C}$  or  $T = 51\text{ }^{\circ}\text{C}$ . When the removal is carried out at  $0.47\text{ m/s}$ , the surface is fully cleaned with water at  $51\text{ }^{\circ}\text{C}$ , while at  $31\text{ }^{\circ}\text{C}$  it still has an amount of shampoo film corresponding to  $A_{inv} = 0.28\text{ V}$ .

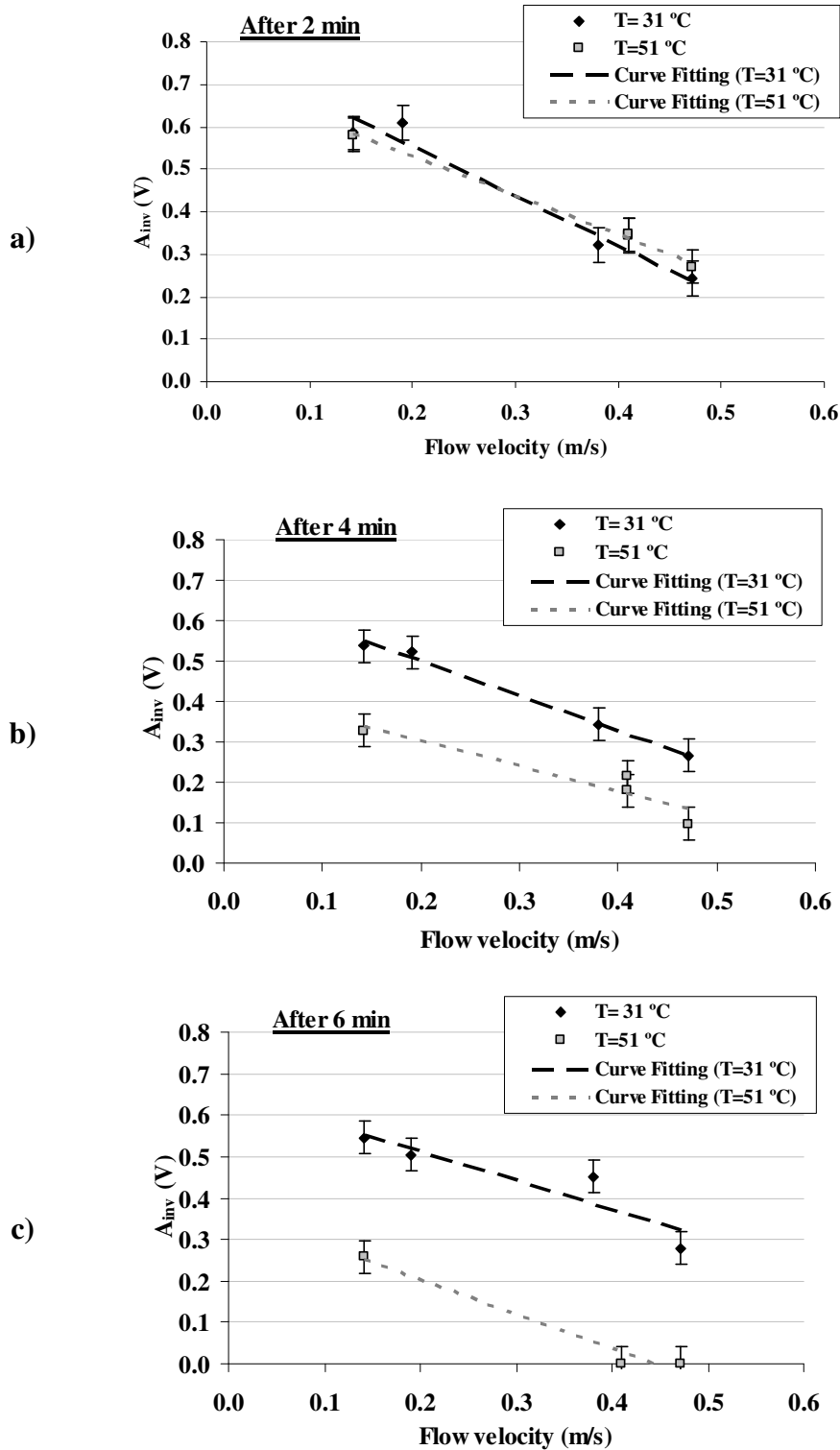


**Figure 5.7:** Variation of the  $A_{inv}$  signal with the flow velocity for  $T = 31\text{ }^{\circ}\text{C}$  and  $T = 51\text{ }^{\circ}\text{C}$ , after different removal times: a)  $t = 2\text{ min}$ , b)  $t = 4\text{ min}$  and c)  $t = 6\text{ min}$

#### **5.4. CONCLUSIONS**

The MSS (Mechatronic Surface Sensor) is a fully integrated on-line monitoring device that provides information about the amount and rates of build-up or removal of deposits and their nature. This paper shows that the MSS can also be used to detect cleaning end-points on shampoo cleaning processes. It also demonstrates that different cleaning conditions result in different rates of cleaning, which are accurately monitored by the MSS. The end-points determined by the MSS have been positively confirmed by spectrophotometry and contact angle measurements.

The characteristics of the MSS respond to three important questions regarding the optimization of industrial production and cleaning procedures: i) When should the plant be cleaned?; ii) How should the plant be cleaned?; iii) When is the cleaning end-point achieved and when should the cleaning procedure be stopped? Answering these questions contributes to the optimization of the cleaning-in-place process, improving the operational cycles of the plant, increasing the quality of the final product and saving in processing costs associated with the consumption of water, chemicals and energy, as well as reducing the pollutant load in wastewater treatment.

#### **REFERENCES**

Asteriadou, K., T. Hasting, M. Bird and J. Melrose (2007). "Predicting cleaning of equipment using computational fluid dynamics." Journal of Food Process Engineering 30(1): 88-105.

Balzer, D., S. Varwig and M. Weihrauch (1995). "Viscoelasticity of personal care products." Colloids and Surfaces A: Physicochemical and Engineering Aspects 99: 233-246.

Friis, A. and B. B. B. Jensen (2002). "Prediction of hygiene in food processing equipment using flow modelling." Food and Bioproducts Processing: Transactions of the Institution of Chemical Engineers, Part C 80(4): 281-285.

Hasting, A. P. M. (2002). Industrial experience of monitoring fouling and cleaning systems. Fouling, cleaning and disinfection in food processing. Cambridge, UK.

Hasting, A. P. M. (2005). Improving the monitoring of fouling, cleaning and disinfection in closed process plant. Handbook of hygiene control in the food industry. H. L. M. Lelieveld, M. A. Mostert and J. Holah. Cambridge - UK, Woodhead Publishing limited.

Hay, T. R. and J. L. Rose (2003). "Fouling detection in the food industry using ultrasonic guided waves." Food Control 14(7): 481-488.

Janknecht, P. and L. F. Melo (2003). "Online Biofilm Monitoring." Reviews in Environmental Science and Biotechnology 2(2): 269.

Lohr, K. R. and J. L. Rose (2003). "Ultrasonic guided wave and acoustic impact methods for pipe fouling detection." Journal of Food Engineering 56(4): 315-324.

Mendes, J., L. F. Melo, A. Mendes and A. Pereira (2005). Method and device for the measurement and identification of biofilms and other deposits using vibrations. FEUP. Portugal. N° 103 344.

Mendes, J., L. F. Melo, A. Mendes and A. Pereira (2006). Method and device for the measurement and identification of biofilms and other deposits using vibrations. FEUP. *Pending Patent* (PCT/IB2006/052992).

Merheb, B., G. Nassar, B. Nongailard, G. Delaplace and J. C. Leuliet (2007). "Design and performance of a low-frequency non-intrusive acoustic technique for monitoring fouling in plate heat exchangers." Journal of Food Engineering 82(4): 518-527.

Pereira, A., R. Rosmaninho, J. Mendes and L. F. Melo (2006). "Monitoring deposit build-up using a novel mechatronic surface sensor (MSS)." Food and Bioproducts Processing 84(4 C): 366.

Rosmaninho, R. and L. F. Melo (2006). "Calcium phosphate deposition from simulated milk ultrafiltrate on different stainless steel-based surfaces." International Dairy Journal 16(1): 81-87.



Rosmaninho, R., F. Rocha, G. Rizzo, H. Müller-Steinhagen and L. F. Melo (2007). "Calcium phosphate fouling on TiN-coated stainless steel surfaces: Role of ions and particles." Chemical Engineering Science 62(14): 3821-3831.

Taylor, J. R. (1997). An Introduction to error analysis: The study of uncertainties in physical measurements, University Science Books.

Wilson, D. I. (2005). "Challenges in cleaning: Recent developments and future prospects." Heat Transfer Engineering 26(1): 51-59.



## 6. OPTIMIZATION OF THE MSS CONFIGURATION

### OVERVIEW OF CHAPTER 6

In order to improve the MSS performance a new setup will be devised. The design of this new device will be based on the discussion of the vibration fundamentals behind the MSS. Some constraints (mainly due to its practical usage) to the build-up of this new prototype will be previously established. Fulfilling those requirements the dimensions of the monitored plate were optimized according to two criteria. Those simulations studies can be read in Section 6.2. Several simulations of the changes that different conditions (e.g. plate dimensions or different boundary conditions) have on the modal frequencies and shapes will be performed. In Section 6.3 the experimental modal analysis procedure (EMA) will be introduced as an approach to assess the vibrating characteristics of the system: the modal frequencies and damping ratios. This methodology (methodology 2) and the ‘standard’ procedure (methodology 1) used along the former chapters (the one that allowed to determine the  $A_{FFT}$  and of the  $DF$ ) will be compared. The preliminary tests of the new configuration of the MSS setup as well as the determination of the best sealing option can be read in Section 6.4. This section also discusses the linearity of the system as well as the effect of the water on the modal characteristics. Furthermore, a comparison between the results obtained by the two methodologies described will be established. The proof of concept (with calcium phosphate deposition) of this new configuration is discussed in Section 6.5. The ability of the two additional methods in following the adhesion/removal of deposit will also be evaluated. Some preliminary discussion about the effect of the temperature, flow velocity and flow regime in the modal characteristics of the system is accomplished in Section 6.6.

### 6.1. INTRODUCTORY NOTES

As widely reported in the former chapters the functioning principle behind the MSS is based on vibration. Vibratory phenomena occur permanently in the daily life (e.g. noise, music, driving, among many others). The theory of vibration studies the oscillatory motion of physical systems. In general a vibratory system includes (Rao 2004) a way:

a) for storing potential energy (spring or elasticity) -  $m$ ; the elastic components provide flexibility and store or absorb energy in mechanical systems. These elastic components restore the body forces according to its stiffness.

b) for storing kinetic energy (mass or inertia) -  $k$ ; inertia is a property of an object that makes it resist to any effort to change its state of motion or rest.

c) by which energy is gradually dissipated /lost (damper) -  $\zeta$ ; damping is the process of energy dissipation, reducing the amplitude of motion during the vibration process.

So, a vibratory phenomenon occurs from the balance between the inertial forces and from the restoring forces of the system (Rao 2004). Additionally, all of the mechanical systems are subjected to dissipative phenomenon which results from the transformation of mechanical energy into heat. It is possible to demonstrate (Appendix A, Equation A.3) that the essential parameters that characterize a given vibration system are: its natural frequency  $\omega_n$  (rad/s) and its damping  $\zeta$  (adimensional). When a system is actuated and left to vibrate on its own, the frequency with which it oscillates is named natural frequency. The damping, as already mentioned, is related with the energy dissipation of the system.

The definitions previously presented are the basis of the vibration studies. Since the analysis and results interpretation provided in the present chapter are intrinsically related with several concepts established and studied within the ‘theory of vibration’, an appendix with the most important concepts of such discipline is provided – Appendix A. Along this chapter several references to this appendix will be made.

## **6.2. SIMULATION STUDY**

Along the years, rectangular thin plates have gained the interest of structural engineers (Shuyu 2001). Analytical methods have been used to deal with the vibration of these plates with different boundary conditions. Based on some of these methods described in literature, different studies will be discussed during the present section:

a) The optimization of the plate dimensions based on two different approaches: i) maximization of the frequency separation of the first  $n$  modes; and ii) minimization of the frequency of the first  $n$  modes. This study was done for a clamped boundary condition. Based

on the output results, the most suitable criterion and the dimensions of the plate (to be used in this new configuration) were established.

b) Discussion of the effect that the boundary conditions have on the modal characteristics (frequencies and modal shapes) of a given plate. Applying the criterion chosen in the former point, the plate dimensions were optimized for the other two boundary conditions: free and simply-supported. The comparison between the different boundary conditions allows to discuss about the effect that each of them has on the plate vibration.

c) The modal characteristics of the new plate will be compared with the ones of the plate used in Chapter 4. The main difference between the two plates is their size (the thickness is constant – 0.6 mm).

The studies previously described were performed using a software developed in MATLAB<sup>®</sup>. This software has been kindly programmed by Dr. José Vieira Antunes (ITN - Nuclear Technology Institute, Lisbon). A brief explanation of the features of this software will be provided in Section 6.2.3.

### **6.2.1. Setup requirements**

The dimensions/configurations of the new plate have to fulfill some additional requirements, being:

1. The device should be inserted into a flow cell similar to the one used in Chapters 3 and 4. The structural characteristics of this flow cell make it quite practical to be used as a prototype model, because it has coupons and it is made of a transparent material - PERSPEX<sup>®</sup>. This latter point is important for adhesion/removal experiments since it enables visually control of what happens with the deposit.

2. The plate to be monitored should not be glued to any structure of the flow cell. The glue can be a problem on warranting reproducibility of the system, since: i) the amount of glue (used to keep the plate and the PERSPEX<sup>®</sup> structure together) is critical to the vibrating characteristics of the system, since different amounts of glue can lead to different vibration responses (e.g. more or less damped systems); ii) the physical properties of the glue change with temperature, which modifies the structural characteristics of the plate/structure system. The latter point may lead ultimately to leaking points between the plate and the structure (the sealing of the flow cell may be endangered).

3. The plate should be made of stainless steel, since this material is one of the most commonly used in industrial equipment. Furthermore, it has some advantages from the vibration point of view since it has a lower damping ratio (e.g. when compared to PVC). The plate should also have the same thickness of the ones used in the previous chapters that is 0.6 mm.

Based on these assumptions and requirements, the plate should be clamped between two PERSPEX<sup>®</sup> structures, similar to the schematic representation in Figure 6.1.

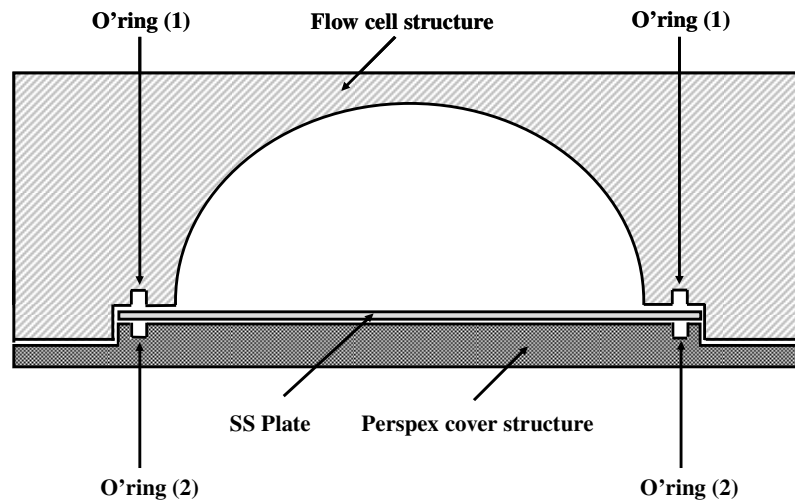


**Figure 6.1:** Schematic representation of the flow cell and the way the SS plate can be fixed

Due to assembly/manufacturing constraints, the maximum allowed plate dimensions are:  $A_{max}$  (length) = 225 mm and  $B_{max}$  (width) = 41 mm. According to Shuyu (2001) the physical characteristics of the stainless steel are:

Young's modulus,  $E$  (N/m<sup>2</sup>):  $1.95 \times 10^{11}$

Density,  $\rho$  (kg/m<sup>3</sup>):  $7.8 \times 10^3$

Poisson coefficient: 0.28

### 6.2.2. Optimization of the plate dimensions – governing equations

As discussed in the Appendix A, Section A.1.2 the systems can be modeled as multi-degree-of-freedom systems. This approach considers that the systems are modeled as lumped-parameters systems. That means that the motion at each point is modeled as if the mass were concentrated at that point. The parameters of the system are thus discrete set of finite numbers. There are also other approaches that model the mass and stiffness properties as

being distributed throughout the structure through infinitely small elements. When a structure vibrates, each of these infinite number of elements moves relative to each other in a continuous way. This area of vibration analysis is typically known as addressing ‘distributed-parameter system’ or as ‘continuous systems’. The choice between lumped or distributed parameters models depend on the nature of the system and the purpose of the study. Since continuous systems deal with partial differential equations (more difficult to solve than the ordinary differential equations of the multi-degree-of-freedom discrete models) there are only a few distributed-parameters models that have a closed-form solution (e.g. strings, bars, shafts, beams, plates and membranes with simple shapes and boundary conditions).

Distributed-parameters systems can be described spatially (in the time domain) by a continuous function of the relative position along the system (this spatial description for the lumped-parameters systems recurs to vectors). These systems are considered to have an infinite number of natural frequencies, which will be represented as:  $f_{m,n}$  for a two-dimensional structures. In order to find out those natural frequencies of the system, boundary conditions should be applied. A huge number of boundary conditions can occur for a rectangular plate, since each edge can have one of the three types of boundary conditions: free, simply-supported or clamped. In the case of the present Thesis, the analysis will be limited to the three cases previously mentioned, since the same boundary conditions will be equally applied to the four edges of the plate.

The software used in the present section uses analytical methods developed elsewhere. Since the discussion about how these methodologies were determined is not under the scope of the present Thesis, they will not be discussed here. The analytical solutions for the modal frequencies and the ones corresponding to their respective mode shapes can be found in:

- Vibration of rectangular thin plates with free boundary conditions – (Shuyu 2001);
- Vibration of rectangular plates with simply-supported (articulations) boundary conditions – (Reddy 2007);
- Vibration of rectangular clamped plates – (Arenas 2003);

### **6.2.3. Software design**

When an optimization procedure is performed it is necessary to define under what conditions/criteria it should be made. However, typically this is not an obvious choice and in

most cases a rigorous and realistic analysis of the results is desired and helps on determining if a given criterion is suitable or not for a given system. As analyzed in Appendix A, knowing the natural frequencies ( $f_n$  or  $\omega_n$  since  $\omega_n=2\pi f_n$ ) of the system are key parameters for an efficient vibration test. The two independent criteria that will be used to optimize the plate dimensions are:

- Criterion 1 - The maximization of the frequency separation between the  $n$  lower frequency modes: the separation between any two consecutive resonant frequencies is very important during damping quantification. It can be read in Appendix A, Section A.4 that the accuracy may be lost if during the modal identification, two consecutive peaks are closely spaced.

- Criterion 2 - The minimization of the frequency of the first  $n$  modes: recall the definition of transfer function represented by Equation (A.21) in Appendix A. When a vibrating mode is considered, the amplitude of such vibration is higher as the natural frequency of the system is smaller. So, in order to maximize the displacement response of the system, the frequencies of the first modes should be as small as possible.

These two criteria are independent, and may lead to different conclusions, giving an important input to the discussion of the dimensions of the MSS plate.

The software is able to perform:

**a) Optimization of the plate dimensions.** This part of the software requires the minimum and maximum dimensions of the plate to be considered (length -  $A$  and width -  $B$ ). For each pair of dimensions  $A$  and  $B$  the software determines the frequency of the  $n$  first modes and keeps them on memory. These calculations are done according to the specific equation found in the literature and mentioned above (according to the boundary condition established). Then, one of the following criteria is applied:

1. Maximization of the separation between the first  $n$  modes. The target function defined is the frequency separation between two consecutive modes, normalized by the frequency of the first mode:

$$f_{target}^{C1}(A,B) = \text{Min} \left( \frac{F_{i+1} - F_i}{F_1} \right), \quad \text{for } i = 1, 2, \dots, n-1 \quad (6.1)$$



It is not sufficient to look for the maximization of the target function since, for example, mode 1 and mode 2 can have frequencies very much separated while modes 3 and 4 may have almost identical frequencies (lower separation). In order to avoid this situation, for each plate dimensions the software stores the minimum frequency separation (the closest modes). So, the optimum plate dimensions are given by maximizing the target function given by Equation (6.1).

2. Minimization of the frequencies of the first  $n$  modes. For this criterion, the target function was defined as:

$$f_{target}^{C2}(A, B) = \frac{1}{\text{Max}(F_i)}, \quad \text{for } i = 1, 2, \dots, n \quad (6.2)$$

Maximizing the target function warranties that the optimum plate dimensions have the lower frequencies for the  $n$  modes considered. Since the software sorts the calculated frequencies, the maximum of  $F_i$  is always the frequency of the highest mode considered  $n$ ; so, the target function can be defined as:

$$f_{target}^{C2}(A, B) = \frac{1}{F_n} \quad (6.3)$$

**b) Determination of the frequency and mode shapes of the first  $n$  modes.** The dimensions of the plate to be studied should be entered on the software ( $A_{calc}$  and  $B_{calc}$ ). Note that these dimensions can be the ones determined in point a). The frequencies and modal shapes are analytically determined according to the boundary conditions of the system.

#### 6.2.4. Dimensions optimization: clamped boundary condition

The software maximizes the target function in the range of the considered dimensions, and outputs the pair of values that fulfills the chosen criterion requirements. As a first approach the clamped boundary condition will be studied.

Recall that the maximum dimensions of the plate have been previously established (Section 6.2.1). Let us consider that the plate could have as minimum dimensions, 50 mm long and 10 mm wide. The following parameters were used to perform the optimization:

- The range of dimensions is:

$$A_{min} \text{ (length): } 50 \text{ mm} \qquad A_{max} \text{ (length): } 225 \text{ mm}$$

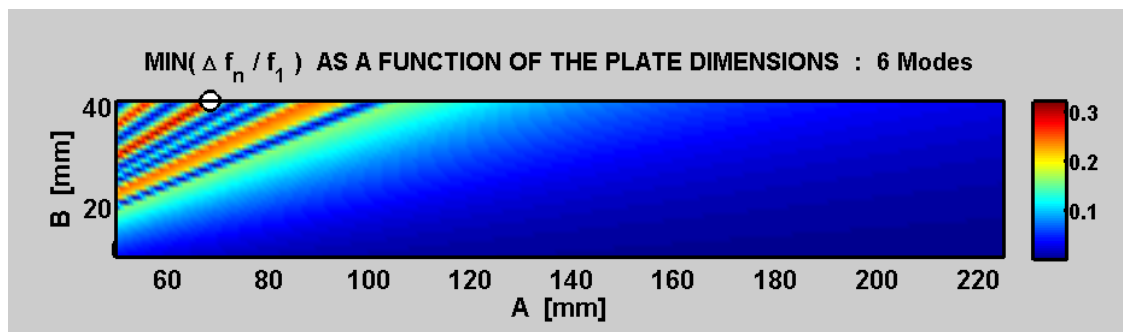
$$B_{min} \text{ (width): } 10 \text{ mm} \qquad B_{max} \text{ (width): } 41 \text{ mm}$$

- The thickness is constant for all of the simulations: 0.6 mm;
- The number of calculated modes is  $n = 6$ ;
- The boundary condition is clamped;

#### 6.2.4.1. Criterion 1 – Maximization of the frequency separation between the $n$ modes

The minimum frequency separation between two consecutive modes is plotted in Figure 6.2.

Criterion 1 - The maximization of the frequency separation between the  $n$  modes



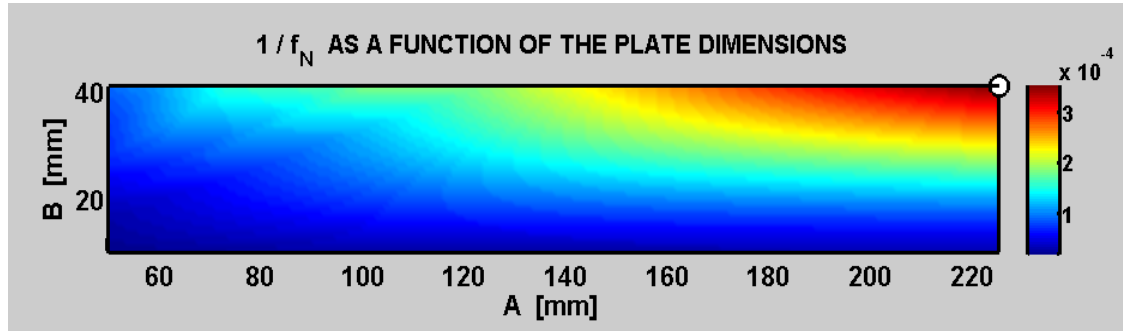
**Figure 6.2:** Target function values according to criterion 1 for plate with dimensions  $A$  and  $B$

Figure 6.2 shows the calculated values from the target function C1 – Equation (6.1). The optimum solution is indicated in Figure 6.2 with a white circle and the corresponding dimensions are:  $A = 68.5$  mm and  $B = 41.0$  mm. The color bar on the right side of the figure indicates the values of the target function: red color means higher values and blue color occurs to the lower frequencies separations. The type of representation in Figure 6.2 is very useful since it allows predicting which set of dimensions maximizes the frequency separation. It can also be seen that there are other sets of dimensions with target values similar to the ones obtained for the optimal solution.

#### 6.2.4.2. Criterion 2 – Minimization of the frequency of the first $n$ modes

An equivalent graphical representation is provided for the target function of criterion 2 in Figure 6.3.

Criterion 2 - The minimization of the frequency of the first  $n$  modes



**Figure 6.3:** Values of the target function according to criterion 2 for plate dimensions  $A$  and  $B$

Figure 6.3 shows that the set of dimensions that maximizes the target function are the ones in the top-right end of the plate:  $A = 225.0$  mm and  $B = 41.0$  mm. In fact, according to criterion 2 the best dimensions of the MSS plate are the maximum ‘allowed’ for this simulation. It also shows that, when the maximum length ( $A$ ) is considered, there is an increase of the frequencies of the first  $n$  modes (decrease of the values of the target function) with the decrease of  $B$ . Similarly, it is possible to see that the function values decrease (the frequencies of the first  $n$  modes increase) with the decrease of  $A$ , when  $B$  is maximum. Again, the red color corresponds to the lower frequency values while the blue occur to the higher frequencies.

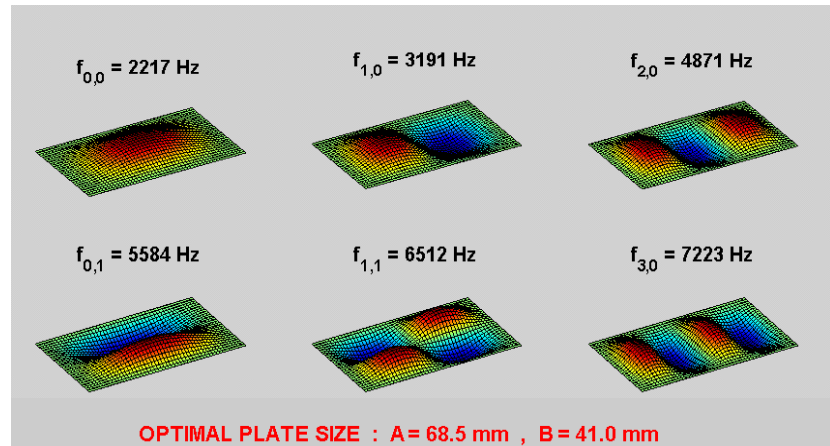
According to the procedure b) described in Section 6.2.3, the frequencies and respective modal shape of the first 6 modes are shown in Figure 6.4 (for each pair of dimensions given by the two establish criteria). This figure plots the frequencies of the first 6 modes. The notation  $f_{m,n}$  is used, where  $m$  is the number of nodal lines (see definition of nodal lines on Appendix A, Section A.3) parallel to dimension  $B$  and  $n$  is the number of nodal lines parallel to dimension  $A$ . This figure corroborates the results discussed so far, since the modal frequencies are lower for the dimensions obtained by criterion 2, ranging between 1931 Hz and 2826 Hz. These frequencies are much lower than the ones determined for the plate with the dimensions obtained by criterion 1, being: from 2217 Hz to 7223 Hz. On the other hand, criterion 1 leads to a higher separation between the frequencies. For example, let us consider the first two modes ( $f_{0,0}$  and  $f_{1,0}$ ); according to criterion 1, their normalized separation is 0.439

(since,  $\Delta f/f_j = (3191 - 2217)/2217 = 0.439$ ). The frequency separation of the equivalent first two modes, for the plate with the dimensions obtained by criterion 2, is 0.030. These results show that the optimization procedures (according to each specific criterion) give accurate results.

- a) According to critereon  
1: maximization of the  
separation between the  
first 6 modal frequencies

**Area of the plate:**

$$28.1 \text{ cm}^2$$



- b) According to critereon  
2: minimization of the first  
6 modal frequencies

**Area of the plate:**

$$92.3 \text{ cm}^2$$

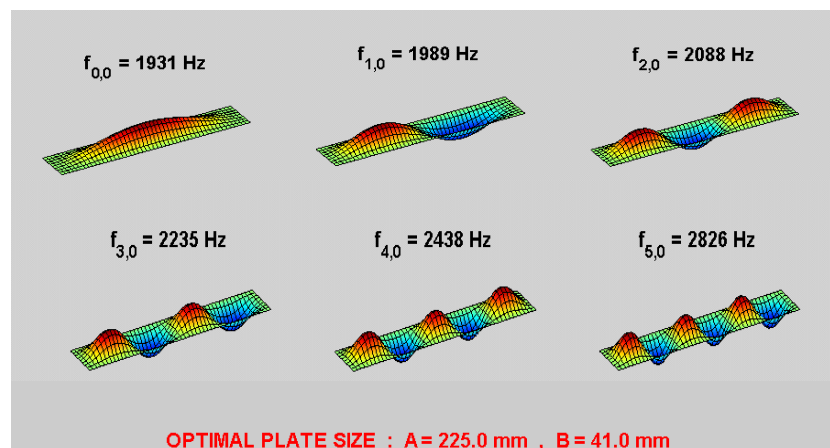


**Figure 6.4:** Representation of the frequencies and modal shapes of the first 6 modes, according to the two applied criteria

It is also interesting to note in Figure 6.4, that the modal shapes of the first 6 frequencies are highly dependent on the dimensions of the plate. The plate with smaller length (Figure 6.4 a) shows the vibration modes with lines parallel both to the  $A$  dimension (all the  $f_{0,i}$ ) and to the  $B$  dimension (all the  $f_{i,0}$ ). On the other hand the first 6 mode shape of the vibration of the plate with higher length only shows nodal lines parallel to the  $B$  dimension.

As can be seen in Figure 6.2, Figure 6.3 and Figure 6.4, the results from criteria 1 and 2 are quite different. The first criterion points out that the  $A$  dimension should be around 3.3 times smaller than the maximum value established, while in Figure 6.3 it can be seen that the lower frequency values are obtained for a maximum value of length ( $A$ ). Concerning the width ( $B$ )

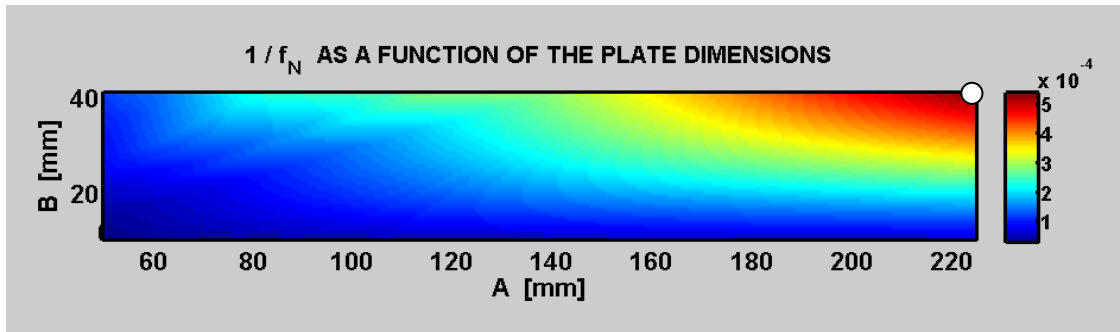
both indicate that this should be the maximum value considered. This shows, as previously mentioned, that the different criteria to optimize a given characteristic of the system (in the present case the dimensions of the plate), may lead to different results. In such cases, a realistic analysis of the results is determinant in choosing what criterion should be adopted. In the present case, since the main goal of the MSS is to detect the adhesion/removal of deposits to a given surface, the plate should have the dimensions that maximize its area. This is an important characteristic of a good fouling monitor since a large area lowers the biasing problems (the integration measurement area is also bigger). So, it is obvious that the second criterion fulfills this necessity and the plate dimensions to be used in the new configuration are:  $A = 225.0$  mm and  $B = 41.0$  mm.

### **6.2.5. Effect of the boundary conditions: free and simply-supported**

The previous results were determined for a clamped plate. However the real plate fixing procedure is not purely clamped (nor neither of the other boundary conditions). So, the optimum dimensions obtained for the clamped solution (applying criteria 2) will be compared with the results for the two other boundary conditions: free and simply-supported. For the reasons above mentioned only criterion 2 will be applied.

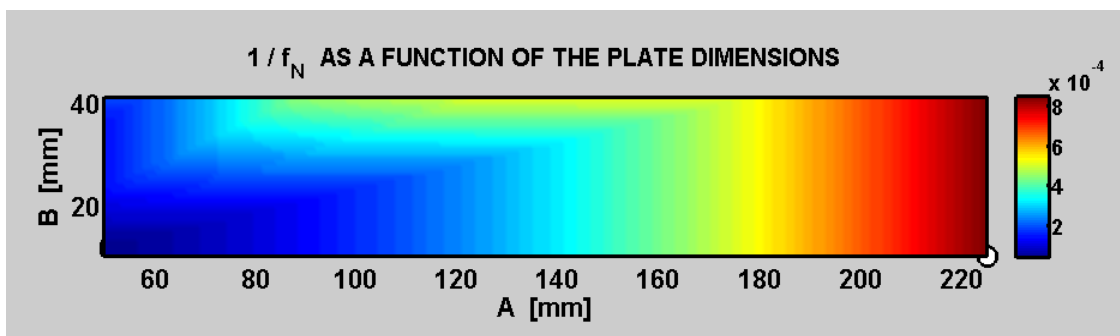
The comparison between Figure 6.3 and Figure 6.5 a), which correspond respectively to the clamped and to the simply-supported boundary conditions, shows that the target function has similar behavior (just higher values for the simply-supported condition). This increase on magnitude occurs since the simply-supported condition has fewer constraints than the clamped one and so, it vibrates more freely (at lower frequencies). On the other hand, if the free condition is examined - Figure 6.5 b) - the results lead to a completely different situation. It shows that lower frequencies (of the first  $n$  modes) occurs to longer plates (higher  $A$  value) almost independently of the  $B$  dimension, especially for  $A$  higher than 160 mm. The lower vibration frequencies happen because in the free vibration situation no constraint to the plate movement is observed.

Simply-Supported boundary condition



a)

Free boundary condition



b)

Figure 6.5: Target function values according to criterion 2 for the plate dimensions  $A$  and  $B$  for: a) simply-supported condition and b) free condition

Using the procedure explained in point b (Section 6.2.3), the first 6 vibration frequencies for the 3 boundary conditions studied are shown in Figure 6.6. The frequencies were studied for the dimensions  $A = 225$  mm and  $B = 41$  mm.

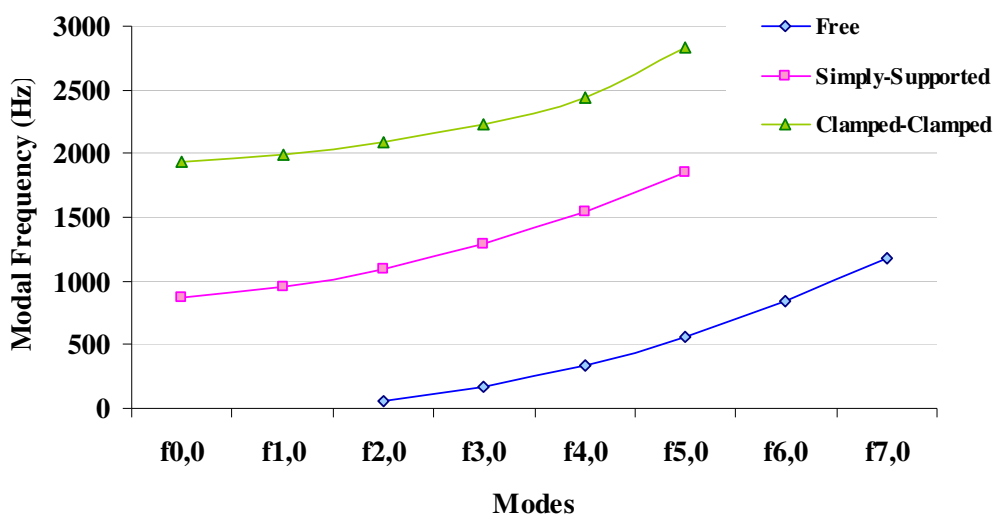


Figure 6.6: Frequencies of the first 6 vibration modes of a plate subject to the following boundary conditions: a) free, simply-supported and clamped-clamped

Figure 6.6 confirms that an increase of the constraints to the plate movement increases the frequency of the vibration modes. In fact, the fundamental vibration mode only appears to  $m=2$  (mode  $f_{2,0}$ ). As far as the constraints to the plate movement increase, the fundamental frequencies tend to be high. For example, for the first vibration mode the determined frequencies are: for free plate - 63 Hz; for simply-supported plate - 871 Hz; and for clamped plate - 1931 Hz.

### 6.2.6. Modal analysis of the new and of the old configurations

Let us now consider the SS plate used in Chapter 4 with the following dimensions:

**Plate 1:**  $A = 212 \text{ mm}; B = 29 \text{ mm}; h = 0.6 \text{ mm}$

This plate will be designated as plate 1 and the plate used in the new configuration will be plate 2. Recall that the dimensions of plate 2 were obtained by simulation in Section 6.2.4 and are:

**Plate 2:**  $A = 225 \text{ mm}; B = 41 \text{ mm}, h = 0.6 \text{ mm}$

Similarly to what happened in the previous section, the modal frequencies and their mode shape will be compared for the two plates (only for clamped boundary conditions). Figure 6.7 shows the frequencies and modal shapes for plate 1.

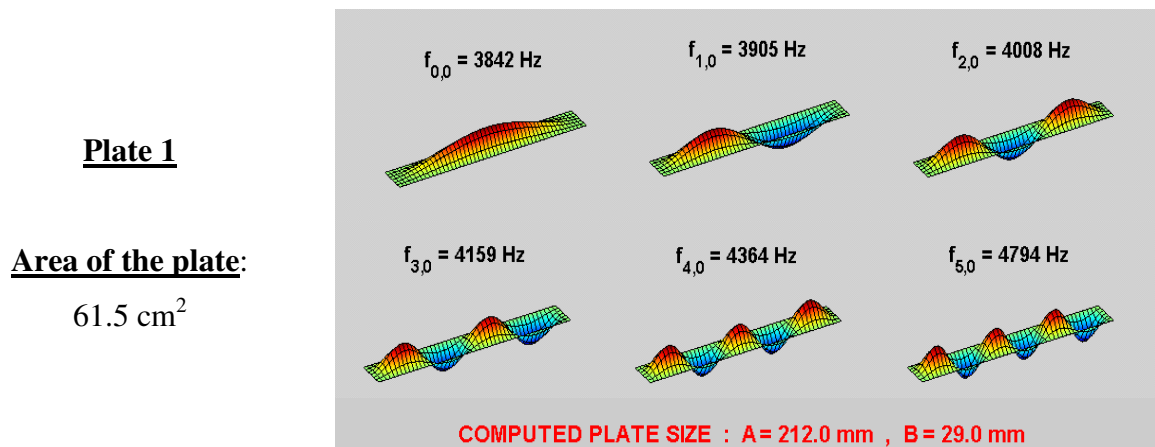


**Figure 6.7:** Representation of the frequencies and modal shapes of the first 6 modes, for plate 1

Comparing the modal frequencies of plate 1 - Figure 6.7, with the ones obtained for plate 2 - Figure 6.4 b) it is possible to observe that the latter has much lower frequencies than the ones of plate 1. It is possible to find in literature some mathematical relations that determine the frequencies of different modes for rectangular plates with clamped edges (Fletcher and

Rossing 1998). The frequencies can be obtained by multiplying a constant (which is tabled and depend on the  $A/B$  quotient) by  $1.654c_L h/B^2$ , where  $c_L$  is the longitudinal wave velocity (which depends on the plate material) and  $h$  the thickness of the plate. The  $c_L$  and the  $h$  are equal for the two considered plates, since the material and the thickness are the same. Furthermore, the constant is also the same because the relation  $A/B$  is higher than 3 for both plates. Being so, after introducing these simplifications the relation between the fundamental frequencies of the two plates is given by:

$$\frac{F_{Plate1}}{F_{Plate2}} = \frac{B_{Plate2}^2}{B_{Plate1}^2} \quad (6.4)$$

For the present case the relation between the widths of the two plates gives rise to the following relation:  $\text{Frequency}_{\text{plate 2}} = 0.5 \times \text{Frequency}_{\text{plate 1}}$ . In fact, the fundamental frequency obtained for plate 1 (3842 Hz) is almost twice the value of plate 2 (1931 Hz). From these output results it can also be concluded that the dimensions of the new plate (plate 2) lead to modal frequencies lower than the ones observed for plate 1. Furthermore, the separation between the modes is higher for plate 2 than for plate 1. For example, the normalized separation between the first two modes is: 0.01 for plate 1 and 0.03 for plate 2. A similar trend is observed for separation of the other modes.

Regarding the applicability of both plates to monitor the adhesion of deposit, it is more interesting to consider the plate with higher surface area (which is the case of plate 2), since the sampling area is higher.

### **6.3. METHODOLOGIES FOR RESPONSE ANALYSIS**

The present section will briefly discuss the generation/acquisition procedures and the signal processing analysis applied in the previous chapters. The features of the methodology used so far (which will be designated from now on as methodology 1) were already highlighted along the present Thesis. This sinusoidal excitation technique (methodology 1) enables the determination of the  $A_{FFT}$  and of the damping factor, which are not characteristic parameters of a vibrating system. In the present chapter the experimental modal analysis (EMA) will be introduced (and called methodology 2) in order to determine such characteristic parameters



that are able to provide information about the real vibrating properties of the system: the modal frequencies and the modal damping (or also called damping ratio). The fundamentals of the EMA technique can be read in further detail on Appendix A, Section A.3.

### 6.3.1. Methodology 1

The first generation/acquisition system implemented was shown in Figure 3.2 (Chapter 3). This system was replaced by the one represented schematically in Figure 6.8. Contrarily to what happened with the first system, the latter one (used in the other 2 chapters) concentrates the generation and acquisition in a data acquisition system (NIDAQ-Card PCI-6221) that is connected to a computer (where the signal processing is performed). Both the actuation and sensing processes are automatically carried out during each period of time ( $\Delta t$ ), providing real-time information to the user.

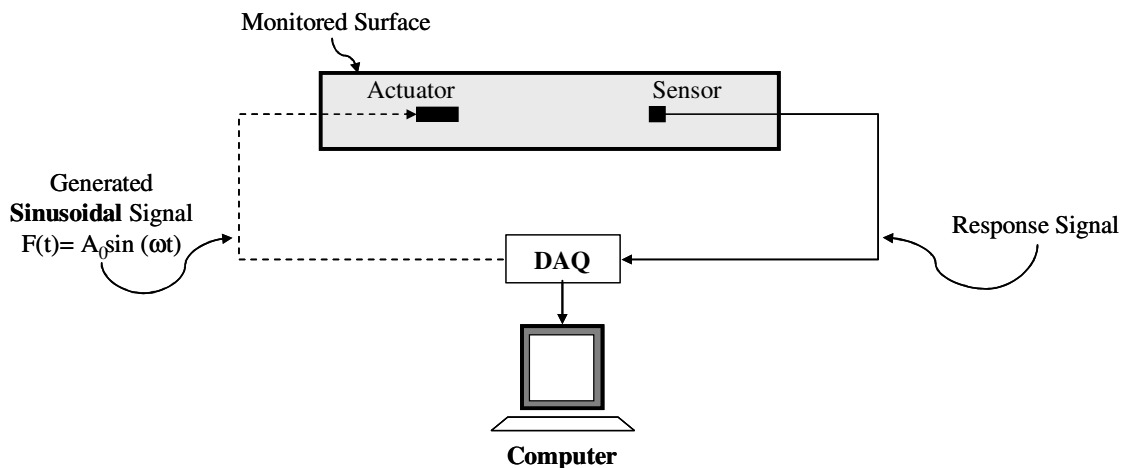


**Figure 6.8:** Schematic representation of the generation and acquisition system (methodology 1)

When setting up a new experimental trial the resonant frequency of system with higher peak-to-peak amplitude – see Figure 6.9 - is determined (i.e. the frequency at which the system has the highest response). In the former chapters it was mentioned that the frequency used was the one that matches the resonant frequency of the system. The sinusoidal wave sent to the actuator is characterized by a given amplitude and frequency. In order to determine the ‘better’ sinusoidal wave parameters, a LabVIEW<sup>®</sup> software (named ‘resonant frequency determination’) was programmed to perform the following tasks:

- generate and actuate the system with a sinusoidal wave that combines different set of amplitudes ( $A_{in}$ ) and frequencies ( $f_{in}$  or  $\omega_{in}$ , since  $\omega_{in} = 2\pi f_{in}$ );

- b) for each set  $A_{in}$  and  $f_{in}$ , the output response is measured and its peak-to-peak amplitude ( $A_{out}$ ) is determined – see Figure 6.9; and the ratio  $A_{out}/A_{in}$  is calculated
- c) after running the previous procedures as much times as the combination between the frequencies and amplitudes imposes, the higher ( $A_{out}/A_{in}$ ) value determines the frequency ( $f_{in}$ ) and the amplitude ( $A_{in}$ ) of the sinusoidal wave that generates the system's highest response;

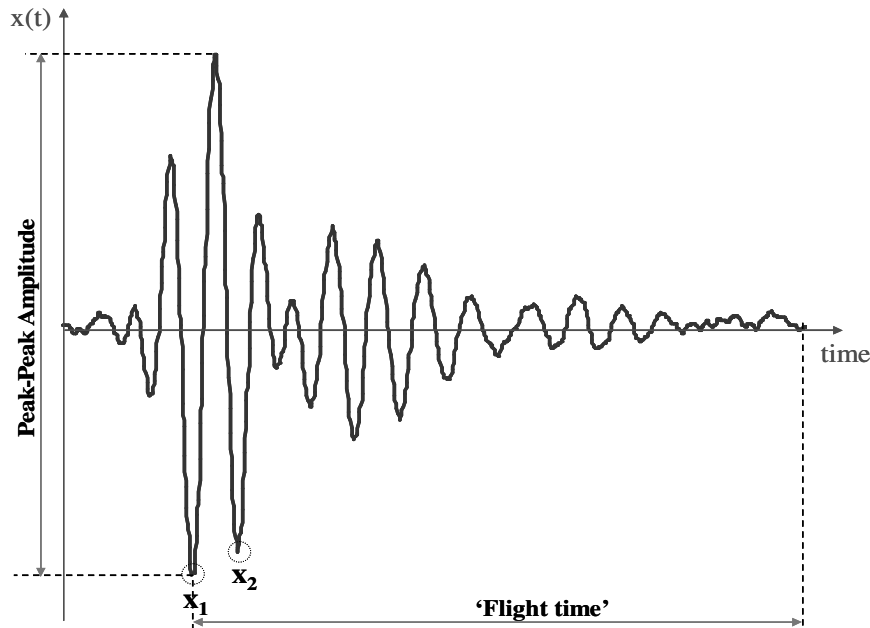


**Figure 6.9:** A typical output wave with the time-measurements indicated – peak-to-peak amplitude, ‘flight-time’ and the points  $x_1$  and  $x_2$  for damping factor calculation

It is important to mention that the maximum amplitude that can be generated by the DAQ is 10 V and that the range of studied frequencies is between 2000 and 8000 Hz. The former range was defined based on the information gathered from an extensive frequency scan that indicated the inexistence of important data below and above the established frequency range.

The determined parameters ( $A_{in}$  and  $f_{in}$ ) are then introduced into the main program (also built in a LabVIEW<sup>®</sup> application) that periodically performs the following tasks:

- a) generate a sinusoidal wave with the characteristics ( $A_{in}$  and  $f_{in}$ ) previously determined, and send it to the actuator;
- b) capture the vibration response of the plate (to the former excitation) with the sensor;
- c) the acquired response is then mathematically processed, for:

- time-domain measurements (see Figure 6.9): peak-to-peak amplitude, ‘flight-time’, and the damping factor are determined. The latter is calculated by the ‘Logarithm Decrement Method’ and the points  $x_1$  and  $x_2$  are represented in Figure 6.9.
- frequency-domain measurements: FFT determinations with a number of samples equal to 512 (recall from Appendix A, Section A.2.2 that the number of samples should be a power of 2). For each collected wave, only the amplitude with higher value and damping factor were considered.

The parameters used to perform the acquisitions and the calculations were the following:

- Sampling rate of the response waveform ( $\Delta t$ ): 4  $\mu$ s, so  $f_{sampling}=250$  kHz; recall from Appendix A, Section A.3.2, that the sampling rate should be 2.5 time the maximum frequency.
- Waveform total time: 16 ms (4000 points)

The user interface of the LabVIEW<sup>®</sup> program developed to run the procedure described for methodology 1 can be seen in Figure 6.10 .

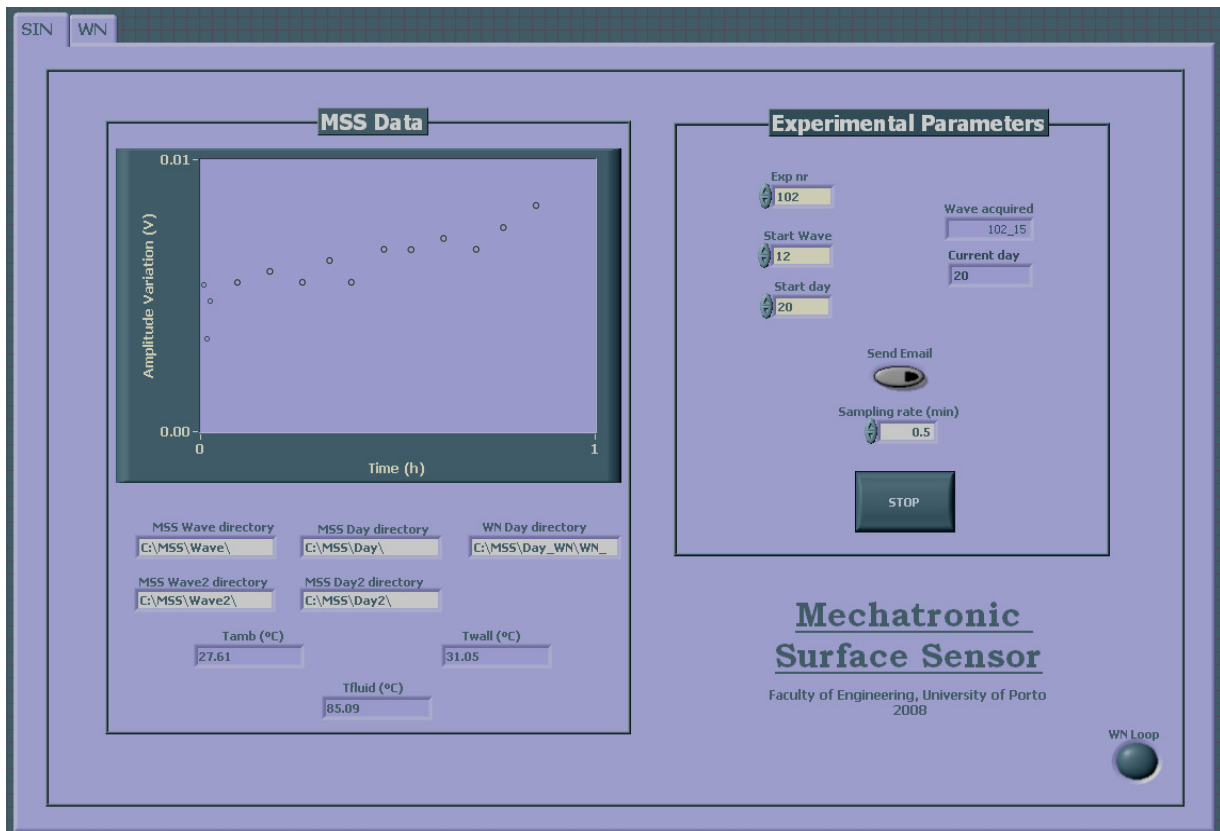


**Figure 6.10:** User interface of the software used to perform methodology 1

### 6.3.2. Methodology 2

The use of random excitations has some advantages over the frequency excitations – more information can be read in Appendix A, Section A.2.1. The main differences between them rely on the fact that the random excitation integrates more information since it excites all the natural vibration modes of the system rather than restricting the excitation to one of these resonances (as it happens with methodology 1). Nevertheless, the sinusoidal excitations showed so far (under the scope of the present Thesis) to be an efficient way to evaluate the amount of deposit attached to the monitored surface.

As previously reported, the experimental modal analysis assumes a quite important role in testing vibrating systems. Most practical vibrating problems are related with resonance phenomena, where external forces excite one or more vibrating modes. These modes have an important characteristic related to the fact that any response of a system can be reduced to a set of discrete modal parameters: the modal frequency, the modal damping and the modal shape. The analysis of such parameters within the frequency range of interest is a complete dynamic description of the system (Dossing 1988). The experimental modal analysis is the (experimental) process of determining the modal parameters. The EMA is based on the determination of the transfer function of the system (more information can be read in Appendix A, Section A.3), which describes the dynamic properties of a system. With a proper extraction procedure, the frequency and damping ratio can be determined and used to characterize the system.

Figure 6.11 shows a schematic representation of the generation/acquisition system implemented in this methodology. The main difference between the physical inputs/outputs of the data acquisition system is the fact that in order to determine the transfer function of the system, it should measure not only the system's response but also the signal that is generated.

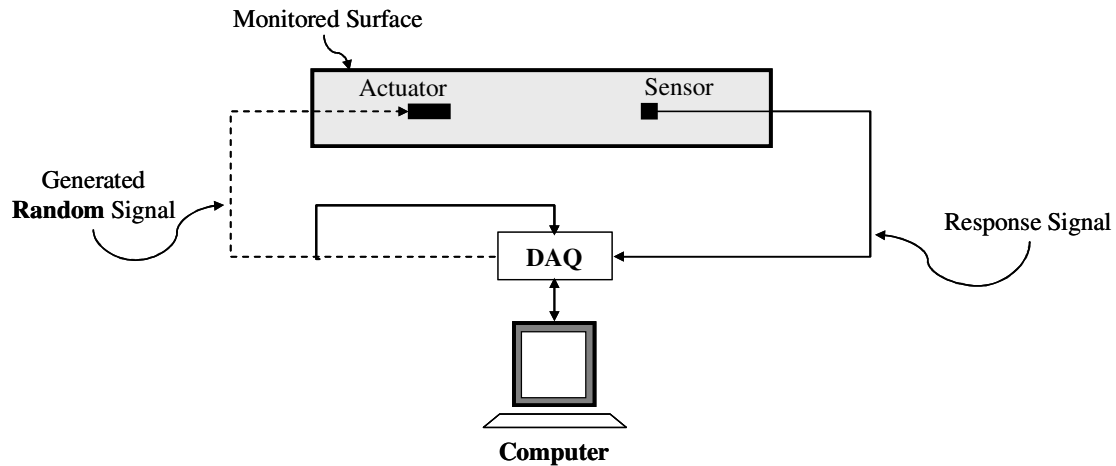


**Figure 6.11:** Schematic representation of the generation/acquisition system (methodology 2)

The system was excited with white noise - a large spectrum excitation - since it excites the whole frequency range with constant energy. It is important to determine the frequency range and the amplitude level that conveniently excites the vibration modes of interest. The frequency range used to excite the system along the following trials was between 0 Hz and 20 000 Hz.

The parameters used to perform the acquisitions and the calculations were the following:

- Sampling rate of the response waveform ( $\Delta t$ ): 20  $\mu\text{s}$ , so  $f_{\text{sampling}}=50$  kHz; the maximum admissible frequency 20 kHz;
- Waveform total time: 328 ms (16384 points)
- For the transfer function determination an averaging procedure with the following characteristics have been accomplished:
  - Averaging mode: linear RMS;
  - Number of averages: 100;
  - Averaging window: Hanning. The Hanning window is the best weighing function to use with random data in order to minimize leaking errors (Dossing 1988). These errors are associated with the fact that the excitations are random and continuous in time although the record length is finite. The signal is typically windowed in order to soft the entry and exit for each record.

The user interface of the LabVIEW<sup>®</sup> program developed to run the procedure described for methodology 2 can be seen in Figure 6.12.

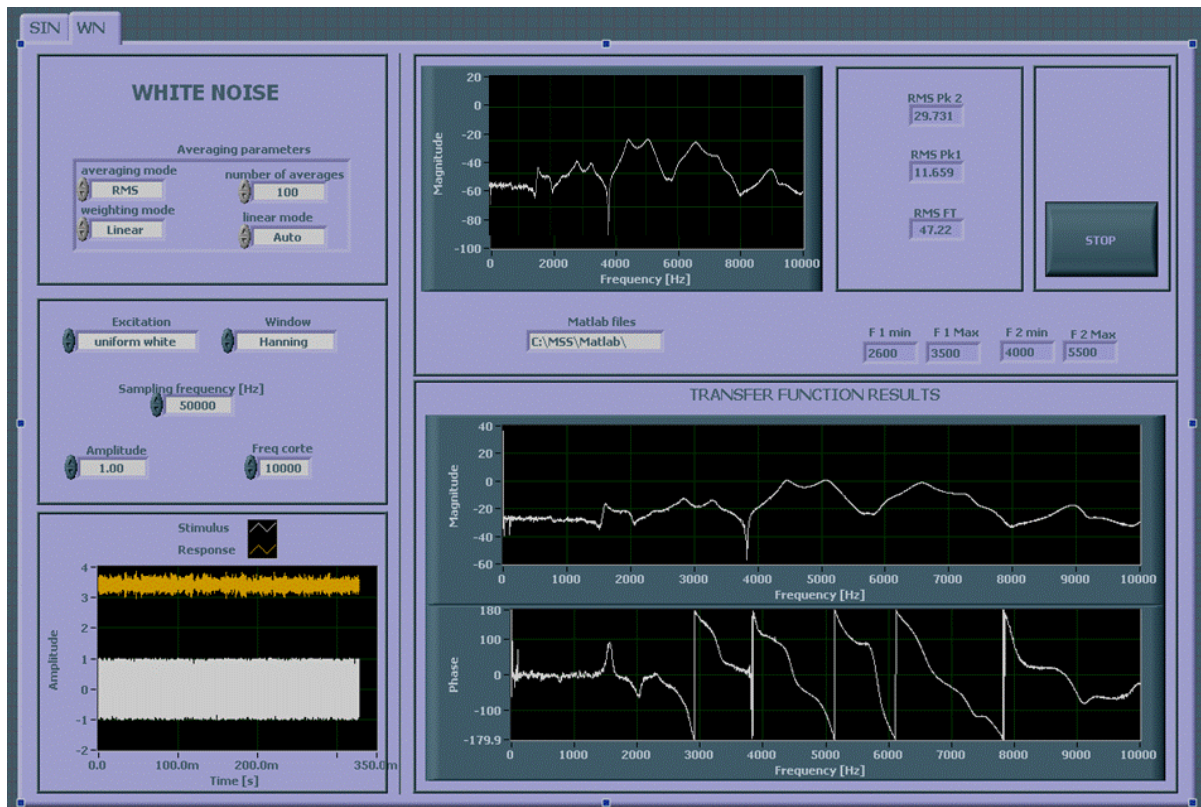


Figure 6.12: User interface of the software used to perform methodology 1 and methodology 2

### 6.3.2.1. Transfer function determination

The methodology 2 has been integrated into the original LabVIEW<sup>®</sup> software (previously described for methodology 1). After the established period, the software runs the procedure for methodology 1 and then the one for methodology 2, which is defined by the following tasks:

- the system generates and actuates the MSS plate with white noise;
- The software averages (100 times) the transfer function (TF), with the generated and the response signal;
- The transfer function is stored in the computer, and three RMS calculations (of the transfer function) are determined, being:
  - **RMS<sub>TF</sub>**: it calculates the RMS of the magnitude function in the range:  $0 < \text{Frequency (Hz)} < F_{cutoff}$ , where  $F_{cutoff}$  is the cutoff frequency.
  - **RMS<sub>Pk1</sub>**: it calculates the RMS of the magnitude function in the range:  $F_1 < \text{Frequency (Hz)} < F_2$ .
  - **RMS<sub>Pk2</sub>**: it calculates the RMS of the magnitude function in the range:  $F_3 < \text{Frequency (Hz)} < F_4$ .

Note that the frequencies ( $F_i$ ,  $i=1, 2, 3$  and  $4$ ) will be defined latter on based on the TF of the adopted configuration (Section 6.4.5). Those ranges should include the frequencies where the magnitude function shows more defined (less damped) peaks. Regarding the  $F_{cutoff}$ , it was found that for all the analyzed situations (e.g. flow cell with: air, water, deposit, etc) no important information appear above the 10 000 Hz. Being so, the  $F_{cutoff}$  was set to be the 10 000 Hz which will be maximum frequency shown in the following transfer functions.

The determination of the modal characteristics (with the tools available at the time) of the signal can not be done automatically. The RMS procedure was introduced as an expedite way to measure the effect of the deposits on the vibration properties. It is easy to implement and gives an integrated measurement. Furthermore, since it is possible to define the RMS of different zones all the important information is integrated.

### 6.3.2.2. Modal extraction

An example of a technique used to extract the modal characteristics from the TF is described in Appendix A, Section A.4. That method can be used for lightly-damped systems and with well-separated modes, and a simple inspection of the transfer function curve is enough to determine the natural resonant frequencies of the system. But in practice, for heavily damped systems, the overlap between consecutive modes can make it very difficult to determine the response of the individual modes. When such thing happens, it is necessary to implement more sophisticated approaches. The procedure used in the present chapter was the one described by Inácio et al. (2006) and Dr. José Vieira Antunes gently let their software be used for modal identification within the scope of the present Thesis. In summary, the modal identification was achieved by developing a multi-degree-of-freedom (a brief description of multi-degree-of-freedom systems can be read in Appendix A, Section A.1.2) curve-fitting algorithm in the frequency domain. For all measurements in a given frequency range  $[\omega_{min}, \omega_{max}]$  encompassing  $n$  modes, the modal parameters were optimized in order to minimize the error  $\mathcal{E}(\omega_n, \zeta_n, m_n, \varphi_n)$  between the measured transfer functions  $H_{er}(\omega)$  and the fitted modal model  $\hat{H}_{er}(\omega; \omega_n, \zeta_n, m_n, \varphi_n)$ . The error function is defined by:

$$\mathcal{E}(\omega_n, \zeta_n, m_n, \varphi_n) = \int_{\omega_{min}}^{\omega_{max}} \left[ H_{er}(\omega) - \hat{H}_{er}(\omega, \omega_n, \zeta_n, m_n, \varphi_n) \right] d\omega \quad (6.5)$$

With:

$$\hat{H}_{er}(\omega, \omega_n, \zeta_n, m_n, \varphi_n) = \sum_{n=n_1}^{n_1+N} -\omega^2 \frac{A_n^{er}}{\omega_n^2 - \omega^2 + 2i\omega\omega_n\zeta_n} - \omega^2 C_1 + C_2 \quad (6.6)$$

The modal amplitude coefficients are given as:  $A_n^{er} = \varphi_n(\theta_e, Z_e)\varphi_n(\theta_r, Z_r)/m_n$  and the last two terms in Equation (6.6) accounts for the modes located out of the identified frequency-range. Since the modal masses depends on how the mode shapes ( $\varphi_n$ ) are normalized, the normalization used in the present procedure is:  $|\varphi(\theta, Z)|_{max} = 1$ , where  $(\theta, Z)$  are the polar coordinates and the subscripts  $e$  and  $r$  correspond respectively to excitation and response. Such equation cannot be directly solved and so iterative approaches have been developed in which an initial estimative of the desired parameters must be provided. In fact, consider the TF shown in Figure 6.13 and the output of the MATLAB<sup>®</sup> modal identification software. It is possible to see that the transfer function of the free stainless steel plate (2) (dimensions: 225×41×0.6 mm) shows a lot of resonant peaks with low damping ratios (blue curve). In the form developed, the software is only able to identify 5 vibrating modes each time. The initial estimative of the frequency for the optimization procedure were given (vertical green lines) which match approximately the maximum of the  $H(\omega)$  function for each of the considered peak while the initial estimative of the damping ratios ( $DR$ ) was 1%. After using the procedure previously described, the fitted model is represented by the red curve and the modal frequencies and damping ratios values are shown in the bottom part of the layout. It is possible to see that the fitted model adjusts quite well in the range of the considered modes.

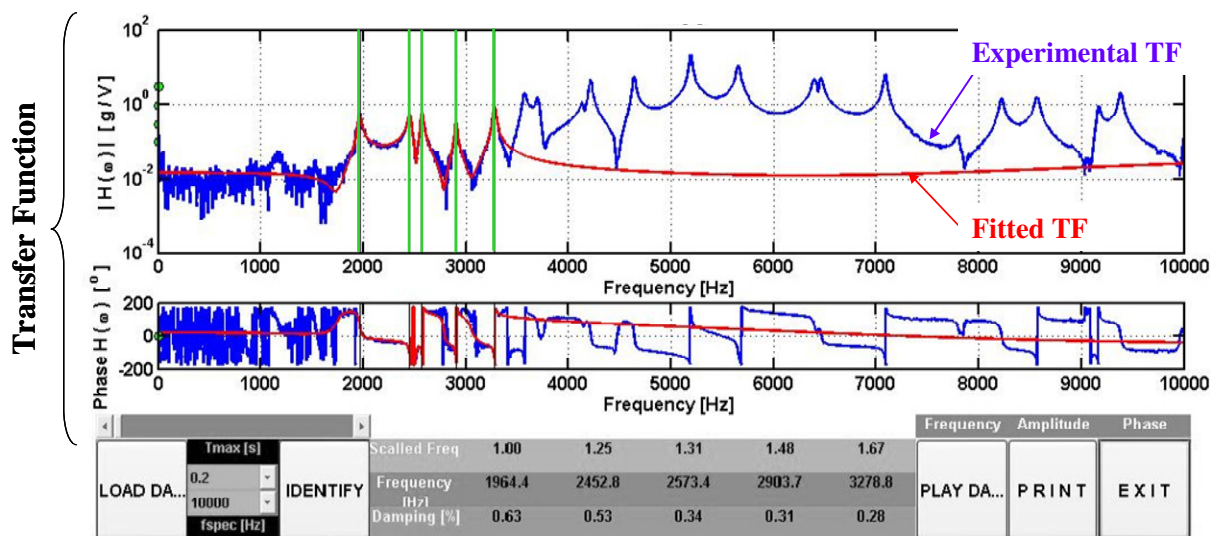


Figure 6.13: Output results steering from the modal identification of a transfer function (in the MATLAB<sup>®</sup> software developed to determine the modal characteristics of the system) of the stainless steel plate



Similar determinations to the one shown in Figure 6.13 were performed along the experimental trials in order to determine the effect of the parameters under test (e.g. adhesion of deposit), on the modal characteristics (frequency and damping ratios) of the system.

A comparison between the two damping determinations: the damping factor ( $DF$ ) and the damping ratio ( $DR$ ) will be provided in Section 6.4.5. Recall that the  $DR$  has only been introduced in the present chapter while the  $DF$  was used in Chapters 3 and 4.

#### **6.4. PRELIMINARY TESTS OF THE NEW MSS SETUP**

The transfer function measurements will be used to evaluate the characteristics of the plate under study (free boundary condition). The analysis of the best way to fix this plate into the flow cell (mainly in what concerns the sealant characteristics and configurations) will also be based on modal determinations and evaluations.

##### **6.4.1. Experimental modal analysis of the SS plate**

The SS plate (recall that the dimensions of the plate are  $225 \times 41 \times 0.6$  mm) was supported in expanded polystyrene, according to what is shown in Figure 6.14 (this material is commonly used in this type of vibrating tests).

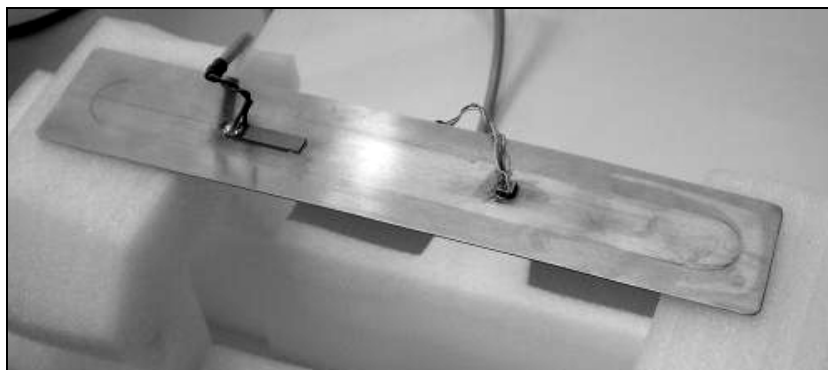


**Figure 6.14:** Experimental setup for measuring the transfer function of the SS plate (under free boundary conditions)

The transfer function is characterized by three variables: magnitude, phase and coherence. Figure 6.15 shows the magnitude, phase and coherence functions for the free plate in the conditions shown in Figure 6.14. As it will be shown in Section 6.4.3 the system meets the

linearity requirements, which makes the output response independent on the input amplitude. In spite of this, all the transfer functions discussed in the present chapter were obtained exciting the system with white noise with amplitude of 1.0 V. The actuator and the sensor elements were the ones used in the previous two chapters.

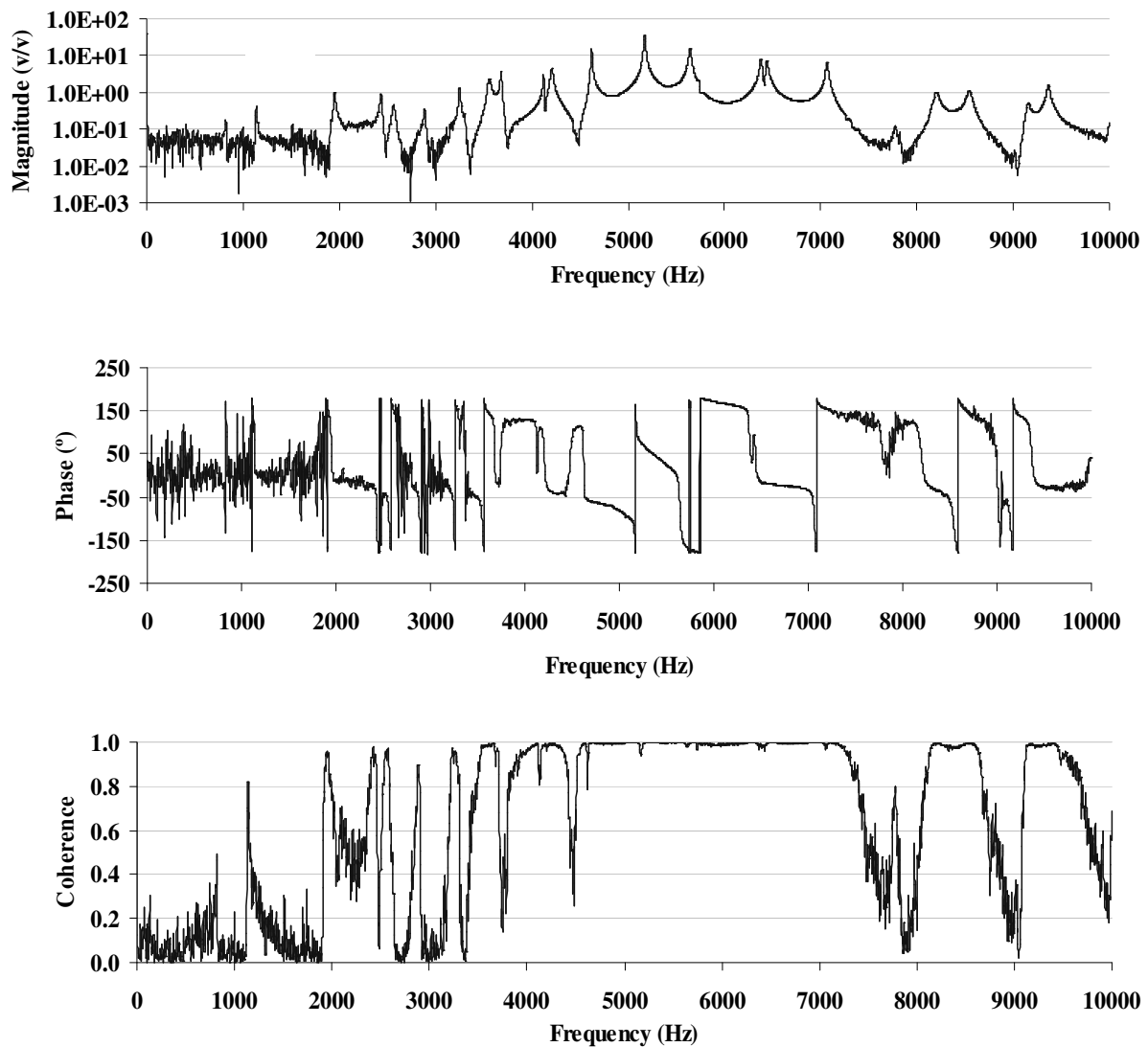


**Figure 6.15:** Transfer function (magnitude and phase) and coherence functions of the free vibrating plate

When these results are compared with the ones obtained for the simulation shown in Figure 6.6, it is possible to see that the first 6 vibrating modes for a free boundary-condition occur theoretically at much lower frequencies (63 than it happens in the experimental case. In fact, the analysis of the coherence function (in Figure 6.15), determined from the experimental data, indicates that there are no accurate measurements for frequencies lower than 1000 Hz. This seems to indicate that the excitation system is not suited to excite the system below

1000 Hz which also explains the non-existence of resonant peaks in the range of frequencies obtained in the simulation study. The first modes may have additional information that enables to improve the overall results. Despite the positive input that this point could bring to the overall results/analysis, it will not be contemplated in the present Thesis but it should be taken into consideration when devising a new MSS prototype.

In Figure 6.15 a number of well defined, low damped resonant peaks can be observed. When placing the SS plate on the flow cell the damping ratio is expected to increase (the peaks will be less defined) and possibly some resonances will disappear. This is expected to occur since the O’rings will certainly damp the vibration and add constraints to the movement.

In our discussion from now-on, only the magnitude function will be considered, so the phase and the coherence will not be represented in this chapter. Nevertheless, since the analysis of the phase and coherence function is important to a correct interpretation of the results, these two variables and the magnitude will be presented in Appendix D, for all the situations discussed here.

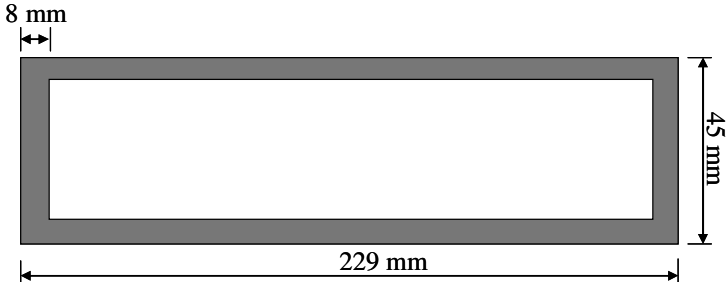
#### **6.4.2. Choice of system’s best configuration**

Three different types of sealants – listed in Table 6.1 - have been tested. Each type of sealant has been tested under two different configurations according to the schematic representation of the flow cell and of the way to fix the SS plate, observed in Figure 6.1. The different tested configurations can be summarized as:

- a) One sealant: placed in the flow cell (designated in Figure 6.1 as O’ring (1));
- b) Two sealants: one placed in the flow cell and another placed in the PERSPEX<sup>®</sup> cover part (designated in Figure 6.1 as O’ring (2));

Since one of the most studied possibilities is to apply the MSS in tubings/flow cells filled with water, it becomes important to analyze the magnitude function not only in air but also when the flow cell is filled with water. The choice of the sealing material is a very subtle procedure since in one hand it should be able to seal the flow cell and at the same time it should be made of a material that absorbs the minimum amount of energy as possible. Additionally, the sealant should be able to provide some freedom in order to let the plate vibrate. So, the best sealing solution will be determined by analyzing the magnitude function.

**Table 6.1:** List of the tested sealants

| Type of sealant                           | Dimensions   |
|---|--|
| Normal O'ring<br>Higher hardness O'ring   | Diameter = 0.8 mm  |
| Polyurethane plate*<br>(thickness = 1 mm) |  <p>The diagram shows a rectangular polyurethane plate with a thickness of 8 mm. The outer dimensions are 229 mm in length and 45 mm in width. The plate is shown as a shaded rectangular frame.</p> |

\* Note that the polyurethane was cut according to the scheme represented in Table 6.1 and so it was not introduced in the PERSPEX<sup>®</sup> depressions (represented in Figure 6.1 as O'rings), but rather sandwiched between the PERSPEX<sup>®</sup> structures and the SS plate.

Presenting the transfer functions and discussing all the combinations of sealants and their possible configurations would be a repetitive task. So, only the worst and the best cases will be considered for analysis within this chapter. The decision about the best sealing configuration was established under air conditions.

#### 6.4.2.1. Worst solution

One of the worst solutions occurred for the case of two polyurethane plates placed between the PERSPEX<sup>®</sup> structures and the SS plate. Contrarily to what happened when the plate was subject to no constraints - Figure 6.15, no defined resonance peaks are observed in the magnitude function shown in Figure 6.16.

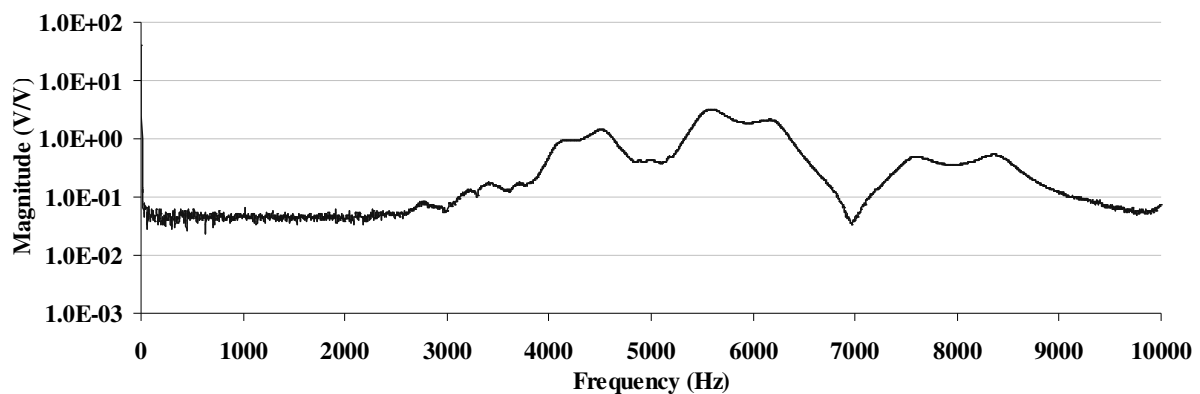


**Figure 6.16:** Magnitude function of the system – SS plate clamped between 2 polyurethane plates

This occurs because the system is highly damped which is contrary to what is desired.

#### 6.4.2.2. Best solution

The solution with two normal O’rings (with lower hardness) showed to be the one with better defined resonant peaks – see Figure 6.17. Based on this result, this was the adopted configuration and, from now on, only this configuration will be analyzed.

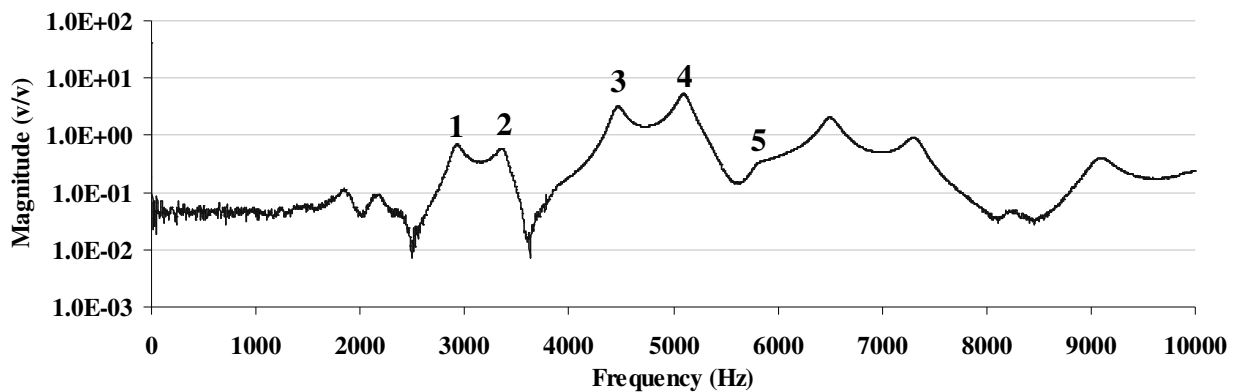


**Figure 6.17:** Magnitude function of the system configuration adopted – two normal O’rings as sealant

This configuration can be seen in Figure 6.18, which shows: i) the flow cell with the O’ring placed in the depression indicated in Figure 6.1 as ‘O’ring (1)’; ii) the PERSPEX<sup>®</sup> structure with the respective O’ring (placed in the position O’ring (2)); and iii) the flow cell with the SS plate fixed between the two previous mentioned structures. The SS plate and the respective actuator and sensor elements can be seen in Figure 6.14.

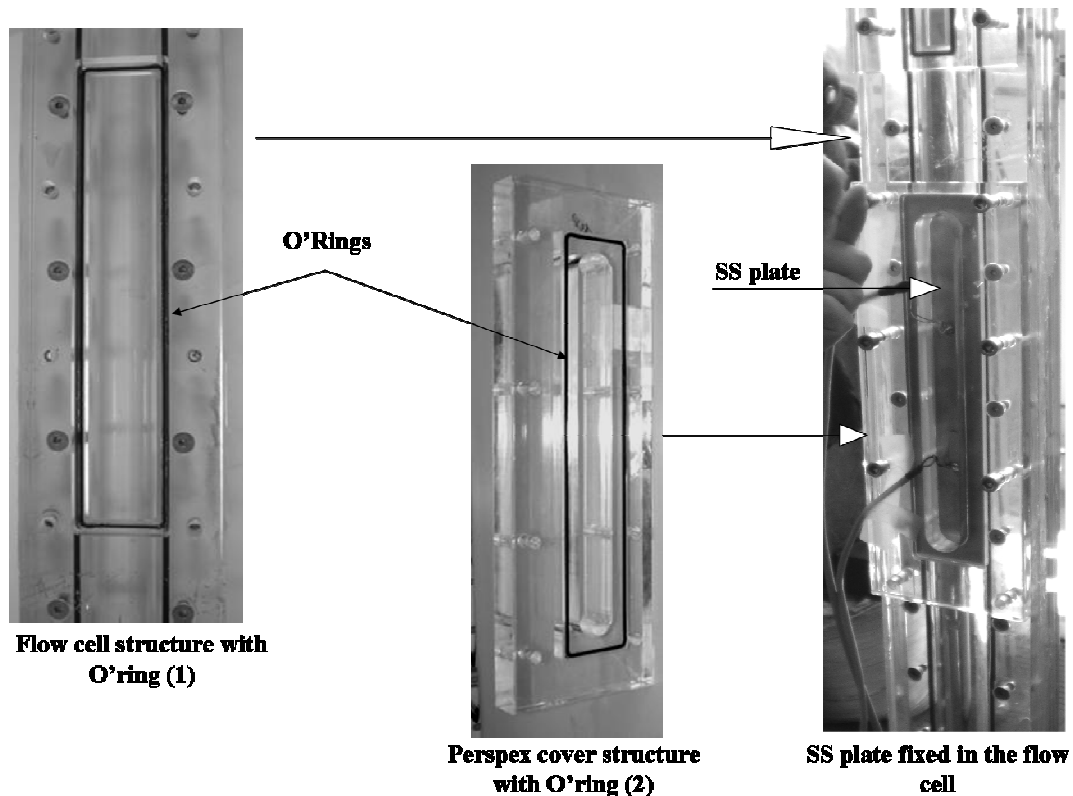


**Figure 6.18:** Photos of the flow cell and of the PERSPEX<sup>®</sup> cover structure (with the respective O’rings) and the SS plate fixed between these two structures

### 6.4.3. Linearity test

In order to start the modal characterization of the system, it is important to determine if the system is linear (recall from Appendix A, Section A.3 that the modal analysis can only be performed for linear systems). This linearity test has been carried out for all the tested configurations as well as for the free SS plate (previously studied). However, since the conclusions are similar for all of them, the results of the linearity test will only be presented and analyzed for the adopted configuration.

In a linear system, the output modal parameters (resonant frequencies and damping ratios) are independent of the excitation amplitude. In order to study that, the system was actuated by white noise at different amplitudes (0.1 V, 0.5 V, 1.0 V and 1.5 V). The modal characteristics of the five resonances indicated in Figure 6.17 with numbers 1 to 5 will be identified. The results of the linearity test are shown in Figure 6.19, as well as the average and standard deviation of the frequency and damping ratio of the five considered vibration modes.

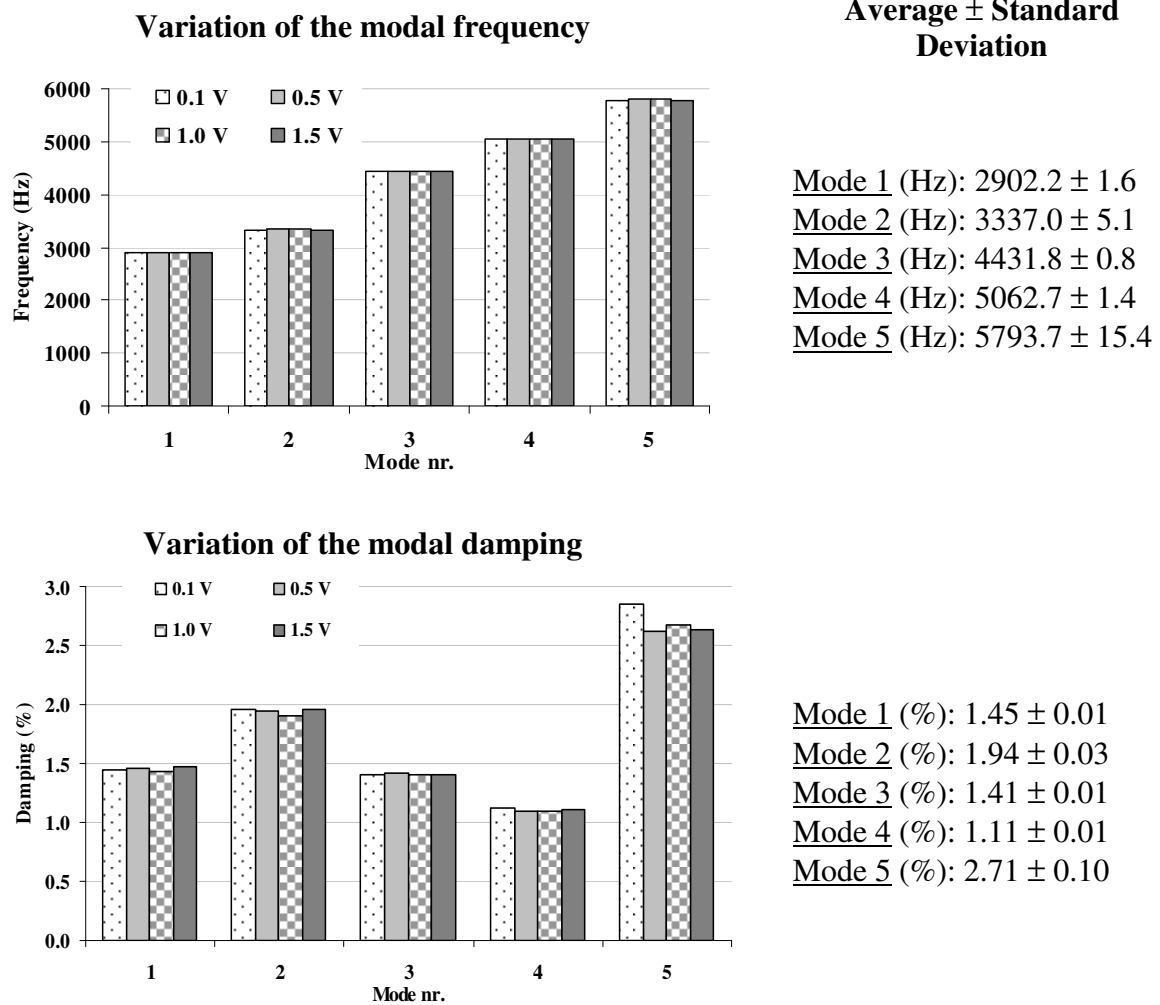


**Figure 6.19:** Frequency and damping ratio average and standard deviation of the five considered modes

The results provided in Figure 6.19 show that there are no significant differences between the modal frequencies and damping ratios for different amplitudes of the excitation signal. In fact, in the worst case (mode 5) the standard deviation represents 0.3% of the mean frequency and 3.7% of the mean damping ratio. Since the linearity requirement is fulfilled (all the results are independent of the excitation amplitude) and the modal analysis can be performed without additional concerns.

The following trials involving modal analysis have been accomplished by exciting the system with white noise (between 0 and 20 000 Hz) and 1.0 V, according to the procedure described in Section 6.3.2.

#### 6.4.4. Effect of water on the transfer function of the system

The MSS has been designed to measure the adhesion/removal of deposits in aqueous environments. So, it is crucial to study the magnitude function of the system when it is filled with water. Those results are shown in Figure 6.20.

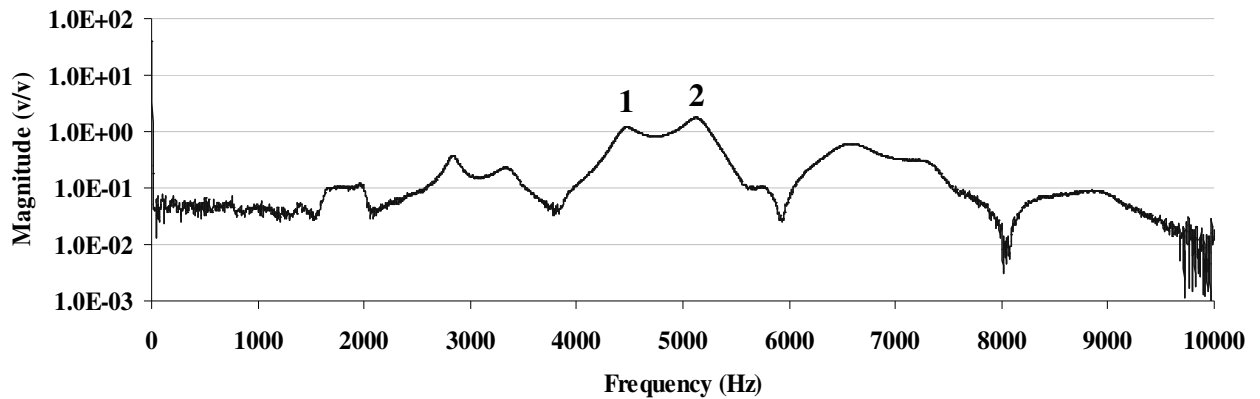


Figure 6.20: Magnitude function of the system filled with water

The comparison between the transfer functions in Figure 6.17 and Figure 6.20 shows that the magnitude is higher when the system is empty (air conditions). This means that the SS plate responds less to the same excitation, when the system is filled with water. Additionally, the water also increases the damping ratio of the vibration modes and the peaks with higher frequencies almost disappeared (for example, the one at 9000 Hz). This happens because the water acts as an additional source of energy dissipation as well as it increases the mass of the system (which is another constraint to the vibration of the plate). The modal identification software is only able to correctly adjust two modes (mode 1 and mode 2) between 4000 and 5500 Hz. These modes correspond to the modes 3 and 4 in Figure 6.17. When the flow cell is filled with water (no flow,  $T=30\text{ }^{\circ}\text{C}$ ) the modal frequencies and damping ratios are:

Mode 1 (Hz): 4445.7

Mode 1 (%): 2.11

Mode 2 (Hz): 5081.5

Mode 2 (%): 1.36

The comparison between the empty and the filled system shows that the frequencies of the two modes slightly increased (around 0.4% in both cases). On the other hand, the damping ratio variation was much higher: for mode 1 the increase was approximately 50%; and for mode 2 the increase was around 23%. In fact, these results are in accordance to what was expected and confirm that the main effect of the water in the system is the increase of the damping ratio.



### 6.4.5. Comparison of the 2 methodologies

The former conclusions were based on the experimental modal analysis – methodology 2. It should however be recalled that, based on the magnitude function on Figure 6.20, additional determinations were performed: the RMS of the overall magnitude function and two other defined according to the frequency zones that have higher magnitude. Based on the TF results previously obtained, the RMS will be evaluated for:

$$RMS_{TF}: 0 < \text{Frequency (Hz)} < 10\,000$$

$$RMS_{Pk1}: 2600 < \text{Frequency (Hz)} < 3500$$

$$RMS_{Pk2}: 4000 < \text{Frequency (Hz)} < 5500$$

The RMS absolute value does not provide information to characterize a given vibrating system. It is only indicative of changes that occur within a given range of frequencies. It is an integrated measurement that may help follow what happens in a system, rather than a methodology to characterize that system.

In fact, the RMS determinations are similar to the ones evaluated by methodology 1:  $A_{FFT}$  and  $DF$ , since they do not characterize a given vibrating system (they are not intrinsic properties of such systems). However they are a way to quantitatively follow changes that occur in such vibrating system. For comparison purposes of the two methodologies the output waves obtained by methodology 1 for the system empty and filled with water are shown in Figure 6.21. For each condition the resonant frequency of the system has been found and the latter was actuated at that frequency and amplitude.

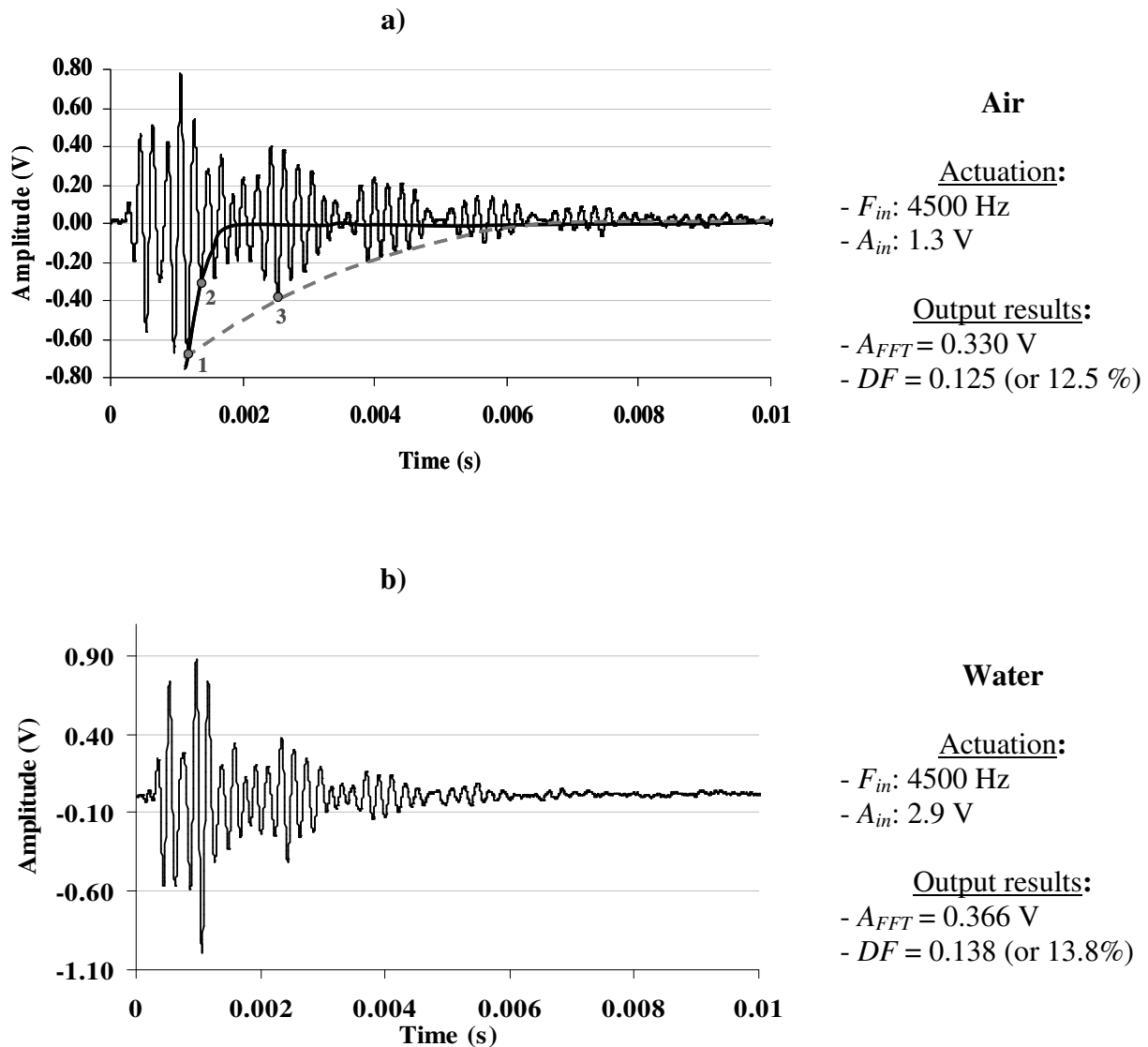


**Figure 6.21:** Output waves determined by methodology 1, the respective excitation parameters and output results (where  $A_{FFT}$  is the higher amplitude obtained after FFT and  $DF$  is the damping factor)

The results shown in Figure 6.21 shows that from the output waves under different conditions it is not possible to draw conclusions about the system vibration characteristics. This happens because it is very complicated to determine both the modal frequencies and damping ratios from the output waves, since these are the result of the interaction of several vibrating modes. Furthermore the output responses have different amplitudes (and so different  $A_{FFT}$  values) according to the excitation voltage ( $A_{in}$ ). This excitation voltage is adjusted for each condition air/water (according to the procedure mentioned in Section 6.3.1). For example, to excite the system when the flow cell is filled with water, the amplitude is almost 2.3 times higher than the one for the air condition. If the system filled with water was actuated with 1.3 V, it would

respond with lower output amplitude, which in terms of its analysis is not desirable (the output signal should be as higher as possible in order to increase the sensitivity of the system). Regarding the damping factor determinations it was already mentioned in Section 6.3.1, that the determination of this parameter is accomplished with the ‘Logarithm decrement method’ and using the consecutive points as represented in Figure 6.9. These points correspond to points 1 and 2 in Figure 6.21 a). The damping factor determined for the air conditions is approximately 0.125 which is very different from the damping ratio (determined from modal analysis) shown in Figure 6.19. According to the information provided in that figure, the damping ratio is 1.4 % for approximately 4400 Hz (the closest frequency to the excitation one in Figure 6.21). The methodologies used to calculate the damping factor (‘logarithm decrement method’) and damping ratio (modal extraction – Section 6.3.2.2) are alternative procedures to determine the damping of a given system. Being so, the  $DF$  and the  $DR$  values are expected to be at least in the same magnitude order. However, as previously mentioned, they show very different values and the  $DF$  (12.5%) is almost 9 times higher than the  $DR$  (1.4%). Note that the  $DF$  values presented so far are absolute values contrarily to the  $DR$  values which were always expressed as percentage. If one analyzes carefully the output wave in Figure 6.21, when points 1 and 2 are used to characterize the system’s response for  $DF$  determination ( $DF = 12.5\%$ ) the system returns very quickly to its rest position (see the trend line that crosses points 1 and 2). According to that trend line the system would achieve its rest position before 2 ms, which is not what happens with the real output wave since it only reaches the rest position around 8 ms. On the other hand, if the damping factor is recalculated using points 1 and 3, the obtained value is 1.5% which is very close to the one obtained for the damping ratio 1.4%. In fact, when considering the trend line that crosses point 1 and 3 (dashed line) it can be seen that the system gets to its rest position at 6 ms which is a more realistic figure compared to what happens with the output wave. So, the use of the damping factor to characterize the modal damping, as it was determined along the present Thesis, should be regarded with careful since depending on the output wave points  $x_1$  and  $x_2$  can not be representative of the real system’s damping. Nevertheless, the damping factor has been positively used, in the present work, to provide information about the type of deposit.

Note that the experimental results obtained by methodology 1, which will be discussed in the next chapters were obtained by exciting the system with a sinusoidal wave with characteristics:  $A_{in} = 2.9$  V and  $F_{in} = 4500$  Hz.

## **6.5. EXPERIMENTAL RESULTS**

The discussion of the ability that the different methodologies have to characterize the system in terms of its vibration parameters has already been presented. The question to address now is to find out if methodology 2 is a good procedure to monitor the adhesion/removal of deposits from the system. In order to do that, an experiment similar to the one described in Chapter 4, where fouling caused by calcium phosphate was induced on the MSS stainless steel surface, was performed. It is important to mention that the present chapter will not be focused on the description of the experimental methods nor on the characterization of the adhered fouling layers (see Chapter 4). It will rather discuss the output results, based on visual inspection and on the fact that the normalized amplitude (obtained from methodology 1) is an accurate and efficient way to follow the development of the deposit.

### **6.5.1. Error associated with each methodology**

In order to correctly interpret the adhesion/removal results, it is important to evaluate the error associated with each methodology (i.e. each parameter under study). This was accomplished by determining the standard deviation of 10 consecutive measurements at the same experimental conditions. The former procedure was performed for all the parameters except for methodology 2 (modal characterization), which only includes 4 consecutive measurements (since the modal identification is performed manually and is a time consuming procedure). This standard deviation was determined for different fluid temperatures and flow velocities and the averages of such standard deviations are shown in Table 6.2.

**Table 6.2:** Parameters evaluated under each methodology and respective standard deviations obtained under different temperatures and flow velocities

| Methodology                                      | Parameter   | Standard deviation mean |
|--|---|-------------------------|
| <u>Methodology 1</u>                             | Amplitude ( $A_{FFT}$ ) – (V)                       | 0.003                   |
|  | Damping factor ( $DF$ )                             | 0.005                   |
| <u>Methodology 2</u><br>(Modal characterization) | Frequency ( $Freq_{M1}$ ) – Mode 1 - (Hz)           | 6.9                     |
|  | Frequency ( $Freq_{M2}$ ) – Mode 2 - (Hz)           | 6.6                     |
|  | Damping ratio ( $DR_{M1}$ ) – Mode 1 - (%)          | 0.06                    |
|  | Damping ratio ( $DR_{M2}$ ) – Mode 2 - (%)          | 0.10                    |
| <u>Methodology 2</u><br>(RMS determinations)     | RMS Transfer function ( $RMS_{TF}$ ) - (V Hz/V)     | 0.05                    |
|  | RMS in frequency range 1 ( $RMS_{Pk1}$ ) - (V Hz/V) | 0.03                    |
|  | RMS in frequency range 2 ( $RMS_{Pk2}$ ) - (V Hz/V) | 0.06                    |

Note - recall that the RMS determinations were made in the following frequency ranges:

$$RMS_{TF}: 0 < \text{Frequency (Hz)} < 10000$$

$$RMS_{Pk1}: 2600 < \text{Frequency (Hz)} < 3500$$

$$RMS_{Pk2}: 4000 < \text{Frequency (Hz)} < 5500$$

The calculated “Standard Deviation Mean” is going to be considered as the error associated with the determination of each parameter.

### 6.5.2. Experimental results

The system was stabilized during 10 h with water recirculating at 51 °C and 0.45 m/s,  $Re \sim 15000$ ). After that period of time, the SMUF solutions were added to the water and the pH was adjusted to 6.70. Contrarily to what happened in Chapter 4, the SMUF solutions were added to the water that was recirculating (the flow has never been stopped). The solution of calcium phosphate was set to recirculate within the system for approximately 17 h. After that period of time,  $HNO_3$  has been injected into the system. The temperature and flow velocity of the solution was kept constant.

The adhesion and removal curves of calcium phosphate deposits on the SS plate monitored by methodology 1 ( $A_{FFT}$ ) are shown in Figure 6.22. A detailed view of the removal curve is additionally provided.

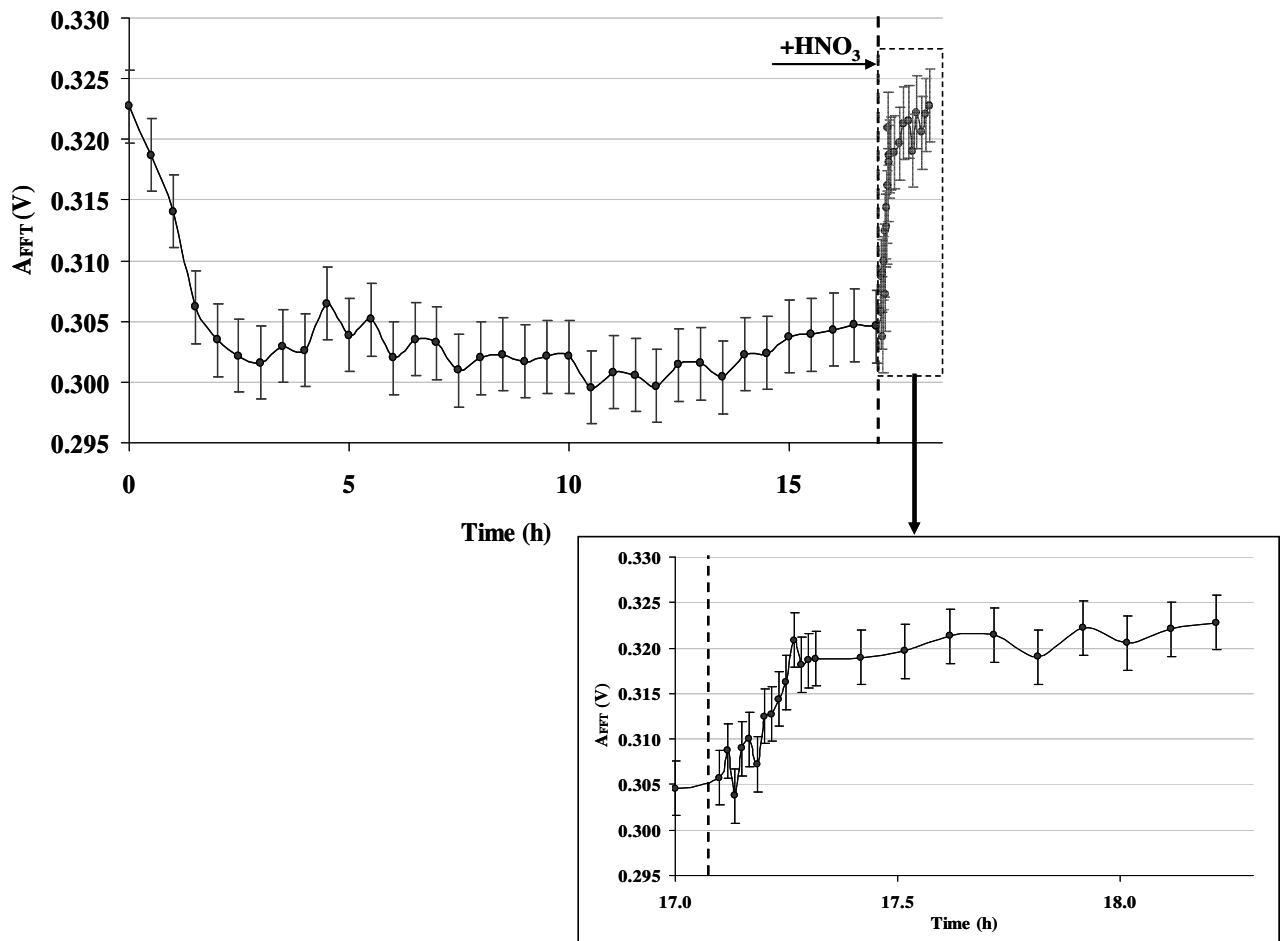


**Figure 6.22:** Adhesion and removal curves of calcium phosphate monitored with the  $A_{FFT}$  (methodology 1) and a detail graph of the removal

It is important to recall that the normalized amplitude (presented in Chapter 3 and 4) is a normalization of the  $A_{FFT}$ , where all the data points are subtracted from the first point value (corresponding to the clean plate) since the  $A_{FFT}$  is inversely related to the amount of deposit as shown in Figure 6.22. This means that the  $A_{FFT}$  curve in Figure 6.22 decreases with the increase of the amount of deposit. It can be seen that the deposit increased faster during the first hours until it reached a constant  $A_{FFT}$ . When the  $HNO_3$  was added to the SMUF solution, the amount of deposit rapidly decrease until the system reached its clean state ( $A_{FFT} \sim 0.323$  V).

One way to determine the best parameter to control the adhesion/removal phenomena is to compare its value variation during this process to its associated error (as determined in Section 6.5.1). The ratio between these two figures enables the comparison of the several presented parameters. The highest the ratio between the maximum variation and the mean

standard deviation the better is the parameter, as long as its variation is according to the phenomena occurring.

Consider the variation that occurred for  $A_{FFT}$  in Figure 6.22, where the maximum value corresponds to the clean plate and is around  $(A_{FFT})_{max} \sim 0.323$  V and the minimum value corresponds to the maximum amount of deposit  $(A_{FFT})_{min} \sim 0.300$  V. The variation from the start of the adhesion process is approximately 0.023 V and so, the ratio between this variation and the mean standard deviation (0.003 V) is around 7.7.

The ratio variation/standard deviation for all the parameters under study are shown in Table 6.3. It is obvious that the results shown on this table depend on the amount of deposit attached to the MSS plate. If a linear relation between each parameter and the amount of deposit is assumed to occur, one can assume that better parameters will always be better no matter the deposit amount.

**Table 6.3:** Percentage error for the parameters under study (during the adhesion process)

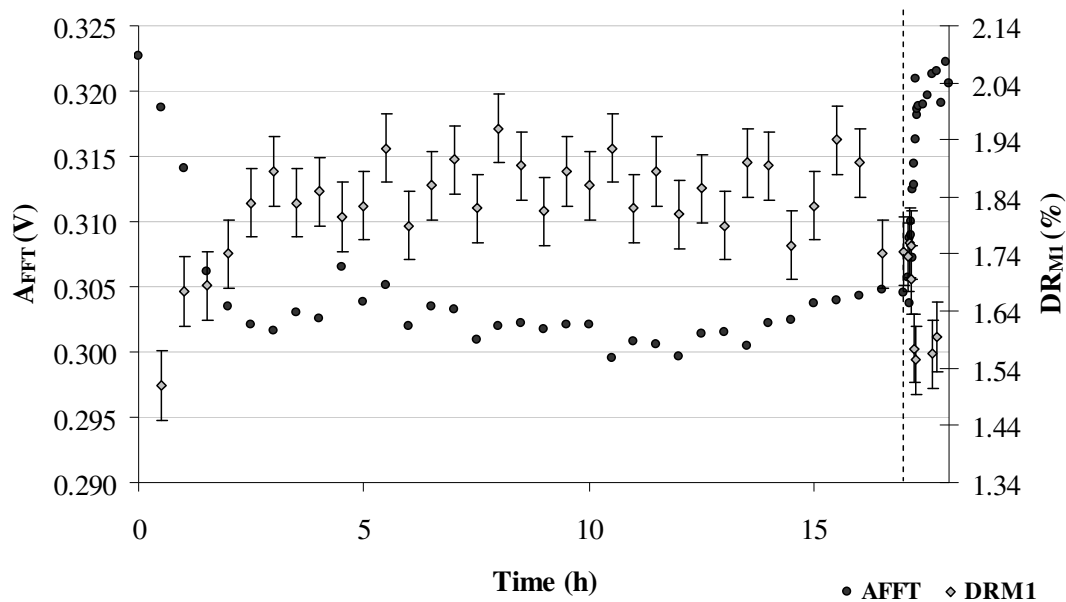
| <b>Methodology</b>                               | <b>Parameter</b>       | <b><u>Maximum Variation</u><br/>Standard Deviation</b> |
|--|------------------------|--|
| <u>Methodology 1</u>                             | $A_{FFT} - (V)$        | 7.7  |
|  | $DF$                   | 4.3  |
| <u>Methodology 2</u><br>(Modal characterization) | $Freq_{M1} - (Hz)$     | 2.3  |
|  | $Freq_{M2} - (Hz)$     | 3.2  |
|  | $DR_{M1} - (\%)$       | 7.5  |
|  | $DR_{M2} - (\%)$       | 4.3  |
| <u>Methodology 2</u><br>(RMS determinations)     | $RMS_{TF} - (V Hz/V)$  | 62   |
|  | $RMS_{Pk1} - (V Hz/V)$ | 42   |
|  | $RMS_{Pk2} - (V Hz/V)$ | 22   |

Table 6.3 shows that the ratios variation/standard deviation is very different from parameter to parameter. Since the MSS is intended to be an accurate and sensitive method to determine the adhesion of deposits on its surface, the controlled parameter variation should be as high as possible compared to the error associated with its determination. The previous chapter already demonstrated that the  $A_{FFT}$  is a good parameter to follow the adhesion of deposit on the MSS surface and that it has a linear variation with the amount (mass) of deposit. According to that

information, only parameters with ratios variation/standard deviation higher than 7 (similar to  $A_{FFT}$ ) will be analyzed in more detail.

a) **Methodology 1** ( $A_{FFT}$  and  $DF$ ): the analysis of the  $A_{FFT}$  has already been discussed. Regarding the damping factor, the ratio variation/standard deviation is not high enough. In fact, this is according to what was observed in the previous chapter, since the  $DF$  was only used to give indications about the type of deposit rather than to provide information about the amount of such deposit. In fact the  $DF$  shows different mean values according to the type of adhered deposit.

b) **Methodology 2 – Modal characterization** ( $Freq_{M1,M2}$  and  $DR_{M1,M2}$ ): the frequencies of the two modes and the damping ratio ( $DR$ ) of the mode 2 shows low ratio variation/standard deviation. Only the  $DR_{M1}$  shows an acceptable ratio variation/standard deviation of 7.5. The variation of the  $DR_{M1}$  and of the  $A_{FFT}$  with time is shown in Figure 6.23. Note: for simplicity purposes in Figure 6.23 and Figure 6.24 only the error bars associated with the parameter  $DR_{M1}$  and  $RMS$ 's will be provided (the  $A_{FFT}$  error bars can be seen in Figure 6.22).



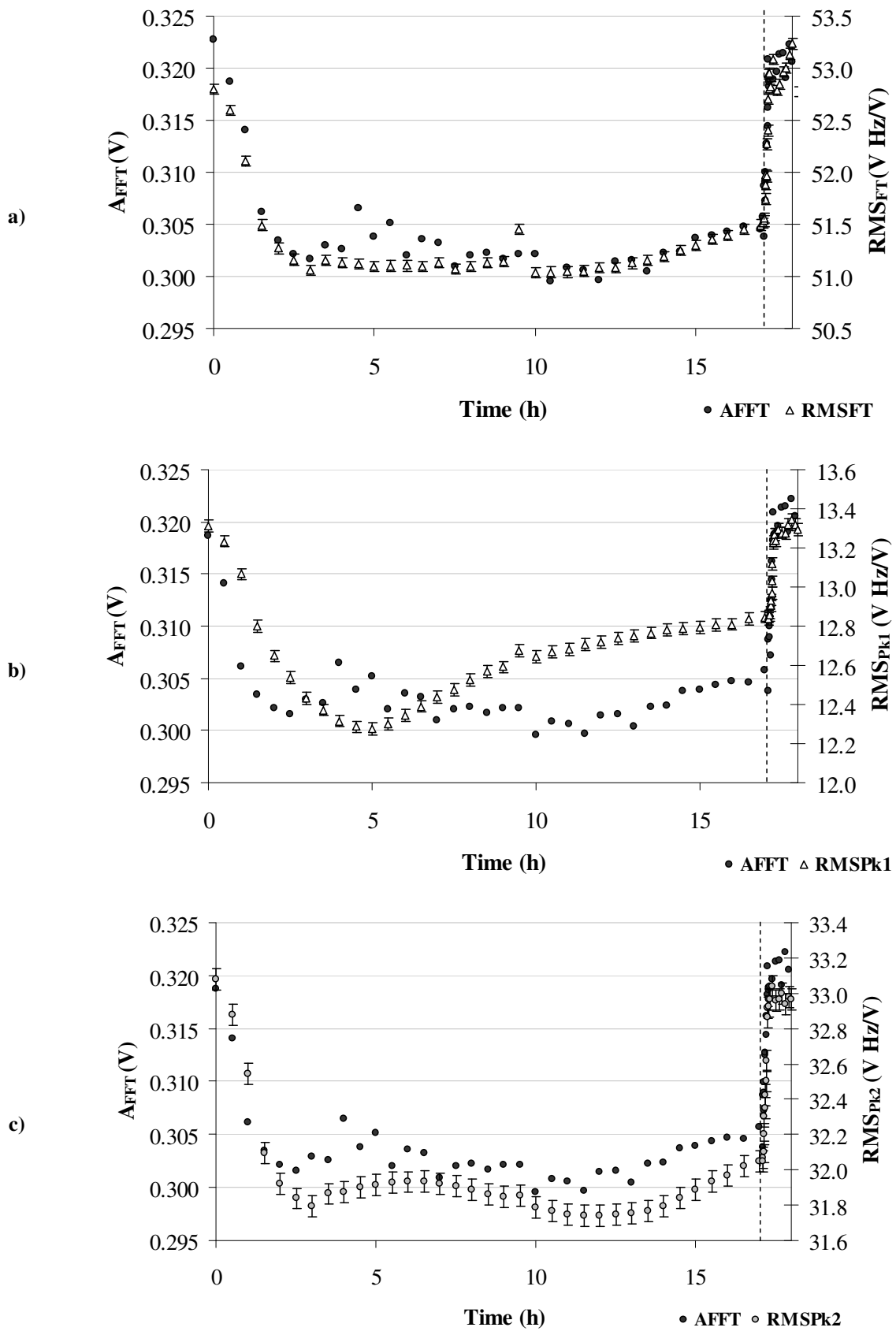
**Figure 6.23:** Comparison between the variation of the amplitude ( $A_{FFT}$ ) and of the damping ratio of the first mode ( $DR_{M1}$ ) with the adhesion/removal of calcium phosphate deposit



Figure 6.23 shows that the  $DR_{MI}$  is also a good indicator of what happens with the deposit, since it is able to follow both its adhesion and removal. According to what was expected, the damping ratio increases with the increase of the attached layer since the deposit is an additional source of energy dissipation. Since the ratio variation/standard deviation of the  $DR_{MI}$  is similar to the one observed for the  $A_{FFT}$ , one can consider this parameter as a good one to monitor the amount of deposit. Since the damping ratios and frequencies are the parameters that characterize the vibration of a given system, the  $DR_{MI}$  should be regarded as an important element to be analyzed.

It is important to highlight that in spite of the physical concept behind the  $DF$  and  $DR$  being the same (the measurement of the system's ability to dissipate energy) these parameters are differently affected by the deposit, according to what was previously discussed. In fact, this happens because the methodologies used to determine each of them are quite different (cf. Section 6.4.5). The quantification of the  $DF$  is based on the output wave which reflects the interaction of several different modes. When using the transfer function to calculate the  $DR$ , one determines the energy dissipation associated with just one specific vibration mode. Each mode can be differently affected by the deposit. That explains why the  $DR_{MI}$  follows the adhesion of the deposit, and the  $DF$  is only able to provide qualitative information about the type of adhered deposit.

c) **Methodology 2 – RMS determinations** ( $RMS_{TF}$ ,  $RMS_{Pk1}$ ,  $RMS_{Pk2}$ ): the ratio variation/standard deviation associated with these determinations is much higher than for any of the other parameters under study. This means that the error associated with the determination of these parameters is very low when compared to their variation with the deposit's formation. The representation of the RMS's and  $A_{FFT}$  curves against time is shown in Figure 6.24. Figure 6.24 a), b) and c) show, respectively, the comparison between the curves of  $A_{FFT}$  and of  $RMS_{TF}$ ,  $RMS_{Pk1}$  and  $RMS_{Pk2}$ .



**Figure 6.24:** Comparison of the curves of the adhesion and removal process given by the  $A_{FFT}$  and the RMS determinations – a)  $RMS_{TF}$ , b)  $RMS_{Pk1}$ , c)  $RMS_{Pk2}$

Figure 6.24 shows that in spite of the low error associated with the 3 parameters not all the RMS determinations are able to properly monitor what happens with the deposit. For example, Figure 6.24 b) shows that there is a difference between the behavior of the  $RMS_{Pk1}$  and of the  $A_{FFT}$  curves. In fact, according to the  $RMS_{Pk1}$  curve the deposit started to decrease after 6 h which was not visually confirmed, nor observed in the  $A_{FFT}$  curve (or any of the other parameters). This suggests that the  $RMS_{Pk1}$  should not be used to monitor the adhesion/removal of fouling layers, in spite of a good ratio variation/standard deviation of 42. Possibly the vibration modes between 2600 Hz and 3500 Hz are not linearly affected by the deposit attached to the MSS surface.

On the other hand, the  $RMS_{Pk2}$  (represented in Figure 6.24 c)) seems to be another good parameter that provides valuable and accurate information about the amount of deposit. Its ratio variation/standard deviation is improved when compared to  $A_{FFT}$  ( $22 > 7.7$ ).

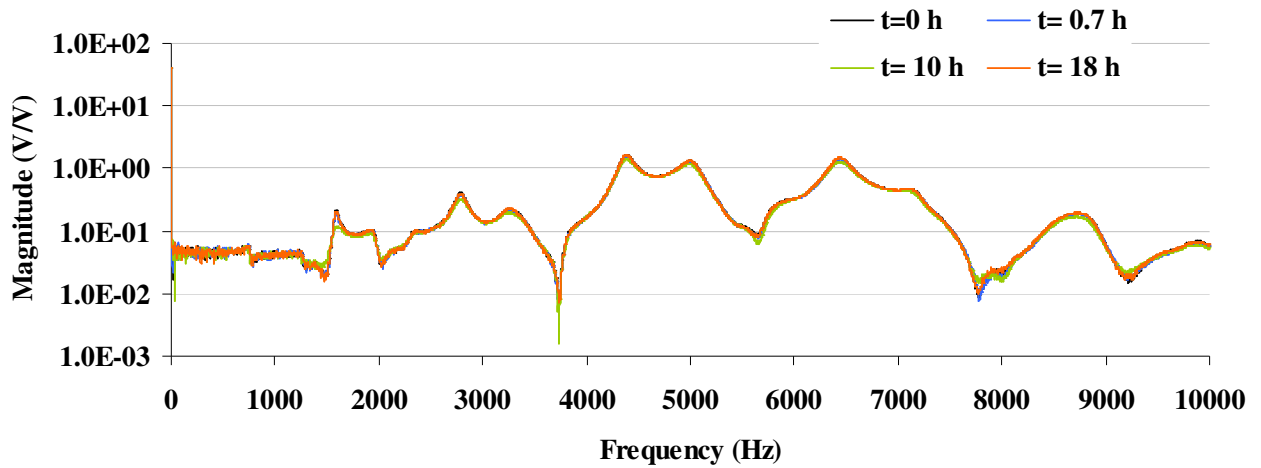
The  $RMS_{TF}$  (which integrates the information of the transfer function between 0 and 10000Hz) showed to be the parameter that best describes what happens in the MSS surface. It can be seen in Figure 6.24 a) that the  $RMS_{TF}$  and the  $A_{FFT}$  curves are almost superimposed confirming the accuracy of the  $RMS_{TF}$  determination which was able to increase the resolution of the system (its ratio variation/standard deviation was 62 against the 7.7 of the amplitude measurement). As already demonstrated, the former showed to be the most robust technique to evaluate the amount of deposit attach to the MSS surface.

### 6.5.3. Overall discussion of the results and methodologies

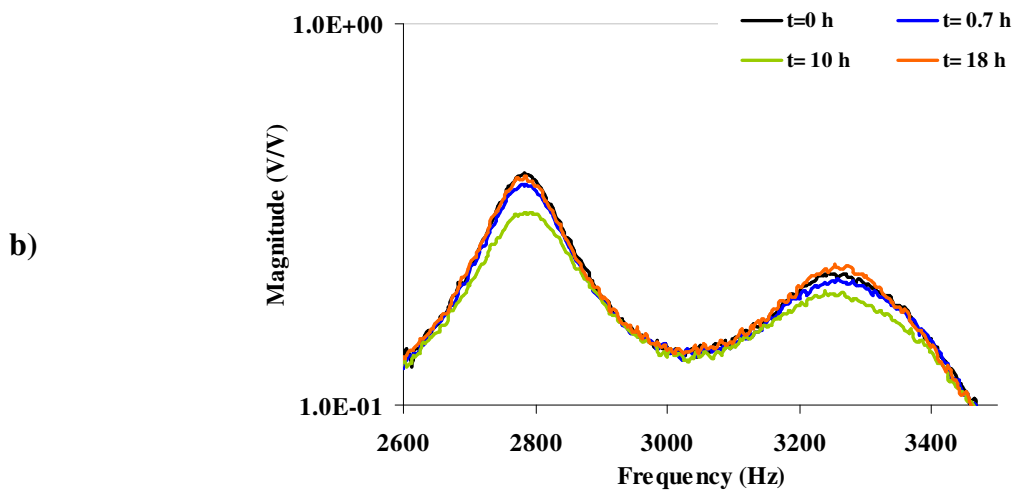
Let us consider the transfer functions obtained at four distinct points of the adhesion/removal curve in Figure 6.22: i)  $t=0$  h; ii)  $t=0.7$  h; iii)  $t=10$  h and iv)  $t=18$  h. These points correspond to:

- (i) and (iv) to the SS clean state respectively at the beginning and at the end of the experiment ( $A_{FFT}$  is 0.323 V for i) and 0.321 V for ii));
- ii) and iii) correspond to two different  $A_{FFT}$  values (i.e. different stages of the deposit formation is considered and so, different amounts of deposit are adhered to the SS surface and mass of point iii) is higher than point ii)), being respectively 0.313 V and 0.300 V.

Figure 6.25 shows the magnitude function of the four curves for the instants previously indicated (0, 0.7, 10 and 18 h). Additionally, a detail of such transfer function can be seen in graphs b) and c), in the range of frequencies chosen to perform the RMS calculation, respectively: between 2600 – 3500 Hz (peak 1) and between 4000-5500 Hz (peak 2).



a)



b)

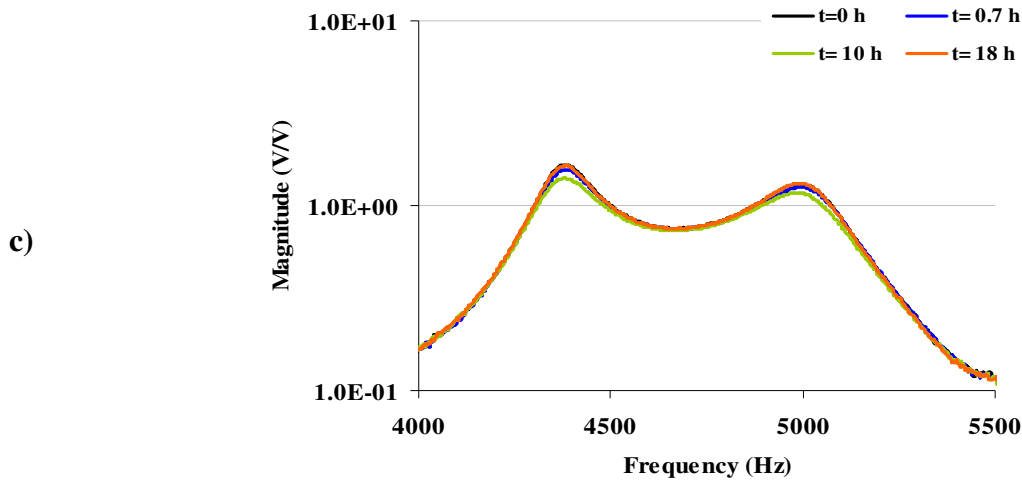


**Figure 6.25:** The magnitude of the transfer functions for the system at different deposit stages for frequencies between: a) 0-10000 Hz; b) 2600-3500 Hz (peak 1); c) 4000-5500 Hz (peak 2)

It can be seen that the magnitude of the functions at different adhesion/removal periods are globally very similar. In fact, the differences observed in their magnitude are very subtle and are more perceptible around the resonant modes. The characteristics of the resonant peaks found in Figure 6.25 are summarized in Table 6.4.

**Table 6.4:** Modal characteristics of the resonant peaks in Figure 6.25 c)

| Methodology                                      | Parameter                  | Time (h) |        |        |        |
|--|----------------------------|----------|--------|--------|--------|
|  |                            | 0        | 0.7    | 10     | 18     |
| <u>Methodology 1</u>                             | $A_{FFT} - (V) \pm 0.003$  | 0.323    | 0.313  | 0.300  | 0.321  |
| <u>Methodology 2</u><br>(Modal characterization) | $Freq_{M1} - (Hz) \pm 6.9$ | 4381.3   | 4374.2 | 4373.2 | 4376.8 |
|  | $Freq_{M2} - (Hz) \pm 6.6$ | 5008.8   | 5001.5 | 5003.0 | 5012.7 |
|  | $DR_{M1} - (\%) \pm 0.06$  | 1.51     | 1.68   | 1.92   | 1.58   |
|  | $DR_{M2} - (\%) \pm 0.10$  | 1.71     | 1.82   | 2.05   | 1.77   |

The graphs in Figure 6.25 illustrate that, according to what was expected, the curves corresponding to the clean plate (for 0 h and 18 h) are almost coincident. This conclusion is also corroborated by the data in Table 6.4, since the frequencies and damping ratios for  $t=0$  and  $t=18$  h are very similar (under the error associated with each parameter). On the other hand, the curve with lower magnitude occurs when there is more deposit attached to the SS plate ( $t=10$  h). The results in Table 6.4 indicate that the frequency of the resonance modes is almost constant for different amounts of deposit (being their average and standard deviation

respectively:  $4376.4 \text{ Hz} \pm 3.6$  for mode 1 and  $5006.5 \text{ Hz} \pm 5.2$  for mode 2), while the damping ratio increases with the increase of the amount of the deposit. By visual inspection of the output transfer functions curves, it is possible to conclude that the damping ratio is the modal parameter affected by the adhesion/removal of deposit, although as already demonstrated only the  $DR_{M1}$  should be analyzed since the  $DR_{M2}$  has a high error associated with its determination. In fact, the problem lies on the damping identification, which has high errors (standard deviation) associated with its quantification, since the system is highly damped. For example, the effect of the deposit on the damping ratio of the resonant peaks observed in Figure 6.25 b) is quite noticeable, although the identification software used was not able to accurately adjust a model to determine this damping ratio. Furthermore, these results indicate that the dynamic characteristic of the system that is affected by the deposit (its increase or decrease) is the damping ratio. Being so, the both the  $A_{FFT}$  and the  $RMS_{FT}$  are indirect measurements of the effect that the deposit has on the damping ratio.

It is also perceptible from Figure 6.25 that the effect of the deposit on the modal characteristics of the system (as previously mentioned on the damping ratio) is observed not only for a specific modal frequency but occurs also for many of them. This conclusion clarify why the integrated measurements of the transfer functions (the  $RMS_{TF}$ ) showed to be more accurate (and with high resolution) than the other determinations. In fact, the RMS determination integrates the information on a given frequency zone of the transfer function and so, the effect that the deposit has on all of the resonant frequencies (included in such range) is taken into account.

Another important observation that can be taken from Figure 6.25 c) is that the modes that respond with higher magnitudes are comprised between the 4000 and 5500 Hz. In fact, this observation is in accordance to what was concluded from methodology 1 since the excitation sine wave is in the range of frequencies that respond with higher magnitude. According to Figure 6.25, it can be seen that methodology 1 would respond more positively to the adhesion/removal of deposit if the excitation frequency was 4380 Hz instead of 4500 Hz because the separation between the four curves is more perceptible around the 4380 Hz. This conclusion brings an important input to the future work since a more precise method to determine the resonant frequency of the system should be used alternatively to the method

presently implemented: it is more accurate to analyze the magnitude function to determine the resonant frequency than to use the ‘resonant frequency determination’ software.

## **6.6. OTHER STUDIES**

The effects of temperature, flow regime and flow velocity on the measured parameters were also studied. In the previous chapters two distinct situations occurred: the external operating variables (temperature and flow velocity) were kept constant (e.g. Chapters 3 and 4) or, in the case of the shampoo removal (Chapter 5), a previous calibration between the amplitude ( $A_{FFT}$ ) and those variables was performed. For the latter case, a correction of the  $A_{FFT}$  with the temperature and flow velocity has been introduced in the processed data (according to Appendix C). With proper calibration, the effect of these experimental conditions on the analyzed parameters can be eliminated.

As already demonstrated, all the evaluated vibration parameters are based on the effect that the deposit has on the modal characteristics of the system (as seen before on the damping ratio). Thus, the following discussion will contemplate the effect that the experimental conditions have on such modal parameters of the system. A special attention will be provided to the analysis of the transfer function since it allows an important assessment of the changes that occur on the modal characteristics of the system. For simplicity purposes, the transfer function will be only represented between 4000 and 5500 Hz, since the two identified modes lie on this range.

The study provided in the present section is only preliminary, since the effect of the temperature and flow velocity engages a lot of other factors whose quantification and characterization is not under the scope of the present Thesis. This section will be focused on analyzing the results in a way that may substantially contribute to the future work. Two different approaches will be evaluated: i) the effect that the external conditions have on the modal characteristics, and ii) this effect compared with the error associated with the determination of such parameters. Regarding point i), the variations observed in the modal parameters will be compared with the standard deviation mean associated with their determination (according to Table 6.2, Section 6.5.1). On the other hand, the discussion of point ii) will be based on the determination of the ratio variation/standard deviation. The

value 5 was established as limit for the ratio variation/standard deviation: below this number the effect will be considered negligible, while above this figure the external condition will be considered to have a significant effect on the parameter.

### 6.6.1. Temperature

The study of the effect of the temperature on the evaluated parameters is highly dependent on the way the monitoring system is assembled. The temperature affects the whole system in a variety of different ways, among them: i) it affects the actuator and/or the sensor measurement; ii) the flow cell and plate materials expand with the increase of the temperature; iii) the sealant mechanical properties (hardness) might change with temperature and it can also expand; iv) the water viscosity decreases with the increase of temperature. It is obvious that the output results will be a combination of these individual factors exert into the system. Let us consider three different water temperatures: 30 °C, 35 °C and 45 °C. The system's TFs without flow are compared in Figure 6.26.

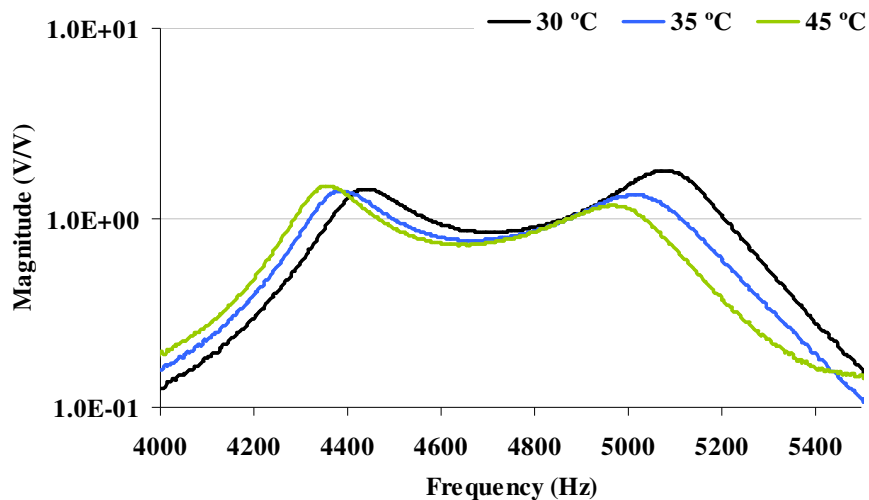


**Figure 6.26:** Magnitude function of the system when the flow cell is filled with water at different temperatures (no flow)

Figure 6.26 shows that the temperature has an effect on the transfer functions which can also be confirmed in Table 6.5 where the results of the modal characterization are presented. In this table it can be seen that an increase of 15 °C (from 30 °C to 45 °C) causes a decrease of 85.3 Hz on the frequency of mode 1 and of 102.3 Hz for the frequency of mode 2. These differences are quite high when compared to the standard deviation mean associated with each parameter which is around 7 Hz (the variation of the frequency of the two modes caused by



an increase of 15 °C is several times superior to the standard deviation associated with the frequency determinations). And so, it can be seen that the increase of the water temperature decreases the frequency of the system's vibration modes. Furthermore, it can be seen that the variation of the frequency modes is also considerably high even for a 5 °C variation (from 30 to 35 °C), where the modal frequencies decreases for mode 1 and for mode 2, respectively, 55.5 Hz and 49.2 Hz. The decrease on modal frequencies can probably be explained by a decrease of the system's rigidity. The reduction in rigidity associated to a temperature increase is probably due to the effect of the O'rings dilatation and/or hardness decrease.

**Table 6.5:** Modal parameters (frequency and damping ratio) for three water temperatures (no flow)

| Methodology                               | Parameter                    | Temperature (°C) |        |        |
|---|------------------------------|------------------|--------|--------|
|   |                              | 30               | 35     | 45     |
| Methodology 2<br>(Modal characterization) | $Freq_{M1}$ - (Hz) $\pm$ 6.9 | 4445.7           | 4390.2 | 4360.4 |
|   | $Freq_{M2}$ - (Hz) $\pm$ 6.6 | 5081.5           | 5032.2 | 4979.3 |
|   | $DR_{M1}$ - (%) $\pm$ 0.06   | 2.11             | 2.07   | 1.73   |
|   | $DR_{M2}$ - (%) $\pm$ 0.10   | 1.36             | 1.71   | 2.04   |

The ratios variation/standard deviation associated with the modal frequencies observed for a 15 °C increase are 12.4 for  $Freq_{M1}$  and 15.4 for  $Freq_{M2}$  which is well above the limit 5. The effect of the temperature on the modal frequencies is still important for a 5 °C variation (from 30 °C to 35 °C), since the ratios variation/standard deviation are 8.1 for mode 1 and 7.5 for mode 2. Considering these results, the effect of the temperature on the modal frequencies can not be neglected.

Concerning the damping ratio, the two analyzed modes showed a different behavior for an increase of 15 °C:  $DR_{M1}$  decreases 0.38, while the  $DR_{M2}$  increases 0.68. Since the standard deviation mean associated with the  $DR_{M1}$  and  $DR_{M2}$  is respectively 0.06 and 0.10 it can be seen that there is also a significant effect of the temperature increase on these two modal parameters. The effect of an equal temperature variation of 15 °C on the ratio variation/standard deviation of the damping parameters is approximately 6.3 to 6.8 for both modes. On the other hand when an increase of 5 °C is considered, the effect on the damping ratio can be neglected since the ratios variation/standard deviation are very low: 0.7 for the  $DR_{M1}$  and 3.5 for the  $DR_{M2}$  (both below 5). In fact, the effect of a 5 °C variation on the

damping ratio of the mode 1 is totally neglected, since the variation of such parameter is smaller than the mean standard deviation associated with its determination. So, the effect of the temperature on the damping ratios should only be considered for high temperature variations while it can be neglected for low ones (especially when considering the  $DR_{M1}$ ). It is also important to note that the temperature changes does not have the same effect on all the modal damping ratios, since of the two analyzed modes react in opposite way: one increases with the increase of temperature and the other decreases.

From the former discussion it can be concluded that the temperature has an effect on the frequencies and the damping ratios. This effect showed to be much more important on the modal frequencies than on the damping ratios. It is also interesting to note that the effect caused by the adhesion of deposit on the frequency can be neglected (recall that the ratio variation/standard deviation was low: 2.3 for  $Freq_{M1}$  and 3.2 for  $Freq_{M2}$  – according to Table 6.3). But on the other hand, the effect of temperature causes an important variation of modal frequencies (even for just a 5 °C change). Being so, it seems to indicate that during the monitoring of an adhesion process it is possible to follow independently the temperature variation by recurring to the frequency analysis. In fact, if one recalls the adhesion process in Section 6.5, the frequency variation of both modes was neglected indicating that no significant changes in the temperature occurred. This observation was confirmed by the temperature values observed (measured with PT 100 sensors) along the adhesion/removal process, being  $51.1\text{ °C} \pm 0.3$ . This opens a very interesting window for further research and suggests that the analysis of the frequency (in parallel with one of the other parameters that are used to monitor the deposit amount) can be an indicative of the temperature changes in the bulk.

### **6.6.2. Flow velocities**

Similarly to what was observed for the temperature, the flow velocity is also a quite complex condition to be analyzed. In parallel with the former conditions it is necessary to consider their effect on the flow regime, since when it changes from laminar to turbulent, vortices start to appear in the flow. The flow regime (based on the Reynolds number criterion) is dependent not only on the characteristics of the pipes – which are constant within these experiments – but also on the flow velocity and on the fluid temperature. Additionally, the fluid temperature

has a direct effect on the density and on the viscosity of the fluid. So, again, a lot of additional and interchangeable effects are simultaneously observed.

In order to evaluate the effect of the flow velocity variation in the modal characteristics of the system, the magnitude function was compared for three different flow velocities: i)  $v=0$  m/s - no flow; ii)  $v=0.08$  m/s - laminar flow ( $Re\sim 1800$ ) and iii)  $v=0.39$  m/s - turbulent flow ( $Re\sim 9000$ ), being  $T=30^\circ\text{C}$  (see Figure 6.27).

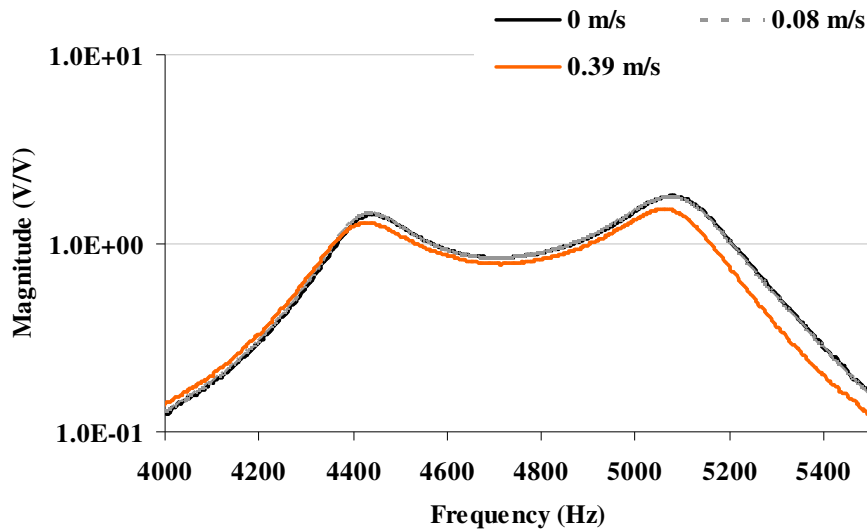


**Figure 6.27:** Magnitude function for three flow conditions:  $Re=0$ ,  $Re\sim 1900$ ,  $Re\sim 9000$  (for  $T=\text{constant}=30^\circ\text{C}$ )

According to what was expected there is no significant difference between the transfer functions with no flow and with laminar flow (the two curves are superimposed). When these curves are compared with the one obtained for the turbulent flow ( $Re\sim 9000$ ) a change on the modal parameters occurs – see Table 6.6.

**Table 6.6:** Modal parameters (frequency and damping ratio) for three flow velocities ( $T=30^\circ\text{C}$ )

| Methodology                               | Parameter                    | Flow Velocity (m/s) |                      |                        |
|---|------------------------------|---------------------|----------------------|------------------------|
|   |                              | 0                   | 0.08                 | 0.39                   |
|   |                              | Re=0<br>(no flow)   | Re~1900<br>(laminar) | Re~9000<br>(turbulent) |
| Methodology 2<br>(Modal characterization) | $Freq_{M1}$ - (Hz) $\pm 6.9$ | 4445.7              | 4439.5               | 4419.4                 |
|   | $Freq_{M2}$ - (Hz) $\pm 6.6$ | 5081.5              | 5077.6               | 5071.5                 |
|   | $DR_{M1}$ - (%) $\pm 0.06$   | 2.11                | 2.10                 | 2.18                   |
|   | $DR_{M2}$ - (%) $\pm 0.10$   | 1.36                | 1.41                 | 1.66                   |

When the flow passes from laminar to turbulent regime, there is a slight effect on the  $Freq_{M1}$  which decreases 20 Hz and is insignificant on the  $Freq_{M2}$  which decreases only 6.1 Hz (the latter variation is smaller than the standard deviation associated with its measurement). However, for  $Freq_{M1}$  it can be seen that the effect is much smaller when compared to the effect, for example, of the temperature (changed 55.5 Hz with 5°C increase) and is similar to the one introduced by the deposit adhesion. Being so, since the ratio variation/standard deviation (2.9) is smaller than 5 the effect of the flow regime on the  $Freq_{M1}$  can be neglected.

The data shown in Table 6.6 points out that there is an increase of the damping ratio of the two considered modes: 0.08 (for mode 1) and 0.25 (for mode 2). In fact, this damping ratio increase may be related with the existence of vortices in the turbulent regime, which are additional sources of energy dissipation, increasing the system's damping. It should, however, be noted that the ratio variation/standard deviation associated to the damping ratio measurements for the regime variation is very low when compared with the established 5 (1.3 for  $DR_{M1}$  and 2.5 for  $DR_{M2}$ ). Being so, the effect of the flow regime on the variation of the DR can be neglected.

### **6.6.3. Simultaneous effects of the temperature and flow velocity**

The temperature and the flow regime effects were analyzed separately, although in real situations simultaneous changes are likely to occur. For analysis purposes let us consider two temperatures (30 °C and 45 °C) and two flow velocities (~0.09 m/s and 0.39 m/s). The magnitude function of such combined conditions is compared in Figure 6.28.

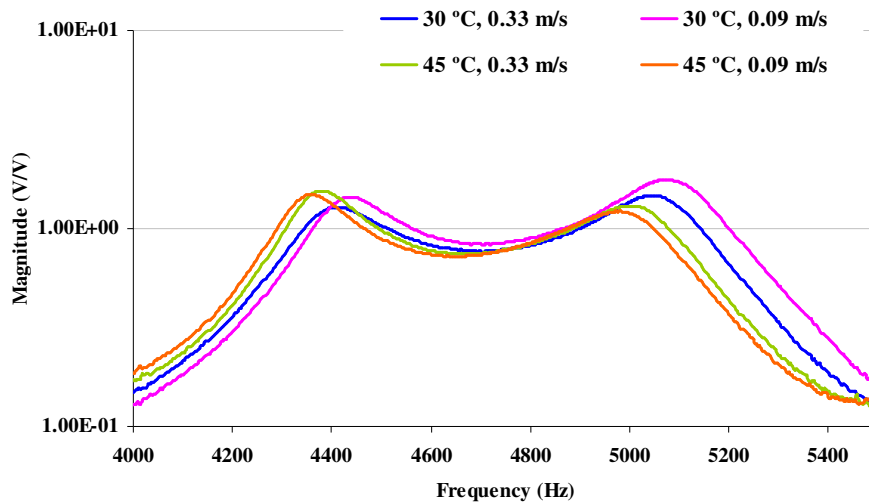


**Figure 6.28:** Magnitude function for different temperatures (30 and 45 °C) and different flow velocities (~0.09 m/s and 0.39 m/s)

The modal identification of the former transfer curves are shown in Table 6.7.

**Table 6.7:** Modal parameters (frequency and damping ratio) for different experimental conditions

| Methodology                                      | Parameter                         | $T=30\text{ }^{\circ}\text{C}$ |               | $T=45\text{ }^{\circ}\text{C}$ |                |
|--|-----------------------------------|--------------------------------|---------------|--------------------------------|----------------|
|  |                                   | 0.08 m/s                       | 0.39 m/s      | 0.09 m/s                       | 0.39 m/s       |
|  |                                   | $Re\sim 1900$                  | $Re\sim 9000$ | $Re\sim 2900$                  | $Re\sim 11800$ |
| <u>Methodology 2</u><br>(Modal characterization) | $Freq_{M1} - (\text{Hz}) \pm 6.9$ | 4439.5                         | 4419.4        | 4358.4                         | 4387.7         |
|  | $Freq_{M2} - (\text{Hz}) \pm 6.6$ | 5077.6                         | 5071.5        | 4987.7                         | 5025.9         |
|  | $DR_{M1} - (\%) \pm 0.06$         | 2.10                           | 2.18          | 1.73                           | 1.89           |
|  | $DR_{M2} - (\%) \pm 0.10$         | 1.41                           | 1.66          | 1.86                           | 1.88           |

It can be seen that the frequency of the two modes decreases with the increase of temperature. In fact, this is in accordance with the conclusions taken in Section 6.6.1, and reemphasizes the idea that the system gets less rigid with the increase of the temperature (and so the frequency becomes lower). It is also interesting to observe that the effect of the temperature decreases for higher flow velocities. For example, for a temperature variation from 30 to 45 °C, the frequency of mode 1 decreased: 81.1 Hz at 0.09 m/s and 31.7 Hz at 0.39 m/s. These results seem to indicate that for turbulent flow the temperature has lower effect than for laminar flow. When considering the same temperature (30 °C), the increase of the flow velocity decreased the frequency of both modes, while for 45 °C an increase on the frequency modes was

observed. Concerning this velocity effect, it is obviously not linear and is not yet fully studied and understood, so no further considerations will be made here.

Once again it is observed that the damping ratio and the temperature are not linearly related, since (for similar flow velocities) an increase of the temperature is reflected on a decrease of the damping for mode 1 and on an increase of the damping for mode 2. The ratio variation/standard deviations associated with the variations introduced by the temperature on the  $DR$  values are: 6.1 (at 0.09 m/s) and 4.8 (at 0.39 m/s) for mode 1; 4.5 (at 0.09 m/s) and 2.2 (at 0.39 m/s) for mode 2. These values are near the limit value 5, reemphasizing that the simultaneous effect of the temperature and of the flow velocity on the  $DR$  should be carefully studied for each specific case under analysis.

When considering the same temperature it can be seen that the increase of the flow velocity increases the  $DR$  of both modes. However these changes are almost insignificant since the highest ratio variation/standard deviation is 2.5 (for  $DR_{MI}$ , 45 °C and 0.39 m/s), which is half the established limit value of 5.

From the previous discussion it is clear that the most important effect is exerted by the temperature on the modal frequencies of the system. That effect is smaller for higher flow velocities. For a given system it is crucial to evaluate the effect of the temperature and flow velocity on the output parameters. In laboratory experiments where those operating conditions are fully controlled, this is not usually a problem. For example, recall what happened in the shampoo removal experiments (Chapter 5) where a relation between the  $A_{FFT}$  and the temperature and flow velocity was determined. For each measured point the  $A_{FFT}$  was corrected by that calibration (recall that the software also acquired the temperature of the system). The effect of the temperature and flow velocity becomes a major issue when addressing industrial applications. In industrial facilities the systems are affected by all type of external factors and the calibrations should be carefully done. A bad calibration may lead to a misinterpretation of the output results. Temperature and flow velocity measurements should be done in parallel with the MSS determinations, since this information will allow to easily implement an automatic correction of the output data.

## 6.7. CONCLUSIONS

The present chapter compared the methodology (sinusoidal excitation) used in the former chapters with the experimental modal analysis (EMA). The implementation of the EMA technique was a very important improvement since it enabled the determination of the vibrating modal parameters: modal frequency and modal damping. Furthermore, this technique allowed to determine the best configurations to seal the SS plate within the flow cell (based on such vibrating parameters).

Regarding the monitorization of the adhesion/removal processes, the results seem to suggest that a combination between the two methodologies is desirable since the sinusoidal excitation allows the quantification of the  $A_{FFT}$  and of the  $DF$ , which were found to be related respectively to the amount and to the type of adhered layer. On the other hand, the  $RMS_{FT}$  (gathered with the EMA) showed to be the parameter that is able to follow the adhesion/removal of the deposits with lowest inherent error. Additionally, it was found out that the amount of deposit has an effect on the damping ratio of the system, and being so, both the  $A_{FFT}$  and the RMS are indirect measurements of the variation occurred on that vibrating characteristic.

Concerning the effect of other external conditions on the modal characteristics it was found (for the specific conditions under study) that: i) the modal frequencies are highly affected by the temperature, while the same effect on the damping ratios can be neglected for small temperature variations; ii) the effect of the flow regime in spite of the variation introduced both on the modal frequencies and on the damping ratios can be neglected when the errors associated with their determinations are considered; iii) the effect of the temperature on the modal frequencies is higher for lower flow velocities. The former point highlights the importance of a proper analyzes for each specific case and suggests that a calibration between the monitored parameter and the temperature and flow velocity could be necessary in some situations. Nevertheless, it is important to recall that these studies are still preliminary and should be studied in further detail.

Another relevant conclusion is related with the importance that the simulations have on the interpretation of the results or on the devising of new solutions. A software was used in order

to optimize the dimensions of the MSS plate (based on two previously established criteria). Additionally, a simulation study has been performed in order to evaluate the effect of the boundary conditions and of the plate dimensions on the vibrating modal frequencies and on modal shapes of the plate.

### **REFERENCES**

Arenas, J. P. (2003). "On the vibration analysis of rectangular clamped plates using the virtual work principle." Journal of Sound and Vibration 266(4): 912-918.

Dossing, O. (1988). Structural testing. Part I: Mechanical mobility measurements, Brüel & Kjaer.

Fletcher, N. H. and T. D. Rossing (1998). The physics of musical instruments. New York, Springer-Verlag.

Inácio, O., L. L. Henrique and J. Antunes (2006). "The dynamics of Tibetan singing bowls." Acta Acustica united with Acustica 92(4): 637-653.

Rao, S. S. (2004). Mechanical Vibration (4th edition), Prentice Hall.

Reddy, J. N. (2007). Theory and analysis of elastic plates and shells (Chapter 9), CRC Press.

Shuyu, L. (2001). "Study on the flexural vibration of rectangular thin plates with free boundary conditions." Journal of Sound and Vibration 239(5): 1063-1071.



## 7. MAIN CONCLUSIONS AND FORTHCOMING WORK

### 7.1. CONCLUSIONS

The Mechatronic Surface Sensor (MSS) and its ability to measure on-line the formation and removal of deposits and fluid films that contaminate industrial surfaces were the object of dissertation of the present Thesis. The MSS was found to:

- i) quantitatively determine the amount of layer attached to the surface;
- ii) give semi-quantitative information that enables to distinguish different types of attached layers (inorganic rigid layers versus more viscoelastic biological/organic layers);
- iii) monitor in real time the cleaning operations and determine the respective end-point;
- iv) have applications in distinct processes, from milk pasteurization to cooling water circuits, and shampoo cleaning procedures;

Another important part of the work was focused on studying the working principles behind the MSS. The implementation of the experimental modal analysis methodology showed to be an important improvement to the initial methodology (sinusoidal excitation) enabling the characterization of the MSS in terms of its vibrating properties as well as to conclude about the best configuration to adopt. It was also found that the characteristic of the vibrating system that reflects the effect of the deposit on the monitored surface is the modal damping of the system.

The overall results obtained so far seem to indicate that the MSS has a significant potential for laboratory and field applications. With a proper calibration (as already presented in Chapter 5) the MSS may respond to three important questions regarding the optimization and flexibilization of the production and cleaning procedures: a) When should the plant be cleaned; b) How should the plant be cleaned; c) When is the cleaning end-point achieved. Answering these questions contributes to optimize the cleaning procedures, improving the whole operational cycles of the plant, increasing the quality of the final product and saving in processing costs (mainly associated with water, chemicals, energy and wastewater treatments).

## 7.2. FUTURE WORK

The present work was the beginning of the study of the MSS (and in spite of the good results already achieved), there is still a wide range of work to do mainly regarding the interpretation of the information that is collected from the MSS. This point is crucial because for each type of deposit a calibration between the mass and the signal should be implemented. Furthermore, the modal characteristics of the system were found to be affected by changes of temperature and/or of the flow velocity. This former point demands the implementation of proper and expedites calibration procedures. The design and the mathematical modelling of a more robust prototype (e.g. replacing the PERSPEX<sup>®</sup> structure by a SS one) is another important issue that can minimize both the temperature effect and increase the systems accuracy.

A brief discussion about some of these points that should/could be analyzed on the design of future versions of the MSS and on its practical implementation will be flowingly accomplished.

### 7.2.1. MSS configuration

a) The excitation system could be redesigned in order to excite the system below the 1000 Hz (recall Chapter 6, Section 6.4.1). It was quite clear from the experimental results in that chapter that the system is not being excited below the 1000 Hz. On the other hand, the simulation studies suggest that the first modes of the vibrations of the free plate occur below the 1000 Hz. Concerning the excitation below the 1000 Hz, two different suggestions may be evaluated: the implementation of a different piezoelectric actuator or the use of a signal conditioner to fit properly the impedance of the transducer.

b) Actuator vs sensor position: if one attends the transfer function given in Appendix A by Equation (A.21), it can be seen that its magnitude is dependent on the positions of the actuator and of the sensor, through the modal shapes ( $\varphi_n$ ) of where the transducers are placed, which accounts for the result. Being so, if the structural characteristics of the system are kept constant, the frequency and damping ratio will be also constant and the magnitude becomes only dependent on the modal shapes of where the exciter ( $p_e$ ) and the sensor ( $p_r$ ) are placed. The position of the transducers can be optimized in order to maximize the magnitude of the transfer function, which results in higher output results (e.g. higher *RMS* and *A<sub>FFT</sub>* values).

The optimization software was programmed in MATLAB<sup>®</sup> for this specific purpose. This software determines the first  $n$  modes for the pre-established dimensions of the plate and calculates for each position on the plate the average value of the mode shapes (with the same analytical solutions mentioned in Section 6.2.2) of those first  $n$  modes. The optimum position is given by the higher average value. Since the reciprocity principle is applicable, the software only determines the position of one of the transducers and the other is given by symmetry, in relation to center of the plate.

Figure 7.1 shows the computed average values of the modal shapes (for  $n=6$  modes) for each set of positions  $A$  and  $B$  (recall that the plate dimensions are:  $A=225$  mm and  $B=41$  mm and that the plate is clamped). It can be seen that the pair of dimensions with higher value is observed when the actuator and the sensor are placed in:  $A_{actuator}=30$  mm and  $B_{actuator}=20$  mm; and  $A_{sensor}=195$  mm and  $B_{sensor}=20$  mm – represented in Figure 7.1 by the circles. However, notice that, according to this criterion (maximum average response of the first 6 modes), several other locations along the plate axis fits nearly well.

Indeed, in the MSS plate described in Chapter 6, the two elements were placed in the following dimensions:  $A_{actuator}=75$  mm and  $B_{actuator}=20$  mm; and  $A_{sensor}=150$  mm and  $B_{sensor}=20$  mm. When these pair of dimensions is analyzed in Figure 7.1 (represented by the squares) it can be seen that they are within the red area. This means that they are placed in a position that is favorable to get a high modal shape value, although there is still some margin to increase the output signal by placing them in the positions that maximizes the modal shape values (see Figure 7.1).

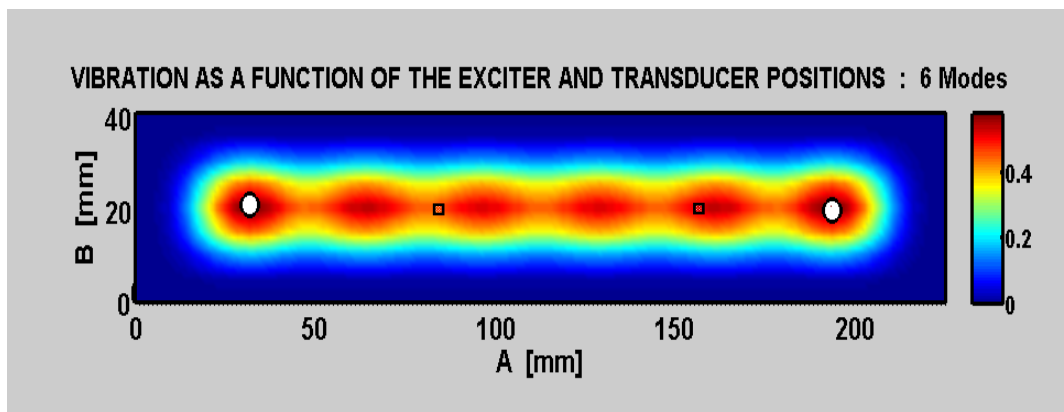


**Figure 7.1:** Representation of optimum position of the exciter and sensor (in the figure designated as transducer) elements – Clamped boundary condition

The type of analysis previously described does not introduce big changes to the conclusions taken so far, but are important regarding the optimization of the system. So, the suggestion to evaluate and implement the results of such simulation/optimization software relies precisely on the last point mentioned before, to improve and get the MSS more accurate and with higher resolution.

c) The MSS physical configuration is another issue that should be taken into account. The possibility of having a transparent flow cell with sampling coupons on its flat surface is very useful in laboratorial prototypes. However, when some specific conditions (e.g. high temperature laboratorial trials or industrial testing) are considered, the use of a PERSPEX<sup>®</sup> creates some disadvantages, which are mainly concerned with the use of high temperatures and chemical reagents. Furthermore, a PERSPEX<sup>®</sup> material is quite fragile and is easily subject to leaking problems. An alternative to this material is to employ stainless steel which is the most commonly used material in industrial equipment. In fact, the SS material is more appealing from the vibration point of view, since it dissipates less energy than the PERSPEX<sup>®</sup>. Another advantage of the SS is that it allows additional fixing procedures than the screwing or gluing, such as soldering. One of the first suggestions regarding the MSS configuration relies precisely on soldering the monitored plate directly to a SS flow cell. Another alternative is the use of a tubular section in spite of the flow cell. This configuration may have some advantages over the configuration used so far, mainly related to the lower damping effect which once again is preferred for the modal analysis, although the vibration modes associated with the cylindrical configuration are typically more difficult to analyze than the ones of the plate.

### **7.2.2. Methodology**

It was already discussed that a future version of the MSS should contemplate the implementation of the two methodologies in parallel. The information given by the damping factor is crucial since it is able to provide indications about the type of deposit that adheres to the monitored surface. The measurement based on experimental modal analysis to quantify the amount of deposit is certainly an unquestionable improvement as well as its ability to characterize the system in terms of its vibration parameters. The analysis of the transfer functions showed to be essential to determine if a given configuration is or not the most suited in terms of the system vibration.

### 7.2.3. Reproducibility

The reproducibility of the MSS needs to be evaluated. Furthermore, it is necessary to assess if the calibrations of the signal *versus* the amount and type of deposit and *versus* the external factors are constant for two setups similarly assembled. This evaluation will help to develop a quality check assembling procedure.

### 7.2.4. Practical implementation

One of the key strategic decisions is the choice of where to place the monitoring devices and it is consensual that the place should be representative of the fouling adhesion/removal of the whole plant. An alternative approach is to place the device on critical points that represent the ‘worst’ case that happens in the plant, since when this part of the equipment is cleaned the rest of the plant is theoretically cleaned as well. The MSS can be directly applied to the equipment pipes although a by-pass configuration is suggested since with the help of CFD it is possible to design a piece of tubing (or flow cell) with similar hydrodynamic conditions to the ones that are observed, for example, in the ‘worst’ part of the equipment.

In spite of the different possibilities to implement the monitoring device, the acquisition system should record not only the information gathered by the MSS but also the temperature (as it already does) and flow velocity, in order to introduce the necessary corrections.

With the previous suggestions in mind, it seems important to concentrate the future work on a unique configuration which should be characterized in terms of its vibrating characteristics. A relation between the output signal and the amount and type of deposit should be established. The calibrations with the experimental conditions should also be trialed. Another suggestion regarding the characterization of the output signal is to precisely determine if the effect of temperature is related with a change on the viscosity of the bulk or with the expansion of the materials.

Once the system is fully tested (in laboratory), it should be implemented within a given pilot plant. These tests should be designed in order to be able to provide the cost advantage of its application (to determine the cost/benefit ratio), to evaluate its robustness and the improvements that should be made regarding its practical operation and performance.



## APPENDIX A - THEORY OF VIBRATION

A brief summary of the analytical methods used to study and characterize vibrating systems will be provided in the present appendix. Most of the real vibrating systems can be ideally modeled by the single-degree-of-freedom oscillator. Thus, and since the latter is also simple and easy to understand, it will be used to discuss some main fundamentals of vibrating systems.

### A.1. SINGLE-DEGREE-OF-FREEDOM SYSTEM

Figure A.1 represents a single-degree-of-freedom system with viscous damper (the viscous force is opposite to the  $x$  direction, so  $f_c = -c\dot{x}$ , where  $c$  is the damping constant). This relation between the force and the velocity ( $\dot{x}$ ) happens in the presence of viscous damping, since a higher vibration velocity yields a higher dissipative force. The damping constant depends on the physical properties of the damper, and may be assumed independent of the time. Besides the damping force there is also a spring force associated with the force applied by the spring ( $f_k = -kx$ , where  $k$  is the stiffness of the spring).

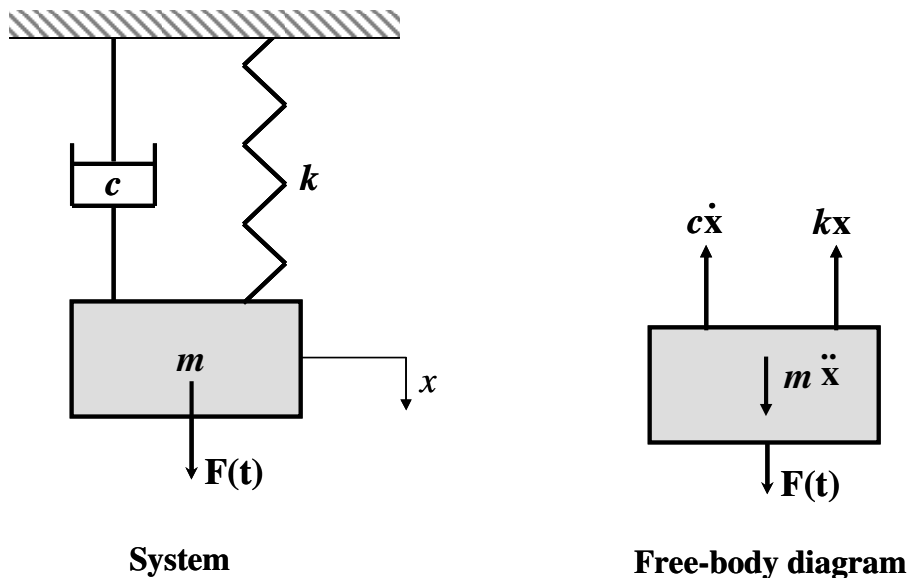


Figure A.1: Schematic representation of a single degree-of-freedom system with viscous damping

The inertial force connected to the mass  $m$  is balanced by these two forces (damping force and spring force) and by an external force  $F(t)$ , according to the Newton's law (when  $x$  is the displacement measured from the equilibrium position), the equation of motion of a single-degree-of-freedom system becomes:

$$m\ddot{x} = -c\dot{x} - kx + F(t) \quad (\text{A.1})$$

This relation is expressed in terms of the physical parameters of the system ( $c$ ,  $k$  and  $m$ ), which is not sufficient to provide information about the oscillation frequency and damping. It is convenient thus to define two new parameters,  $\omega_n$  and  $\zeta_n$ , the frequency and the damping ratio of the system as:

$$\omega_n = \sqrt{\frac{k}{m}} \quad \text{and} \quad \zeta_n = \frac{c}{2m\omega_n} = \frac{c}{2\sqrt{mk}} \quad (\text{A.2})$$

By substituting  $k$  and  $c$  into Equation (A.1) it is possible to define an equivalent equation of motion in terms of its vibration parameters:

$$m\ddot{x} + 2m\omega_n\zeta_n\dot{x} + m\omega_n^2x = F(t) \quad (\text{A.3})$$

Two distinct solution terms can be found from Equation (A.1) or conversely from Equation (A.3): the free response (which occurs when no external force is applied after the initial disturbance that makes the body vibrate,  $F(t)=0$ ) or the forced response (which occurs when the external force  $F(t)$  is applied to the mass).

### **A. Free vibration**

Let us first consider the free vibration, by setting the external force  $F(t)$  equal to zero. Analyzing Equation (A.3) it is possible to find out, from the  $\zeta_n$  and  $\omega_n$  values, the type and in what conditions a motion of a given system occurs.

The solution of the differential Equation (A.3) assumes the form:

$$x(t) = Ce^{\lambda t}, \quad \text{where} \quad \lambda_{1,2} = \omega_n \left( -\zeta_n \pm \sqrt{\zeta_n^2 - 1} \right) \quad (\text{A.4})$$



The value of  $\lambda_1$  and  $\lambda_2$  are obtained by replacing the  $x(t) = Ce^{\lambda t}$  in Equation (A.3), with  $F(t)=0$ . The nature of the roots  $\lambda_1$  and  $\lambda_2$  of the characteristic equation and the behavior of the system depend on the damping magnitude.

And so, different  $\zeta_n$  or  $\omega_n$  values, may lead to different types of motion (see Figure A.2), being:

- DAMPED SYSTEM ( $\zeta_n \neq 1$ )

a) Underdamped motion ( $\zeta_n < 1$ ): the roots of the characteristic equation are complex conjugates ( $\zeta_n^2 - 1 < 0$ ) and it leads to an harmonic motion with an exponential decrease of the amplitude (the amplitude decay is determined by the damping ratio). Its roots becomes:

$$\lambda_1 = \omega_n \left( -\zeta_n + i\sqrt{1 - \zeta_n^2} \right) \quad \text{and} \quad \lambda_2 = \omega_n \left( -\zeta_n - i\sqrt{1 - \zeta_n^2} \right)$$

Since the overall solution in Equation (A.4) includes a term  $e^{-\zeta\omega_n t}$ , the amplitude will exponentially decrease with time (Rao 2004). Equation (A.5) defines the decrease of the frequency of a damped vibration with the increase of the system damping. Most of the engineering systems rely on this type of vibration. It is also the case of all experiments in the present Thesis.

$$\omega_d = \sqrt{1 - \zeta_n^2} \omega_n \tag{A.5}$$

Where  $\omega_d$  is the frequency of the damped vibration, which is always smaller than the undamped natural frequency  $\omega_n$ .

b) Overdamped motion ( $\zeta_n > 1$  or  $\omega_n = 0$ ): the roots of the characteristic are purely real and distinct ( $\zeta_n^2 - 1 > 0$ ). These become:

$$\lambda_1 = \omega_n \left( -\zeta_n + \sqrt{\zeta_n^2 - 1} \right) \quad \text{and} \quad \lambda_2 = \omega_n \left( -\zeta_n - \sqrt{\zeta_n^2 - 1} \right)$$

A non-oscillatory response occurs and the system returns exponentially to its rest position.

c) Critically damped motion ( $\zeta_n = 1$ ): the roots of the characteristic equation are equal corresponding to a non-periodic motion that decreases with time. These roots are:

$$\lambda_1 = \lambda_2 = -\omega_n$$

The amplitude of vibration will never cross the time axis but rather approach it asymptotically. As the damping increases, the motion gets overdamped which means that the amplitudes gets slower toward the rest position. Since  $e^{-\zeta\omega_n t} \rightarrow 0$  as  $t \rightarrow \infty$ , in all damped cases, the motion will decrease until zero amplitude.

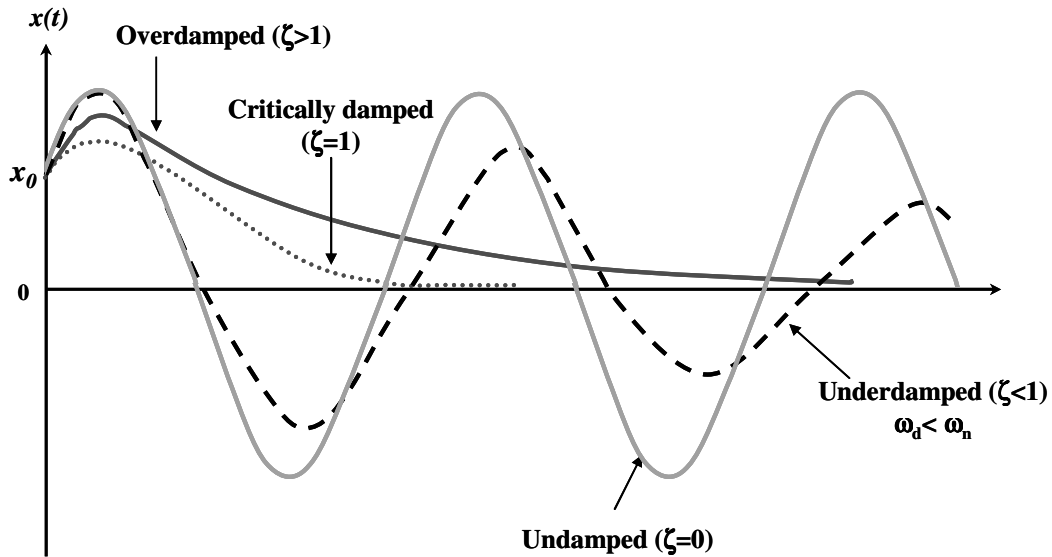


**Figure A.2:** Representations of the motion for different damping ratios ( $\zeta_n$ ), for damped and undamped systems

- UNDAMPED SYSTEM ( $\zeta_n = 0$ )

This motion occurs when there is no resistance or damping in the system and the oscillatory motion would continue vibrating forever at constant amplitude (Figure A.2). In fact, assuming that a system has no damping is purely theoretical, since there is always a given amount of resistance to the motion (which dissipates energy).

## **B. Forced vibration**

In Figure A.1, when we consider that the external force  $F(t)$  is acting on the mass, the forced vibration situation is observed. Let us assume that this system is under an harmonic force with a given excitation frequency ( $\omega$ ) and constant amplitude ( $A_0$ ):  $F(t)=A_0 \sin(\omega t)$ . By changing this excitation frequency it is possible to study the vibratory response of the mass.

It is possible to demonstrate (see for instance, Henrique 2002) that the response of a forced single-degree-of-freedom system can be mathematically described by:

$$\frac{X(\omega)}{F(\omega)} = H(\omega) = \frac{1}{m[\omega_n^2 - \omega^2 + 2i\omega\omega_n\zeta_n]} \quad (\text{A.6})$$

Indeed, the frequency-domain Equation (A.6) is simply obtained by Fourier transforming of the time-domain Equation (A.3). It is important to note that Equation (A.6) is a complex function that can be represented by its magnitude (A.7) and phase (A.8):

$$|H(\omega)| = \frac{1}{m\omega_n^2 \left[ \left( 1 - \left( \frac{\omega}{\omega_n} \right)^2 \right)^2 + 4 \left( \frac{\omega}{\omega_n} \right)^2 \zeta_n^2 \right]^{1/2}} \quad (\text{A.7})$$

$$\phi = \tan^{-1} \left( \frac{2\zeta_n \frac{\omega}{\omega_n}}{1 - \left( \frac{\omega}{\omega_n} \right)^2} \right) \quad (\text{A.8})$$

The graphical computation of the response curves from Equation (A.6) is shown in Figure A.3. This figure shows the magnitude and the phase (normalized by the excitation) of the vibrating system.

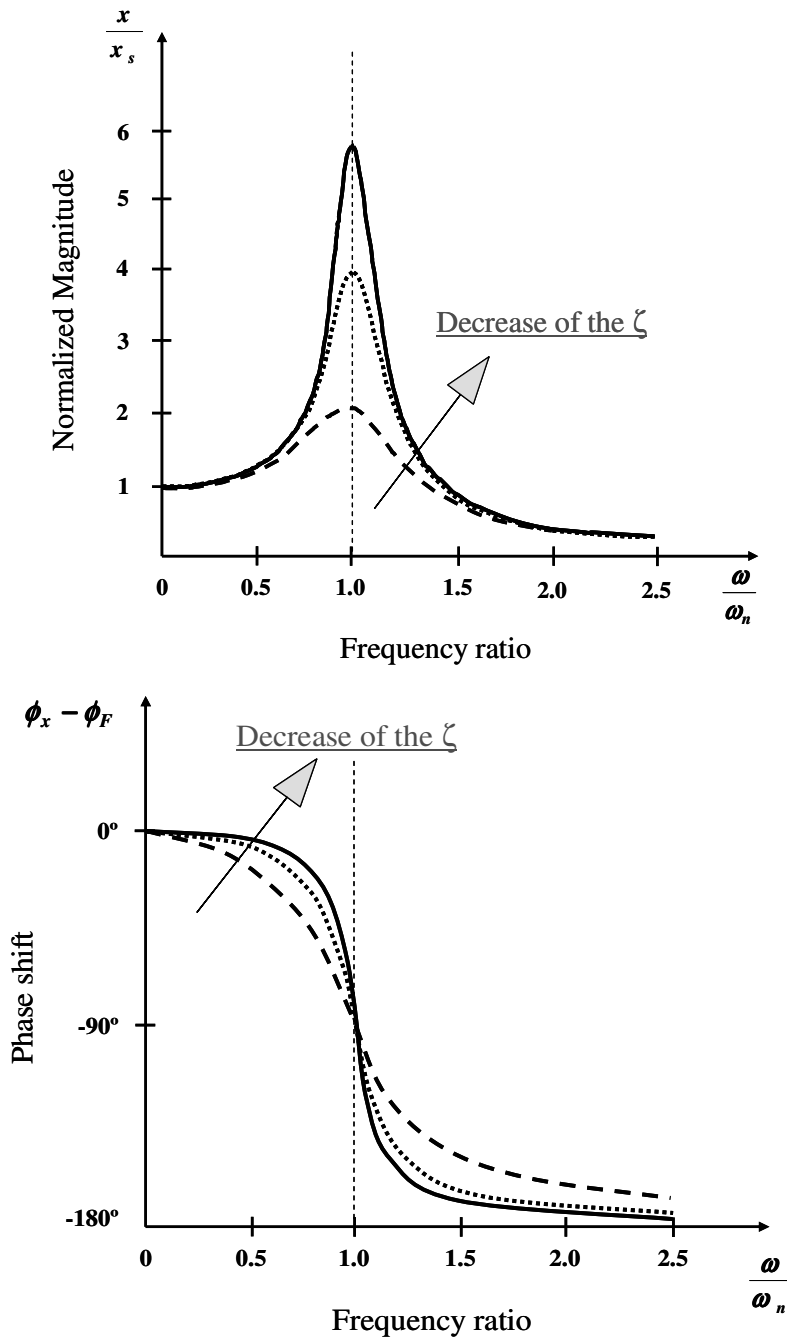


**Figure A.3:** Graphical representation of a) normalized magnitude and b) phase between the excitation and the response of the harmonic system; these parameters were plotted as a function of the frequency ratio (for different damping ratio values)

Equations A.7 and A.8 demonstrate that when changing the excitation frequency ( $\omega$ ) three different situations can be considered:

a)  $\omega \ll \omega_n$ : when the excitation frequency is much smaller than the natural frequency of the oscillator, then the motion of the system is dominated by the rigidity. In this case, Equation (A.6) becomes:

$$|H(\omega)| \approx \frac{1}{m\omega_n^2} = \frac{1}{k} \quad (\text{A.9})$$

When this situation occurs, the vibratory magnitude is almost independent of the excitation frequency and the system behavior as if it was only a spring. On the extreme case when  $\omega \approx 0$ , the phase shift becomes zero, meaning that the vibratory response is in phase with the excitation.

b)  $\omega \approx \omega_n$ : when the excitation frequency is similar/close to the natural frequency of the system, the oscillation amplitude is controlled by the damping forces of the system, as shown in Equation (A.10).

$$|H(\omega)| \approx \frac{1}{(2m\omega_n\zeta_n)\omega} = \frac{1}{\omega c} \quad (\text{A.10})$$

In this case, the system is in resonance with the excitation. The phase difference between the excitation and the response is about  $90^\circ$ , since the dissipative term on Equation (A.6) is associated with the imaginary part.

c)  $\omega \gg \omega_n$ : when the excitation frequency is much higher than the natural frequency of the system, the oscillation is controlled by its inertial forces. So, Equation (A.6) becomes:

$$|H(\omega)| \approx \frac{1}{m\omega^2} \quad (\text{A.11})$$

Equation (A.11) shows that the magnitude of vibration decreases with the increase of the square of the excitation frequency. Additionally, when  $\omega/\omega_n \rightarrow \infty$ , the phase shift tends to  $180^\circ$ , which means that the excitation and the response are out of phase.

Some other conclusions can be taken from Figure A.3:

- a decrease of the damping amount increases the normalized magnitude as  $1/\zeta_n$ ;
- a reduction of the normalized magnitude is very abrupt at or near resonance ( $\omega/\omega_n = 1$ );
- the magnitude of the response becomes smaller with increasing values of the forcing frequency, i.e. if  $\omega/\omega_n \rightarrow \infty$  then  $x/x_s \rightarrow 0$ ;

The analysis of the single-degree-of-freedom model is quite important since more complicated systems, which have many resonances behave quite similar to this model in the neighborhoods of each one of their resonances (specially the lightly damped). On the other hand, the type of analysis previously described is very useful when we want to decide what changes should be made to improve the system's behavior.

### **A.1.1. Measurement of damping**

Dynamic systems show always some form of mechanical-energy dissipation. When modeling a system, damping can be neglected (as far as modal computations are concerned) if the mechanical energy dissipation for cycle is small when compared to the total mechanical energy of the system. Three primary mechanisms of damping are typically reported in mechanical systems:

- a) *Internal damping* (of the material) results from mechanical-energy dissipation within the material due to internal structural processes.
- b) *Structural damping* (joints and interfaces) is caused by mechanical-energy dissipation between components of a mechanical structure with common contact points, joints or supports.
- c) *Fluid damping* (through fluid-structure interactions) results from the fluid viscosity and drag dynamic interaction forces when a mechanical system or its components moves in a fluid.

It is extremely complicated to develop a realistic model for damping determination mainly when the system is complex and influenced by different conditions and different mechanical interactions. The difficulties also arise from the fact that usually it is not possible to distinguish between the various types of damping. Concerning the elements of a vibrating system the damping ratio is the most difficult quantity to be determined since pertains to dynamic forces which are often one or two order magnitude smaller than those of the inertial and stiffness effects.

It is usual though to assume linear viscous behavior when estimating damping parameters from experimental data (De Silva 2000). There are two general ways to measure damping: time-response methods (use time-response signals) and frequency-response methods (use frequency-response signals). For time-response signals stemming from single-degree-of-

freedom systems the methods used for damping ratio estimation are: Logarithmic Decrement Method, Step-Response Method and Hysteresis Loop Method. On the other hand, the most common frequency-response methods are: Magnification-Factor Method and Bandwidth Method. In this section only the Logarithmic Decrement Method will be described, since it is the most popular method and was the one used to determine damping in the previous chapters. For multiple degree of freedom systems, a more detailed focus will be provided on the frequency – response methods further on, in Section A.4.

**Logarithmic Decrement Method:** this is perhaps the time-response method most used to measure damping. Consider a record of displacement response of an underdamped system (for example, similar to Figure A.2 – underdamped motion). The Logarithmic Decrement Method is based on the decrease of the maximum amplitude of the output (response) wave per unit time. For example, if the response of the system is similar to the one shown in Figure A.4, it is possible to establish a decay displacement (indicated by the dashed line) of the type  $Ae^{-\zeta\omega_n t}$ .

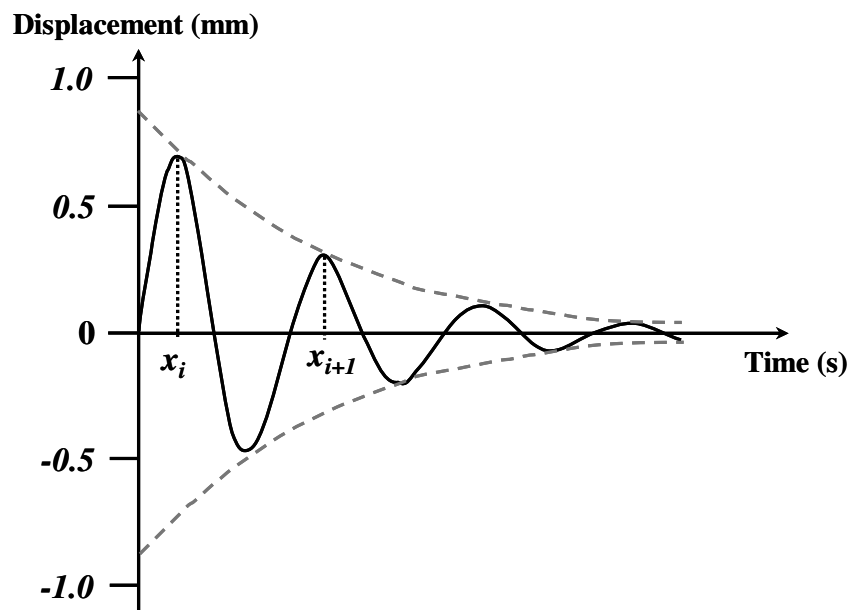


**Figure A.4:** Underdamped response used to measure damping – Logarithmic Decrement Method

It is possible though to determine  $\zeta_n$  after  $\omega_n=2\pi/T_n$  is known (where  $T_n$  is the oscillation period). The damping ratio can be determined by the following equation:

$$\zeta_n = \frac{\frac{1}{n} \ln \left( \frac{x_i}{x_{i+1}} \right)}{\sqrt{(2\pi)^2 + \frac{1}{n^2} \ln^2 \left( \frac{x_i}{x_{i+1}} \right)}} \quad (\text{A.12})$$

where  $\frac{x_i}{x_{i+n}}$  is the ratio of two non or consecutive amplitudes;  $n$  is an integer value such as

$(n+1)$ =number of peaks, and  $\zeta_n$  is the damping ratio (see Figure A.4).

### A.1.2. Multi-degree-of-freedom systems

In real-world situations, most engineering systems are continuous and have an infinite number of degrees of freedom. Continuous systems are difficult to study since they often involve the solution of partial differential equations (and in many situations there is not an analytical solution for those equations). So, a continuous system is often approximated by a discrete multi-degree-of-freedom system, since the latter requires the solution of a set of ordinal differential equations (which is usually simpler than the partial differential ones). The number of degrees of freedom is typically established from the number of moving parts and the number of directions in which each part can move. More than one degree of freedom means that the system has more than one natural frequency and so the opportunity of resonance greatly increases. The concepts discussed in Section A.1 (Single-degree-of-freedom systems) can be extrapolated for the multi-degree-of-system systems. In other words, it is possible to say that a system with  $n$  degrees of freedom has  $n$  natural frequencies associated with a corresponding mode shape and damping ratio.

The previous section has shown how it is possible to characterize/model the response to known inputs. As mentioned before, it is possible to develop similar models for systems with more than one degree of freedom. This type of analysis, often called modal analysis is quite an important tool in vibration design, diagnosis and control, for example to establish the extent and the location of severe vibrations in a given mechanical system. In this approach, given the matrices (for more than one-degree-of-freedom it is most convenient to work with matrices)  $\mathbf{M}$  (inertia),  $\mathbf{K}$  (stiffness) and  $\mathbf{D}$  (damping) along with appropriate initial conditions and forcing functions, it is possible to determine the solution of the equation that describes the dynamics of the structure. This approach is often named ‘forward problem’ (Inman 2001). In



opposition to this approach there is the ‘inverse problem’ approach which determines the matrices  $M$ ,  $K$  and  $D$  from the knowledge of the excitation forces and output responses of the system (position, velocity or acceleration). Since the present Thesis is focused on gathering and analyzing information about the system through experimental determinations, more attention will be provided to the ‘inverse problem’ approach. More detailed information about the modal analysis and identification can be found in the literature (e.g. Inman 2001; Rao 2004).

## **A.2. VIBRATION SIGNALS**

Many examples of every-day vibrating systems can be presented – an airplane in-flight, a car in movement, a musical instrument playing, etc. The excitations and the responses (inputs and outputs) are a function of time but they can also be represented as a function of frequency, through Fourier transformation techniques. The result – the Fourier Spectrum of a signal – can be interpreted as a set of frequency components in which the original signal contains energy. The frequency-domain analysis emphasizes many characteristics of the signal and of the system that can not be easily found in the time-domain. That is why Fourier analysis is used in a huge variety of applications – experimental modeling, modal analysis, data interpretation, acoustics research, etc. The present section will analyze in more detail the type of signal that can be used to excite a given system, as well as to briefly describe the Fourier transformation techniques.

### **A.2.1. Excitation methods**

It was previously discussed that a given system can be actuated by an external force  $F(t)$ . In Section A.3 the importance of this external force will gain a new dimension, since the excitation signal is crucial for an efficient experimental design. Vibration testing can employ both deterministic and random signals as excitation sources:

- *Deterministic signals* are time signals completely predefined that can be divided into two main categories: single-frequency signals and multi-frequency signals, each being composed by periodic and transient signals.
- *Random signals* are signals that are generated by some random (stochastic) mechanism. Each time a mechanism is operated, a different signal is usually generated. The likelihood of

any two sample functions becoming identical is governed by some probabilistic law. Further details on the way to evaluate the characteristics of a given random signal can be read in Section A.3.3. Some examples of random signals are: white and pink noise or random impacts.

A brief description of the most used excitation methods will now be provided:

a) Frequency excitation: the signals have a predominant frequency component at a given time and they can typically be represented by simple mathematical expressions. Some examples of such signals are: sine sweep, sine beat, among many others. On the other hand, if multi-frequency signals are considered they appear irregular and have more than one predominant frequency component at a given time.

b) Impulsive excitation: it is a very simple excitation technique which typically needs a shaker or an impact hammer. Its main advantage rely on the fact that there is no need to attach the exciter to the system (no additional mass load is observed). The excitation energy is concentrated on a short period of time, which can make the system to behavior (respond) non-linearly. On the other hand, since the excitation duration is very short, it makes this method quite sensitive to the environmental noise (mainly when it is intense). The limit of the impulsive excitation is the Dirac function, which has infinite amplitude in a very short period of time. Impulsive excitations contain energy in a large spectral frequency range, which is a definite advantage.

c) Random excitation: it is possible to excite the system with energy simultaneously in a given wide range of frequencies. The *white noise* has constant spectral magnitude for all the frequencies in which it is generated. This signal is quite used in mechanical vibration while the pink noise is more applied in acoustic tests. The *pink noise* is a signal in which energy is constant for all frequencies and so the spectral magnitude decreases with the increase of frequency.

### **A.2.2. Signal analysis**

A measured signal is a time history, where the independent variable is the time and the signal is represented in the time domain. A limited amount of information can be extracted by examining the time history, and most of that information is related (directly or indirectly) with either the amplitude or the frequency. The present section will be devoted to discuss the frequency analysis.

The frequency domain representation of a time signal is obtained through Fourier analysis. One of the main advantages of the Fourier transform is that differentiation and integration operations (in the time domain) are converted into simple algebraic operations (such as multiplication and division) in the frequency domain. Three interrelated versions of the Fourier transform are important to consider:

a) Fourier series expansion: applicable only to periodic signals; according to the Fourier theory, any periodic function  $x(t)$ , with period  $T$ , can be represented by an infinite series of the form:

$$x(t) = \frac{a_0}{2} + \sum_{j=1}^{\infty} \left( a_j \cos \frac{2j\pi t}{T} + b_j \sin \frac{2j\pi t}{T} \right) \quad (\text{A.13})$$

The  $\omega_T = 2\pi/T$  and the  $a_0$ ,  $a_n$  and  $b_n$  are the *Fourier coefficients* for the periodic function  $x(t)$ . The former coefficients can be calculated by applying the following formulas (for  $j = 1, 2, \dots$ ):

$$a_0 = \frac{2}{T} \int_0^T x(t) dt, \quad a_j = \frac{2}{T} \int_0^T x(t) \cos \frac{2j\pi t}{T} dt, \quad b_j = \frac{2}{T} \int_0^T x(t) \sin \frac{2j\pi t}{T} dt \quad (\text{A.14})$$

It can be seen that  $a_0/2$  represents the average value of  $x(t)$ .

b) Fourier integral transform: applied to any general signal; considering the Fourier series of a non-periodic function  $x(t)$  it becomes that its transform  $X(\omega)$  is defined by:

$$X(\omega) = \frac{1}{2\pi} \int_{-\infty}^{\infty} x(t) e^{-j\omega t} dt \quad (\text{A.15})$$

Equation (A.15) transforms the variable  $x(t)$  from a function of time into a function of frequency  $\omega$ . Writing the series represented by Equation (A.13) in a complex form and allowing the period to go to infinite, it is possible to define the Fourier transform integral described by Equation (A.15).

c) Discrete Fourier Transform (DFT): applied for discrete signals; the discrete-time history value are accomplished using the digital Fourier transform series by:

$$x(t_k) = \frac{a_0}{2} + \sum_{j=1}^{N/2} \left( a_j \cos \frac{2\pi t_k}{T} + b_j \sin \frac{2\pi t_k}{T} \right), \quad \text{with } k=1, 2, \dots, N \quad (\text{A.16})$$

Where  $T$  stands here for the duration of the time acquisition.

The *digital spectral coefficients* are now defined by:

$$a_0 = \frac{1}{N} \sum_{k=1}^N x_k, \quad a_j = \frac{1}{N} \sum_{k=1}^N x_k \cos \frac{2j\pi k}{N}, \quad b_j = \frac{1}{N} \sum_{k=1}^N x_k \sin \frac{2j\pi k}{N} \quad (\text{A.17})$$

For any acquired signal  $x(t_k)$  the Equation (A.16) should be solved in order to determine its DFT. For reasons of computation efficiency, the transform size or number of samples  $N$  is usually fixed as a power of 2 (such as 256, 512 and 1024). The former Equation (A.16) to (A.17) can be written in a matrix form:

$$\vec{X} = [A] \vec{d} \quad (\text{A.18})$$

where  $\vec{X} = \{x_1 \ x_2 \ \dots \ x_N\}^T$  is the vector of samples with elements  $x_n$ , the vector of spectral coefficients is given by  $\vec{d} = \{a_0 \ a_1 \ a_2 \ \dots \ a_{N/2} \ b_1 \ b_2 \ \dots \ b_{N/2}\}^T$  and  $[A]$  is the matrix composed by the coefficients  $\cos \frac{2j\pi t_k}{T}$  and  $\sin \frac{2j\pi t_k}{T}$  of  $a_0$  on Equation (A.17). Formally, it is possible to determine the frequency content of the signal/response of the system, from the relation (A.19):

$$\vec{d} = [A]^{-1} \vec{X} \quad (\text{A.19})$$

The matrix  $[A]^{-1}$  is efficiently computed using Fast Fourier Transform (FFT) by the analyzer.

### **A.3. EXPERIMENTAL MODAL ANALYSIS (EMA) OF VIBRATING SYSTEMS**

The main idea behind modal testing (the ‘inverse problem’ approach) relies on the determination of the system’s natural characteristics, being: frequency, damping and mode shapes (Dossing 1988). These dynamic properties occur in all structures and they depend on the weight, stiffness and damping of such system (recall Equation A.3). When a theoretical model is developed the experimental modal analysis enables to verify this predicted frequencies and mode shapes. This section will be focused on experimental modal analysis (EMA) – also called modal testing – which deals with the determination of the natural frequencies of the system, mode shapes and damping ratios from experimental vibration measurements. When a system is actuated at resonance, its response exhibits two distinct aspects – amplitude and phase (as indicated by Equation (A.7) and (A.8)). As the driving frequency approaches the natural frequency of the system, the magnitude at resonance rapidly

approaches a sharp maximum value. On the other hand, a resonance phenomenon is that where the phase of the response shifts by  $180^\circ$  as the frequency sweeps through resonance (phase at resonance is around  $90^\circ$ ). Several assumptions are made to apply this type of experimental test, although the most essential is that the system under test has to be linear. Some important concepts should be introduced and defined before starting to discuss the EMA approach.

Let us consider a tightly elastic string or cable with length 'l' subject to a transverse force  $f(x,t)$  and with both ends fixed. In the time domain, it is possible to determine the equation that characterizes the system response, which can be expressed in terms of  $x$ ,  $t$  and of two arbitrary constants ( $C_n$  and  $D_n$ ). The solution of this equation is called the  $n^{\text{th}}$  mode of vibration of the string (more information can be read in Rao (2004)). By Fourier transforming such solution, the system response may be expressed in terms of its modal properties:  $\omega_n$ ,  $\zeta_n$ ,  $m_n$  and  $\varphi_n(x)$ .

Figure A.5 shows the first three modes of vibration of the string.

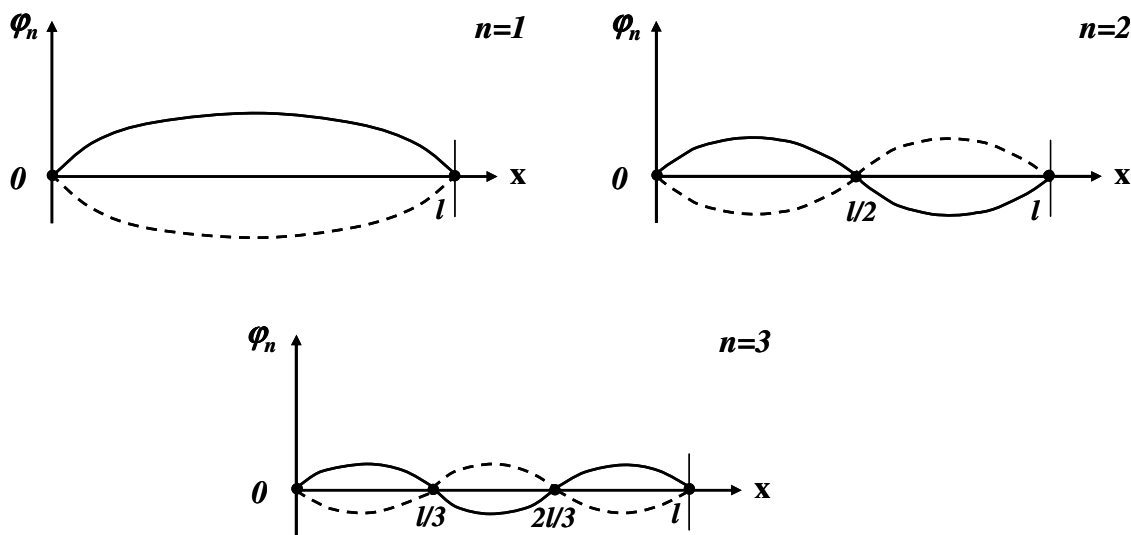


Figure A.5: Modal shapes of a vibration string (adapted from Rao (2004))

- Fundamental mode: is the mode that corresponds to  $n=1$  and  $\omega_1$  is called *fundamental frequency*.

- Modal motions: are the configurations at which the system naturally ‘prefers’ to vibrate at (when it is let to freely vibrate). Each modal configuration has: an own frequency ( $\omega_n$ ) and damping ( $\zeta_n$ ) associated to its motion and is also defined with a vibration shape  $\varphi_n(x)$ . Finally, the so-called modal mass  $m_n$  expresses how the mass distribution of the system contributes to the inertia forces for any given mode shape  $\varphi_n(x)$ . Typically, the vibration of a given system is quite complex and results from the superimposition of different modal motions, depending on the excitation force  $f(x,t)$ .

- Nodes of a mode: a node of a mode shape is simply the coordinate of a zero entry in the mode shape, i.e. the points at which  $\varphi_n = 0$  are the *nodes of vibration*. For example, it can be seen in Figure A.5 that the fundamental mode ( $n=1$ ) has two nodes of vibration at  $x=0$  and  $x=l$ ; the second mode has three nodes at  $x=0$ ,  $x=l/2$  and  $x=l$ , and so on.

- Nodal lines: is a similar notion of the ‘nodes’ but applied to a two dimension structure, i.e. are the lines defined by the set of points with 0 displacement ( $\varphi_n = 0$ ).

- Transfer function: for any linear system, the transfer function  $H(\omega)$ , can be defined as the relation between the excitation  $F(\omega)$  and the response  $X(\omega)$  of that system in the frequency domain, which in its conceptualized form can be represented by:

$$H(\omega) = \frac{X(\omega)}{F(\omega)} \quad (\text{A.20})$$

The transfer function depends on the governing equations of the system. The transfer function of multimodal vibratory systems is a generalization of Equation (A.6) previous studied (Henrique 2002):

$$\frac{X(\omega, p_r)}{F(\omega, p_e)} = H(\omega, p_r, p_e) = \sum_{n=1}^N \frac{\varphi_n(p_e)\varphi_n(p_r)}{m_n[\omega_n^2 - \omega^2 + 2i\omega\omega_n\zeta_n]} \quad (\text{A.21})$$

Where:  $\varphi_n$  is the modal shape of the mode  $n$ ;  $p_e$  is the excitation point;  $p_r$  is the response point.

It is thus possible to make for multiple degrees of freedom systems an analysis similar to the one made for the force vibration in Section A.1. For example, an interesting consequence that can be taken from Equation (A.21) is the fact that if the system is excited on a node of  $\varphi_n$ , this mode  $n$  does not respond. This equation also illustrates quite well the *reciprocity principle* which states that exciting a system at a point  $p_e$  and measuring at a point  $p_r$  is identical to excite it at a point  $p_r$  and measure at a point  $p_e$ .

### A.3.1. Vibration measuring system

The basic vibration features and hardware used to perform an experimental vibration test can be seen in Figure A.6.

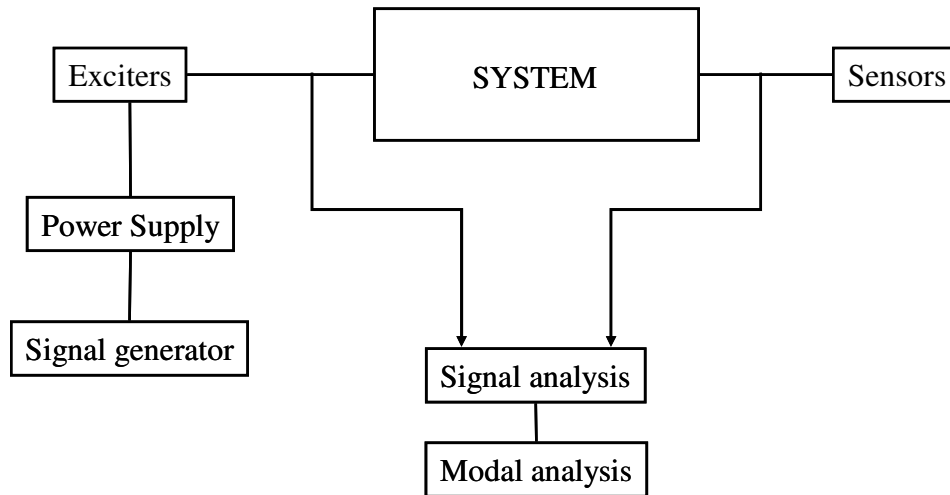


**Figure A.6:** Schematic representation of the basic vibration measurement scheme

The basic hardware elements can be divided into three main groups:

a) *Exciter (or actuator)*, provides a known and controlled input to the system. The excitation system denoted as ‘exciter’ consists of the device that provides the input motion (the driving force  $F(t)$  in Equation (A.1)). This device may assume different physical configurations and characteristics, such as for example: shaker (electromagnetic or electrohydraulic), piezoelectric materials. More information about the piezoelectric materials can be read in Appendix B. Since the exciters are typically attached to the test system, their size and dimension should be taken into account when choosing this device. The excitation signal can be chosen (and is generated on the signal generator) to match the requirements of the test design, and it can be for example: a sine wave, random or any other signals (recall information from Section A.2.1). The choice of the excitation device is quite an important step mainly due to the mass that it adds to the system and due to the frequencies that it is able to excite.

b) *Sensor*, to measure vibrations the most popular and widely used are the ones made of piezoelectric materials. The main characteristics that should be taken into account when choosing the transducer are: their linearity and the dynamic range of their response. Similarly to what happened with the exciter, the sensors can be of different configurations and physical

principles, for example: resistive, piezoelectric, capacitive, etc. More information about accelerometers is provided in Appendix B.

c) *Spectrum analyzer (Analysis system)*, is a device in which signal processing and modal analysis can be executed. The spectrum analyzer determines the response of a system under a known excitation and presents it in a convenient way. Typically, these analyses are done in the frequency domain since they are able to obtain more useful information than the time domain. The standard analyses are called digital or discrete Fourier analysis or Fast Fourier Transform (FFT). Basically, after acquiring the analog voltages signals (e.g. acceleration), the signal is digitalized for computation and the discrete frequency spectra (plots of magnitude vs frequency) of individual signals and cross-spectra between the input and the output are determined. The analyzed signals can be computed in a variety of ways to produce the type of desired information, such as: natural frequencies, damping ratios, magnitudes at resonance, etc. In parallel with the frequency domain analysis, some time domain characteristics can be determined, such as: flight-time, peak-to-peak amplitude, damping factor, etc.

Depending on the characteristics and demands of the overall system, some auxiliary equipment may be needed, such as signal conditioners. The impedance of most transducers is not fitted to be directly inputted into signal analysis equipment. In these cases, signal conditioners (e.g. charge amplifiers, voltage amplifiers) should be introduced.

### **A.3.2. Digital signal processing**

As discussed in the previous section, the measurement of a vibration is performed in the following way:

- i) an exciter applies a known input force to the system;
- ii) the force is applied to the system, and the response of the system to such force is then collected with a transducer. The transducer converts the physical motion of the system into an electrical signal;
- iii) in some cases, the signal collected with the transducer passes through a signal conditioning (amplifier) to make the characteristics of such transducer compatible with the input of the electronics of the digital acquisition system;



iv) the signal processing and data analysis of the collected signal are then performed in an analyzer or data acquisition system;

The acquisition system that accepts the analog output signals of the transducer has to convert them into digital records. It samples the signals  $x(t)$  at many different equally spaced values and produces a digital record of the signal  $x_j=x(t_j)$ , where  $t_j$  is the discrete value of the time ( $j=1, 2, \dots, N$  where  $N$  is the number of samples collected). This process is performed by an analog-to-digital converter (A/D). To better understand how this A/D conversion is performed one can imagine a gate that samples the signal every  $\Delta t$  seconds and passes through the signal  $x(t_j)$ . Figure A.7 shows a signal in the time domain with its Fourier and digital representation (Rao 2004). Note that the total record length ( $T$ ) of the signal is given by:  $T=N\Delta t=1/\Delta f$ .

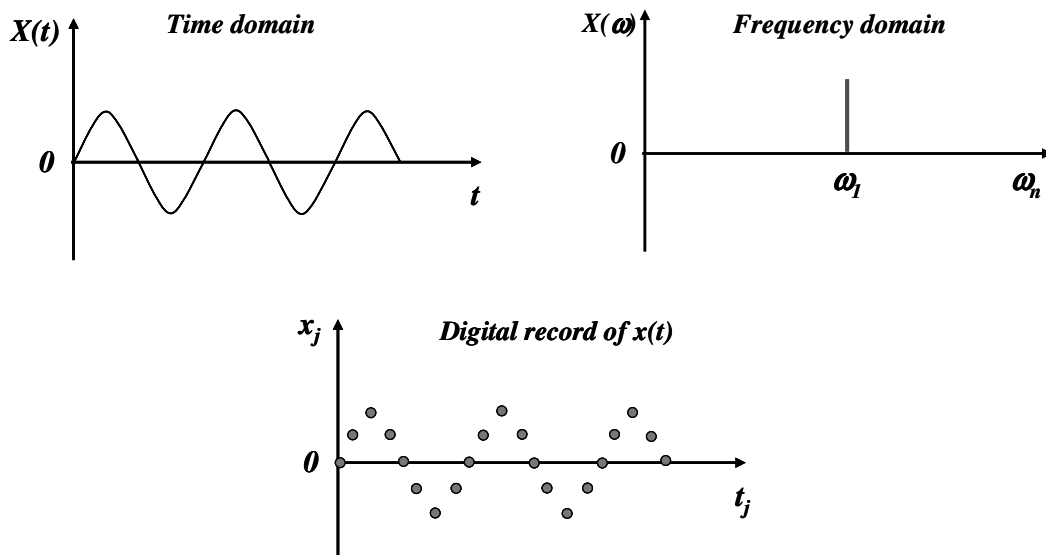


**Figure A.7:** Schematic representation of a sinusoidal signal in three different forms: time-domain, frequency-domain and the signal  $x(t)$  in the digital form

When determining the Digital Fourier Transform of a continuous signal it is important to properly interpret the digital results. The sampling time (the time between successive  $t_j$ ) is a critical parameter when performing the DFT since *aliasing* (which is a common error) may occur. *Aliasing* refers to misrepresentation of the analog signal by the digital record and may happen during the A/D conversion. If the sampling rate (of the acquiring equipment) is too slow to catch the details of the analog signal, the digital representation will be misrepresented and will cause high frequencies to appear as low frequencies. To avoid *aliasing*, the *Shannon's sampling theorem* should be applied. This theorem states that to recover a signal

from its digital samples, it should be sampled at a rate at least twice the highest frequency of the signal. The experience indicates that it is better to perform the acquisition at least at 2.5 samples per cycle (of the highest frequency). Another option is to subject the analog signal to an *antialiasing* filter, which is a low-pass sharp-cutoff analog filter (only allows low frequencies through). As soon as the digital signal is available the DFT can be performed according to Equation (A.16).

### **A.3.3. Analysis of random signals**

The analysis of random signals is quite an important subject in experimental modal analysis, since the input and output signals typically contain some random noise (which is difficult to analyze in a deterministic manner). In some cases, the random signal is used to perform the vibrating tests which increase the need to analyze this type of noise. Disturbances are often characterized as random if the  $x(t)$  for a given value of  $t$  is only known statistically. This means that from random signals it is not possible to predict the details of the signal, as it is with a pure deterministic signal (e.g. as a sine function) – Figure A.8 a) and d) illustrate this problematic (Inman 2001). Thus, random signals are characterized in terms of their statistical properties. One record of time history data is not enough to describe the signal, but rather a statistical description of all possible responses is necessary. So, if one considers a random vibration response  $x(t)$ , it should not be seen as a single signal, but rather as a sample from a collection of possible time histories resulting from the same conditions (same system, environment, length of time, etc).

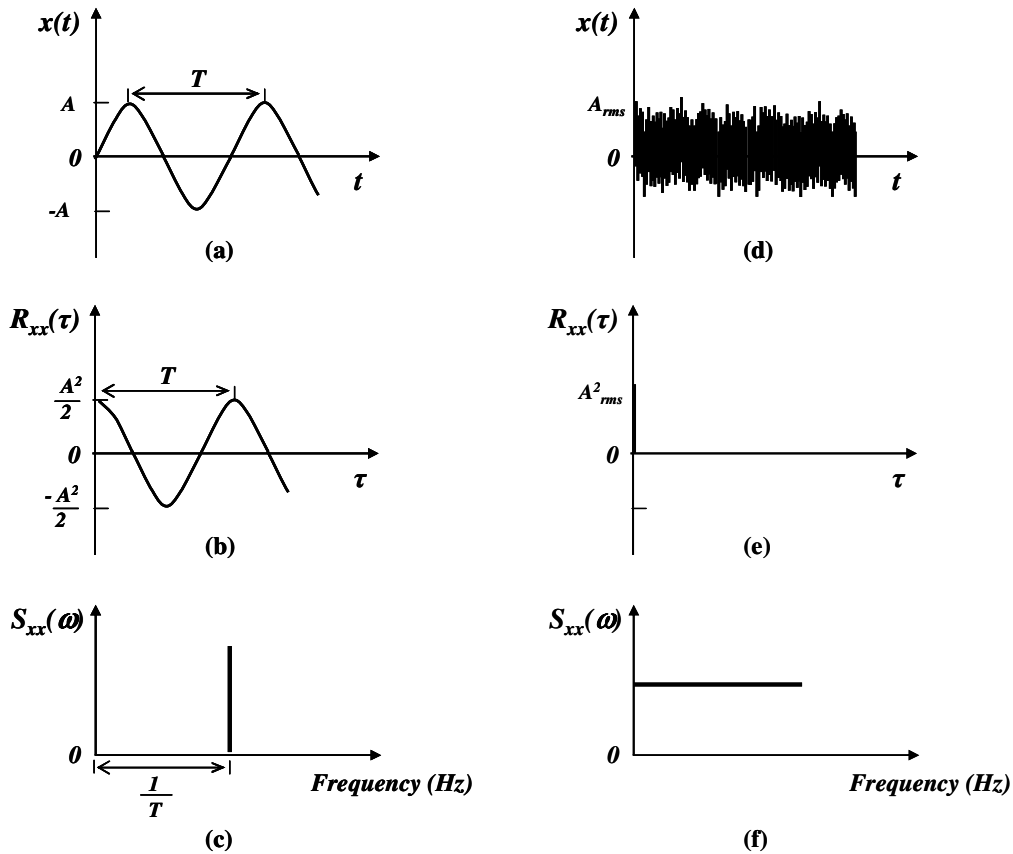


**Figure A.8:** Comparison of the sine function and a random signal, and their respective autocorrelation ( $R_{xx}$ ) and power spectral density – PSD ( $S_{xx}$ )

Consider again the random signal  $x(t)$ , as shown in Figure A.8 d) its *average* will be  $\bar{x}(t)$  defined as:

$$\bar{x}(t) = \lim_{T \rightarrow \infty} \frac{1}{T} \int_0^T x(t) dt \tag{A.22}$$

The former equation is defined for deterministic signals. Since this section deals with random signals it is convenient to consider a signal with zero mean ( $\bar{x}(t)=0$ ). Although this is not restrictive since when a new signal  $\bar{y}(t) \neq 0$ , a new variable may be defined as:  $x(t) = y(t) - \bar{y}(t)$ . This new variable has now a mean equal to zero. So, without loss of generality, it is possible to define the *variance* (or mean-square value) which provides a measure of the fluctuations in the signal  $x(t)$ :

$$\bar{x}^2(t) = \lim_{T \rightarrow \infty} \frac{1}{T} \int_0^T x^2(t) dt \tag{A.23}$$

A related quantity, the *root-mean-square* (RMS), which is the square root of the variance, is given by:

$$x_{RMS} = \sqrt{\bar{x}^2} \quad (\text{A.24})$$

Another important information about a random signal is to know how fast the signal loses the ‘memory’ of its past. This information is given by the *autocorrelation* function ( $R_{xx}(\tau)$ ). The  $\tau$  value is the time difference between the values at which the signal  $x(t)$  is sampled, i.e. the sampling interval.

$$R_{xx}(\tau) = \lim_{T \rightarrow \infty} \frac{1}{T} \int_0^T x(t)x(t+\tau)dt \quad (\text{A.25})$$

If  $x(t)$  is purely random, then  $R(\tau) \rightarrow 0$  as  $T \rightarrow \infty$ , however if  $x(t)$  is periodic or has a periodic component, then  $R(\tau)$  will also be harmonic – this differences can be seen in Figure A.8.

The *power spectral density* (PSD) –  $S_{xx}(\omega)$  - of a random signal  $x(t)$  measures how the signal energy is distributed in the frequency domain and recalls the definition of Equation (A.15):

$$S_{xx}(\omega) = \frac{1}{2\pi} \int_{-\infty}^{\infty} R_{xx}(\tau)e^{-i\omega\tau}d\tau \quad (\text{A.26})$$

Figure A.8 (c and f) shows the PSD of a sine and random signal.

The definitions of autocorrelation and PSD functions can be extended for two signals: the applied force signal  $F(t)$  and the displacement response signal  $x(t)$ . This introduces a new definition of the cross-correlation function –  $R_{xf}(\tau)$  and the cross-PSD –  $S_{xf}(\omega)$ .

$$R_{xf}(\tau) = \lim_{T \rightarrow \infty} \frac{1}{T} \int_0^T x(t)f(t+\tau)dt \quad (\text{A.27})$$

$$S_{xf}(\omega) = \frac{1}{2\pi} \int_{-\infty}^{\infty} R_{xf}(\tau)e^{-i\omega\tau}d\tau \quad (\text{A.28})$$

With the former two Equations (A.27) and (A.28) it is possible to determine the transfer functions of the system under test. The *transfer function*,  $H(\omega)$  is related with the PSD functions as follows:

$$S_{fx}(\omega) = H(\omega)S_{ff}(\omega) \quad (\text{A.29})$$

$$\text{or} \quad S_{xx}(\omega) = H(\omega)S_{xf}(\omega) \quad (\text{A.30})$$

The cross-correlation includes informations about the magnitude and phase of the systems transfer function (note that the transfer function concept has been introduced in previously in Section A.3).

So, if the system under test is excited with a random input  $F(t)$  resulting in the response  $x(t)$ , the two signals (excitation and response) will be measured by the transducers (exciter and sensor) and from Equations (A.29) and (A.30) it is possible to determine the desired transfer function  $H(\omega)$ . In order to determine the influence of the noise associated with the given signal the *coherence function* ( $\gamma^2$ ) should be evaluated, according to:

$$\gamma^2 = \frac{|S_{xf}(\omega)|^2}{S_{xx}(\omega)S_{ff}(\omega)} \quad (\text{A.31})$$

Note that Equations (A.29) and (A.30) uses different PSD densities to determine the same quantity  $H(\omega)$ . In fact, it is quite useful to check the consistency of the  $H(\omega)$  since it should have the same value independently of how it is calculated. The coherence function values lie between 0 and 1: when  $\gamma^2 = 0$  the measurement is pure noise; when  $\gamma^2 = 1$  the measurement of  $x(t)$  and  $F(t)$  do not have any noise, meaning that nearby all the output signal  $x(t)$  is linearly related to the input signal  $F(t)$  (which typically occur near the resonance frequencies of the system). In practice, the coherence is plotted versus the frequency and it indicates how accurate is the measurement process and data with  $\gamma^2 < 0.75$  should not be used (Inman 2001).

#### **A.4. MODAL DATA EXTRACTION**

The main goal of the experimental modal analysis is to determine various vibration parameters from the information gathered during the measurement process. The transfer function  $H(\omega)$  described by Equation (A.29) or (A.30) can be used to determine the most important vibration characteristics: natural frequencies, damping ratios, and modal amplitudes corresponding to all resonant peaks observed in the  $H(\omega)$  plot. There are several methods to accomplish this purpose. An exhaustive review of the methods used to gather information from the  $H(\omega)$  function is not under the scope of the present Thesis, so as an example, one of the simpler methods will be described.

As an illustrative example, let us consider that the  $H(\omega)$  is represented by Figure A.9 (Rao 2004), with four resonances (peaks) suggesting that the system can be modeled as a four-degree-of-freedom system. In fact, determining the number of degrees of freedom is one of the difficult areas in modal identification studies, but in many cases the number of degrees of freedom is established by counting the number of clearly defined resonances within a given frequency range. However this may not be quite accurate if the  $H(\omega)$  plot has closely spaced resonant frequencies or high damping values.

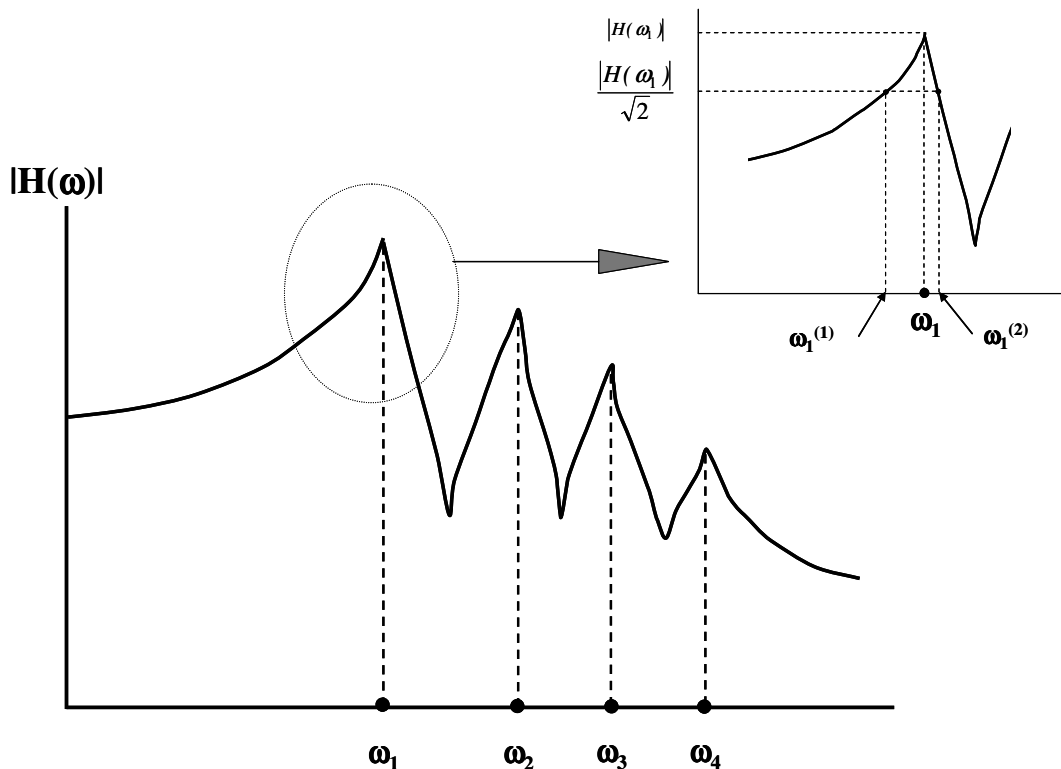


Figure A.9: Typical frequency-response function, adapted from Rao (2004)

One of the simple methods to find modal data is the single-degree-of-freedom approach, which deals with the concepts discussed in Section A.1 (forced vibration). Basically, the  $H(\omega)$  graph is divided into several frequency ranges. Each partitioned frequency range will be considered as a transfer function of a specific single mode (and so of a single-degree-of-freedom). The resonant frequencies can be confirmed with the phase measurement, since at a resonant point the phase angle is  $90^\circ$ . The damping ratio of the peak  $j$ , with resonant frequency  $\omega_j$  can be denoted by  $\zeta_j$ . Consider the first peak ( $\omega_1$ ) in Figure A.9. For systems lightly damped the peak  $|H(\omega)|$  at resonance is well defined, and the modal damping can be related to the frequencies corresponding to the two points on magnitude plot, where:

$$\left| H(\omega_j^{(1)}) \right| = \left| H(\omega_j^{(2)}) \right| = \frac{|H(\omega_j)|}{\sqrt{2}} \quad (\text{A.32})$$

Assuming that:  $\omega_l^{(2)} - \omega_l^{(1)} = 2 \zeta_n \omega_l$ , so

$$\zeta_n = \frac{\omega_1^{(2)} - \omega_1^{(1)}}{2\omega_1} \quad (\text{A.33})$$

From Equation (A.33) it is possible to determine the damping of a given resonant peak.

The determination of the mode shape from transfer functions measured experimentally is more difficult than the damping or the natural frequency, since it involves the measurement of several transfer functions.

### **REFERENCES**

- De Silva, C. W. (2000). Vibration: Fundamentals and Practice, Boca Raton: CRC Press LLC.
- Dossing, O. (1988). Structural testing. Part I: Mechanical mobility measurements, Brüel & Kjaer.
- Henrique, L. L. (2002). Acústica Musical. Lisboa, Gulbenkian Educação.
- Inman, D. J. (2001). Engineering Vibration (2nd edition), Prentice Hall, Inc.
- Rao, S. S. (2004). Mechanical Vibration (4th edition), Prentice Hall.





## APPENDIX B - ACTUATOR AND SENSOR CHARACTERISTICS

In the present Thesis two different types of transducers have been used: a piezoelectric ceramic (BM 70/25/200M, from Piezomechanick) and an accelerometer (ADXL 103, from Analog devices).

### **B.1. PIEZOELECTRICITY**

One of the best examples of these piezoelectric crystals is Quartz since when stress is applied to such crystal it develops an electrical moment proportional to the applied stress. This is known as *direct* piezoelectric effect. On the other hand, if an electric field is applied, the crystal slightly changes its shape and this is known as *inverse* piezoelectric effect (Morgan 2000).

Several crystals exhibit this piezoelectric property, such as Quartz, tourmaline and Rochelle salt. However piezoelectric ceramics, such as the PZT, has been designed in order to increase the small piezoelectric effect observed by the natural crystals. The PZT (lead zirconium titanate) has a perovskite structure, since each unit of which consists: of a small tetravalent metal ion, (usually of zirconium or titanium) in lattice, of large divalent metal ions (usually lead or barium) and  $O^{2-}$  ions. These ceramics can assume the generic configuration  $(Pb[Zr_xTi_{(1-x)}]O_3)$ , where  $0 < x < 1$ .

The main advantages associated with the PZT ceramics are (Mendes, 2003) that: i) they have a strong piezoelectric effect; ii) they can be fashioned elements of almost any shape and size; iii) they are chemically inert and iv) they are not affect by humid environments. These ceramics are used in a wide range of applications, such as: acoustics, optics, medical among many others.

The PZT elements can have different configurations. One of the most typical configurations consist of two or more layers (in the present case two) of piezoelectric material that are poled in a way that the layers on opposite sides have an opposite strains. This opposition strain

creates an internal bending moment and makes the entire bender to flex (Niezreckri et al. 2001), as shown in Figure B.1.

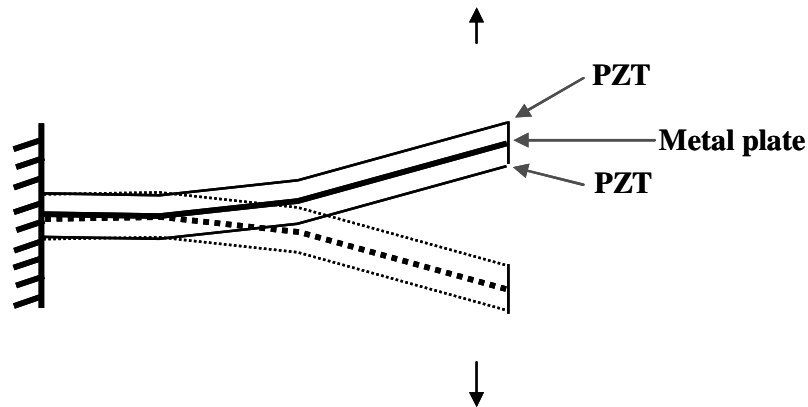


**Figure B.1:** Schematic representation of a bimorph piezoelectric ceramic (in a cantilever bending configuration)

The PZT type used along the present Thesis (dimension: 25x7.5x0.4 mm) is a parallel bimorph piezoelectric bending element, since it operates in a bending configuration with a thin metal plate sandwiched between the two piezo ceramic elements. The parallel operation is related to the fact that each of the ceramic strips is connected individually to the voltage source (Morgan 2000). In the present Thesis, the PZT element is glued to the monitored plate and only the upper strip is connected to the voltage source, according to the schematic representation shown in Figure B.2.

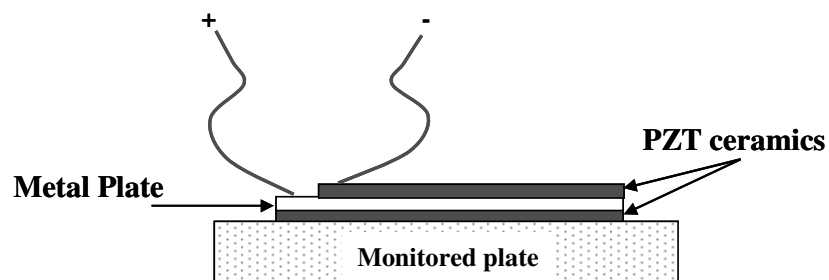


**Figure B.2:** Schematic representation of the piezoelectric element glued to the monitored surface and with the soldering wires (lines represented by + and – signals)

## B.2. ACCELEROMETER

Accelerometers, as the name indicates are acceleration measuring devices which can have different configurations. The acceleration can be determined through the indirect measurement of capacitance, piezoelectricity, etc. The sensor used in the present Thesis (5 x 5 x 2 mm) is a surface-micromachined polysilicon structure which is built on top of the silicon wafer. A polysilicon proof mass is suspended by folded tethers at each end and which deflects when acceleration is applied to the substrate. Independent movable beams are attached to the centre mass and form side-wall air-gap capacitors with the fixed beams (according to the schematic representation shown in Figure B.3). The acceleration deflects the beam and unbalances the differential capacitor, resulting in an output square wave whose amplitude is proportional to acceleration. This means that the acceleration of the mass changes the space between the moving and the fixed plates of the capacitor (such as: C1 and C2) which is proportional to the acceleration. The main advantages associated with these accelerometers are its high precision, low power consumption and low mass.

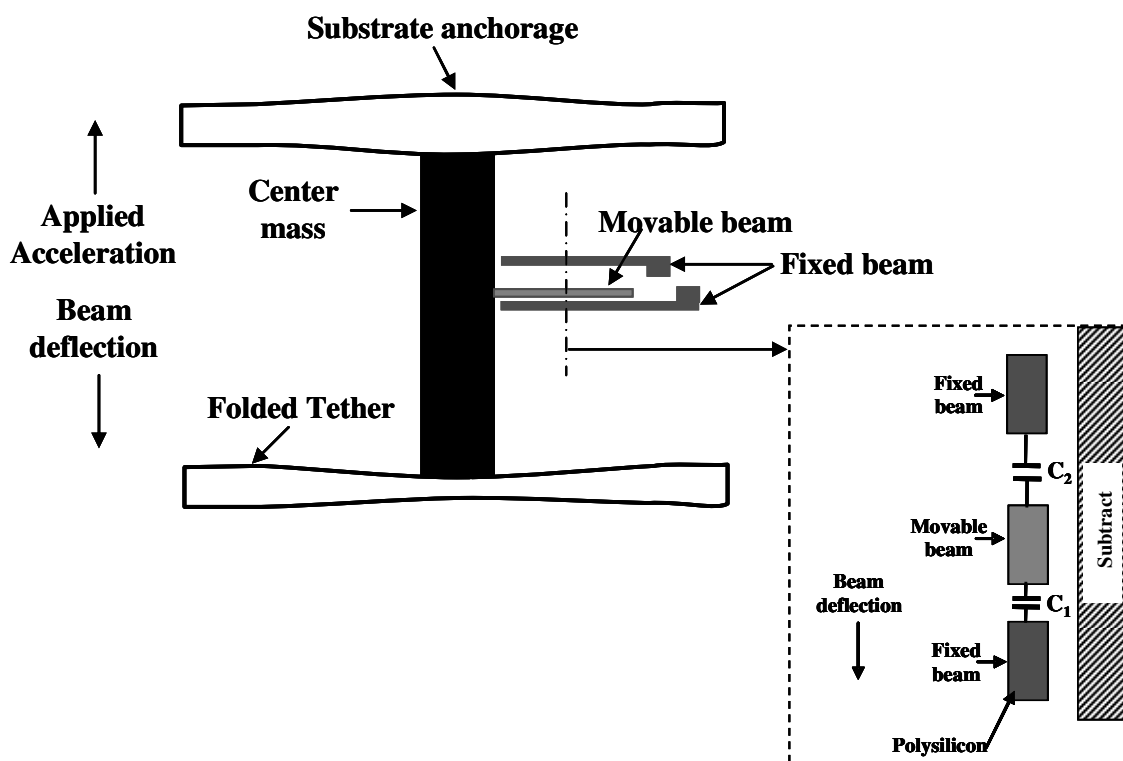


Figure B.3: Schematic representation of a surface-micromachined polysilicon structure (based on (Chau et al. 1996))

**REFERENCES**

Chau, K. H. L., S. R. Lewis, Y. Zhao, R. T. Howe, S. F. Bart and R. G. Marcheselli (1996). "An integrated force-balanced capacitive accelerometer for low-g applications." Sensors and Actuators, A: Physical **54**(1-3): 472-476.

Mendes, J. (2003). "Two novel Piezo-Actuations: an accurate micropositioning device and an active vibration system for sewing machines." PhD dissertation.

Morgan (2000). Piezoelectric ceramics Catalogue from Morgan (Electro ceramics).

Niezreckri, C., D. Brei, S. Balakrishnan and A. Moskalik (2001). "Piezoelectric Actuation: State of the Art." The Shock and Vibration Digest **33**(4): 269-280.

## APPENDIX C - CALIBRATION OF THE $A_{FFT}$ WITH THE TEMPERATURE AND THE FLOW RATE

The temperature and the flow velocity have an effect on the  $A_{FFT}$  acquired during the shampoo cleaning trials (Chapter 5). Being so, since the cleaning procedure used in that chapter was performed for different temperatures and different flow velocities, each  $A_{FFT}$  acquired have been corrected according to a previously determined relation between the  $A_{FFT}$  and the experimental conditions (temperature and flow rate). Note, that the flow is represented in Chapter 5 as a velocity although in the present appendix it will be used as a flow rate (recall that the surface area is constant,  $3.5 \times 10^{-4} \text{ m}^2$ , and so it is easy to convert one in another).

The variation of the  $A_{FFT}$  with the temperature, for two different flow rates can be seen in Figure C.1. The error bars associated with each condition is the standard deviation of the 10 consecutive measurements at that specific condition.

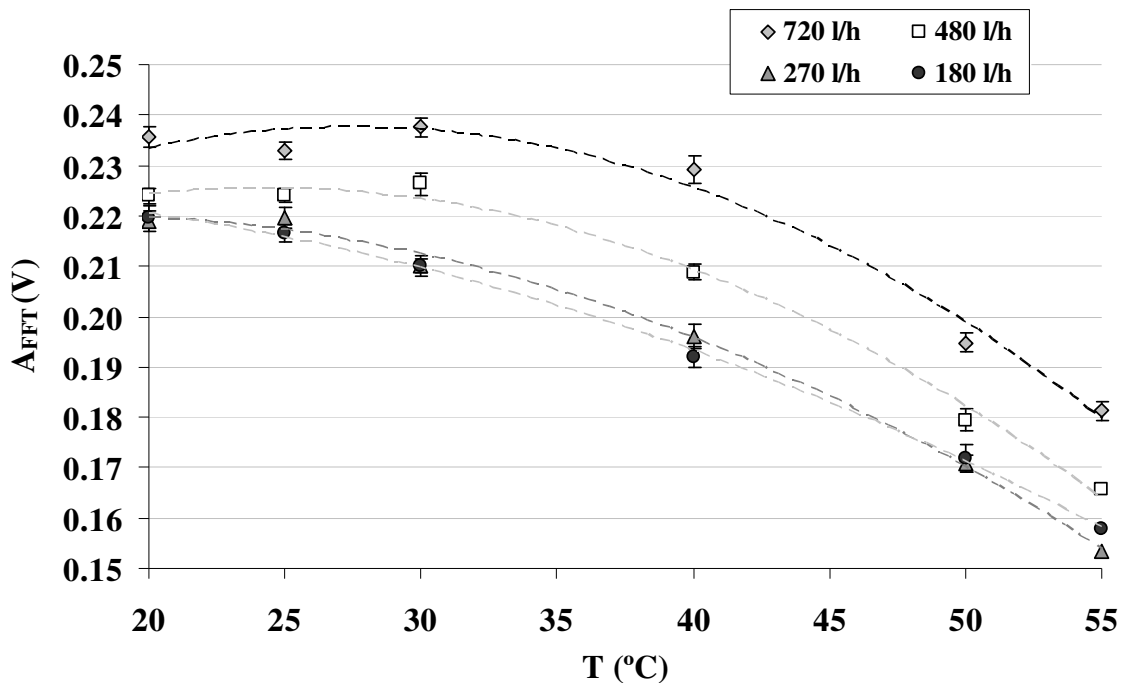


**Figure C.1:** Variation of the  $A_{FFT}$  with the temperature for four different flow rates

Figure C.1 shows that an increase of the temperature (mainly over 30 °C) decreases the value of the FFT amplitude (for all the tested flow rates). It also indicates that the  $A_{FFT}$  values obtained for the two lower flow rates are almost superimposed.

As can be read in Chapter 6, the  $A_{FFT}$  is not a vibrating characteristic of the system. Being so, a second degree polynomial model between the measured parameter and the temperature ( $T$ ) and flow rates ( $Q$ ) was determined:

$$A_{FFT} = 0.197 + 2.077 \times 10^{-3} T - 1.895 \times 10^{-5} Q - 5.356 \times 10^{-5} T^2 + 4.952 \times 10^{-7} TQ + 5.185 \times 10^{-8} Q^2$$

Where,  $T$  is expressed in °C and  $Q$  in l/h.

The relation between the experimental data and the predicted one is shown in Figure C.2. It can be seen that the model adjusts quite well the experimental data since the obtained slope is almost 1.

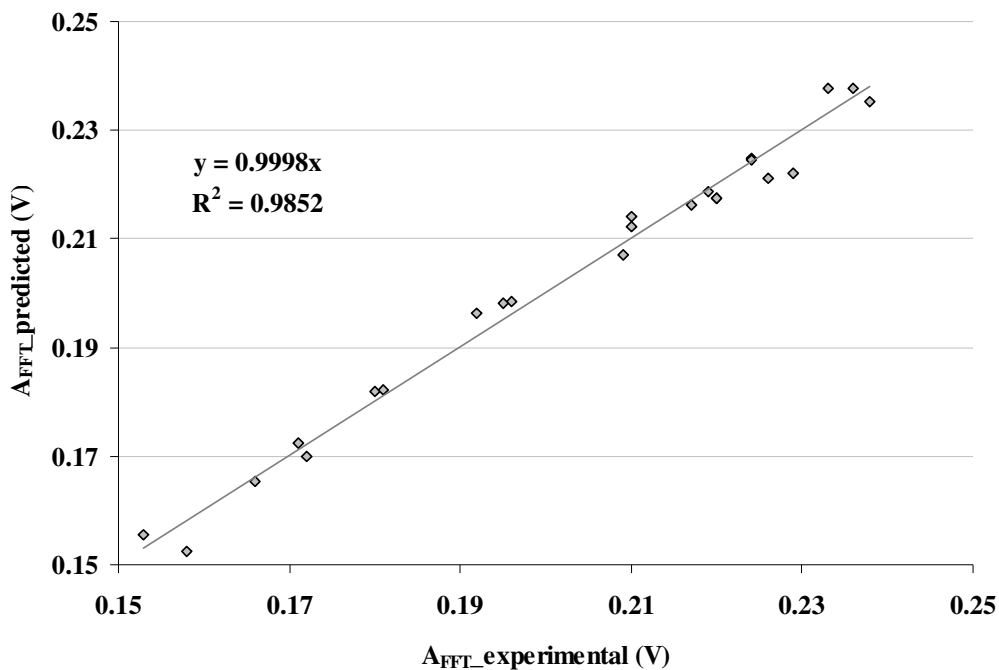


Figure C.2: Relation between the experimental and the predicted data

# APPENDIX D - TRANSFER AND COHERENCE FUNCTIONS

Transfer and coherence functions analyzed along the present chapter are shown in the following graphs.

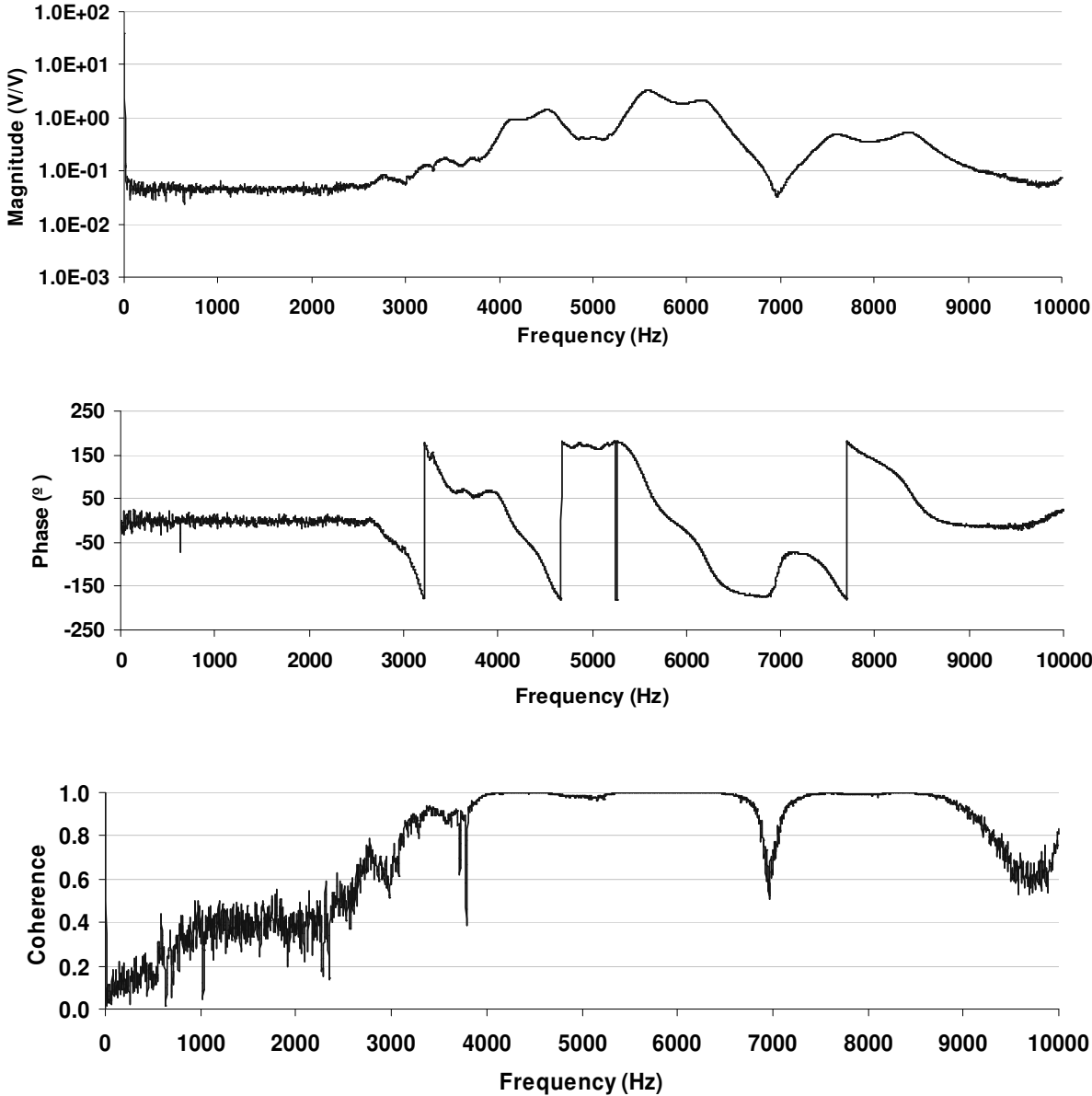
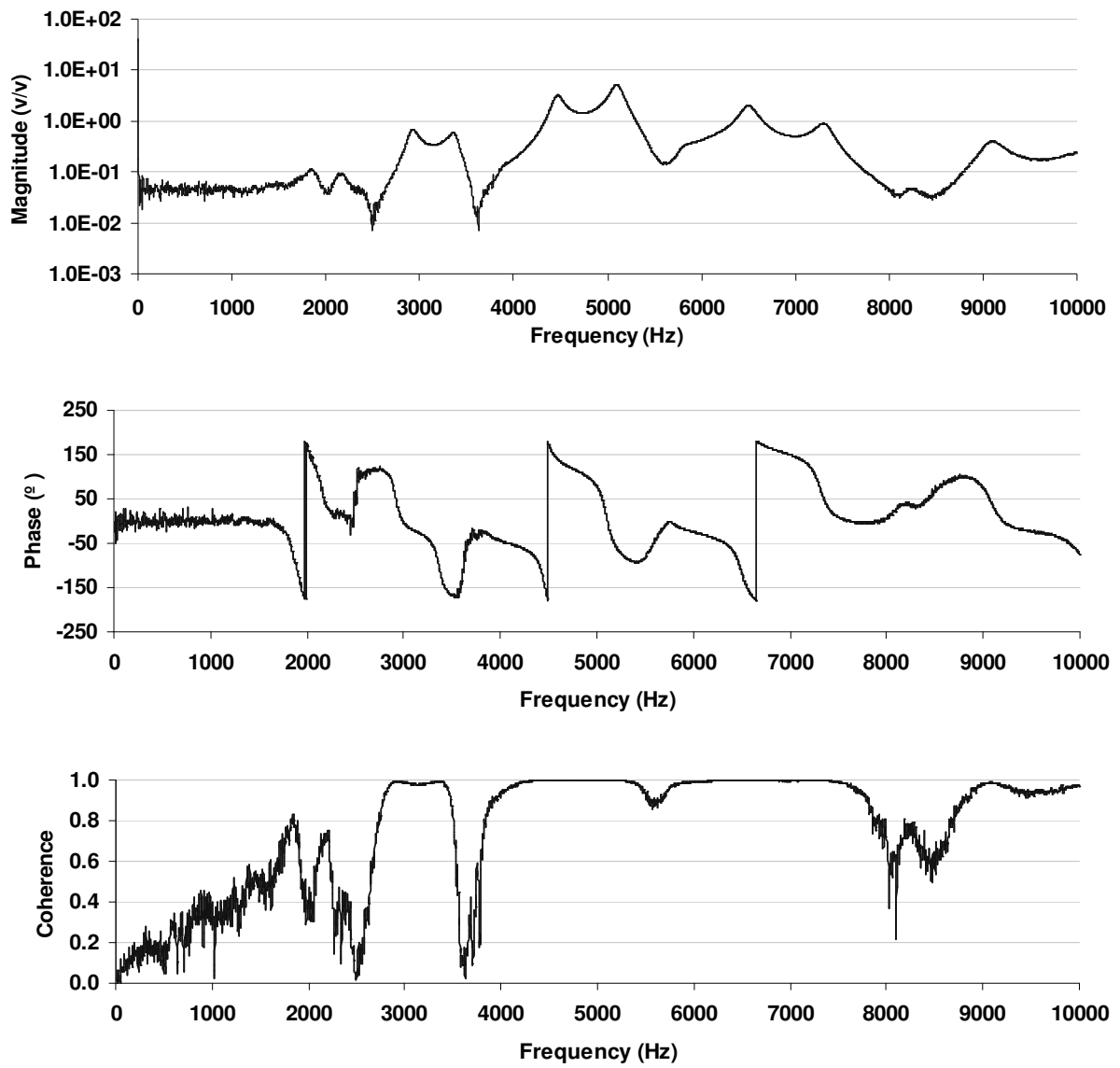
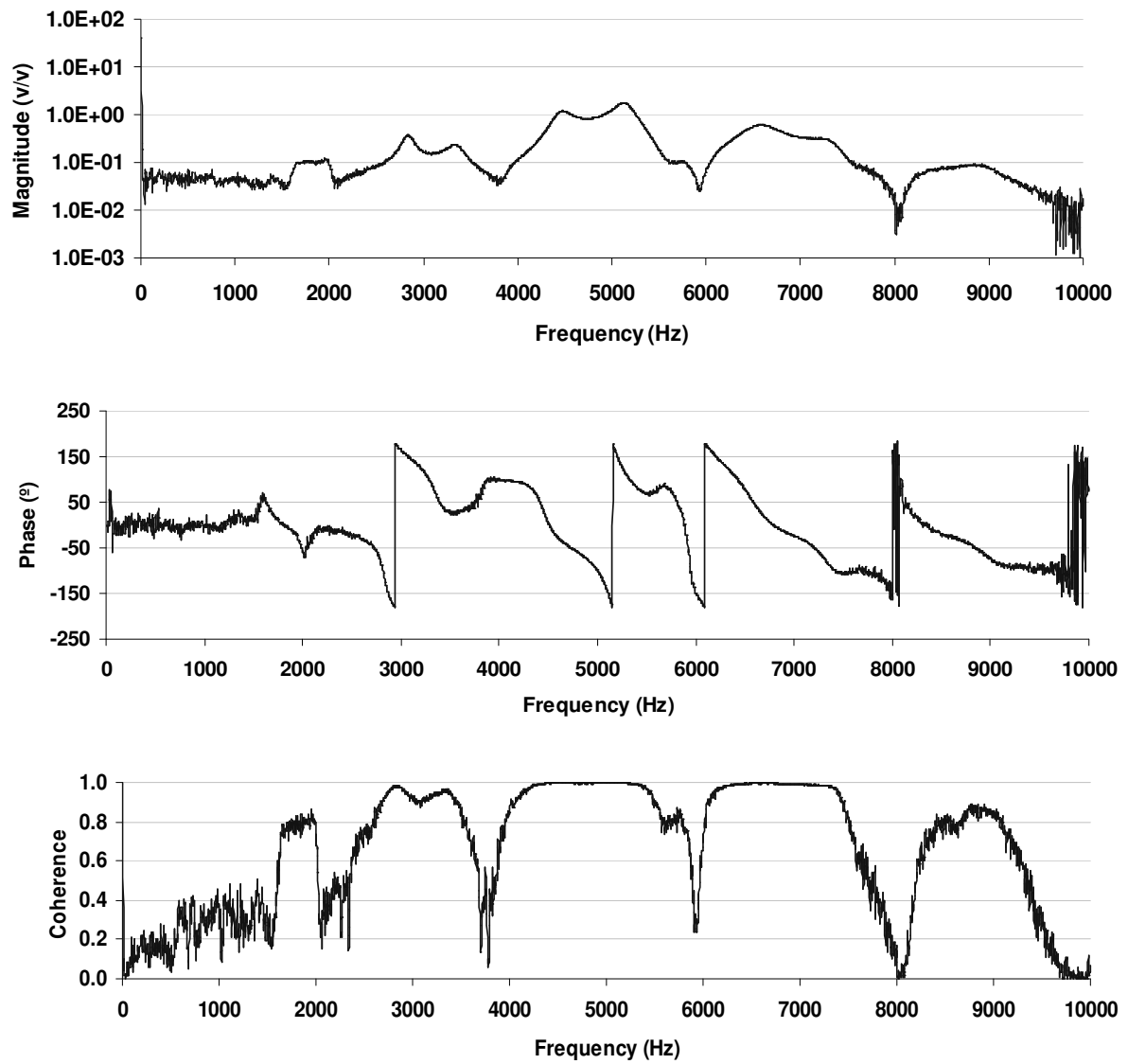


Figure D.1: SS plate clamped between 2 polyurethane plates (functions corresponding to the magnitude curve shown in Figure 6.16)



**Figure D.2:** SS plate clamped between 2 normal O’rings sealants (functions corresponding to the magnitude curve shown in Figure 6.17)





**Figure D.3:** system filled with water (functions corresponding to the magnitude curve shown in Figure 6.20)

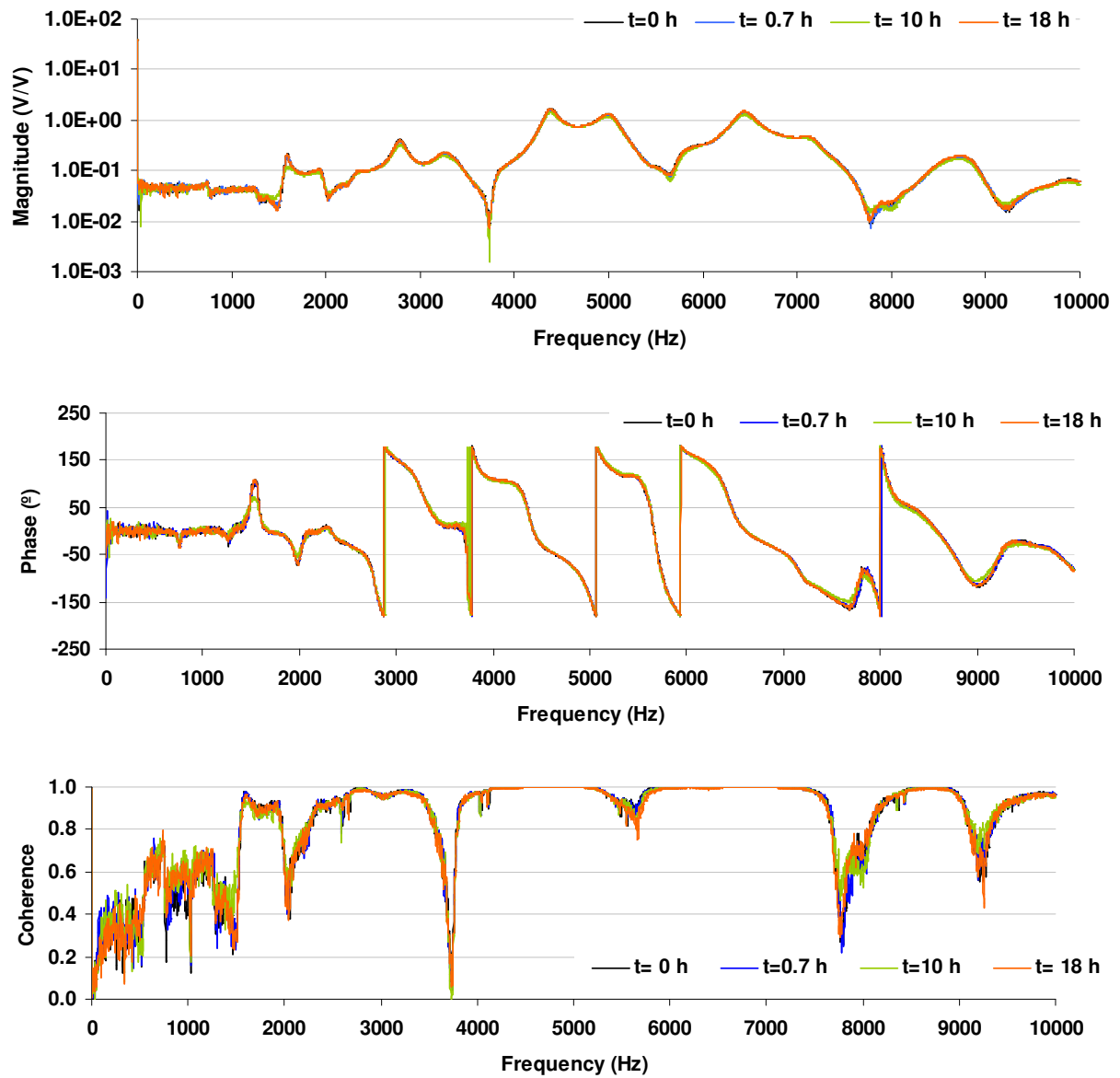


**Figure D.4:** transfer function of the system at different deposit stages (corresponding to the magnitude transfer curves shown in Figure 6.25)

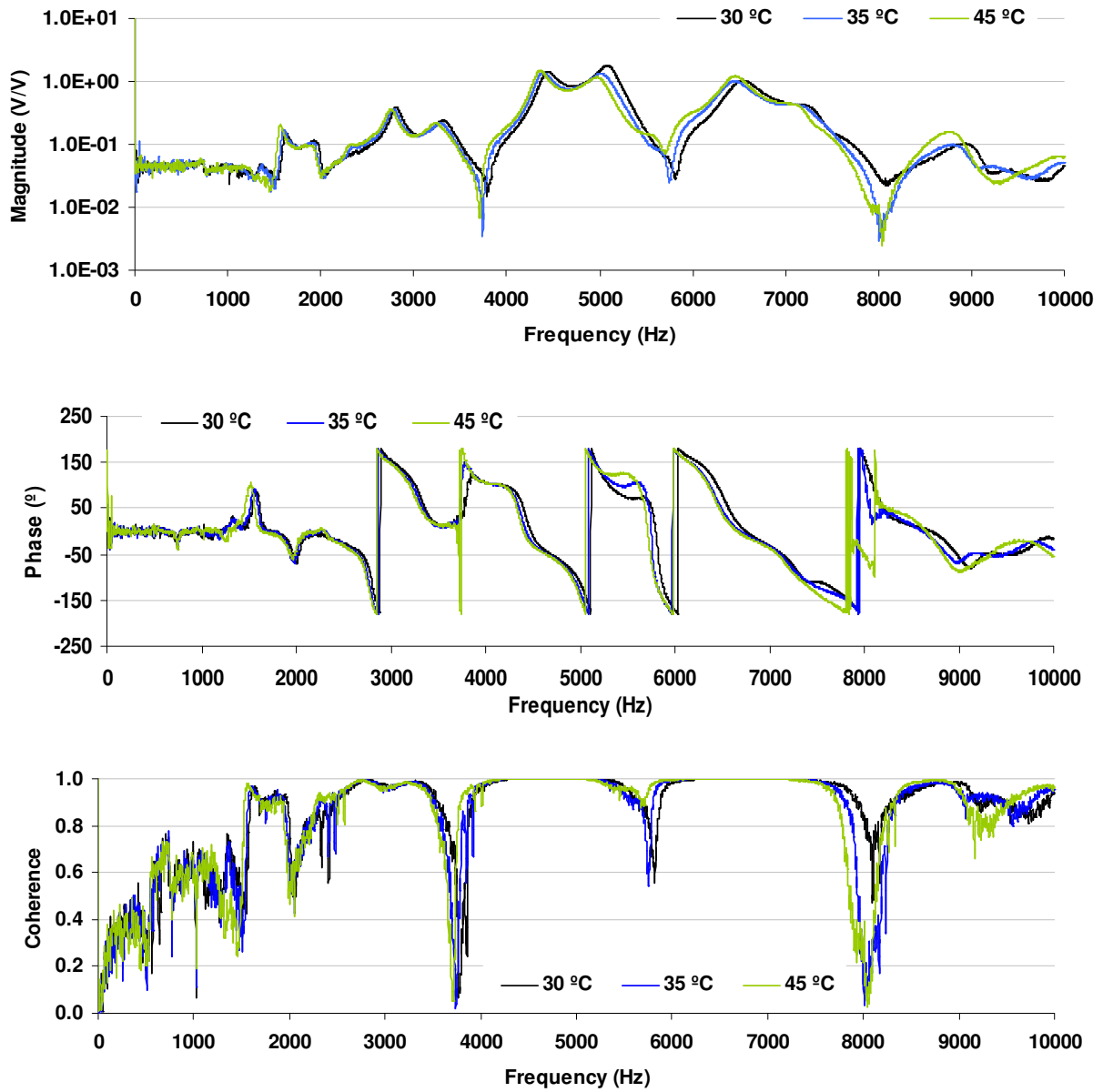


**Figure D.5:** transfer function of the system filled with water at different temperatures (corresponding to the magnitude transfer curves shown in Figure 6.26)

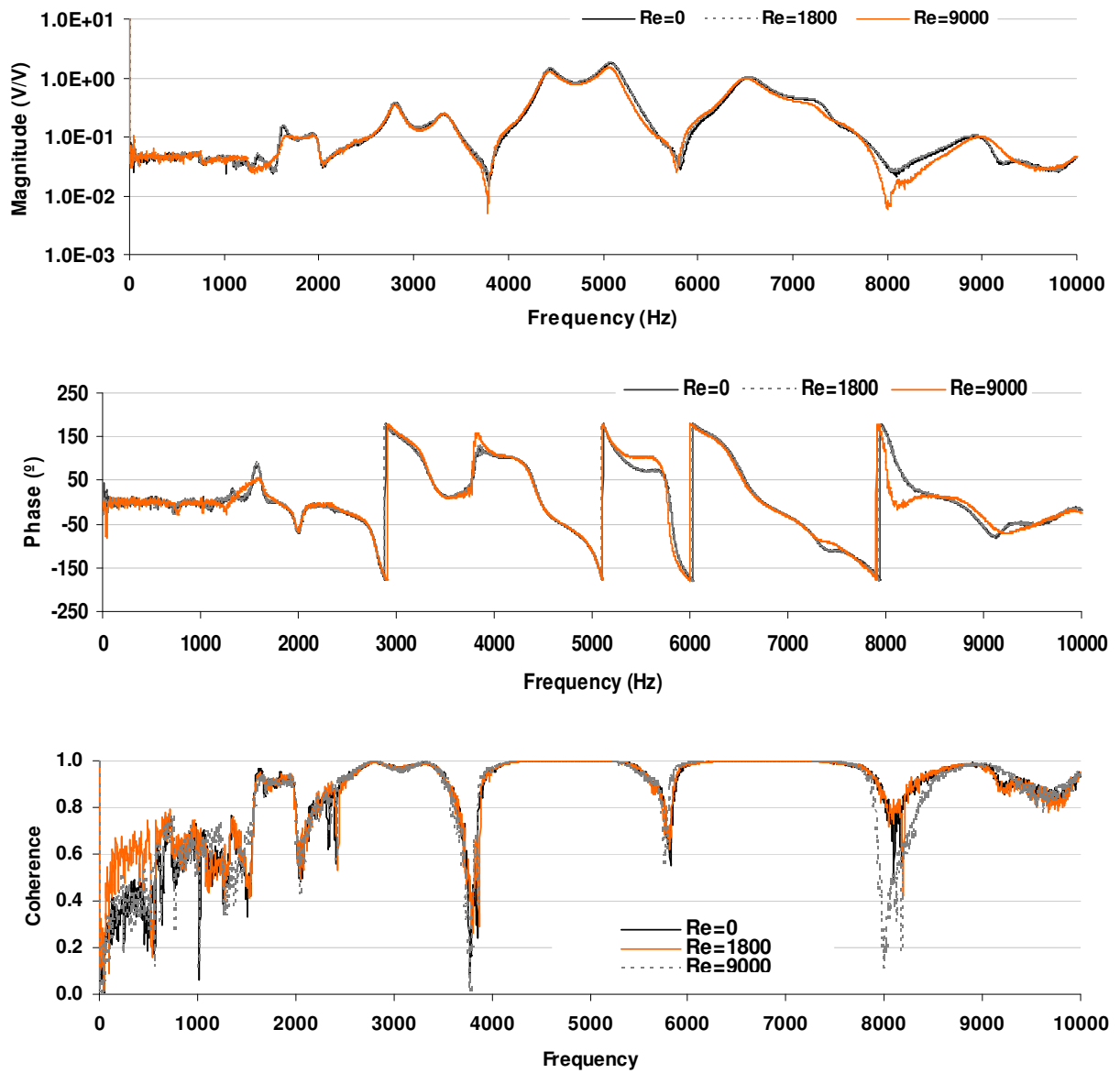


**Figure D.6:** transfer function of the system for different flow regimes (corresponding to the magnitude transfer curves shown in Figure 6.27)

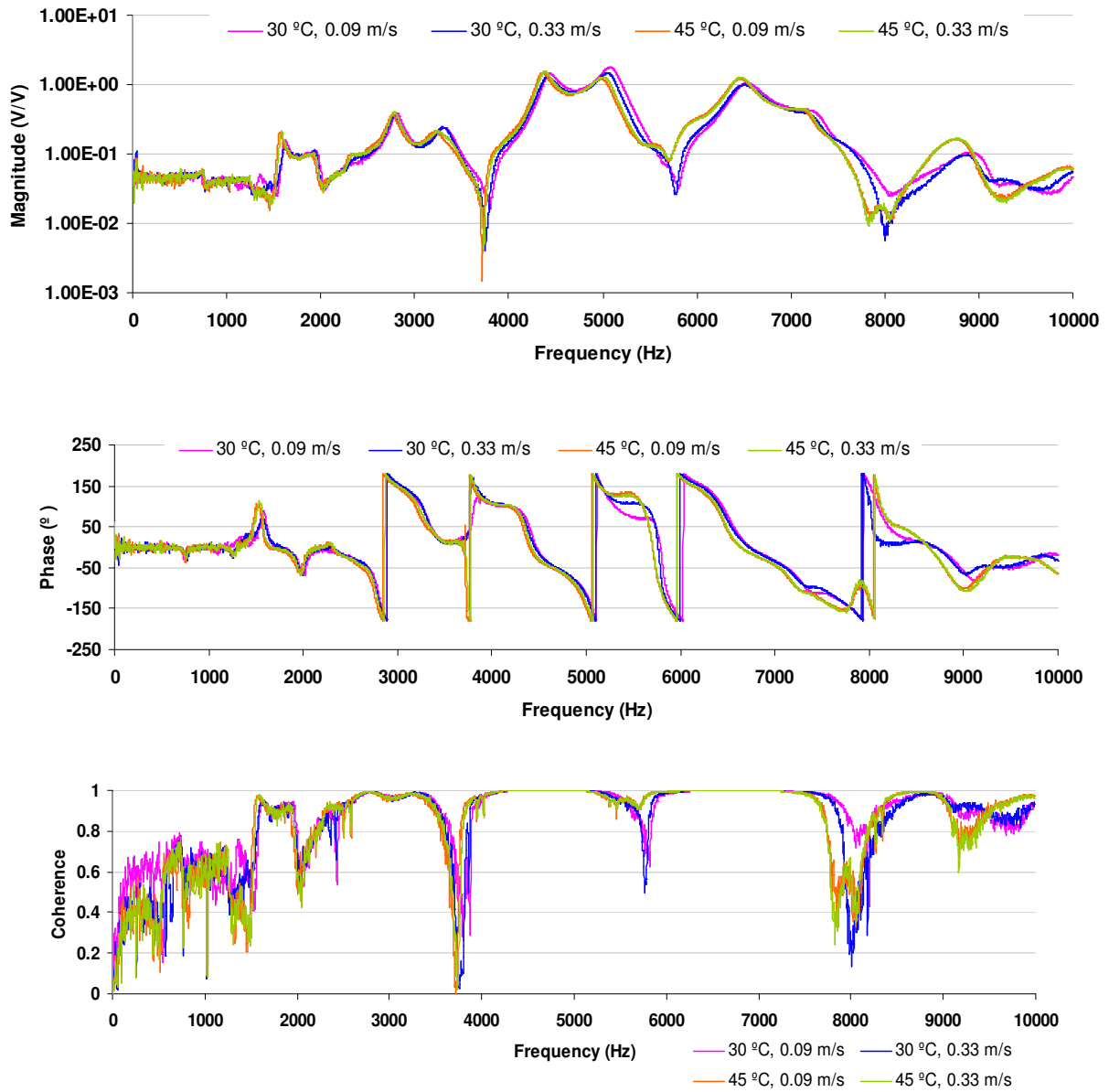


**Figure D.7:** transfer function of the system for different temperatures and different flow velocities (corresponding to the magnitude transfer curves shown in Figure 6.28)